



Topology Optimisation and Additive Manufacturing of Structural Nodes of Gridshell Structures

A thesis submitted in fulfilment of the requirements for the degree of

DOCTOR OF PHILOSOPHY

Hamed Seifi

B.Sc. (Civil Engineering, Tehran University)

M.Sc. (Structural Engineering, Tehran University)

School of Engineering

College of Science, Engineering and Health

RMIT University

March 2019

Declaration

I certify that except where due acknowledgement has been made, the work is that of the author alone; the work has not been submitted previously, in whole or in part, to qualify for any other academic award; the content of the thesis is the result of work which has been carried out since the official commencement date of the approved research program; any editorial work, paid or unpaid, carried out by a third party is acknowledged; and, ethics procedures and guidelines have been followed. I acknowledge the support I have received for my research through the provision of an Australian Government Research Training Program Scholarship.

Hamed Seifi

March 2019

Acknowledgments

I would like to take this opportunity to express my sincerest thanks to people who have provided generous help during my PhD candidature. The research in this thesis would not have been successfully performed without the significant support from them.

First and foremost, I would like to express my sincere gratitude to my senior supervisor, Distinguished Professor Yi Min (Mike) Xie for his valuable suggestions, continuous support and encouragement throughout this research project. Professor Xie has been an excellent supervisor and role model who has encouraged and inspired me to strive for success during my PhD study. I would like to thank Professor Xie who has always been wise and patient in instruction, meticulous in revising my papers and supportive to my research. Without the outstanding supervision of Professor Xie, this PhD work would not have been accomplished smoothly and successfully. It is my greatest honour and fortune to be one of his students.

Secondly, I would like to express my special appreciation to my associate supervisors Dr. Shanqing Xu and Dr. Xiaoshan Lin, for their encouragement, advice, comments and contributions.

Thirdly, I would like to thank my wife and fellow PhD candidate, Anooshe Rezaee Javan, for her great help, continuous support, insightful comments and encouragement, which have enabled me to complete my PhD research. Also, I am very grateful for all the care and support from other colleagues in the Centre for Innovative Structures and Materials (CISM). I appreciate their company with me to experience the unforgettable and fruitful life during my PhD candidature.

My sincere thanks go to all the academic and administrative staff in the Civil and Infrastructure Engineering discipline in the School of Engineering at RMIT University.

Last but not least, I would like to express my sincerest and deepest gratitude to my parents for their spiritual support over the years. I would also like to thank my parents-in-law for their supports. I would like to dedicate this thesis to my mother for being my first teacher.

Publications during the period of the PhD candidature

Directly related to this thesis:

1. **Seifi, H.**, Rezaee Javan, A., Xu, S., Zhao, Y., and Xie, Y. M. (2018). Design optimization and additive manufacturing of nodes in gridshell structures. *Engineering Structures*, **160**, 161-170.
2. Donnellan, J., **Seifi, H.**, Sitler, B., Williams, N., Crolla, K., and Xie, Y. (2015). Smart nodes pavilion: Bi-directional evolutionary structural optimization and additive manufacturing. In: Proceedings of the International Association for Shell and Spatial Structures (IASS) Symposium 2015, Amsterdam, 1-12.
3. Williams, N., Prohasky, D., Burry, J., Crolla, K., Leary, M., Brandt, M., Xie, M., and **Seifi, H.** (2015). Challenges of scale modelling material behaviour of additive-manufactured nodes. In: Proceedings of the 5th Designing Modelling Symposium 2015, Copenhagen, Denmark, 45-51.
4. **Seifi, H.**, Xie, Y. M., O'Donnell, J., and Williams, N. (2015). Design and Fabrication of Structural Connections Using Bi-directional Evolutionary Structural Optimization and Additive Manufacturing. In: Proceedings of the 2nd Australasian Conference on Computational Mechanics (ACCM 2015), Brisbane, Australia, 571-576.

Indirectly related to this thesis:

1. Ding, C., **Seifi, H.**, Dong, S., and Xie, Y. M. (2017). A new node-shifting method for shape optimization of reticulated spatial structures. *Engineering Structures*, **152**, 727-735.
2. Ding, C., **Seifi, H.**, and Xie, Y. M. (2016). Form-finding of spatial grid structures with volume constraints. In: Proceedings of the International Association for Shell and Spatial Structures Annual Symposium (IASS 2016), Tokyo, Japan, 1-8.

Other publications in structural engineering:

1. **Seifi, H.**, Rezaee Javan, A., Ghaedizadeh, A., Shen, J., Xu, S., & Xie, Y. M. (2017). Design of Hierarchical Structures for Synchronized Deformations. *Scientific Reports*, **7**, **41183**, 1-7.

-
2. Lu, D., Li, Y. F., **Seifi, H.**, Zhou, S., Zhao, Z.-L., & Xie, Y. M. (2018). Designing novel structures with hierarchically synchronized deformations. *Extreme Mechanics Letters*, **19**, 1-6.
 3. Rezaee Javan, A., **Seifi, H.**, Xu, S., Ruan, D., & Xie, Y. M. (2017). The impact behaviour of plate-like assemblies made of new interlocking bricks: An experimental study. *Materials & Design*, **134**, 361-373.
 4. Rezaee Javan, A., **Seifi, H.**, Xu, S., Lin, X., & Xie, Y. M. (2018). Impact behaviour of plate-like assemblies made of new and existing interlocking bricks: A comparative study. *International Journal of Impact Engineering*, **116**, 79-93.
 5. Rezaee Javan, A., **Seifi, H.**, Xu, S., & Xie, Y. M. (2016). Design of a new type of interlocking brick and evaluation of its dynamic performance. In: *Proceedings of IASS Annual Symposia, 2016*, **7**, 1-8.

Table of Contents

Declaration.....	i
Acknowledgments.....	ii
Publications.....	iii
Table of Contents.....	v
Abstract.....	ix
Chapter 1: Introduction.....	2
1.1. Background.....	2
1.2. Motivation of the thesis.....	4
1.3. Scope and aims of the thesis.....	5
1.4. Thesis outline.....	6
References.....	7
Chapter 2: Literature.....	9
2.1. Gridshells.....	9
2.1.1. History.....	9
2.1.2. Structural principle.....	20
2.1.3. Nodes in gridshell structures.....	22
2.2. Structural optimisation.....	30
2.2.1. Topology optimisation.....	31
2.3. Manufacturing.....	34
2.3.1. Formative manufacturing (casting).....	35

2.3.2. Subtractive Manufacturing (computer numerical control machines).....	36
2.3.3. Additive manufacturing (AM):.....	37
2.4. Knowledge gap in designing and manufacturing nodes for gridshell structures	43
References	43
Chapter 3: Topology optimisation and advanced manufacturing of structural nodes	50
3.1. Introduction	51
3.2. Loading and geometrical conditions	53
3.2.1. Geometrical design of initial model	53
3.2.2. Load cases.....	56
3.3. Design of geometrically simple nodes for basic load cases.....	59
3.3.1. Effect of the non-design domain shape on BESO results.....	71
3.4. Design of geometrically complex nodes for general load cases	74
3.4.1. Node design for a prototype canopy.....	74
3.4.2. Design of nodes for arbitrary load conditions	78
3.5. Effect of design domain size	82
3.6. Smoothing	85
3.7. Manufacturing:.....	94
3.8. Conclusions	101
References	102
Chapter 4: Comparison between new and conventional designs of nodes for gridshell structure.....	105
4.1. Introduction	106

4.2. Design of structural nodes for gridshell structures.....	108
4.2.1. Loading conditions	108
4.2.2. Transitional section design	111
4.2.3. BESO design.....	116
4.2.4. Conventional designs.....	124
4.3. Finite element modelling.....	131
4.4. Results and discussion.....	132
4.5. Conclusions	141
References	142
Chapter 5: Experimental and Numerical Studies of Nodes for Gridshell Structures	145
5.1. Introduction	146
5.2. The design concept of test setup	149
5.3. Case study	154
5.3.1. BESO design.....	163
5.3.2. Material test.....	165
5.3.3. Numerical simulation	166
5.3.4. Estimation of load cell force.....	172
5.3.5. Manufacturing	175
5.3.6. Experiments.....	175
5.4. Discussion and conclusions.....	180
References	181

Chapter 6: Conclusions and Future Research 183

6.1. Conclusions 183

6.2. Future Research..... 185

Abstract

Gridshells, also called lattice shells or reticulated shells, are lightweight spatial structures. Their organic shape, column-free space, free-form surface and maximised transparency have provided limitless design freedom for architects and structural engineers. The design and manufacturing of structural connections (nodes) have been the bottle neck in the design and construction of gridshells, which is due to their complicated geometries and the three-dimensional loading conditions applying on these nodes. The invention of additive manufacturing (AM) provides the possibility of optimising the nodes by using topology optimisation (TO) algorithms. Instead of rationalising the geometry of the nodes to provide simplified connections for conventional production system, custom-designed connections can be achieved with lower weight and higher accuracy using combination of TO and AM. As a consequence, the optimised nodes help reduce the structure size and foundation requirements which leads to saving in the material cost. Furthermore, other features also make the newly designed nodes promising, such as the aesthetical features, high stiffness, high precision and less labour.

In this study, Bi-directional Evolutionary Structural Optimisation (BESO) techniques are used to minimise the weight and the printing time required for each node. Firstly, the effect of general load cases on the optimised topology of structural node is studied by comparing the optimised results for the nodes under different individual load cases and combined load cases. Furthermore, the effect of the size of the design-domain on the final weight and topology of a node designed by BESO is examined by using different initial sizes. In addition, various smoothing methods for the final geometry are explored and compared with each other. The challenges of using AM in manufacturing nodes are also investigated through 3D printing individual optimised nodes and the optimised

nodes for a case study of a prototype gridshell structure. Besides, comparisons made between optimised nodes and conventional nodes show the efficiency of the optimised nodes.

An innovative experimental setup for quasi-static test of nodes under dominant design loads is also proposed in this study. Two nodes are designed and manufactured using BESO and AM to test by a test rig designed based on the proposed setup. In addition, a 3D finite element analysis is conducted, and the numerical model is validated against the test results.

CHAPTER 1

INTRODUCTION

Chapter 1: Introduction

1.1. Background

Gridshell structures, which are also known as lattice structures, are widely used in civil infrastructure including large-scale commercial buildings and stadia. In the design and manufacturing of gridshell structures, structural connections (nodes) have been reported as a bottleneck [1]. Basically, most of geometrical and topological information of gridshell structures is stored in their nodes in the form of geometry. Therefore, it is often required to generate a bespoke shape with complex geometry for each node. Besides, the limitations of conventional manufacturing methods necessitate a certain level of simplicity for the nodes to be manufactured through these methods. To consider the simplicity required by manufacturing methods and the complexity resulted from external geometrical constraints, node designs are often structurally inefficient. Furthermore, the standard design codes and conventional design methods are usually not applicable to these nodes due to complex internal force fields.

The newly developed design algorithms, such as the structural optimisation algorithm, have effectively responded to the demand for efficient structural design for complex nodes. The form-finding algorithms, structural optimisation algorithms and powerful simulation packages are helping designers to virtually realise their ideas. Although these methods and algorithms produce structurally optimal designs, the geometries of these designs are too complex to be fabricated using conventional manufacturing methods. Newly developed additive manufacturing (AM) technologies are able to realise the most complex geometries. Although the cost of AM is higher than conventional methods, the structural optimisation methods decrease the node volumes in design, and hence the total cost of additive manufacturing.

Structural nodes can be considered as one of the most important elements in a gridshell structure due to their vital role in load transferring process. They are critical links in design and construction of structures, due to the geometrical and topological complexity, as well as a great amount of forces transferred through the small volume [2]. Therefore, it is desirable to optimise the designs of structural nodes.

Structural optimisation can be classified into three main types: size optimisation, shape optimisation and topology optimisation. In size optimisation, the optimal design would be obtained by changing the size variables of the structure, such as the cross-sectional dimensions of trusses and frames and the thicknesses of plates. This is the easiest and earliest approach for improving structural performance. In shape optimisation, which is mainly used in continuum structures, the variables are the parameters defining the boundaries of a structure. In topology optimisation, the variables are the structural elements. In discrete structures, such as trusses and frames, topology optimisation will find the optimal connectivity by adding or removing bars/beams between predefined nodes. In continuum structures, determining the best locations of cavities will lead to the optimal design. Topology optimisation for continuum structures is considered to be the most technically challenging and economically rewarding structural optimisation method [3]. At present, this method has been extensively used in the automotive and aerospace industries for component designs.

The conventional manufacturing method in construction, including cutting and welding separate parts, is not able to realise the complex designs of structural nodes. The manufacturing processes include machining/subtractive process and casting/formative process. In machining/subtractive process, the part is produced by material removal. While in casting/formative process, the part is produced by a mould. Both processes require a high degree post-processing of design results. To ensure a feasible design, several significant manufacturing constraints must be taken into account during the design stage when using

these methods. For example, the need for tool access in the case of machining, and the need for part removal from a mould in the case of casting. These constraints limit the physical realisation of the optimal topology, and a compromise has to be made between optimality and ease of manufacture. Usually, these constraints are either included in the actual optimisation by limiting the topology to feasible designs, or considered by subsequent simplification of the unconstrained design. The former is normally preferable, but not all constraints can be included easily in the optimisation process [4].

By contrast, additive manufacturing technologies open the possibility to overcome limitations currently encountered by conventional manufacturing techniques, and enable the solid free-form manufacture of complex geometries. AM technologies are usually working on a layer-by-layer approach. They are a further development from rapid prototyping (RP), and are becoming more versatile, stable, accurate and economical at a steady pace, aimed at producing end-use parts rather than prototypes. In recent years, significant efforts have been made to process metals, and several commercial metal processes are now available for producing end-use parts.

1.2. Motivation of the thesis

The main objective of structural design is to develop load carrying systems that can economically satisfy structural safety and performance requirements. From the economical point of view, it is desirable to reduce the number of steps involved in a product manufacturing. Besides, the economic considerations also include the reductions in construction materials and labour intensity. Gridshell structures could perfectly cope with the aforementioned constraints and satisfy the requirements of canopy and façade type structures due to aesthetical advantages and environmental compatibility. Besides, these structures are easy to be assembled and disassembled due to the use of prefabricated customised nodes and

elements. Many nodes in gridshell structures are unique in shape and design. Manufacturing these nodes using conventional methods is usually very challenging and labour intensive. Besides, the structural behaviour of a gridshell is very sensitive to the node imperfection especially in steel structures. By exploring and solving challenges in design and construction of gridshell structures with topologically optimised and additively manufactured nodes, insights into the new opportunities and design freedom will be obtained.

The application of structural optimisation techniques to find the best material distribution within the design domain has significant positive environmental impacts, such as the reductions of construction material and wastes.

1.3. Scope and aims of the thesis

This study aims to explore the potential of using topology optimisation and additive manufacturing in the design and manufacture of structural nodes for gridshell structures, especially steel gridshells.

The main research objectives to this study are as follows.

1. Investigating the main structural behaviour of the nodes of gridshell structures, and studying key parameters in the design of nodes.
2. Exploring the challenges and opportunities in using topology optimisation for the node design and additive manufacturing for fabricated the topologically optimised nodes.
3. Comparing the structural performance of the newly designed nodes with conventional ones.
4. Developing a new method for carrying out the experiments on the topologically optimised nodes.

1.4. Thesis outline

To achieve the research objectives this thesis is structured as follows.

Chapter 2 provides a detailed literature review of the topology optimisation, gridshell structures and additive manufacturing.

In Chapter 3, the structural behaviour of the nodes of gridshell structures as well as the challenges in design, preparation and fabrication of them is studied. A number of nodes with different loading conditions are designed using the bi-directional evolutionary structural optimisation (BESO) method. Besides, a study on the suitable predefined size for the design domain is carried out. Some of the designed nodes are manufactured by additive manufacturing (AM) method.

In Chapter 4, two free-form nodes designed by transitional sections and BESO for gridshell structures are compared with two conventional nodes [5, 6]. Laplacian smoothing algorithm is used for both new nodes to minimise stress concentration in sharp edges. The mechanical performances of the nodes are assessed by finite element modelling and a comparison between the new and conventionally designed nodes is conducted.

In Chapter 5, an innovative approach for designing inexpensive and available test setup for testing the nodes of gridshell structures is proposed. Two types of nodes are designed, fabricated and tested by using a customised test rig which is designed based on the proposed concept. The results of the experiments are compared with the results of the numerical simulations under the similar conditions.

Chapter 6 summaries the major findings of this study followed by recommendations for future research directions [4].

References

1. Tonelli, D., Pietroni, N., Puppo, E., Froli, M., Cignoni, P., Amendola, G., and Scopigno, R. (2016). Stability of statics aware voronoi grid-shells. *Engineering Structures*. **116**: 70-82.
2. Mittendorf, J., and Dodson, D. (2015). *The Art of Reading Buildings*: Fire Engineering Books.
3. Huang, X., and Xie, M. (2010). *Evolutionary topology optimization of continuum structures: methods and applications*: John Wiley & Sons.
4. Brackett, D., Ashcroft, I., and Hague, R. (2011). Topology optimization for additive manufacturing. In: *Proceedings of Annual International Solid Freeform Fabrication Symposium*. **1**: 348-362.
5. Min, C., Dong, X., Yang, Z., Liang, S. U., Shilin, D., Dasui, W., and Anan, Z. (2010). Experimental research and finite element analysis on joints of Sun Valley steel structure for the Expo Axis project. *Journal of Building Structures*.**5**: 006.
6. Knippers, J., and Helbig, T. (2009).Recent developments in the design of glazed grid shells. *International Journal of Space Structures*. **24**(2): 111-126.

CHAPTER 2

LITERATURE REVIEW

Chapter 2: Literature

In this chapter, a literature review is carried out in three sections based on the aims outlined in chapter 1. To optimise connections in gridshell structures, firstly a review on gridshell structures is conducted, covering their history, their structural principle and their structural connections. The second section is on topology optimisation as one of the structural optimisation approaches. The history and different methods of topology optimisation are reviewed. Manufacturing methods are reviewed in the third section, covering casting, computer numerical control (CNC), and additive manufacturing.

2.1. Gridshells

A gridshell structure consists of one layer grid of beam members forming a shell geometry. As the structural behaviour of a gridshell is similar to that of a shell structure, it is beneficial to start the review with shell structures in order to obtain a better understanding of gridshell structures.

Various classifications can be used for structures based on selection criteria, such as different shapes, functions and materials [1]. By using geometrical approach, the shape of a shell structure can be defined as a curved surface, while the thickness (dimension in the direction perpendicular to the surface) is very small compared to the in-plane dimensions of the shell structure. A surface can be double curved, such as a dome and a cooling tower, or single curved like a cylinder.

2.1.1. History

The inspiration in the structural design process comes from nature where right angles and straight lines are not being used frequently [2]. However, in engineering practice, human beings have been constantly using straight lines, orthogonal connections and as much

repetition of elements as possible in structural design. The lack of technology, knowledge, production capability and resources may cause high degree of simplification in design and construction of engineering structures. Nowadays, with the development of new technologies, exceptions from rectilinear designs have become more frequent, and more accurate structural systems with more complexity have been proposed [2].

The first structures, in which humans tried to convert the out-of-plane forces into in-plane forces and then transfer through abutment, are arched structures. These structures are often built with materials strong in compression but relatively weak in tension, like masonry and concrete [3]. Beehive tombs used for burial rituals in Spain and Portugal are the first shell type structures, which can be dated back to 3000 AD (Figure 2-1a), followed by beehive houses in Ireland and Scotland from 2000 AD (Figure 2-1b). Both types of structures were built by piling up blocks of stone.

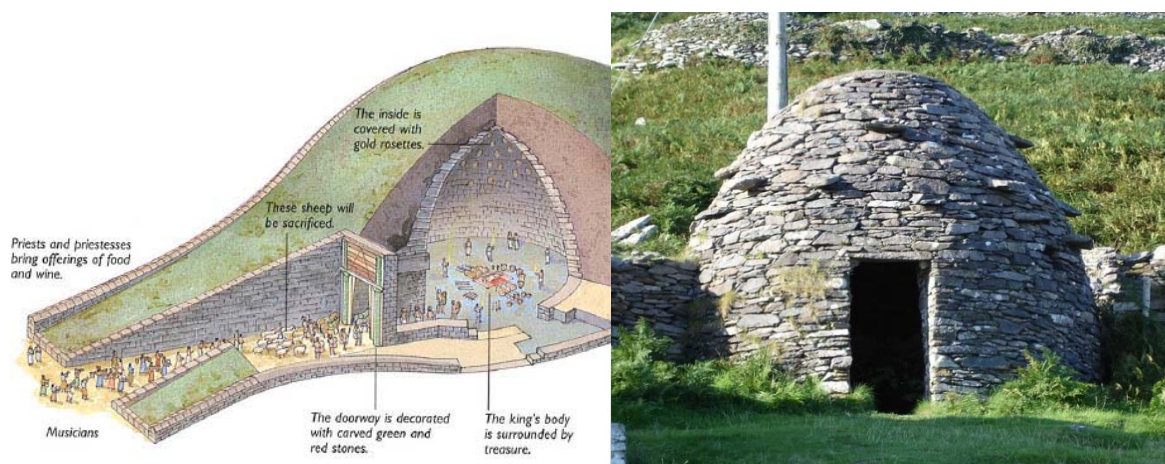


Figure 2-1: a) Beehive tombs, 3000 AD [4], b) beehive houses in Ireland, 2000 AD [5].

The Persian monument Taq-iKisra built in 540AD (shown in Figure 2-2) is one of the best examples of an arch structure made of bricks without centring (supporting structure) [6]. Its central arch-dome is 37 m high and the span is 26m.



Figure 2-2: Taq-iKisra, Persian monument, 540 AD [7].

In Roman period, the construction of arches for aqueducts and amphitheatres brought the Romans the knowledge of transferring out-of-plane forces into normal forces and transferred to the foundation. The oldest known concrete shell structure - the Roman Pantheon (Figure 2-3) was constructed using this concept in 125 AC. With a span of 43 m, it was an incredible piece of engineering at that time.



Figure 2-3: The Roman Pantheon, 125 AC [8].

Another example is the Hagia Sophia dome (Figure 2-4) in Istanbul. With its 32m span, the Hagia Sophia dome is still an impressive structure today. The Hagia Sophia dome is supported by four large columns instead of a solid base as in the Roman Pantheon [9]. Started in the 6th century, hemi domes, abutments and pendentives have often been used as supports, which are different from the Roman Pantheon.

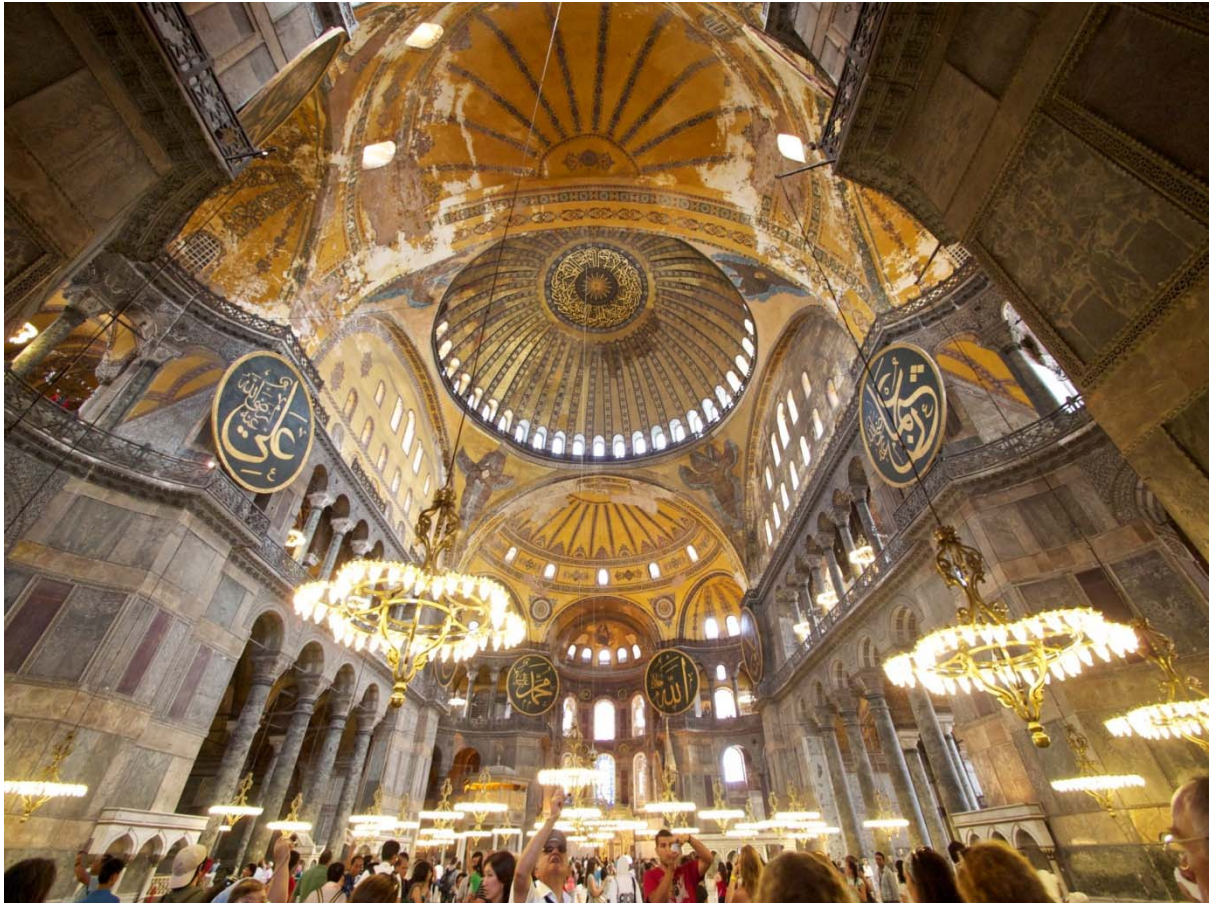


Figure 2-4: Interior of the Hagia Sophia, 6th century [10].

With the introduction of reinforcements (e.g. steel reinforcing bars) to concrete in the 19th century, concrete structures were not only strong in compression, but also could sustain much higher tensile force, leading to further development of curved structures - shells. Casting method in construction has enabled the transformation of flat slabs into shell structures with an even force distribution. But formwork and scaffold represent around 50% of the total cost of a shell structure, even when the shuttering has been reused several times [3].

A successful attempt to replicate a nature structure in an exact manner is achieved by combining the grid systems and double-curved shells to make a creative structural system called gridshell structure. By dividing the whole structure into simple elements using a grid system, the construction issues, such as difficulties in erecting the entire arch structure, are avoided. Besides, a gridshell has the advantage of using the daylight sources comparing with a closed concrete shell. The first gridshell structure was pioneered by Schwedler, who in

1863 built a steel cupola (Figure 2-5) as the roof of a gas holder for the Imperial Continental Gas Association in Berlin. The structural system was able to span a distance of 25-40m [11]. In 1897, a Russian engineer Shukhov constructed a steel mill 150km southwest of Nizhny Novgorod [12]. This building had five doubly curved gridshells, covering an area of 70m×24m (Figure 2-6). Although Shukhov introduced the doubly curved gridshell, he did not make full use of the structural advantage of the double curvature as he neglected the positive impact of the curvature in the cross-direction.



Figure 2-5: Schwedler cupola, J. W. Schwedler, Berlin, 1863 [13].

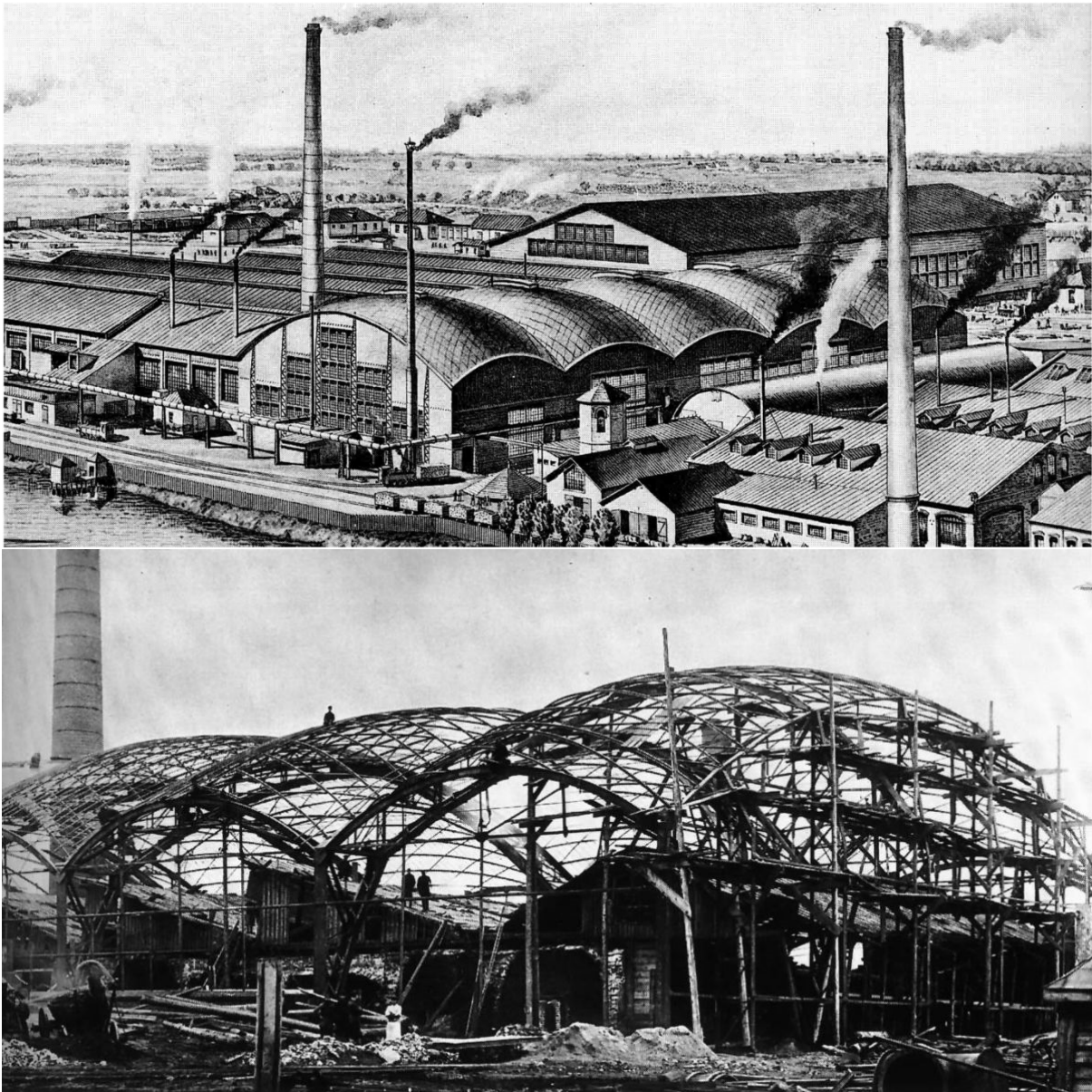


Figure 2-6: Production hall in Vyksa, a) Lithography around 1900 [12], b) during construction [14].

A good example that demonstrates the fusion of a grid structure and a continuum shell is Torroja's Fronton Recoletos, built in Madrid in 1935 (Figure 2-7), where the roof was made as a combination of a concrete shell and a triangular gridshell.

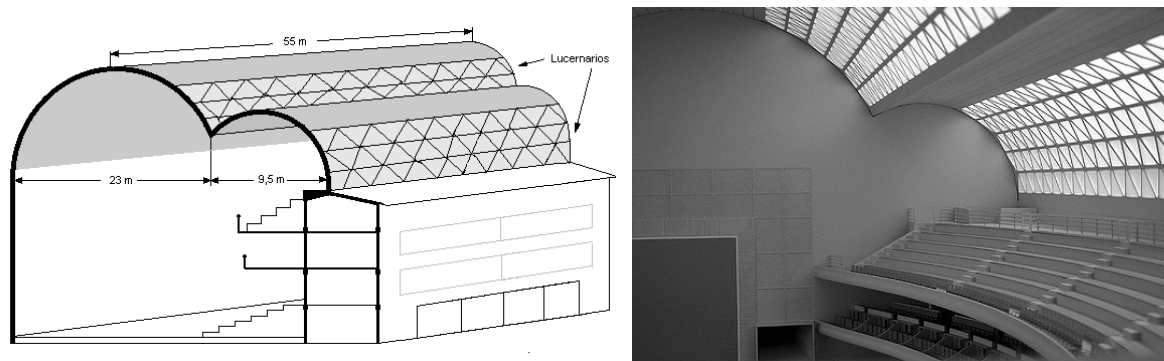


Figure 2-7: Recoletos, Eduardo Torroja, Madrid, Spain, 1935 [15].

An excellent example of the gridshell in reinforced concrete structures is the Palazzetto dello Sport designed by Pier Luigi Nervi, which is an indoor arena located in Piazza Apollodoro in Rome (Figure 2-8).

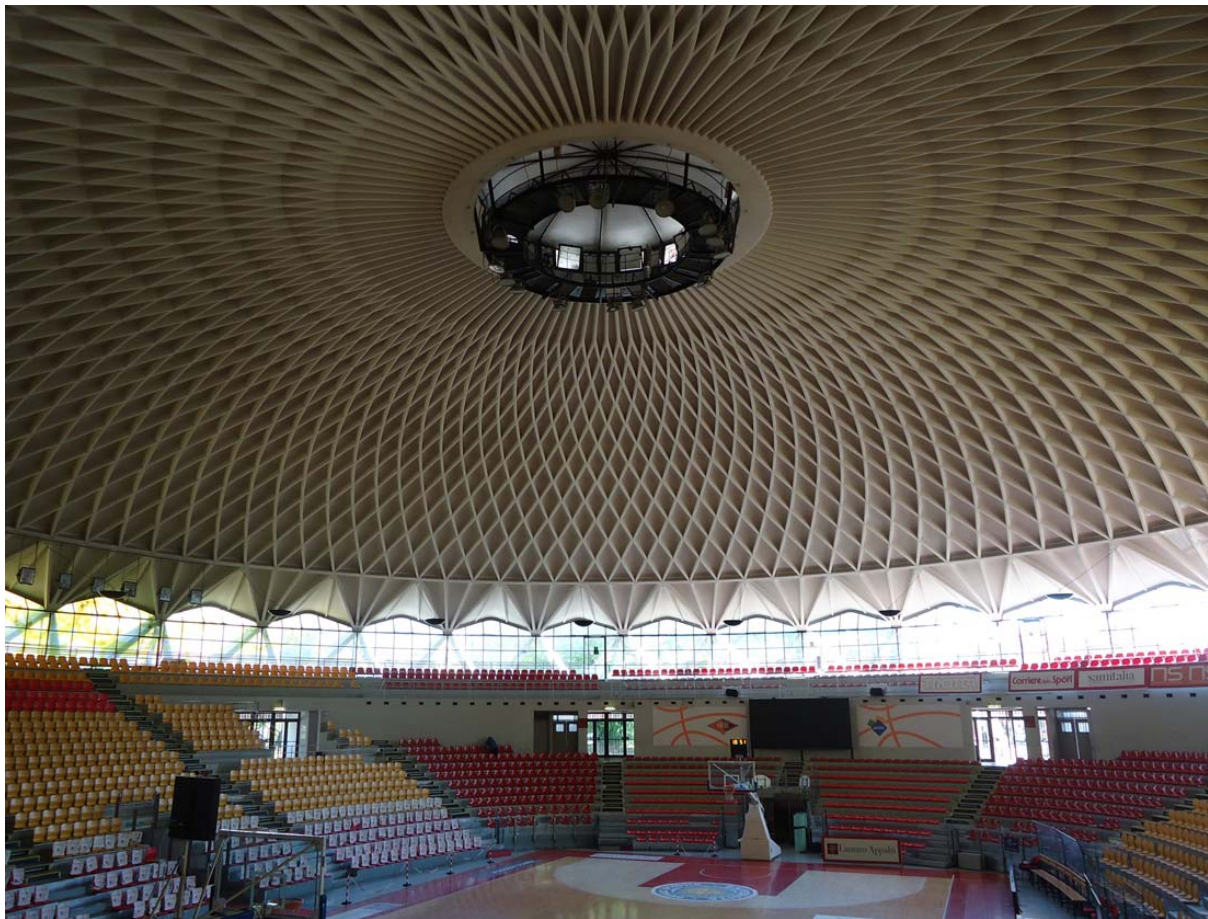


Figure 2-8: Palazzetto dello Sport, Pier Luigi Nervi, Rome, Italy, 1935 [16].

In 1975, a double-curved wooden shell structure (called Multihalle) was built in Mannheim (Figure 2-9) [17]. In contrast to Shukhov's gridshell in Vyksa, the Multihalle made perfect use of its double curvature. This was achieved by Otto using scale models during the form-

finding process [18]. Otto developed models with different forms and shapes to study the behaviour of the grid in a structure. Small load representing the weight of the structure was applied (Figure 2-10). In contrast to steel gridshells, wooden gridshells can be firstly assembled to a flat structure on the ground, and then form their three-dimensional shapes by pushing the boundaries into the exact support locations [19]. This type of gridshell is called active bending gridshell. The gridshell considered in this study is a single-layer lattice frame in which the members are initially made to fit the final form of the structure, and there is no active bending moment in the members.

Having found the desired shape for Multihalle, Otto studied the behaviour of the gridshell using finite element method (FEM). FEM enables the visualisation of stresses and displacements in structures for a wide range of static and dynamic analyses, making the design and analysis of complex structures possible. To remove the restrictions in construction, structural members can be prefabricated using computer numerical controlled (CNC) machines. Thus, all members can be designed to be unique, leading to a free-form gridshell structure. Today, free-form gridshells are very popular as they create attractive (public) spaces. Queen Elizabeth II Great Court (Figure 2-11) which covers the court of the British Museum in London and the Kogod Courtyard (Figure 2-12) in the Smithsonian American Art Museum in Washington are two great examples of gridshell structures.

After more than one century of development, gridshell structures have been evolved in many aspects, including construction material, grid pattern, structural analysis method, structural form-finding method, manufacturing method and connection details.

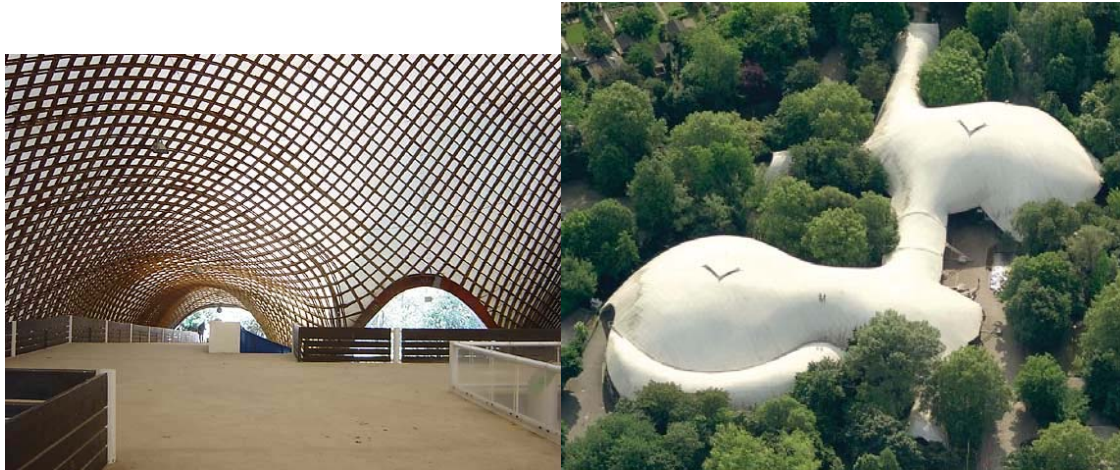


Figure 2-9: Multihalle, Mannheim, Germany, 1975 [18].

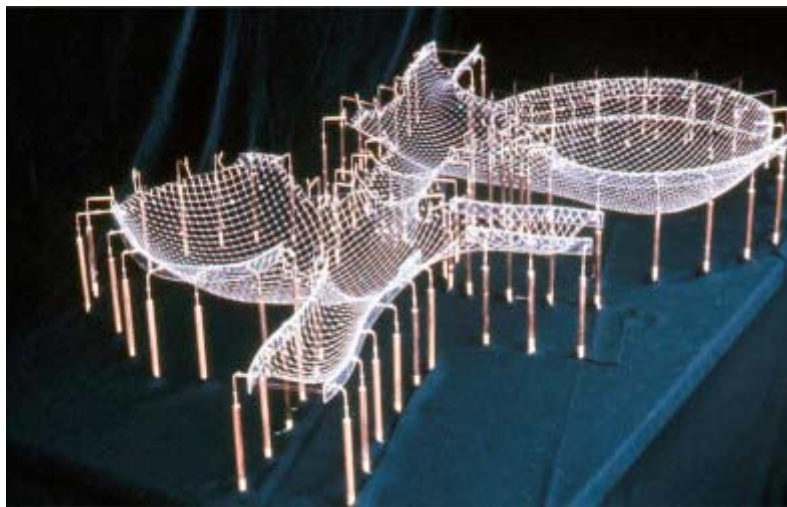


Figure 2-10: Hanging scale model of the Mannheim Multihalle [17].



Figure 2-11: Queen Elizabeth II Great Court, British Museum, London [20].



Figure 2-12: Smithsonian American Art Museum, Washington [21].

2.1.2. Structural principle

The structural behaviour of shells is heavily dependent on their geometries. Free-form gridshells often consist of different kinds of shell surfaces. The best way to classify shell surfaces is based on the definition of Gaussian curvature for that surface. The Gaussian curvature at any point is defined as the multiplication of the minimum and maximum curvatures of the curves fit to the shell surface at that point. These curvatures are called principle curvatures κ_1 and κ_2 . The Gaussian curvature is defined as: $\kappa_g = \kappa_1 \times \kappa_2$. Shell surfaces can be classified using the Gaussian curvature as follows [22]:

- *anticlastic* surface: $\kappa_g < 0$, principal curvatures have opposite signs;
- *synclastic* surface: $\kappa_g > 0$, principal curvatures have the same sign;
- *monoclastic* surface: $\kappa_g = 0$, at least one of the principal curvatures is zero, resulting in a cylindrical surface or a plane when both κ_1 and κ_2 are zero.

Different types of Gaussian curvature are shown in Figure 2-13.

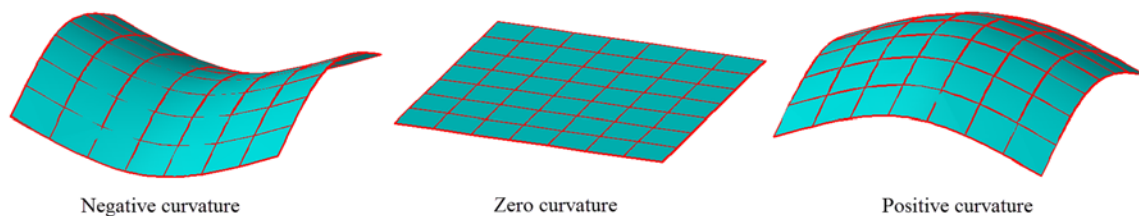


Figure 2-13: Different types of Gaussian curvature.

Shell structures derive their strength from its double curvature. In the experiment (Figure 2-14) conducted by Chilton and Isler [3], a curved plastic element was shown to resist more than 30 times greater load than the flat element.

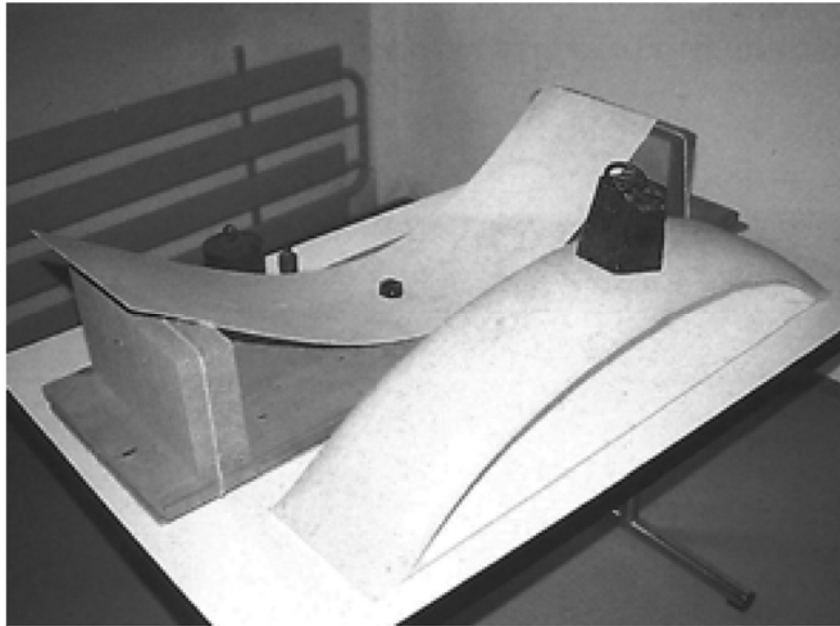


Figure 2-14: Comparison between a plastic double-curved shell and a plastic flat beam over the same span [3].

In the stiffness matrix of a structural member, the axial stiffness is the biggest. By using double curvature in gridshell structures, the axial stiffness of members would spread in other locations of the assembled stiffness matrix [23]. Although all modes of structural actions that are available to beams, struts, arches, cables and plates are involved in shell structures, membrane action prevalently occurs in shell structures [24]. Doubly-curved shells mainly transfer the applied loads to the abutments by membrane internal forces (Figure 2-15). Therefore, the internal force in gridshell structural members is dominated by membrane force.

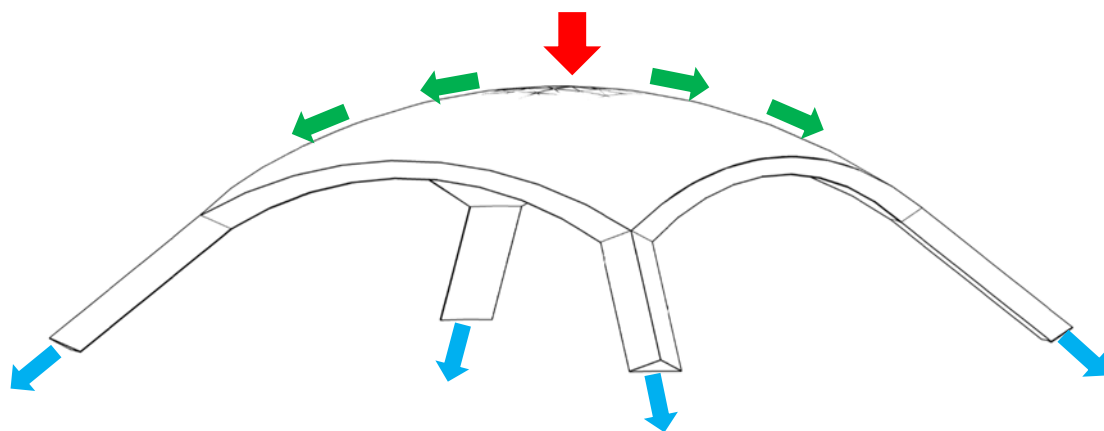


Figure 2-15: Force distribution in shell.

2.1.3. Nodes in gridshell structures

In the early days, limited options were available for designing and constructing gridshells due to the limitations of fabrication, e.g. the number of members with different lengths and nodes with different angles had to be minimised [25]. The development of computer aided manufacturing (CAM) removed many of the manufacturing restrictions. Therefore, more design configurations can be constructed for the gridshell structures. As for steel gridshells with low flexibility, nodes are the most challenging parts in both design and construction stages due to their unusual shapes and complicated stress fields. As nodes are responsible for connecting beam members in gridshell and transfer loads between them, a lack of structural performance in nodes would significantly affect the efficiency of the connected beams and heavily influence the stability and load capacity of the whole structure.

On the other hand, to simplify the geometry of a gridshell system, the structure is divided into numerous simple members (beams and plates) which make the structural connections (nodes) topologically and geometrically complicated and bring challenges for conventional manufacturing methods. Besides, to restrict the node imperfections, a high level of accuracy and quality control during the manufacturing process is required. Many studies have been carried out to investigate the sensitivities of global and local stabilities of a hybrid single layer gridshell to a set of nodal imperfections [26-30]. In addition, customised node production increases the construction cost as well as the possibility of human errors [31]. In steel gridshells, low structural flexibility increases demand for higher accuracy in construction, thus special instruments are needed for manufacturing and construction [25].

Additionally, the sharp edges which emerge from intersecting the prismatic beam members would cause stress concentration in nodes. These sharp edges are usually results of a large amount of welds during the conventional manufacturing process and lead to an increase in the risk of fatigue failure under repeated loads [32, 33]. To avoid this problem, cast steel nodes

are used. These nodes have excellent mechanical performance, beautiful appearance, smooth transitions and flexible forms [34].

There are several types of stability failure in gridshells [35-38], including member buckling, local instability, global instability and a combination of these. Although the overall stability of a gridshell is sensitive to the stiffness of nodes [39-43], the complicated stress field makes it almost impossible to develop a standard configuration and design procedure for nodes.

2.1.3.1. Node categories

In 2011, Fan et al. developed a joint classification system based on the stiffness and the moment capacity of the joint as follow [44]:

1. Rigid: high strength and high bending stiffness;
2. Semi-rigid: moderate strength and moderate bending stiffness;
3. Pinned: low strength and/or low bending stiffness.

Two coefficients, α for stiffness and β for moment capacity, were defined for the joint classification as

$$\alpha = \frac{k}{EI/L_0}, \quad \beta = \frac{M_{i,u}}{M_{e,u}}$$

where EI/L_0 represents the stiffness of the members connected to the joints, k is the flexural stiffness of the joint, and $M_{i,u}, M_{e,u}$ are the moment capacity of the joint and the plastic moment capacity of the member connected to the joint respectively. By taking both coefficients α and β into account, the joint can be classified as

1. Rigid: $\alpha \geq 0.5$ and $\beta \geq 5$
2. Semi-rigid: $\alpha \geq 0.5$ and $0.05 < \beta < 5$, or $0.01 < \alpha < 0.5$ and $\beta \geq 0.05$

3. Pinned: $\alpha \leq 0.01$ or $\beta \leq 0.05$

As the applied loads are mainly transferred through in-plane actions, the main design loads are axial loads from the connecting members. Other member forces are dependent on the grid patterns. The designed node should not only be able to transfer the loads from the connected members, but also be stiff enough to provide desirable stability for the whole structure. Other important parameters in the node design for gridshell structures can be listed below:

- The sensitivity of the design configuration to the angle between elements
- The manufacturability of the designed nodes
- The tolerances of the manufactured nodes which are affected by both manufacturing method and design configuration
- The cost of the nodes
- The weight of the nodes
- The appearance of the nodes

2.1.3.2. Conventional nodes

In practice, different node designs represent solutions to different connecting methods for gridshell members. Depending on the connecting methods, the nodes can be categorised as splice connectors (Figure 2-16) and end-face connectors (Figure 2-17) [45].

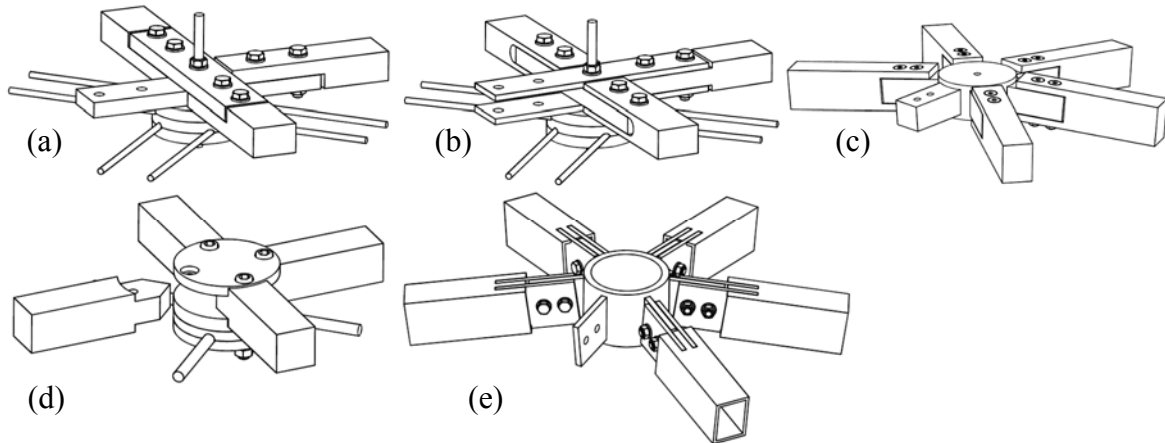


Figure 2-16: Splice connectors of gridshell structures, (a) splice connector SBP-1,(b) splice connector SBP-2,(c) splice connector SBP-3,(d) splice connector HEFI-1,(e) splice connector POLO-1 [45].

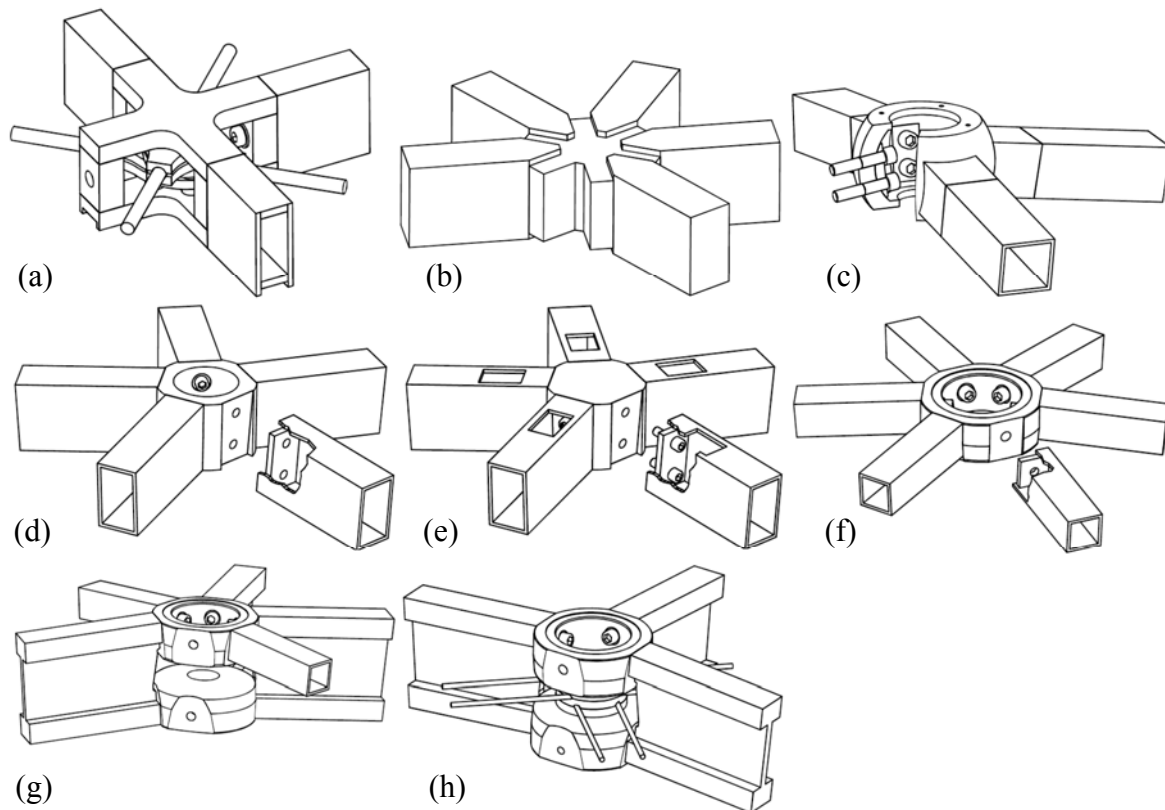


Figure 2-17: End-face connectors of gridshell structures, (a) end-face connector SBP-4,(b) end-face connector WABI-1,(c) end-face connector OCTA-1,(d) end-face connector MERO-1,(e) end-face connector MERO-2,(f) end-face connector MERO-3,(g) end-face connector MERO-4,(h) end-face connector MERO-4 [45].

Figure 2-18 shows examples of end-face nodes of gridshell structures used in projects Palacia de Comunicaciones (Figure 2-18a), Westfield shopping centre (Figure 2-18b) and Frankfurt Hoch Vier (Figure 2-18c).

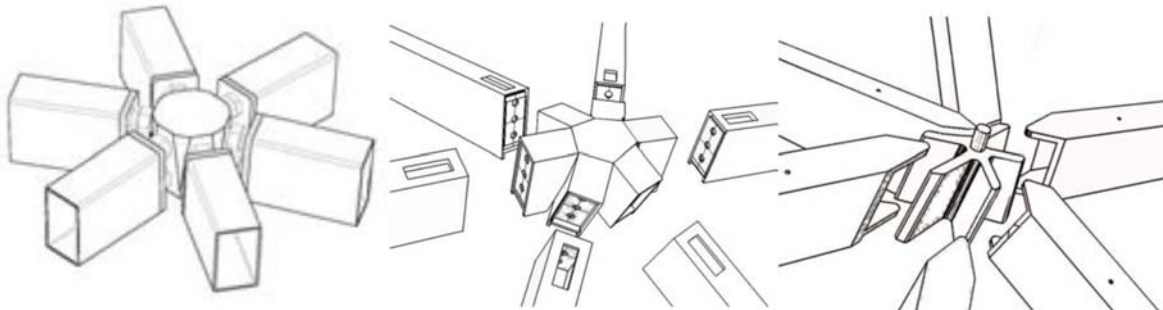


Figure 2-18: End-face nodes used in gridshell structures of real projects, (a) Palacia de Comunicaciones, (b) Westfield shopping centre, and (c) Frankfurt Hoch Vier [46].

2.1.3.3. Unconventional nodes

The aerospace industry has been using the combination of additive manufacturing and structural optimisation for many years. This is due to the fact that the amount of saving in the fuel and consequently the cost of flight is highly dependent on the weight of the flying device. An example of re-design of a structural component based on the topology optimisation and additive manufacturing is shown in Figure 2-19.



Figure 2-19: A small part which is re-designed by topology optimisation and fabricated by additive manufacturing for Airbus A380 airliner [47].

The potential of using the combination of structural optimisation and additive manufacturing in design and construction of nodes for gridshell structures was investigated by Van der Linden in 2015 [46]. He re-designed three nodes of the gridshell structure of Złoty Tarasy in Warsaw, Poland (see Figure 2-20) by using the bi-directional evolutionary structural optimisation (BESO) method, and reduced up to 70% weight of nodes from the original design. The final designs for the nodes are shown in Figure 2-21.



Figure 2-20: Exterior view of the undulating roof Złote Tarasy.

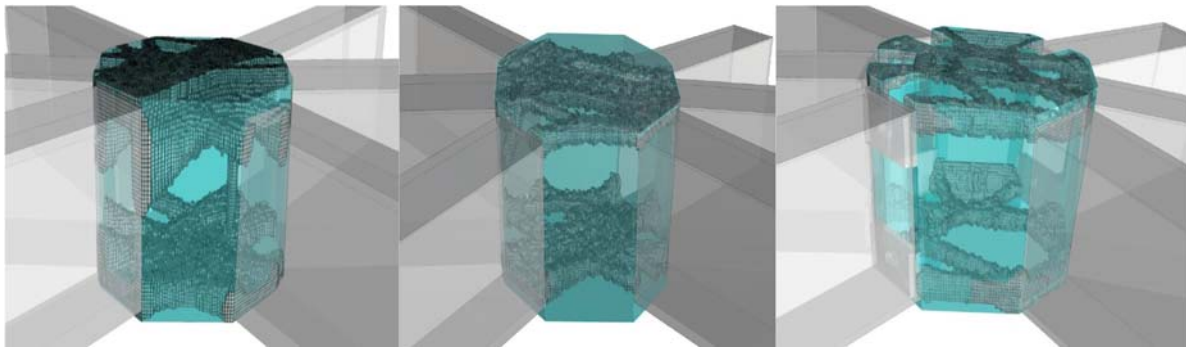


Figure 2-21: Three nodes of Złote Tarasy roof designed using topology optimisation.

In 2015, Galijard et al. [48] optimised the structural connections of a tensegrity structure to explore the topology optimisation method and the opportunity provided by AM technology. The structure consists of 1200 different nodes with attached cables from different angles and positions (Figure 2-22). In the initial design, the mass of the node was reduced from 20kg to 15kg. In their later design, the design process was fine-tuned with a focus on the product integration and the improved control of the optimisation process, leading to a further reduction of the node mass to 5kg (Figure 2-23).



Figure 2-22: Rendering of tensegrity structure in The Hague. This design is not built as such.

Architect: ELV Architecten © Studio i2 [48].

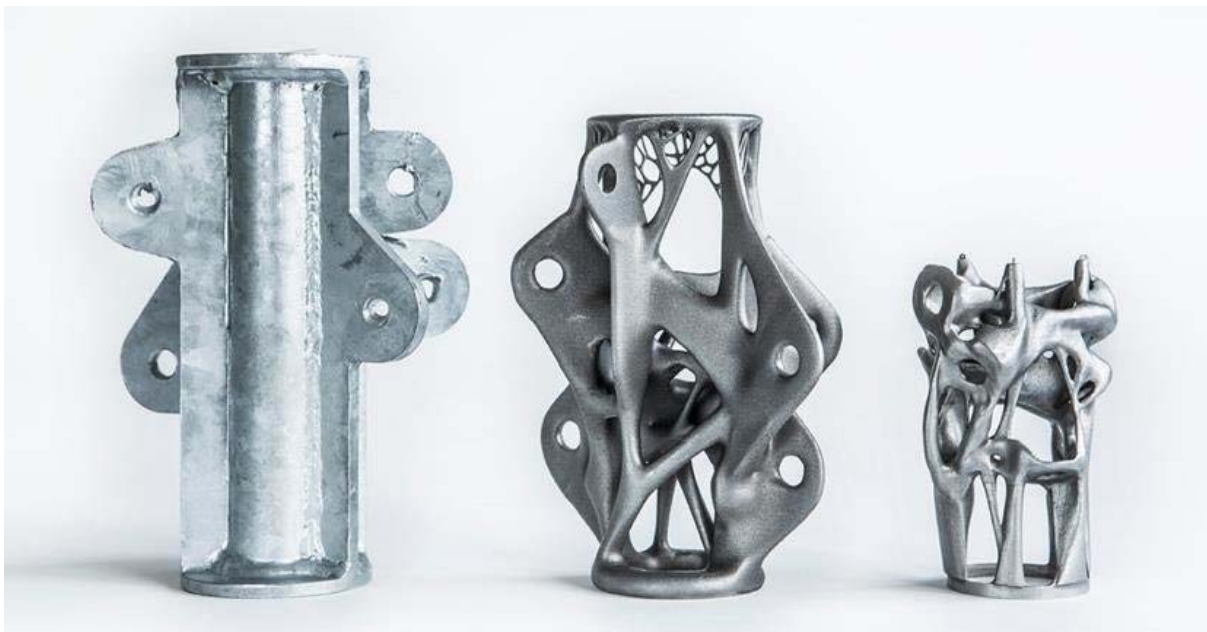


Figure 2-23: Models of the traditional node (left) and the two new nodes, in the middle the first node produced by AM in steel in 2014, at the right the latest optimisation also produced by AM [48].

In 2016, Prayudhi developed a prototype of a gridshell canopy with topology optimised and additively manufactured nodes. The nodes were printed using binder jetting. He carried out a case study by re-designing the structure of an outdoor canopy located at Baku International Airport in Azerbaijan based on the combination of topology optimisation and additive manufacturing [49]. The weight of the new design was reduced by 32%. A structural node designed for this case study is shown in Figure 2-24.



Figure 2-24: Topologically optimised 3D printed node for case study of canopy in Baku International Airport in Azerbaijan [49].

In 2019 Abdelwahab and Tsavdaridis investigated the application of structural optimisation and additive manufacturing in the connections of reticulated structures [50].

2.2. Structural optimisation

The development of mathematical optimisation can be traced back to the introduction of calculus of variations by Bernoulli, Euler and Lagrange between 17th and 18th centuries [51]. In contrast to the classical mathematical optimisation methods, which find solutions using differential equations, the structural optimisation methods often use simplified algebraic equations which are solved by an iterative numerical procedure. Structural optimisation is to find the optimal structural design based on various constraints to achieve the best performance for a structure [52]. It should be noted that modern shape optimisation of continuum is based on variational principles.

Structural optimisation of nodes in gridshell structures is important for a number of reasons. Firstly, structural optimisation could reduce the weight of nodes which is critical to gridshells, especially in large-span roofs. As mentioned before, geometrical and structural complexities of the nodes may lead to heavy and inefficient node designs. Besides, by reducing the nodal weight, the structural performance of the gridshell could be improved which leads to less material cost and less environmental impact.

Topology optimisation

Topology optimisation is a structural optimisation method which treats different element properties (e.g. stiffness, size, existence, etc.) as the variables in the optimisation algorithm to seek for the optimal spatial order and connectivity of bars in discrete structures (i.e. trusses and frames), or the optimal material layout in continuum structures. In a simple maximisation problem, structural topology optimisation techniques often involve the following steps:

1. Selection of the initial design variables (material type, thickness of plate etc.).
2. Evaluation of the objective functions for the current setting of design variables.
3. Comparison between the current properties and the prescribed values.
4. Update the design variables and improve the objective function. Repeat steps 2 to 4 until no further improvement can be achieved.

In order to update the design variables, various strategies can be employed, including the use of the gradient of the objective function. It should be mentioned that the selection of initial topology and the procedure of updating the design variables may result in a solution which is a local optimum, and they may also affect the number of iterations.

The approaches used in topology optimisation for discrete structures (or grid-like structures) and continuum structures are different [53]. Topology optimisation of continuum structures is

the most powerful method among the structural optimisation methods, as it provides much more freedom in the conceptual design to achieve novel and efficient structure [52].

In 1904, Michell introduced the theory of topology optimisation for developing truss-like structures with minimum weight [54]. With the advent of digital computers and the development of linear programming methods in 1950s, the idea of structural optimisation started to gain momentum [55]. In the 1960s, topology optimisation was improved by the introduction of the so-called ground structure (Dorn et al., 1964), in which mathematical programming (MP) algorithms were used [55]. Significant improvement was made in its theory and applications by solving a range of structural optimisation problems, including adding features like section rotation, section type and minimum weight constraint, using finite number of members, and multi-purpose structure subjected to multiple loads or moving loads [56-58]. Other remarkable early works on topology optimisation of discrete structures include the introduction of “optimal layout theory” by Prager (1969) [59] and the maximisation of solid plates stiffness with volumetric constraints by Cheng and Olhoff [60]. The Prager-Shield theory of optimal plastic design [61] and the structural universe [62, 63] were used as the basic concepts in the optimal layout theory. In 1989, Rozvany proposed continuum-based optimality criteria (COC) method for large system optimisation with stress and displacement constraints [64]. Later, Zhou and Rozvany reformulated the COC to a discretised continuum type optimality criteria (DCOC) method using the finite element formulation [65, 66]. The COC/DCOC methods were then extended for solving natural frequency, local buckling and system stability constraints. In 1988 Bendsoe and Kikuchi proposed a methodology for optimal shape design in which a new topology is generated and remeshing of the finite element approximation of the analysis problem is avoided [67]. The development in the field followed another finite element based topology optimisation method called “Evolutionary Structural Optimisation” [68].

Two approaches, namely, macrostructure (geometry) approach and microstructure approach were included in the continuum topology optimisation [54]. The macrostructure approach uses solid isotropic materials (solid elements) while microstructure approach uses porous and microstructural materials (lattice structure unit cells).

Evolutionary structural optimisation

In this study, the bi-directional evolutionary structural optimisation (BESO) technique is employed to create optimal designs for structural nodes. The term evolutionary structural optimisation (ESO) was firstly introduced by Xie and Steven (1993). ESO method seeks the optimal design by systematically removing inefficient materials from the structure [68]. The concept is simple and the residual shape is expected to evolve towards an optimum. In the original version of ESO, the element stress is considered as the element removing criterion, which obtains the optimisation by utilising inner and outer loops. The inner loop firstly defines a threshold element stress as the rejection ratio (RR), and then gradually removes the elements with stress lower than the threshold stress from the structure. Iterations continue until no further elements with the stress lower than the threshold stress remain. In the outer loop, the rejection ratio will be increased with a relatively small step called the evolutionary ratio. Through this loop action, the stress distribution in the structure will become quasi-uniform and a fully-stressed design is expected.

However, the ESO method is not without limitation. As the removed elements are not able to be recovered, the step size has to be very small when removing material. Later, the bi-directional ESO (BESO) was developed [69, 70] in order to allow elements to be added back to the structure after removal. The concept of this method is to remove inefficient material (elements) from the structure and simultaneously add material to the most needed locations of the structure. Although the improvement of BESO over ESO is significant, it was claimed by Zhou and Rozvany that both ESO and BESO were not able to guarantee an optimal design,

and the rejection criterion in ESO might result in very high element rejections [71]. Rozvany claimed that the earlier versions of ESO/BESO were not able to achieve final optimum design, because the estimation of the sensitivity number for void element is highly inaccurate [72, 73].

In order to better represent the element status, Zhu et al. proposed a method in 2007, in which void elements are replaced by a microstructure with low density. In this method, where elements need to be removed, they are replaced by soft material instead [74]. This method is still unlikely to ensure a final optimum, as the evolution procedure is not able to converge sometimes. In 2007, a new version of BESO was proposed by Huang and Xie [75], which could achieve stable and convergent solutions. Later, they proposed a more advanced BESO with the solid isotropic material with penalisation model (SIMP) [76], in which the effective properties of microstructure of element were determined according to the power-law material scheme [66, 77]. In this method, the optimisation for stiffness was carried out by replacing inefficient elements with soft material (soft-kill method). When the material penalty exponent (p) was set to a large value, the results were equivalent to the hard-kill method in which the void elements were removed from the structure completely [75].

2.3. Manufacturing

The widespread use of cast iron as a building material began in the second half of the 18th century. It was mainly used for the structural elements under compression due to its brittle behaviour. The world's first cast iron bridge was built in Coalbrookdale, England (1777–1779). Due to the high compressive strength of iron, it required less material compared to stone arch bridges of a similar scale. Also, a large number of supports and load carrying building façades in New York City were made of cast iron in the 19th century.

However, with the development of steel production technologies, the use of standard rolled steel members became more popular than cast structural elements, due to economic and technical constraints [78].

The conventional manufacturing processes are adapted to the concept of ‘design for production’, which include mechanical cutting operations, material removal techniques – chipping off, forging, casting, stamping, engraving, turning, milling, drilling, grinding, etc. This concept is deeply influenced by the predetermined sizes of the standard parts. In the case of spatial structures, such as space truss and gridshells, the nodes are the conjunctions of a number of members, and their forces are from different directions. The complexity of node geometry is a serious challenge for conventional manufacturing methods. The development of steel production technologies, e.g. welding and rolling techniques, has reduced the use of casting methods in the construction of steel structures. However, in the last few years, the flexibility of new, low-alloy and low-carbon materials for casting has caused a renewed interest in casting in structural engineering. These new materials may meet all functional requirements, such as strength, viscosity, weldability and corrosion resistance [78], and the issues related to fatigue failure are eliminated in this method [32]. However, the node shape could be too complicated to be fed into the mould.

2.3.1. Formative manufacturing (casting)

With the increased research in the field of metallurgy and mould technology, steel casting has been successfully used for oil platforms over the past two decades. Cast steel components have been used in the construction of steel structures since the advent of steel hollow profiles. An overview of the applications of cast steel in roof structures, and pedestrian and traffic bridges is available in [79-81]. The main advantages of using cast steel include the beautiful and free-flowing forms, as well as the capacity of making complicated nodes with numerous

members connecting from different directions. Cast steel allows adjusting the node shape and wall thickness to the flow of forces from the connecting members. Another advantage of using casting method is that the stress concentrations and notch effects could be limited as sharp edges can be avoided in the cross-sections of casted nodes [78].

In the 1980s, advances in casting technology have led to a steady improvement in the weldability [82-84], the material properties [85] and the toughness [86, 87] of cast steel. Cast steel was mainly utilised in offshore structures, high-rise structures and bridges. Previously, welded nodes were considered to be the weak point in the design of offshore structures due to their low fatigue strength and poor welding, and the existence of secondary bending moments [88]. These issues could be solved by using cast nodes. However, typical casting defects may also exist, such as voids, gas bubbles, sand, slag and foam points, hot and cold cracks, segregations and non-metallic inclusions[89].

To manufacture nodes through casting steel, a wooden model is split into two halves with each half pressed into a box filled with sand and resin. The two boxes with negative impressions of node halves are then joined together to form the entire cavity of the node shape, which is used as a mould for casting steel. The cast steel nodes have smooth and flexible shapes, and the connection welds are located outside the nodes for better performance and easier inspection.

2.3.2. Subtractive Manufacturing (computer numerical control machines)

Subtractive manufacturing is a process by which the final shape of a 3D object is obtained by successively and selectively cutting material away from a solid block. Normally, subtractive manufacturing can be done by using a CNC Machine. However, as cylindrical cutters are used for CNC milling, it is difficult to cut the entire internal square corners which are

prevalent in the plastic injection moulding designs. Besides, CNC arm should have access to the parts to be machined, which makes a wide range of 3D designs impossible.

As for designs that can be manufactured using subtracting manufacturing process, this method is comparatively faster and cheaper with a high level of precision. Also, it is available for a wide range of materials, and allows superior surface finishing. One of the major disadvantages is the waste of material. However, some of the material could be recovered and eventually recycled to reduce the overall waste.

2.3.3. Additive manufacturing (AM):

2.3.3.1. History of additive manufacturing

AM is a newly developed manufacturing method, in which objects are manufactured by joining material usually layer-by-layer based on a 3D model data. This method is the opposite of the subtractive manufacturing methodologies, such as traditional machining [90].

The first additive manufacturing process emerged in 1987 based on stereolithography (SL). Stereolithography is a process that solidifies thin layers of ultraviolet (UV) light-sensitive liquid polymer using a laser. Then, different versions of stereolithography were commercialised in Japan in 1988 and 1989 and in Germany in 1990. Later, three non-SL technologies were developed in 1991, including fused deposition modeling (FDM), solid ground curing (SGC) and laminated object manufacturing (LOM). In 1993, QuickCast was introduced to produce investment-casting (lost wax casting) patterns, so that they could be burnt out without fracturing the ceramic shell. In 1994, many new materials and material deposition techniques were introduced for the additive-manufacturing, such as wax material with an inkjet print head, paper lamination material with a knife to produce wood-like models, laser-sintering technology, and so on. With the development of additive-manufacturing materials and technologies, the low cost 3D printers appeared in 1996.

AeroMet (MTS Systems Corp.) introduced laser additive-manufacturing (LAM) in 1997, which worked with a high-power laser and powdered titanium alloys. In 2000, a 3D colour printer was manufactured, which was based on the powder and binder technologies developed by Aad van der Geest of the Netherlands. In 2000, new generations of additive-manufacturing started. The speed of additive-manufacturing process was improved due to the increase in the number of nozzles, improvement in the precision of additive-manufacturing process, development of first metal printer and commercialisation of first 3D multi-colour printer [91]. In 2002, Arcam commercialised powder bed fusion (PBF) technology by using electron beam as energy source instead of laser beam, and launched the first production model namely electron beam melting (EBM) [92]. In the new generations, this technology has been adopted in wider applications, such as aircraft interiors (ULTEM 9085 for its FDM 900mc and 400mc machines from Stratasys, 2008), artistic designs (Shapeways, 2008), dentistry (3D dental printers and its new DentaCast material from Solidscape, 2009), aerospace (DuraForm FR 100 from 3D Systems, 2009), research and development (Dimatix system targeted at the printed electronics market from Fujifilm Dimatix, 2009) and Military (Optomec, 2010). By 2011, several industries had already adopted AM as their main manufacturing method. In 2011, the applications of AM in medical industry experienced a growth [91]. Although a few notable examples of AM metal parts have been made and applied in military aircraft, the first AM part for commercial use was a flow-path sensor housing for a GE-90 commercial engine used in Boeing 777 in 2015 [93].

3D printing with various materials is nowadays available to the public at an acceptable cost. It has created a new market for 3D printed products, including sculptures, jewellery, figurines, and a wide range of other consumer oriented products.

2.3.3.2. Benefits of Additive Manufacturing

Different from traditional manufacturing processes which involve cutting, milling and grinding, AM build parts directly from computer models or from measurements of existing components. Benefits of AM compared to the traditional methods include the potential to vastly accelerate innovation, reduction of supply chains [94], minimisation of material and energy usages, reductions of waste [91], cycle times and unit cost [95], repair of high-value components [96], and manufacture of highly efficient structures [97]. All these advantages make it possible to step away from the concept of ‘design for production’. Therefore, structural designs could start from the performance of the desired product. This can create new opportunities in the building industry, such as production of highly complex objects with free shapes, optimisation and integration of functional features, reduction of processing steps, high degree of design freedom and high degree of product customisation [98].

2.3.3.3. Computer Aided Design (CAD) model

The first step of manufacturing an object through additive manufacturing is to prepare the geometry of the object in a suitable format. Then AM makes the geometry layer-by-layer based on a Computer Aided Design (CAD) representation of the target geometry. The most commonly used file format for 3D printing is Stereolithography (STL) format [98] which contains a single color. VRML is another format which stands for “Virtual Reality Modeling Language”. It is a newer 3D digital file type that includes colour [98]. In addition, enhanced data representations are under development, such as the Additive Manufacturing Format (AMF) [99]. The AM data is converted into a set of two-dimensional scanning paths [100] that are sequentially processed by the AM process.

2.3.3.4. Constraints

Despite having many advantages, additive manufacturing of steel nodes still has constraints, including costly process and machine maintenance, limited dimensions, need of additional support structure, and long production time. Moreover, metallic powders used for 3D printing are quite expensive, and with limited choices. The AM produced metal is also found to be brittle. In some specific AM methods, the design is restricted by the de-powdering process in which slender members break on the shaking table [98]. Therefore, additional temporary support members are needed in the design.

2.3.3.5. Metal systems

One of the most important recent developments in AM has been the proliferation of direct metal processes, which is used for the direct production of metal parts. In most direct metal systems, a point-wise method with metal powders as input is used. There are three different types of direct metal processes, which are powder bed process, powder feed process and wire feed process. In powder bed process, the powder spreading approach is similar to the selective laser sintering (SLS) process, and an energy beam which is normally a high-power laser or an electron beam is used for melting the metal powder (selective laser melting). Most powder bed processes take place in a building space filled with an inert gas to form a protective atmosphere. Therefore, reactive metal powders, such as aluminium and titanium, can be applied. The selective laser melting (SLM) process is schematically shown in Figure 2-25.

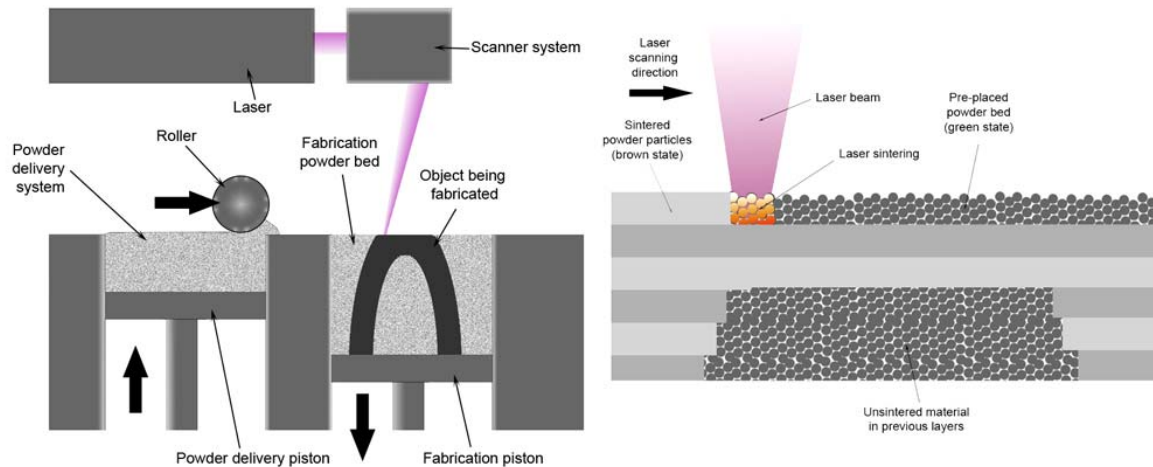


Figure 2-25: Schematic of selective laser melting system [101].

In powder feed process, powder is delivered through a nozzle placed above the part. Laser beam is converged on the layer where the powder is going to be melted and joined to the AM deposit. This approach allows the material to be added to an existing part. Therefore, it can be used for the repair of expensive metal components, like chipped turbine blades and injection mould tool inserts. The schematic of powder feed process is shown in Figure 2-26a. The powder feed systems are capable of manufacturing larger object compared to the powder bed units. Two types of systems are dominant in the market: 1. work piece remains stationary, and deposition head moves; and 2. deposition head remains stationary, and the work piece is moved [98].

The schematic of a wire feed unit is shown in Figure 2-26b. The feed stock is wire, and the energy source for these units include electron beam, laser beam and plasma arc. Initially, a single line of material is deposited and then subsequent lines of material are placed on it to develop a three dimensional structure. In general, wire feed systems are well suited for high deposition rate processing and have large build volumes, however, the fabricated product usually requires more extensive machining than the powder bed or powder fed systems do [98].

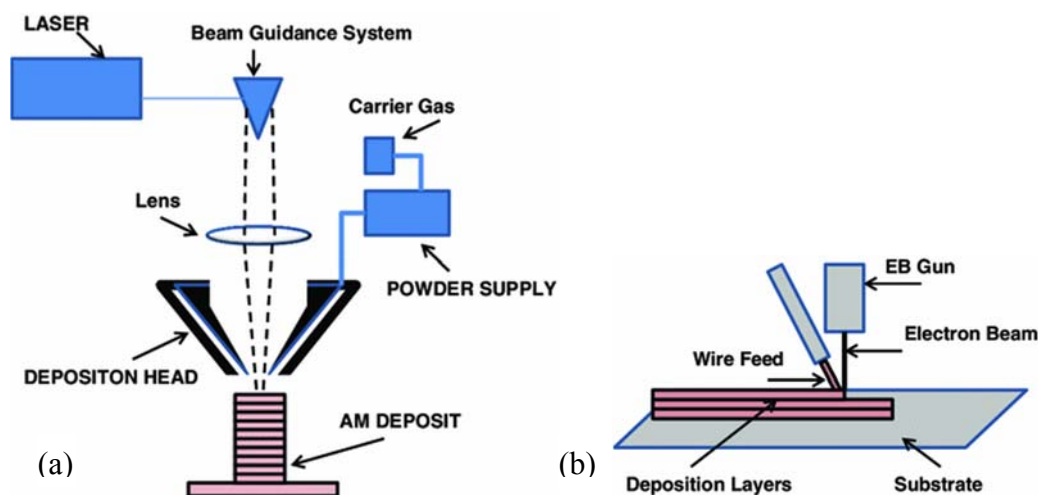


Figure 2-26: Schematics of a) metal powder feed system and b) metal wire feed system [102].

2.3.3.6. Materials

Generally, any metal that can be welded is considered to be a good candidate for powder bed fusion (PBF) processing. To use a PBF process for the creation of complex metal components, four common approaches can be used: full melting, liquid phase sintering (LPS), indirect processing and pattern methods. In the full melting and LPS (with metal powders) approaches, a metal part is typically usable when it comes out of the machine. In the indirect processing approach, a polymer coated metallic powder or a mixture of metallic and polymer powders is used for part construction. In pattern methods, the metal part is created using the mould obtained from either investment casting patterns or sand-casting moulds. In the case of investment casting, polystyrene or wax-based powders are used in the machine, and subsequently invested in ceramic during post-processing. Finally, they are melted out during casting. In the case of sand-casting moulds, mixtures of sand and a thermosetting binder are directly processed in the machine to form a sand-casting core, cavity or insert. These moulds are then assembled and molten metal is cast into the mould, forming a metal part [98].

2.4. Knowledge gap in designing and manufacturing nodes for gridshell structures

The structural behaviour of gridshell structures is influenced by their double curvature and grid system. In most cases, the dominant internal force of a beam member is axial force. The structural nodes which are the most complex members in gridshell structures due to their complex geometries and internal forces are in the focus of the researchers to be designed and manufactured more efficiently.

In this chapter, a literature review is carried out on studies which designed and produced complex geometries for structural nodes in tensegrity structures [48] and gridshell structures [46, 49] using a combination of structural optimisation and additive manufacturing methods. However, in the previous studies, the effects of a number of influencing factors, such as the loading type and the initial node size, on the final node design have not been investigated. Besides, the structural performance of the new nodes is not compared with the conventional node. Furthermore, in the previous studies, there is no experimental validation for the design results. All these issues will be addressed in this thesis for the new node design.

References

1. Adriaenssens, S., Block, P., Veenendaal, D., Williams, C. (2014). *Shell structures for architecture: form finding and optimization*. Routledge.
2. Dimcic, M. (2011). *Structural optimization of grid shells based on genetic algorithms*. PhD thesis, University of Stuttgart.
3. Chilton, J. and Isler, H. (2000). *Heinz isler*: Thomas Telford.
4. Melissa. (2000) Beehive Tomb, Available from: <http://art103fall2009.pbworks.com/w/page/10992785/Mycenaean%20Art>.
5. Huth, D. (2006). Beehive hut, Dingle Peninsula, Co. Kerry, Southern Ireland (Eire), D.b. hut.JPG, Editor.
6. Watson, I. (2013). The Seventy Wonders of the Ancient World: The Great Monuments and How They Were Built. *Reference Reviews*.
7. Janberg, N. (2007). Ctesiphon Palace, Available from: <https://www.britannica.com/place/Taq-Kisra>.
8. Crystal, E. (2009). The Roman Pantheon, <https://www.teggelaar.com/en/rome-day-5-continuation-2>.

9. Croci, G. (2006). Seismic behavior of masonry domes and vaults of Hagia Sophia in Istanbul and St. Francis in Assisi. In: *Proceeding of European Conference on Earthquake Engineering and Seismology*, Geneva, Switzerland, 3-8 September 2006, 3-8
10. Strelau, D. (2011). Hagia Sophia I, I.o.H. Sophia.jpg, Editor.
11. Knippers, J. (2000). Ingenieurportrat Johann Wilhelm Schwedler (1823-94). *DEUTSCHE BAUZEITUNG*. **134**(4): 105-112.
12. Beckh, M. and Barthel, R. (2009). The first doubly curved gridshell structure-shukhovs buildins for the plate rolling workshop in vyksa. In: *Proceedings of the Third International Congress on Construction History*, Cottbus, May 2009, 159-166.
13. lunamtra (2008). Steel-cupola built by F.W. Schwedler in Berlin in 1874. On top of a gas-reservoir (Fichtebunker).
14. Janberg, N. (1897). Vyksa Steel Production Hall.
15. PACO (2007) Sketch of the missing "Recoletos Fronton" of Madrid, F. Recoletos.png, Editor.
16. Rosa, F. (2016). Palazzetto dello sport a Roma.
17. Liddell, I. (2015). Frei Otto and the development of gridshells. *Case Studies in Structural Engineering*. **4**: 39-49.
18. Bobbarton (2012). Mainheim Multihalle. Arup and Frie Otto. The first and still the biggest gridshell in timber.
19. Paoli, C.C.A. (2007). *Past and future of grid shell structures*. 2007, PhD thesis, Massachusetts Institute of Technology.
20. Diliff (2013). View of the Great Court from the second floor of the southern wing, L. British Museum Great Court, UK - Diliff.jpg, Editor.
21. Evanson, T. (2013). Kogod Courtyard - northeast corner and floor - Smithsonian American Art Museum.
22. Toussaint, M.H. (2007). *A design tool for timber gridshells: The development of a grid generation tool*. MSc thesis, Delft University of Technology.
23. Calladine, C.R. (1989). *Theory of shell structures*. Cambridge University Press.
24. D'Amico, B. (2015). *Timber grid-shell structures: form-finding, analysis and optimisation*. PhD thesis, Edinburgh Napier University.
25. Knippers, J. and Helbig, T. (2009). Recent developments in the design of glazed grid shells. *International Journal of Space Structures*. **24**(2): 111-126.
26. Bruno, L., Sassone, M. and Venuti, F. (2016). Effects of the Equivalent Geometric Nodal Imperfections on the stability of single layer grid shells. *Engineering Structures*. **112**: 184-199.
27. Borri, C. and Spinelli, P. (1988). Buckling and post-buckling behaviour of single layer reticulated shells affected by random imperfections. *Computers & Structures*. **30**(4): 937-943.
28. Kato, S., Mutoh, I. and Shomura, M. (1998). Collapse of semi-rigidly jointed reticulated domes with initial geometric imperfections. *Journal of Constructional Steel Research*. **48**(2-3): 145-168.
29. Mak, C.K. and Der-Wang, K. (1973). Finite element analysis of buckling and post-buckling behaviors of arches with geometric imperfections. *Computers & Structures*. **3**(1): 149-161.
30. Yamada, S., Takeuchi, A., Tada, Y., & Tsutsumi, K. (2001). Imperfection-sensitive overall buckling of single-layer lattice domes. *Journal of Engineering Mechanics*. **127**(4), 382-386.

31. Galjaard, S., Hofman, S. and Ren, S. (2015). New opportunities to optimize structural designs in metal by using additive manufacturing, *Advances in Architectural Geometry 2014*. 79-93.
32. Haldimann-Sturm, S.C. and Nussbaumer, A. (2008). Fatigue design of cast steel nodes in tubular bridge structures. *International Journal of fatigue*. **30**(3): 528-537.
33. Haldimann-Sturm, S., Nussbaumer, A. and Hirt, M. (2005). Tubular bridges and the fatigue design of their joints. In: *proceedings of the 6th Japanese-German-Bridge-Symposium*, 67-68.
34. Wang, L., Jin, H., Dong, H. and Li, J. (2013). Balance fatigue design of cast steel nodes in tubular steel structures. *The Scientific World Journal*.
35. Gioncu, V. and Balut, N. (1992). Instability behaviour of single layer reticulated shells. *International journal of space structures*. **7**(4): 243-252.
36. Bulenda, T. and Knippers, J. (2001). Stability of grid shells. *Computers & Structures*. **79**(12): 1161-1174.
37. Knippers, J. and Sailer, S. (1995). Untersuchungen zum Tragverhalten von Netzkuppeln. *Finite elemente in der baupraxis*. Berlin: Ernst and Sohn. 201-12.
38. Knippers, J., Bulenda, T. and Stein, M. (1997). Zum Entwurf und zur Berechnung von Stabschalen. *Stahlbau*. **66**(1): 31-37.
39. Forman, S.E. and Hutchinson, J.W. (1970). Buckling of reticulated shell structures. *International Journal of Solids and Structures*. **6**(7): 909-932.
40. Tonelli, D., Pietroni, N., Puppo, E., Froli, M., Cignoni, P., Amendola, G. and Scopigno, R. (2016). Stability of statics aware voronoi grid-shells. *Engineering Structures*. **116**: 70-82.
41. López, A., Puente, I. and Serna, M.A. Numerical model and experimental tests on single-layer latticed domes with semi-rigid joints. *Computers & structures*. **85**(7): p. 360-374.
42. Lopez, A., Puente, I. and Aizpurua, H. (2011). Experimental and analytical studies on the rotational stiffness of joints for single-layer structures. *Engineering structures*. **33**(3):731-737.
43. Han, Q., Liu, Y. and Xu, Y. (2016). Stiffness characteristics of joints and influence on the stability of single-layer latticed domes. *Thin-Walled Structures*. **107**: 514-525.
44. Fan, F., Ma, H., Cao, Z. and Shen, S. (2011). A new classification system for the joints used in lattice shells. *Thin-walled structures*. **49** (12): 1544-1553.
45. Stephan, S., Sánchez-Alvarez, J. and Knebel K. (2004). Reticulated structures on free-form surfaces. *Stahlbau* **73**(8): 562-572.
46. Van der Linden, L.P.L. (2015). *Innovative joints for gridshells*. Master thesis, TUDelf.
47. Nathan, S. Printing Parts. 2011; Available from: <https://www.technologyreview.com/s/425133/printing-parts/>.
48. Galjaard, S., Hofman, S. and Ren, S. *New Opportunities to Optimize Structural Designs in Metal by Using Additive Manufacturing*. 79-93.
49. Prayudhi, B. (2016). *3F3D: Form Follows Force with 3D printing*. Master thesis, TUDelf.
50. Abdelwahab, M.M. and Tsavdaridis (2019). K.D. *Optimised 3D-Printed Metallic Node-Connections for Reticulated Structures*.
51. Kamat, M. (1993). Optimization, Structural: Status and Promise. *American Institute of Aeronautics and Astronautics, Inc*. **1**.
52. Huang, X. and Xie, M. (2010). *Evolutionary topology optimization of continuum structures: methods and applications*. John Wiley & Sons.

53. Rozvany, G.I.N. (2001). Aims, scope, methods, history and unified terminology of computer-aided topology optimization in structural mechanics. *Structural and Multidisciplinary Optimization*. **21**(2): 90-108.
54. Eschenauer, H.A. and Olhoff, N. (2001). Topology optimization of continuum structures: a review. *Applied Mechanics Reviews*. **54**(4): 331-390.
55. Dantzig, G.B. (1963). *Linear Programming and Extensions*. Princeton landmarks in mathematics and physics. Princeton University Press Princeton.
56. Prager, W. (1969). *Optimality criteria derived from classical extremum principles*. SM Studies Series, Solid Mechanics Division, Univ of Waterloo, Ontario/CANADA.
57. Prager, W. (1974). A note on discretized Michell structures. *Computer Methods in Applied Mechanics and Engineering*. **3**(3): 349-355.
58. Save, M.A. (1975). A general criterion for optimal structural design. *Journal of Optimization Theory and Applications*. **15**(1): 119-129.
59. Prager, W. and Rozvany, G.I.N. (1977). Optimization of structural geometry. *Dynamical systems*. 265-293.
60. Cheng, K.-T. and Olhoff, N. (1981). An investigation concerning optimal design of solid elastic plates. *International Journal of Solids and Structures*. **17**(3): 305-323.
61. Prager, W. and Shield, R.T. (1967). A general theory of optimal plastic design. *Journal of Applied Mechanics*. **34**(1): 184-186.
62. Rozvany, G.I.N. (1981). Optimality criteria for grids, shells and arches. *Optimization of distributed parameter structures*. **1**: 112-151.
63. Rozvany, G.I.N. (1984). *STRUCTURAL LAYOUT THEORY-THE PRESENT STATE OF KNOWLEDGE*, in Unknown Host Publication Title. John Wiley & Sons (Wiley Series in Numerical Methods in Engineering).
64. Rozvany, G.I.N. (1989). *Structural Design via Optimality Criteria: The Prager Approach to Structural Optimization*. Kluwer Academic, Dordrecht.
65. Rozvany, G.I.N. and Zhou, M. (1991). Applications of the COC algorithm in layout optimization. *Engineering optimization in design processes*, Springer. 59-70.
66. Rozvany, G.I.N., Zhou, M. and Birker, T. (1992). Generalized shape optimization without homogenization. *Structural and Multidisciplinary Optimization*. **4**(3): 250-252.
67. Bendsoe, M.P. and Kikuchi, N. (1988). Generating optimal topologies in structural design using a homogenization method. *Computer Methods in Applied Mechanics and Engineering*. **71**(2): 197-224.
68. Xie, Y.M. and Steven, G.P. (1993). A simple evolutionary procedure for structural optimization. *Computers & structures*. **49**(5): 885-896.
69. Querin, O.M., Steven, G.P. and Xie, Y.M. (1998). Evolutionary structural optimisation (ESO) using a bidirectional algorithm. *Engineering computations*. **15**(8): 1031-1048.
70. Yang, X. Y., Xei, Y. M., Steven, G. P., & Querin, O. M. (1999). Bidirectional evolutionary method for stiffness optimization. *AIAA journal*. **37**(11).
71. Zhou, M. and Rozvany, G.I.N. (2001). On the validity of ESO type methods in topology optimization. *Structural and Multidisciplinary Optimization*. **21**(1): 80-83.
72. Rozvany, G.I.N. (2001). Stress ratio and compliance based methods in topology optimization—a critical review. *Structural and Multidisciplinary Optimization*. **21**(2): 109-119.
73. Rozvany, G.I.N. (2009), A critical review of established methods of structural topology optimization. *Structural and multidisciplinary optimization*. **37**(3): 217-237.

74. Zhu, J.H., Zhang, W.H. and Qiu, K.P. (2007). Bi-directional evolutionary topology optimization using element replaceable method. *Computational Mechanics*. **40**(1): 97-109.
75. Huang, X. and Xie, Y.M. (2007). Convergent and mesh-independent solutions for the bi-directional evolutionary structural optimization method. *Finite Elements in Analysis and Design*. **43**(14): 1039-1049.
76. Huang, X. and Xie, Y.M. (2009). Bi-directional evolutionary topology optimization of continuum structures with one or multiple materials. *Computational Mechanics*. **43**(3): 393-401.
77. Bendsøe, M.P. (1989). Optimal shape design as a material distribution problem. *Structural and multidisciplinary optimization*. **1**(4): 193-202.
78. Schober, H. (2003). Steel castings in architecture and engineering. *Modern Steel Construction*. **43**(4): 65-72.
79. Schlaich, J. and Schober, H. (1999) Rohrknotten aus Stahlguss. *Stahlbau*. **68**(8): 652-665.
80. Schlaich, J. and Schober, H. (1999). Rohrknotten aus Stahlguß (Fortsetzung aus Heft 8/99). *Stahlbau*. **68**(9): 734-752.
81. Schober, H. (2000). Rohrknotten aus Stahlguss. *PRUEFINGENIEUR*, (17).
82. Haneke, M. and Gantke, F. (2017). Research into material for cast steel nodes.
83. Ellis, N., Salama, M.M. and Beggs, D.V. (1984). Evaluation of structural steel castings for the Hutton Tension Leg Platform. *Journal of energy resources technology*. **106**(2): 234-239.
84. Koivula, J., Katila, R., Liimatainen, J. and Martikainen, H. (1989). Weldability of a high-purity offshore cast steel. *IRONMAKING & STEELMAKING*. **16**(1): 41-48.
85. Wood, A. M., Gantke, F., Webster, S., & Haneke, M. (1982). Recent advances in the technology of cast steel nodes for use in offshore structures. *Offshore Technology Conference*.
86. Ohba, H., Susei, S., Sakai, Y., Atsuta, T., Ohkuma, Y., Ohminami, R., & Tamura, A. (1979, January). The Development of Casting Leg Nodes for a Jack-Up Rig. In *Offshore Technology Conference*.
87. Richardson, R.C. (1996). *Higher strength cast steel for offshore structures*.
88. Haldimann-Sturm, S.C. (2005). *Ermüdungsverhalten von stahlgussknotten in Brücken aus Stahlhohlprofilen*. Thesis, ÉCOLE POLYTECHNIQUE FÉDÉRALE DE LAUSANNE.
89. Beeley, P. (2001). *Foundry technology*. Butterworth-Heinemann.
90. ASTM-F2792-12a, F2792-12a, 2012, "Standard Terminology for Additive Manufacturing Technologies" ASTM International. West Conshohocken, PA, 2012, DOI: 10.1520/F2792-12A. Laser Enclosure Cooling Head Deposition Head Delivery Powder Ar Carrier Gas Cr, 2012. **2**.
91. Wohlers, T. and Gornet, T. (2014). History of additive manufacturing. Wohlers Report: *Additive Manufacturing and 3D Printing State of the Industry Annual Worldwide Progress Report*.
92. Bhavar, V., Kattire, P., Patil, V., Khot, S., Gujar, K., & Singh, R. (2014). A review on powder bed fusion technology of metal additive manufacturing. In *Proceedings of the 4th International Conference and Exhibition on Additive Manufacturing Technologies-AM-2014*, Bangalore, India, 1-2.
93. Cowles, B.A. (2016). *Summary Report: Joint Federal Aviation Administration–Air Force Workshop on Qualification/Certification of Additively Manufactured Parts*.
94. Véronneau, S., Torrington, G. and Hlávka, J.P. (2017). 3D Printing.

95. Ruffo, M., Tuck, C. and Hague, R. (2006). Cost estimation for rapid manufacturing-laser sintering production for low to medium volumes. In *proceedings of the Institution of Mechanical Engineers, Part B: Journal of Engineering Manufacture*. **220**(9): 1417-1427.
96. Shepeleva, L., Medres, B., Kaplan, W. D., Bamberger, M., & Weisheit, A. (2000). Laser cladding of turbine blades. *Surface and Coatings Technology*. **125**(1): 45-48.
97. Brandt, M., Sun, S. J., Leary, M., Feih, S., Elambasseril, J., & Liu, Q. C. (2013). High-value SLM aerospace components: from design to manufacture. *Advanced Materials Research*. Trans Tech Publ. **663**: 135-147.
98. Gibson, I., Rosen, D.W. and Stucker, B. (2010). *Additive manufacturing technologies*. Vol. 238: Springer.
99. ISO/ASTM, *F2915-13 Standard Specification for Additive Manufacturing File Format (AMF) Version 1.1*, ASTM International. 2014.
100. Zhai, Y., Lados, D.A. and LaGoy, J.L. (2014). Additive manufacturing: making imagination the major limitation. *Jom*. **66**(5): 808-816.
101. Materialgeeza. *Selective laser melting system schematic.jpg*. 2008; [SLS system schematic]. Available from: https://en.wikipedia.org/wiki/File:Selective_laser_melting_system_schematic.jpg.
102. Frazier, W.E. (2014). Metal additive manufacturing: a review. *Journal of Materials Engineering and Performance*. **23**(6): 1917-1928

CHAPTER 3

TOPOLOGY OPTIMISATION AND ADVANCED MANUFACTURING OF
STRUCTURAL NODES

Chapter 3: Topology optimisation and advanced manufacturing of structural nodes

For many years, engineers and architects have been working collaboratively to simplify and rationalise complex freeform structures into practical and cost-acceptable modules. With ingenuity and innovation through geometrical rationalisation, various forms can be found using just a handful of intersecting geometries, such as torus, sphere and cone, and assembled through simple manufacturing processes and standard connections, which can be applied in large engineering constructions [1]. For long span roofs (e.g. sports stadium roofs), about 15-40% of the self-weight is from their connections. The ability to optimise these connections based on the exact loading conditions could significantly reduce the overall weight of a structure, leading to saving in the material cost and reduced requirements for foundations.

When there are a large number of complex structural connections, it is usually required to simplify the node configurations for manufacturing through traditionally manufacturing methods. However, using additive manufacturing (AM) makes it possible to manufacture complex connections. Furthermore, with the use of innovative algorithms, we can optimise parts for specific load cases and criteria. In this study, the Bi-directional Evolutionary Structural Optimisation (BESO) technique [1, 2] is used to minimise the weight and the printing time required for each node. In the BESO method, a structure is optimised by iteratively removing inefficient elements and adding elements where needed [3,4]. In each iteration, all elements are sorted based on their share in the global stiffness of the structure (called sensitivity number). Then a specific percentage of the elements with smallest sensitivity number are turned off and a specific percentage of previously deleted elements with higher sensitivity numbers are added to the model. Then the stiffness matrix of the structure is reconstructed and analysed again. This iterative process results in an efficient topology for the structure. In this study, the BESO code is linked to ABAQUS which is used as a structural analysis engine for optimising the node stiffness.

Although AM is very expensive compared to the conventional manufacturing methods in the construction industry, the ability to fabricate complicated geometries with high accuracy is the advantage of this new manufacturing method over the conventional ones. The price of an additively manufactured member is proportional to the weight. Thus, a reasonable strategy to make AM feasible in construction of structures is to change the conventional trade-off between the weight of a member and its complexity and manufacturability. The structural connections of free-form gridshells which are the smallest and most complicated members of these structures are investigated in this study. In this chapter, the effect of general load cases on the optimised topology of structural node is studied. Besides, the effect of the size of the design domain on the topology and volume of the optimisation result is investigated.

The process of adding and removing elements in BESO is applied to a predefined domain, called the design domain. The parts outside the design domain remain unchanged during the BESO process, which are called non-design domain. In the structural model, the central part of the node is considered as the design domain and the other parts form the non-design domain.

3.1. Introduction

In the node optimisation process, the objective is to achieve the stiffest node with the least amount of material, because the stiffness of a node has a significant effect on the structural performance of the whole structure. One of the aims for topology optimization is searching for the stiffest structure with a given volume of material. In BESO method, elements are treated as design variables. A structure is optimised by removing and adding elements. Thus, the optimisation problem with volume constraint is stated as:

$$\text{Minimize } C = \frac{1}{2} f^T u \quad (1a)$$

$$\text{Subject to: } V^* - \sum_{i=1}^N V_i x_i = 0 \quad (1b)$$

$$x_i = 0 \text{ or } 1 \quad (1c)$$

where f and u are the applied load and displacement vectors, and C is known as the mean compliance. V_i is the volume of an individual element, and V^* the prescribed total structural volume. N is the total number of elements in the system. The binary design variable x_i declares the absence (0) or presence (1) of an element [3]. A flowchart of the BESO method is given in Figure 3-1.

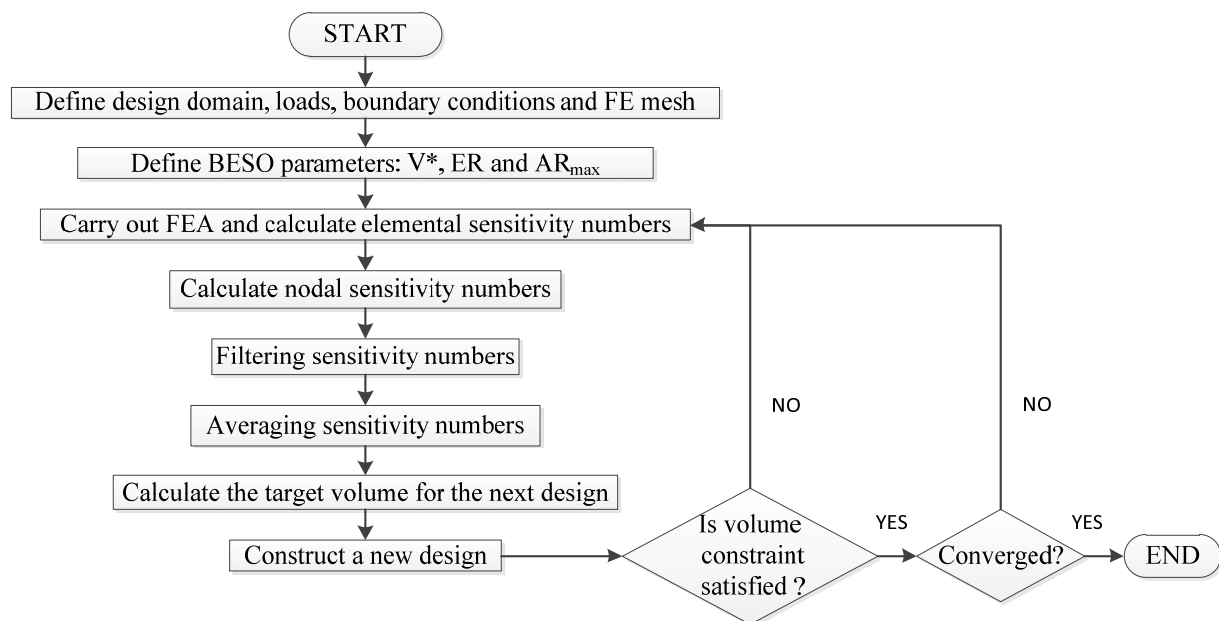


Figure 3-1: Flowchart of the BESO method [3].

Furthermore, the stress level in the node is used to determine the volume of the final design. In the progressive design, the node volume is reduced step-by-step and the stress is checked in each step.

This chapter aims to investigate the effect of different loading types on the topology of the designed nodes. The studied nodes are considered as simple as possible in terms of geometry

and topology. Therefore, the planar nodes are assumed, and the out-of-plane parameters in defining the nodes are excluded from the study.

In this chapter, four symmetrical nodes with different connectivity numbers are considered. The three-way node is optimised under five different general load cases, including axial load, out-of-plane bending, in-plane bending and torsion. The optimisation results are compared to investigate the effect of loading condition. The other three nodes are optimised for the same axial load, and the results are also compared. The optimisation is conducted based on the assumption that the material is isotropic and linear elastic. The optimised results for the nodes under different individual load cases are compared with the results for the nodes under combined load cases. Furthermore, the effect of the size of the design-domain on the final weight and topology of a node designed by BESO is examined by using different initial sizes. In addition, various smoothing methods for the final geometry produced by BESO are explored and compared with each other. The challenges of using AM in manufacturing nodes are also investigated. Finally, the case study of the design and manufacturing procedure of a prototype gridshell structure is demonstrated.

3.2. Loading and geometrical conditions

3.2.1. Geometrical design of initial model

Two approaches have been proposed and investigated to design the general geometry of the nodes with different topological and geometrical conditions in a gridshell structure. The first approach is to use a spherical shape in the middle of the node, which can easily accommodate any directions of the connecting beams in space (Figure 3-2).

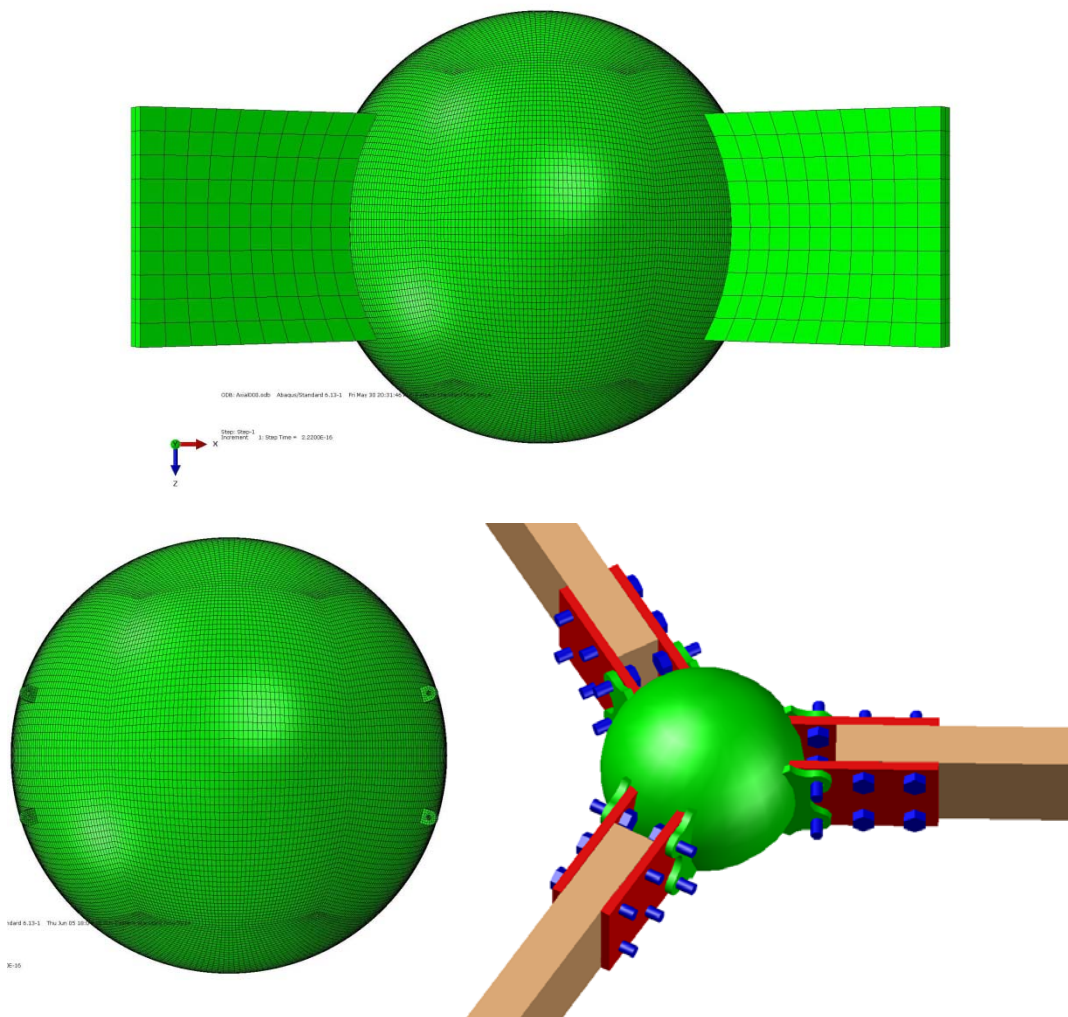


Figure 3-2: Spherical design domain with three different non-designable connecting components.

Although the use of spherical shape as the central part of a node provides maximum capacity for taking the out-of-plane rotations of the connected beams, only a small portion of this capacity is needed in a gridshell structure due to the limited out-of-plane angles. On the other hand, the combination of the spherical design domain and non-designable connecting components produces a complicated geometry, leading to difficulties in generating a consistent overall mesh for the combined shape. Besides, the sharp edges of the non-designable connecting components will usually remain exposed after the adjacent elements in the design domain are removed by BESO.

The second approach is to use a polygonal shape as a generic node configuration. The concept of this approach is to generate an irregular volume enclosed by a series of planar surfaces, including the end faces of the connected beams, bisector planes and top and bottom planes. The schematic diagram of an initial design domain using this approach is shown in Figure 3-3.

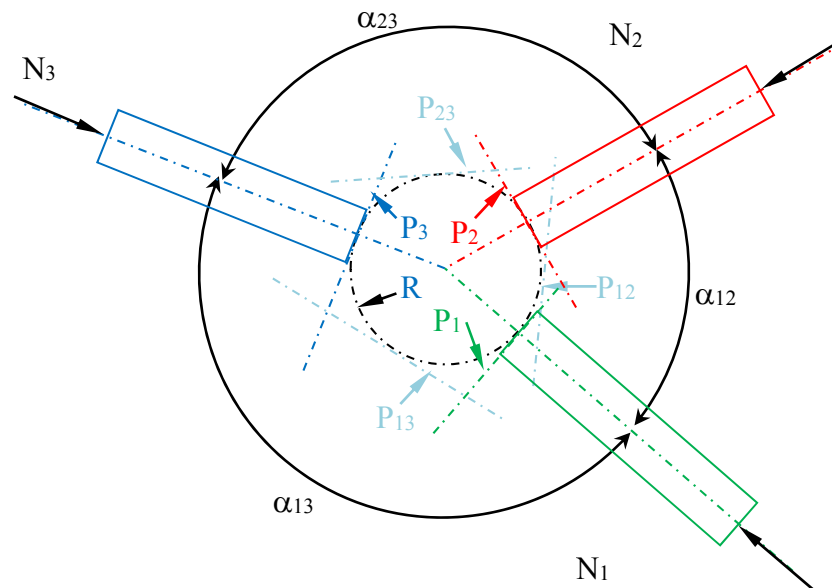


Figure 3-3: Polygonal design domain for a node.

To modify this approach and achieve smaller initial design domain, individual radii can be used for different connecting faces instead of a single radius for all connecting faces.

By using this polygonal configuration, it is easy and straightforward to generate a consistent mesh for both design domain and non-design parts. Figure 3-4 shows the initial model of a three-way node with a polygonal design domain in an unsymmetrical geometrical condition.

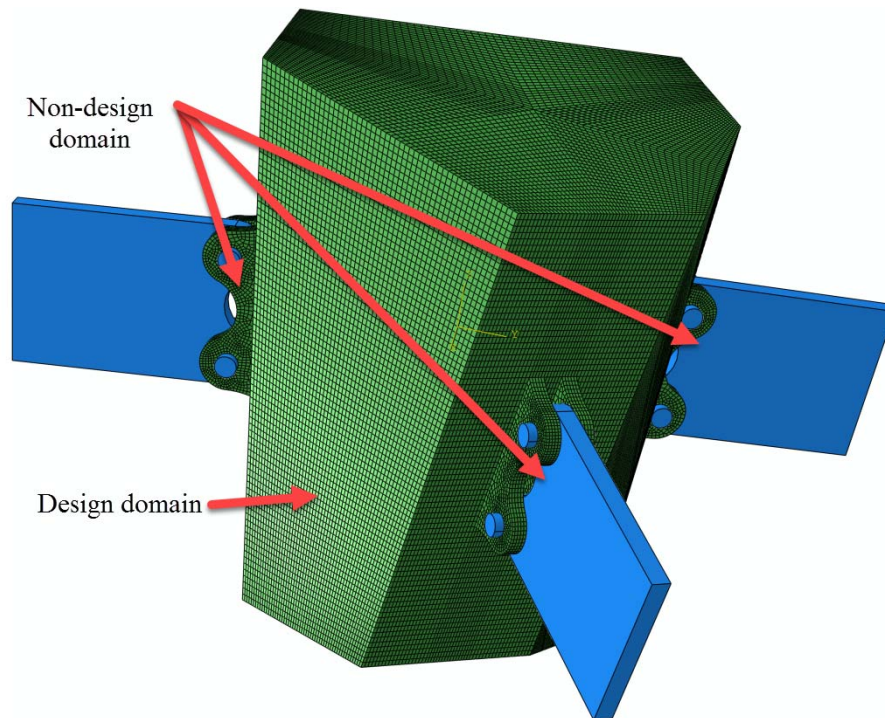


Figure 3-4: Node's model based on polygonal design domain.

Some parts of the node, which serve as the load transferring medium between the connected beam members and the design domain, are considered as the non-design domain. These connecting components need to remain unchanged during the design process. The connecting components which are normally designed by conventional design methods should be capable of transferring all types of loads. Various types of connecting components are used in this study to investigate the effect of non-design domain on the results of topology optimisation. It is found that the dominant loads, including axial load, out-of-plane bending and in-plane bending, can be transferred more effectively by using the connecting components consisting of four regions at four corners of the connecting face. Therefore, four eye connections are used in each connecting face in the model shown in Figure 3-4.

3.2.2. Load cases

Generic load cases for nodes are selected based on six basic load components at the connection between each beam and the node and the equilibrium of the node. The six load

components are axial (F1), out-of-plane bending (M33), torsion (M11), in-plane bending (M22), in-plane shear (V3) and out-of-plane shear (V2). The number of members connected to the node (connectivity number of the node) is important in solving the equilibrium equation of the node. For example, to generate the axial load case (F1) for a three-way node, three equilibrium equations with three variables representing axial forces in space need to be satisfied. Therefore, the three-way node is deterministic for axial load case. This means any three-way node with any geometrical condition can be subjected to only one combination of axial loads. In the case of shear load, due to the eccentricity of the shear loads, six equilibrium equations have only three variables, resulting in all variables equal to zero. Such a load case is not possible for a three-way node. Therefore, for any node in space, the generic load case can have no, one or infinite options which would satisfy the equilibrium equations. The load cases for three, four, five and six-way nodes are shown in Table 3-1.

Table 3-1: Possible load cases in each node.

Load cases	Planar			
	Three-way node	Four-way node	Five-way node	Six-way node
Axial (F1)	One solution	infinite	infinite	infinite
Out-of-plane bending (M33)	One solution	infinite	infinite	infinite
Torsion (M11)	One solution	infinite	infinite	infinite
In-plane bending (M22)	infinite	infinite	infinite	infinite
In-plane shear (V3)	No solution	One solution	infinite	infinite
Out-of-plane shear (V2)	No solution	One solution	infinite	infinite

The number of possible generic load cases increases when the number of the connected members increases. As an example, the possible load cases for planar three-way node and planar four-way node are schematically shown in Figure 3-5 and 3-5 respectively.

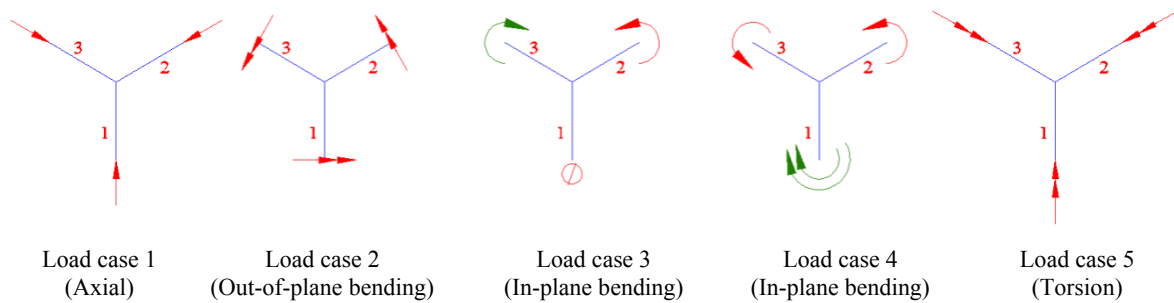


Figure 3-5: Possible load case categories for planar three-way node.

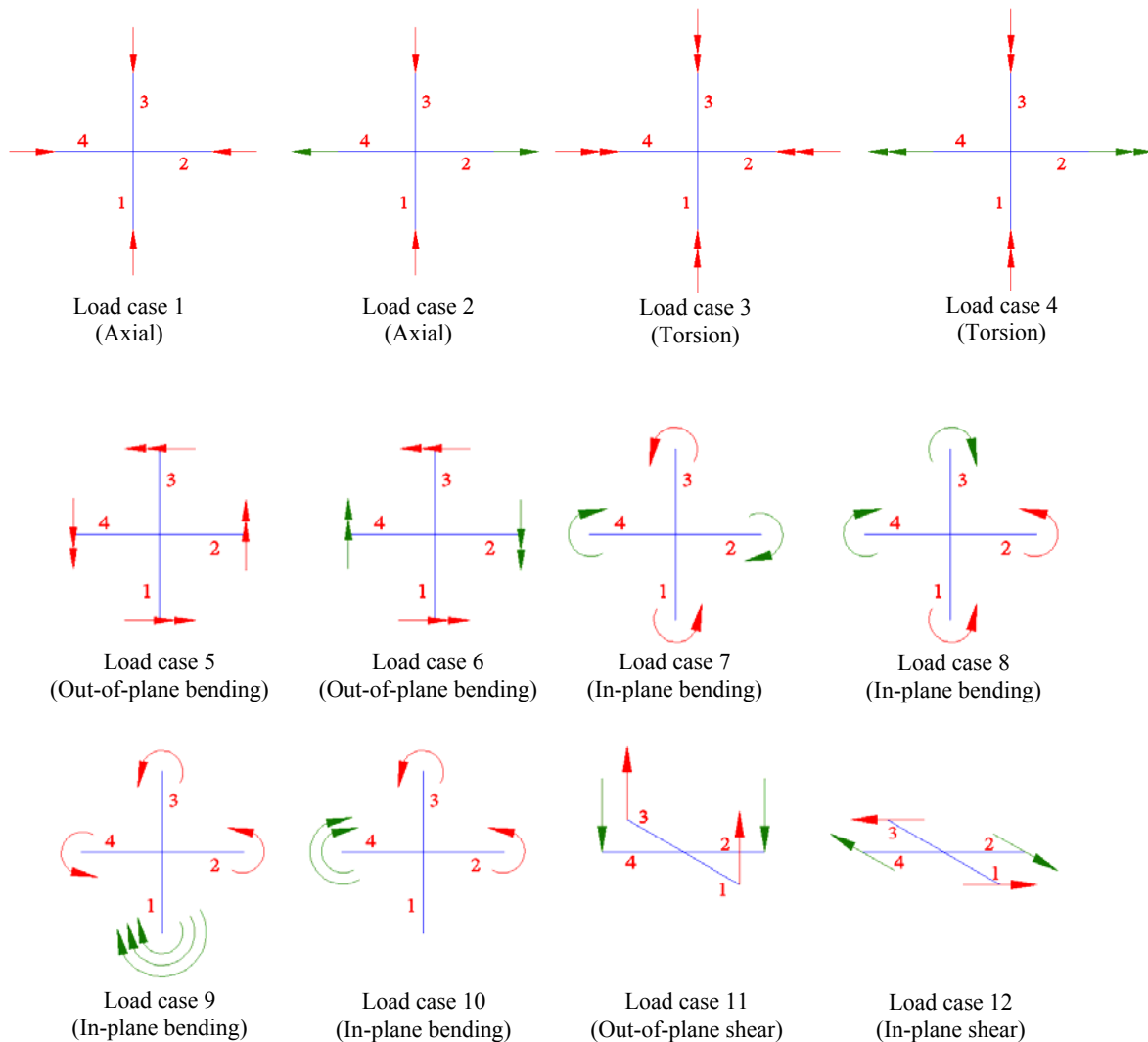


Figure 3-6: Possible load case categories for planar four-way node.

3.3. Design of geometrically simple nodes for basic load cases

To design a node for generic loads, the simplest symmetric 3-way node is topologically optimised using BESO under five different generic load cases as shown in Figure 3-5. The load cases include one axial loading, one out-of-plane bending, two in-plane bending and one torsion. The dimensions and other details of the symmetric 3-way node designed based on the aforementioned five generic load cases are shown in Figure 3-7.

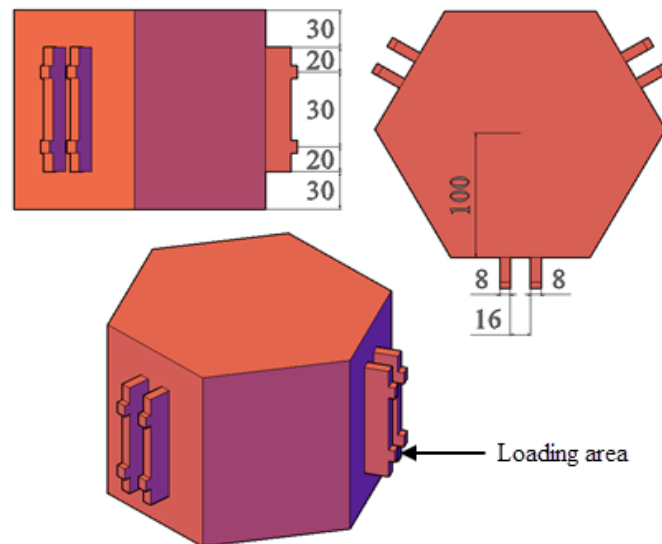


Figure 3-7: The dimensions (in millimetre) and other details of the 3-way node designed by BESO for generic load cases.

As shown in Figure 3-6, loads are applied as surface tractions on the protruding parts of the connecting plates. The BESO optimisation results for the 3-way node under five different generic load cases are shown in Figure 3-8 to 3-11.

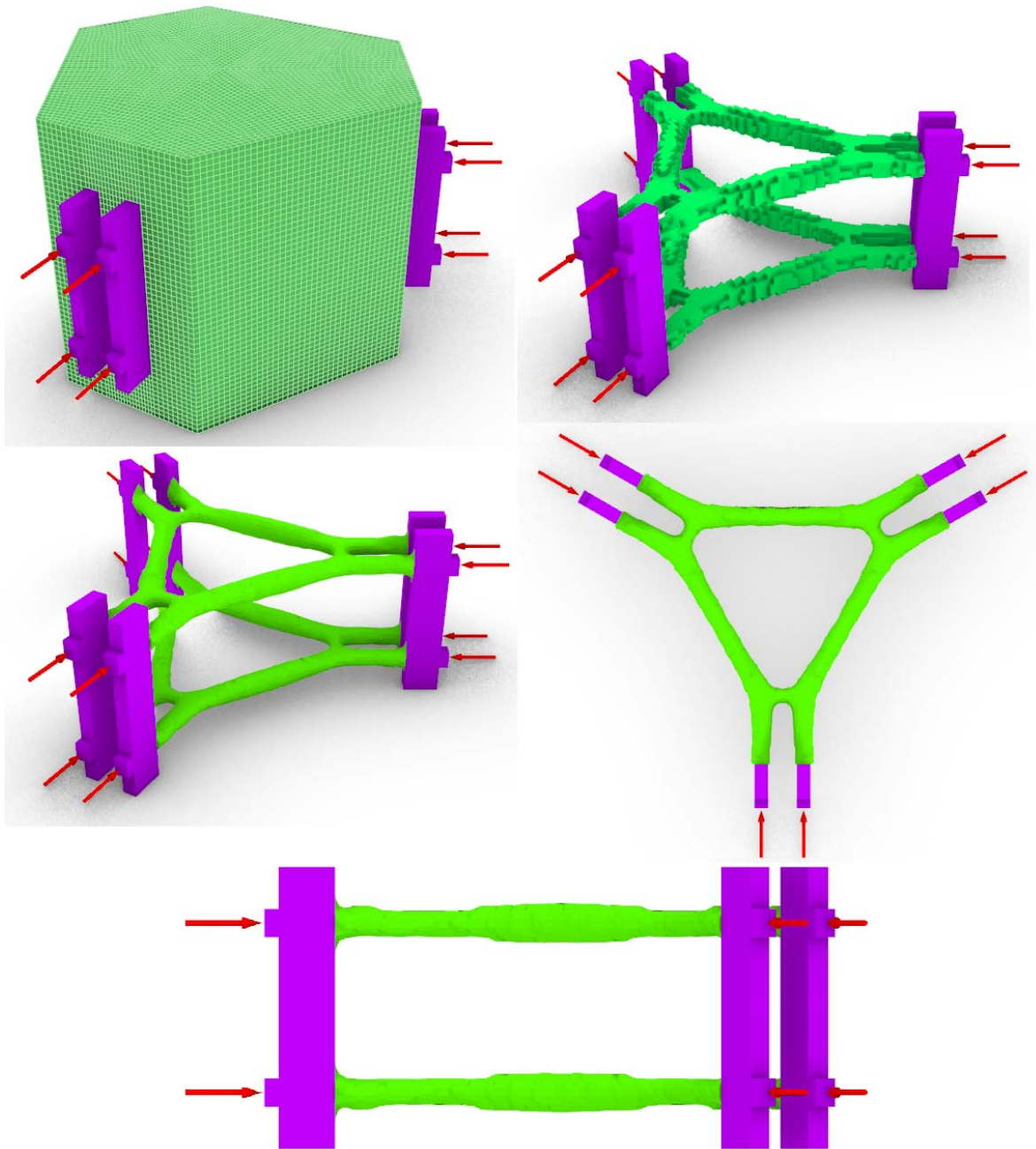


Figure 3-8: Symmetric 3-way node structurally optimised by BESO for axial forces (load case 1).

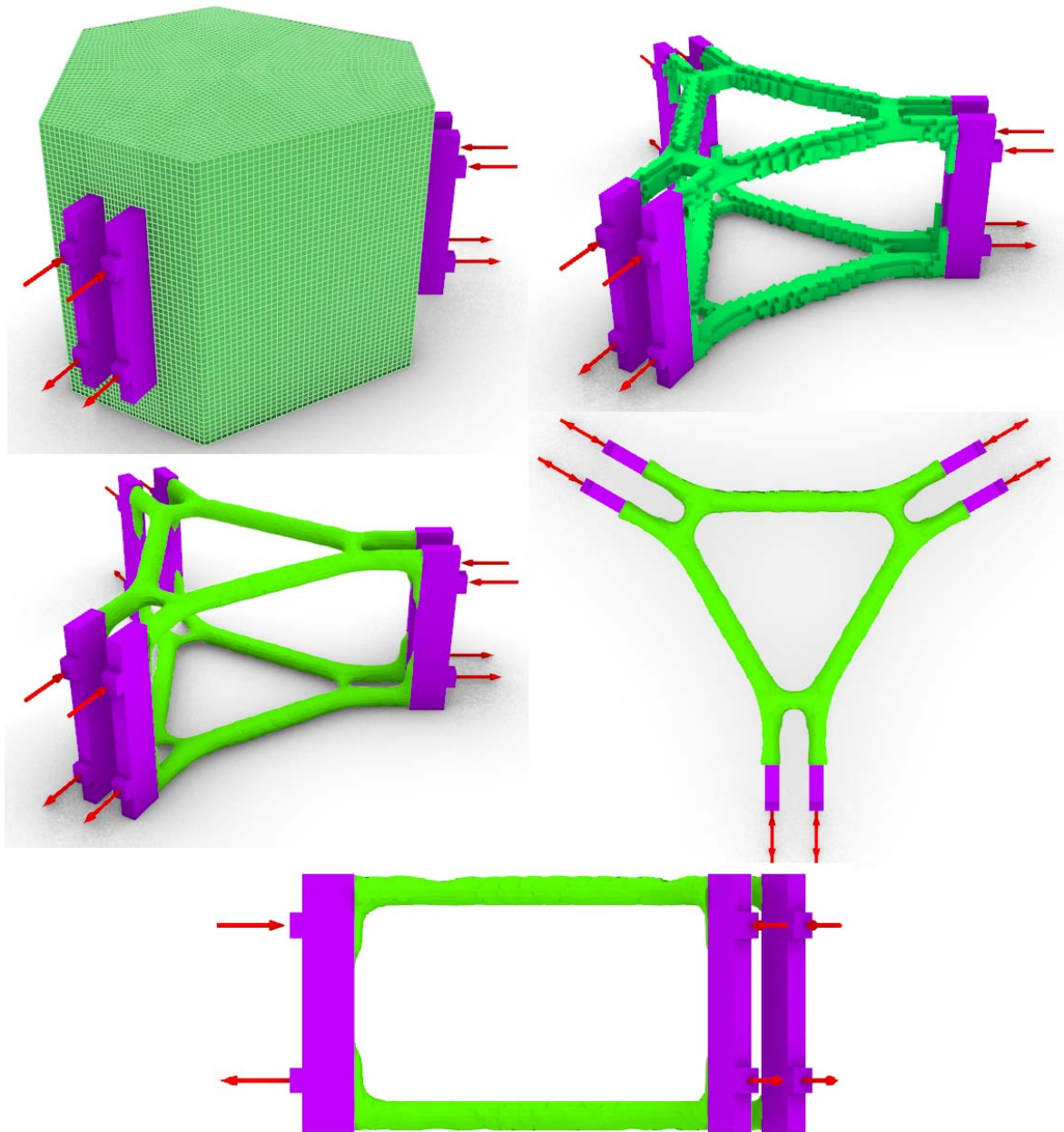


Figure 3-9: Symmetric 3-way node structurally optimised by BESO for out-of-plane bending (load case 2).

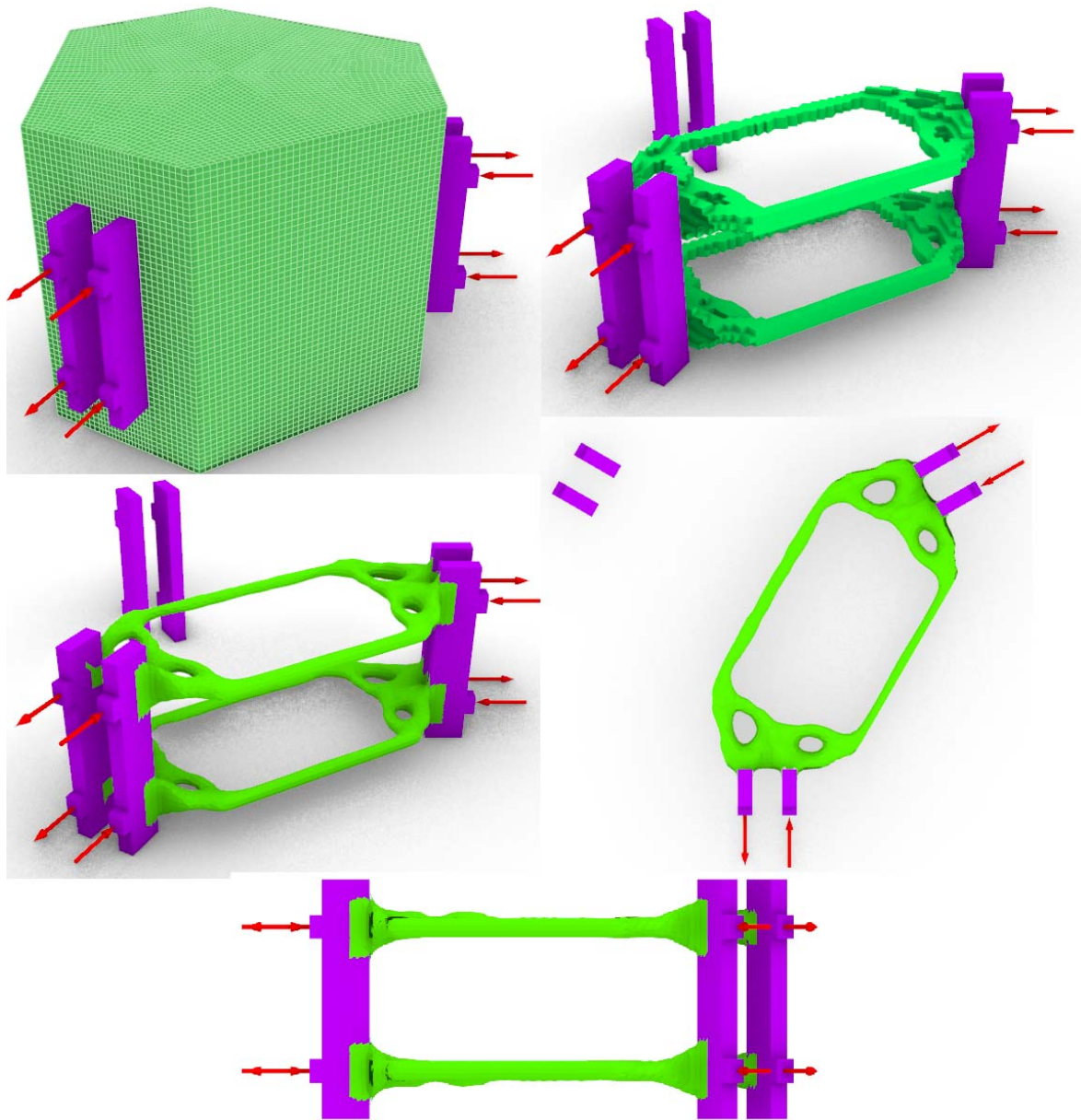


Figure 3-10: Symmetric 3-way node structurally optimised by BESO for in-plane bending between two members (load case 3).

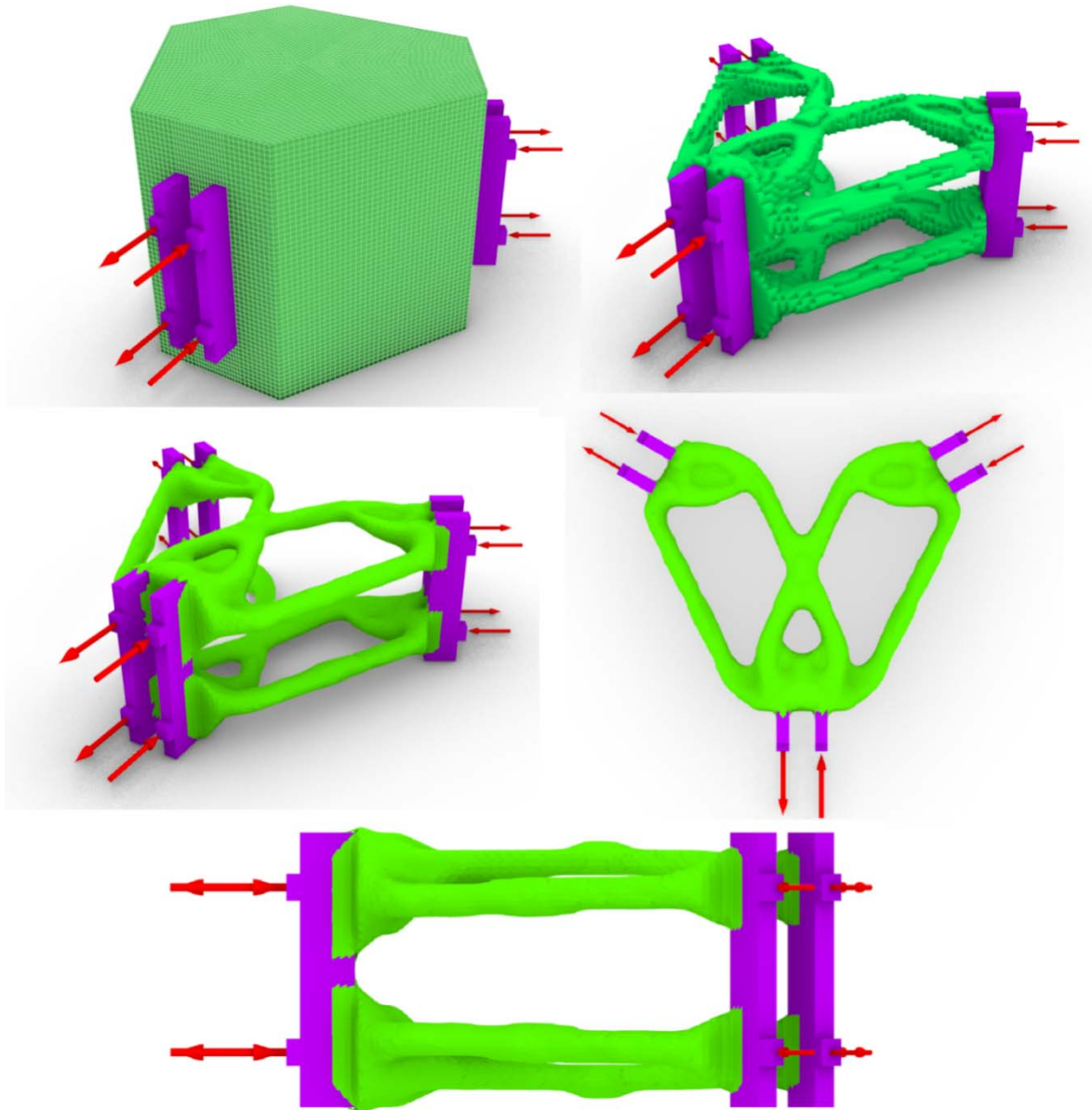


Figure 3-11: Symmetric 3-way node structurally optimised by BESO for in-plane bending among three members (load case 4).

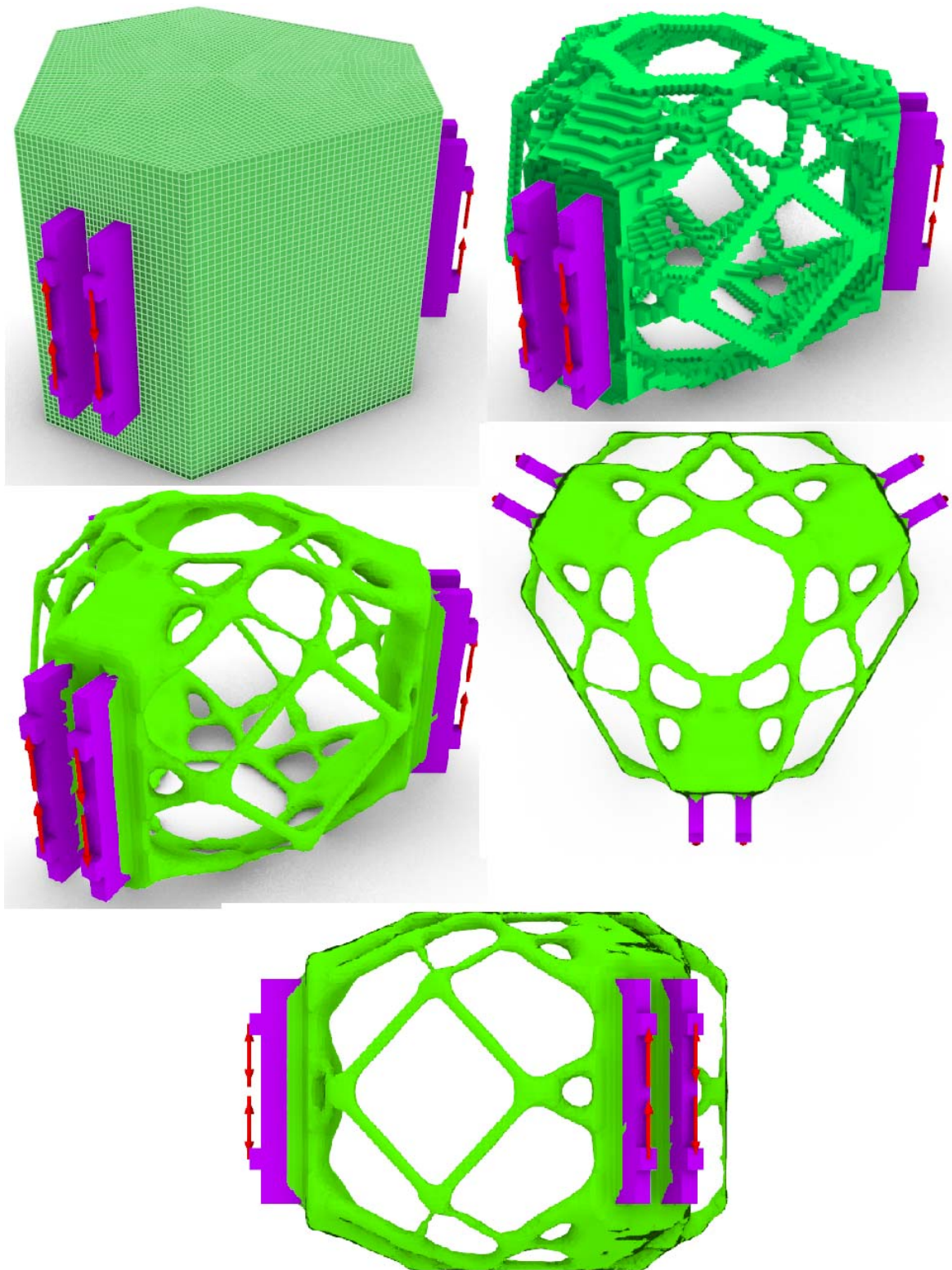


Figure 3-12: Symmetric 3-way node structurally optimised by BESO for torsion moments (load case 5)

The BESO design is dependent on the directions of the loads. When the load is normal to the surface, the generated structural members would for man angle with the loaded surface.

When the applied load is tangent to the surface, the members are generated on the surface. In first four load cases, the applied loads consist of combinations of inward and outward normal loads, which lead to the optimised structures having members inside the design domain. In the last load case generated by the shear surface tractions perpendicular to the normal direction, the members are formed on the surface of the design domain.

Also by comparing the BESO design for axial forces (axial node) in Figure 3-8 with the BESO design for out-of-plane bending (bending node) in Figure 3-9, it can be clearly observed that the optimised planar topologies for both nodes on top and bottom planes are almost identical in geometry. The planar structures in the axial node are aligned with the applied loads whereas in the bending node they are formed in planes different from the planes of the applied loads. The distance between planar substructures in bending node is larger than that in axial node. Additionally, a strengthened part at the connection between the design domain and non-design domain is visible in Figure 3-9. The similarities in the topology and geometry of the planar structures in axial and out-of-plane bending nodes can be explained by the similarity in the load arrangement. In the axial node, the directions of applied loads on the top and bottom planes are the same, and the generated planar structures are performing separately, therefore they are aligned with their attributed applied loads. But, in the bending node, the different load directions on the top and bottom planes would increase the distance between the identical planar structures. It is obvious that increasing the distance of the planar structures would increase the coupling of their axial loads and consequently increase the flexural capacity of the node with the same axial capacity of the planar structures. Therefore, increasing the distance of the planar structures could enhance the flexural stiffness of the node which aligns with the objective of the BESO structural optimisation for bending node. Coupling is performed by the in-plane action of the non-design connecting plates, and the shear and bending deformations of these plates are involved in the calculation of the flexural

stiffness of the node. Unlike planar structures, the in-plane stiffness of the connecting plates decreases with the increase in the distance between the planar structures (Figure 3-13). Therefore, the final distance between the planar structures is obtained from the balance between the stiffness of the planar structures and the stiffness of the non-design connecting plates.

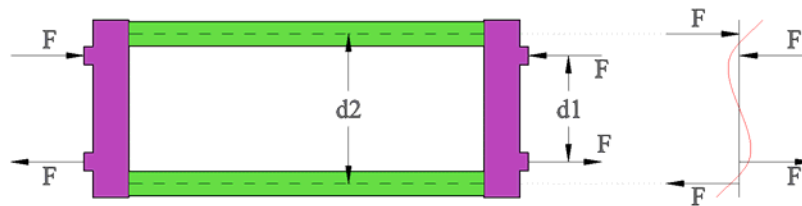


Figure 3-13: Schematic deflection of the non-design connecting plate in bending node.

A similar topology is generated for the in-plane bending between two sides of the node (Figure 3-10). In this node, instead of planar structures, two parallel straight members are generated in each plane to transfer the moment through the node. The parallel straight members are connected at both ends by a truss-like structure to enable the coupling action. As expected, the non-design parts in the third side are disconnected from the structure because they are not subjected to any loading.

Figure 3-11 shows the BESO design for two in-plane bending moments acting in the same direction, which are transferred from the second and third sides to the first side of the node. The final topology is made of two similar structural systems for each of the in-plane bending moments.

Figure 3-12 shows the BESO design for torsion moments applied to three sides of the node. As can be seen from the figure, the structural members are generated on the surface of the design domain, and the material inside the design domain is removed.

To study the effect of the number of the connected nodes on the structural optimisation results, BESO designs are carried out for 4-way, 5-way and 6-way nodes subjected to the axial load case. The dimensions and details of the nodes are shown in Figure 3-14.

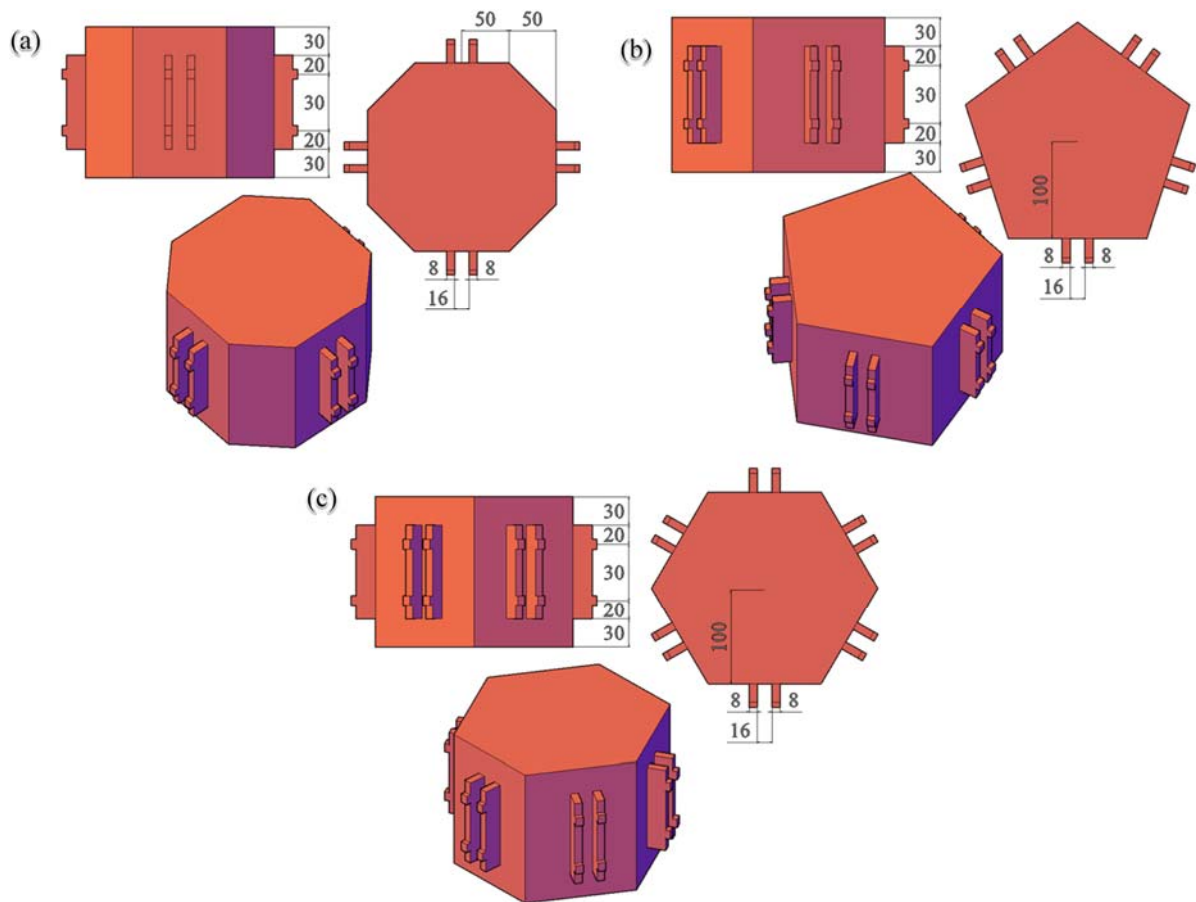


Figure 3-14: The dimensions (in millimetre) and other details of (a) 4-way, (b) 5-way and (c) 6-way nodes designed by BESO for generic load cases (dimensions are in millimetre)

Similar to the 3-way node, loads are applied as surface tractions on the protruding parts at the outer faces of the connecting plates. The optimised designs of the nodes under axial loads are shown in Figure 3-15 to Figure 3-17.

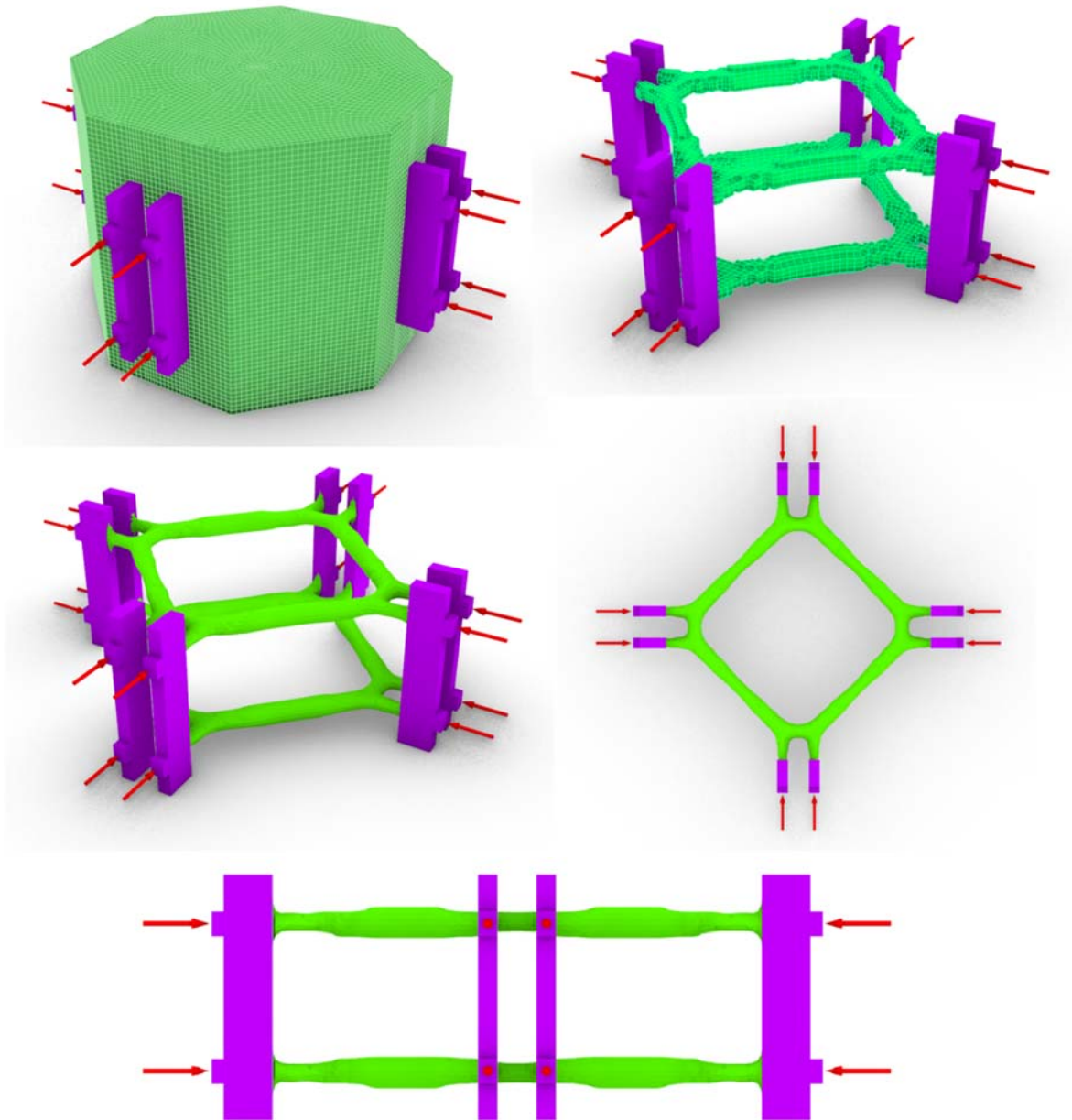


Figure 3-15: Symmetric 4-way node structurally optimised by BESO for axial loads.

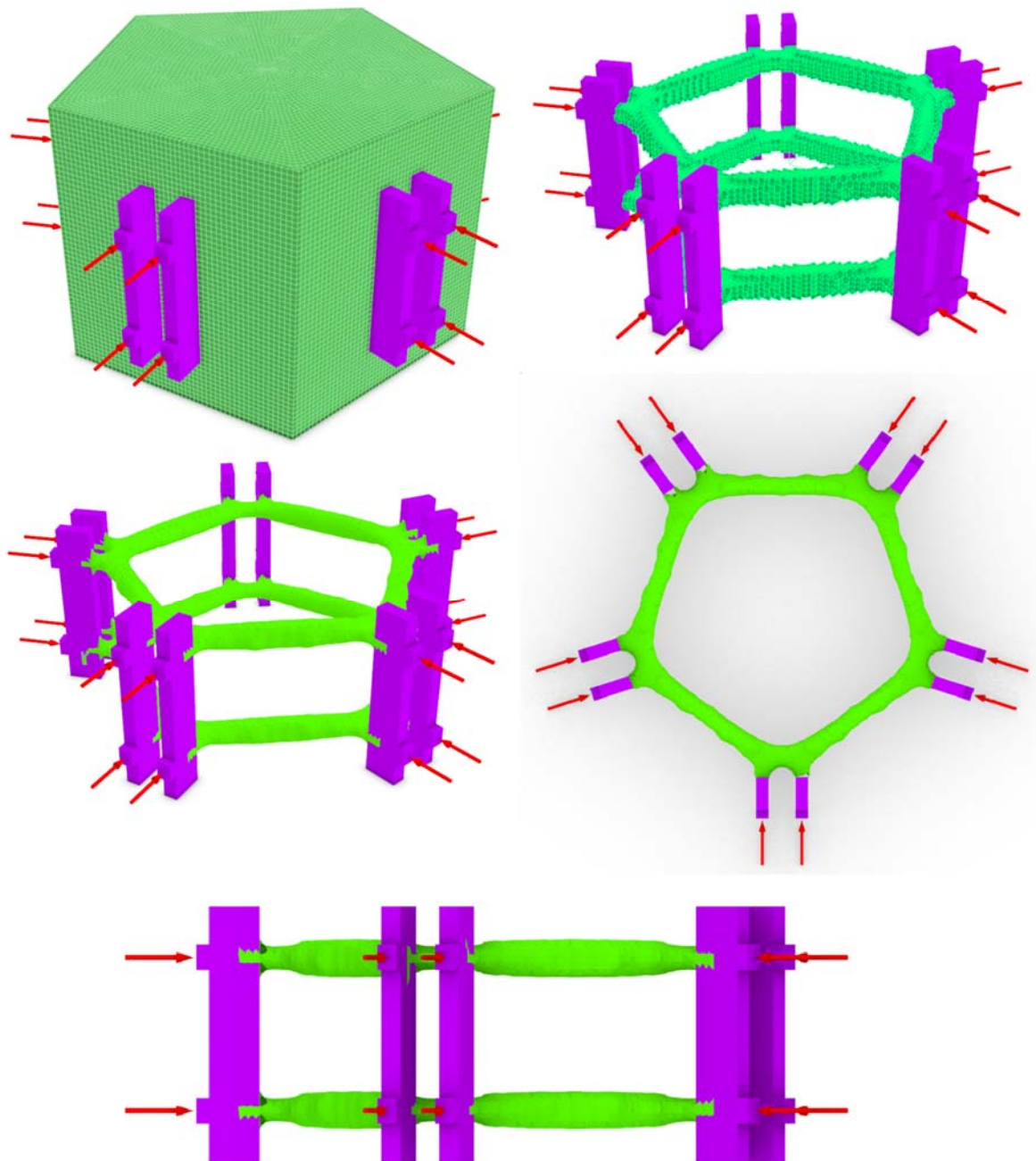


Figure 3-16: Symmetric 5-way node structurally optimised by BESO for axial loads.

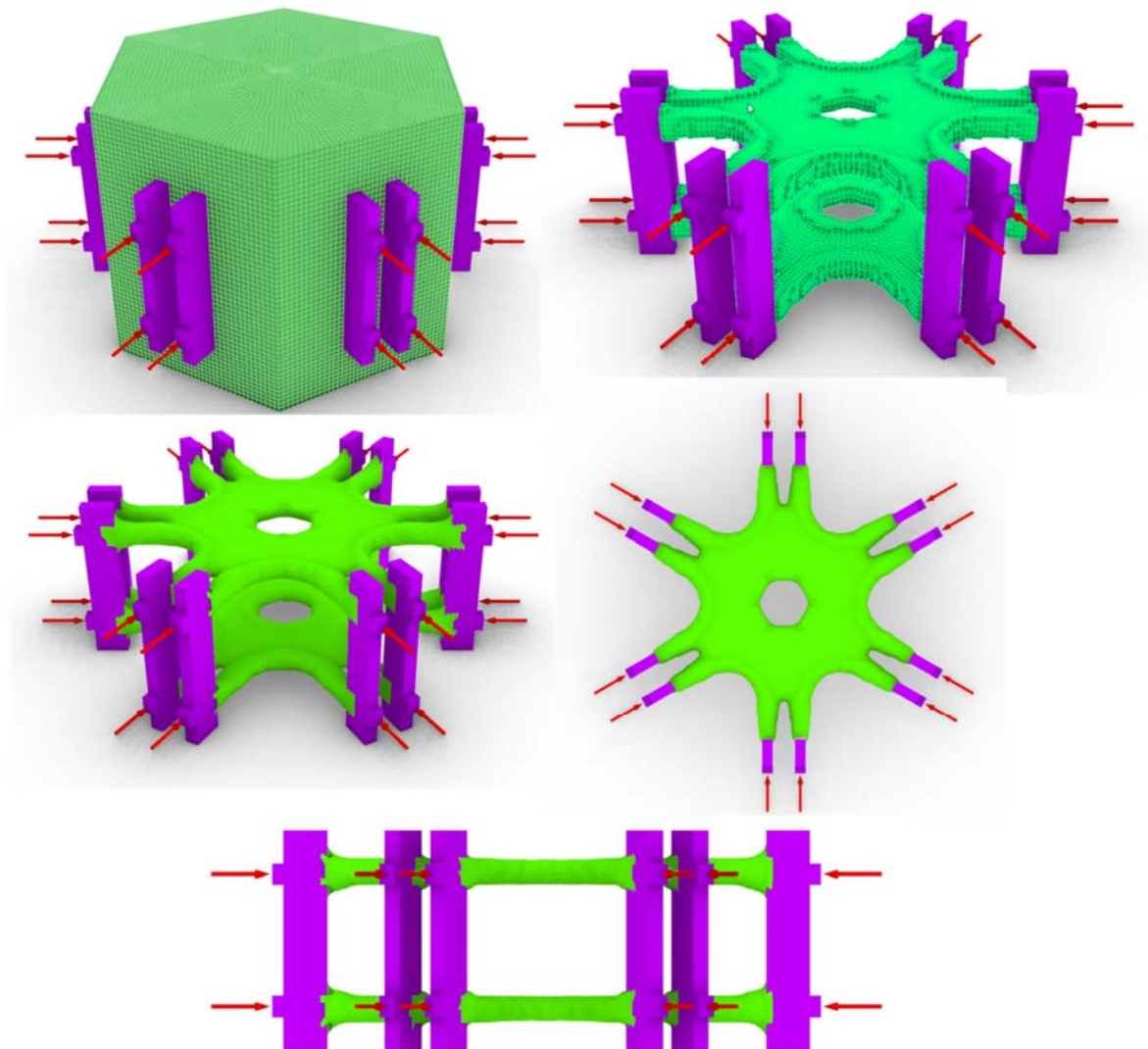


Figure 3-17: Symmetric 6-way node structurally optimised by BESO for axial loads.

Similar to the design for the 3-way node under axial load, the optimised structure consists of two planar substructures in the loading plan. The topologies of the planar substructures for 3-way, 4-way and 5-way nodes are similar, consisting of a truss-like structure with three types of straight members as shown in Figure 3-18. The first type members start from the place of loading and penetrate into the design domain in the direction of the applied load (blue lines in Figure 3-18). The second type members connect the first type members on the neighbouring faces at a certain depth of penetration (red lines in Figure 3-18). The axial force, which is transferred through member type one to member type two, generates a component perpendicular to member type one. To balance the perpendicular component of the internal

forces at the conjunction of the first two sets of members, the third set connects the members of the first type together (black lines in Figure 3-18).

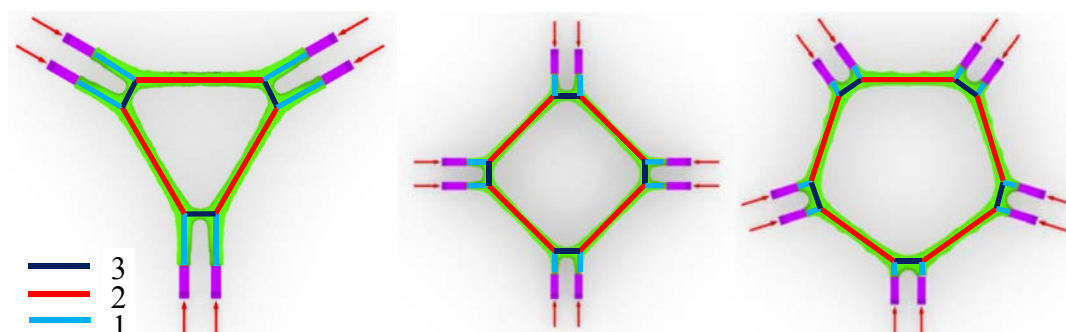


Figure 3-18: Similar members generated by BESO for axial loads in 3-way, 4-way and 5-way nodes.

In the planar substructure of the 6-way node (Figure 3-17), the first set of members are the same as the previous nodes. But the connection of these members to the neighbouring ones is through arch members which are supported by a disk at the centre part of the node. Actually the results of BESO process can be interpreted as the best selected topology among a large number of options as there are many parameters affecting the results. In other words, there might be other topologies rather than the truss-like structure (first three nodes) and the topology with disk (six-way node), which are not selected because of inefficiency. As for the truss-like structure for the first three nodes, the reduction in the length of first type members can be explained as a trade-off between volumes and stiffness, depending on their internal forces and directions. As the connectivity number of the node increases, the angles of the imposed forces decrease, thus the internal forces of the members of set two in truss-like topology increase. Therefore, these members become inefficient in transferring the imposed forces.

Effect of the non-design domain shape on BESO results

In this section, the effect of the non-design domain shape on the final design by BESO is investigated using two axial nodes with different connection details. The first node has three

symmetrical cleat plates connected to a spherical design domain. The initial shape and the final design of the node are shown in Figure 3-19.

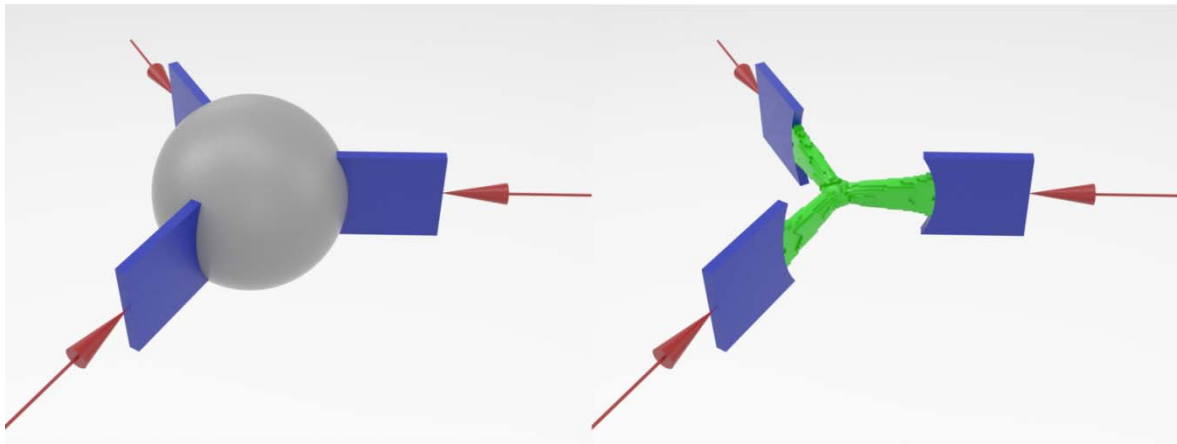


Figure 3-19: Symmetric 3-way node with three cleat plate connections structurally optimised by BESO for axial loads.

Unlike the other axial nodes that have been designed previously, structural members of this node are generated in one layer, with three concentric components connected at the centre of the node.

The second node has six eye connections attached to a spherical design domain. The initial shape and the final design of the second node are shown in Figure 3-20.

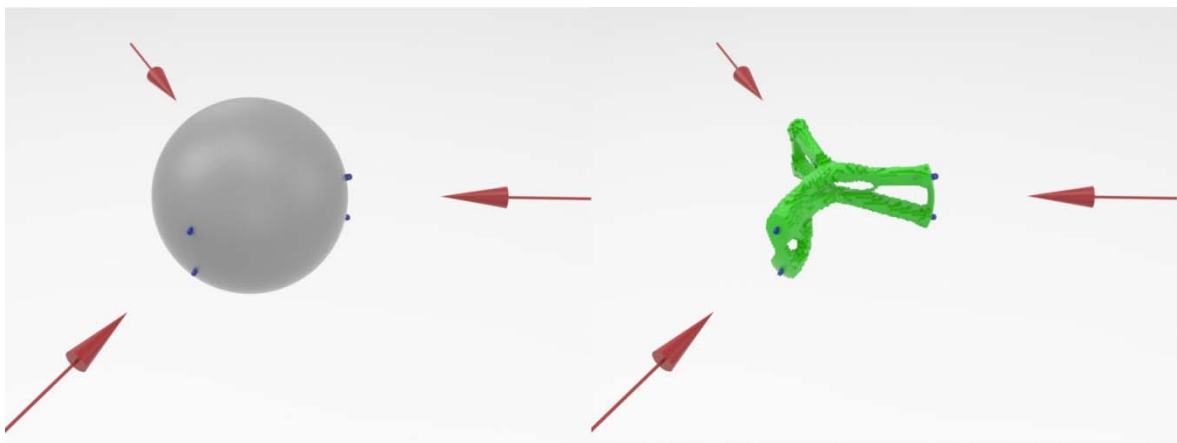


Figure 3-20: Symmetric 3-way node with 6 eye connections structurally optimised by BESO for axial loads.

As shown in the result, the final design of this node is not symmetrical, because the applied forces are not exactly symmetrical due to the small differences introduced by rounding up the load components. This optimisation process is then repeated from the initial step by applying more accurate forces. The result of the second run is shown in Figure 3-21.

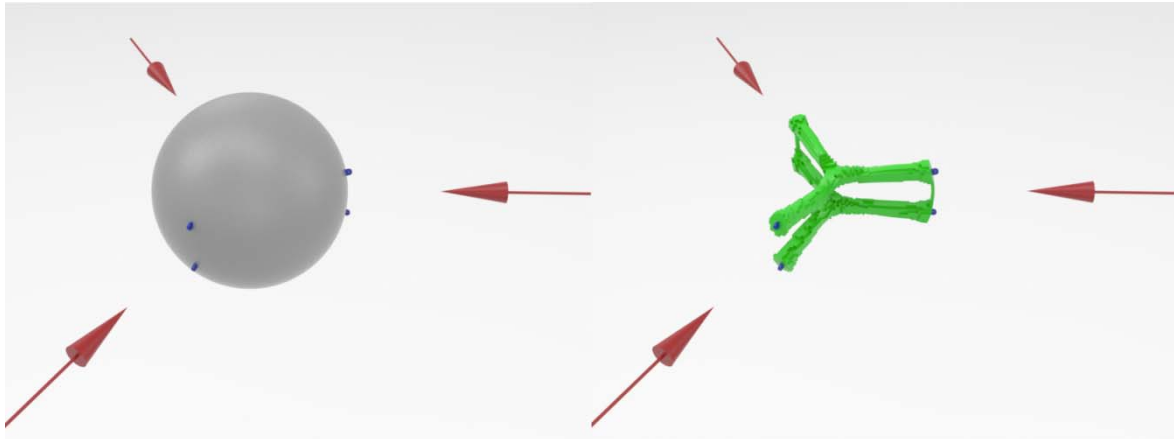


Figure 3-21: Symmetric 3-way node with 6 eye connections structurally optimised by BESO using more accurate forces.

The comparison of the BESO designs for this node and the node shown in Figure 3-20 shows that the topology of the BESO design is very sensitive to the initial conditions defined for the node. In addition, another design is carried out for a spherical node with six eye connections under out-of-plane bending moments. The result is shown in Figure 3-22.

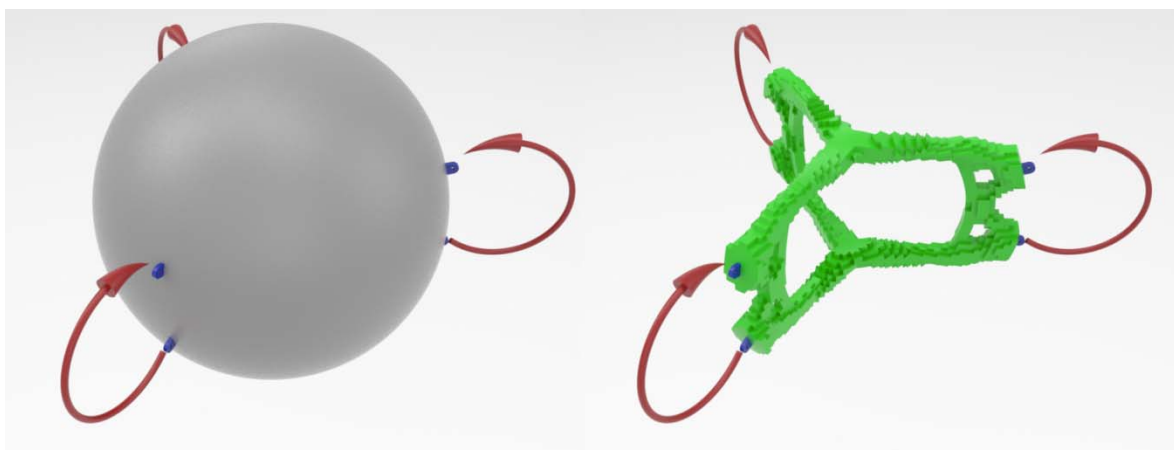


Figure 3-22: Symmetric 3-way node with 6 eye connections structurally optimised by BESO for out-of-plane bending.

As expected, a truss-like structure is formed at each branch to connect the planar substructures and transfer the loads between the loading plane and the substructure plane.

3.4. Design of geometrically complex nodes for general load cases

Having gained insight into the structural behaviour of nodes obtained for the basic load cases, more complex load cases are studied in this section, which can be achieved in two steps. The first step is to design the nodal connections of the prototype of a gridshell structure based on the nodal forces obtained from the analysis of the whole structure. The second step is to design nodes for arbitrary load cases.

3.4.1. Node design for a prototype canopy

As a part of this study, a series of structural nodes of a gridshell canopy prototype are designed using BESO and then 3D printed (Figure 3-23).

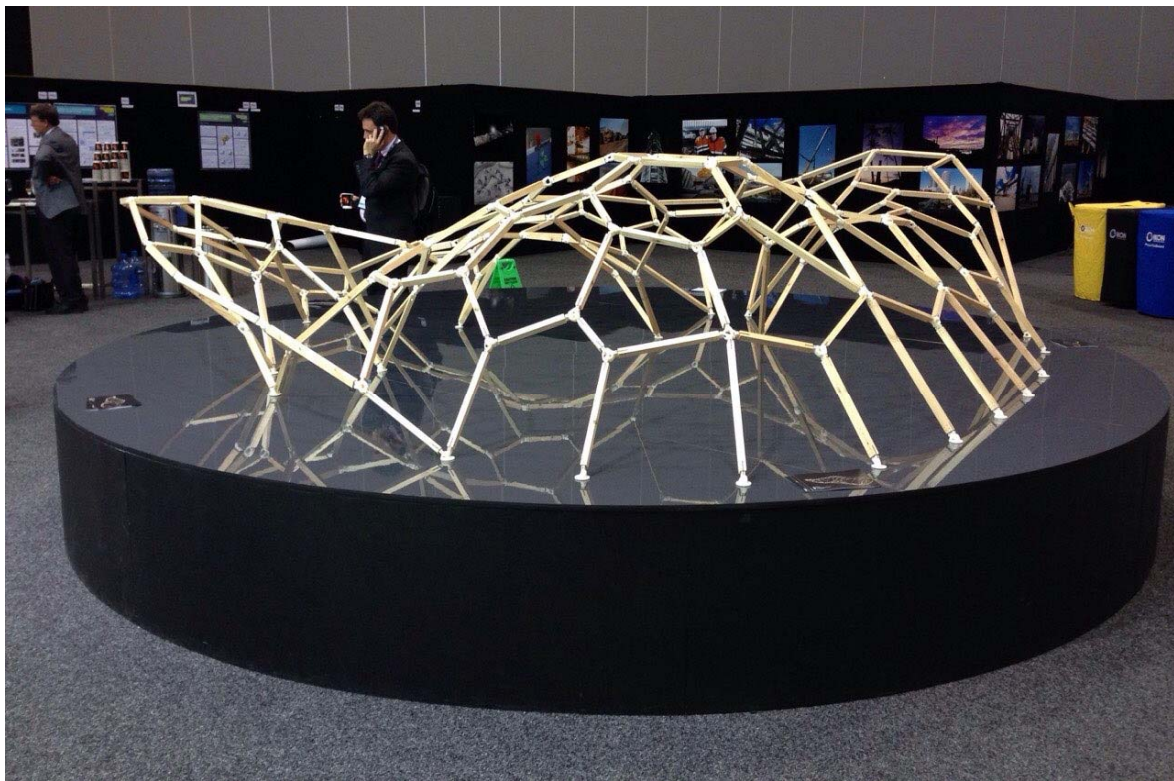


Figure 3-23: A scaled prototype of a gridshell structure designed, manufactured and exhibited during the Engineers Australia Convention in 2014.

A prototype consisting of 137 nodes and 205 beam members is constructed. The design of the nodes is performed based on the nodal forces (Figure 3-24) obtained from the analysis of the whole structure. The analysis and design of the whole structure, in which only self-weight and nominal horizontal loads are considered for the load combination, is carried out by Arup Company [5] in GSA.

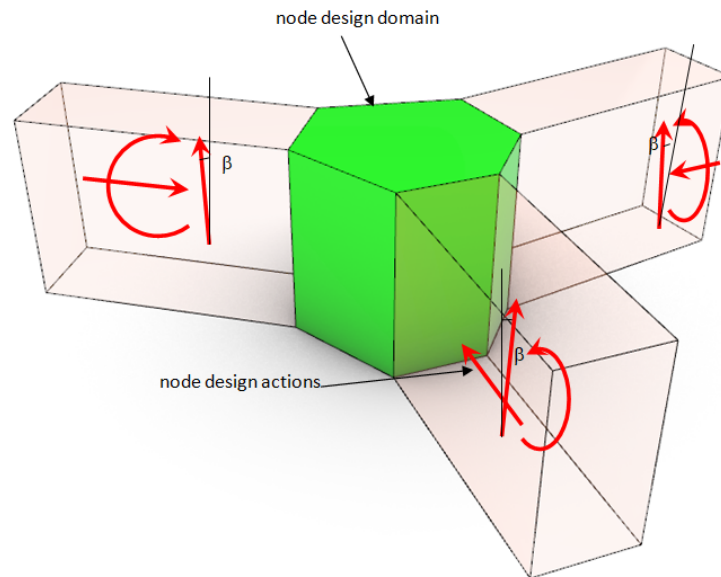


Figure 3-24: Nodal forces from connected members.

Connection detail

In this project, beams are connected to the nodes through an eye-connection. Details of this eye-connection are illustrated in Figure 3-25. Two eye connection plates labelled PL-A in Figure 3-25 are directly connected to the design domain to transfer the loads from beam members.

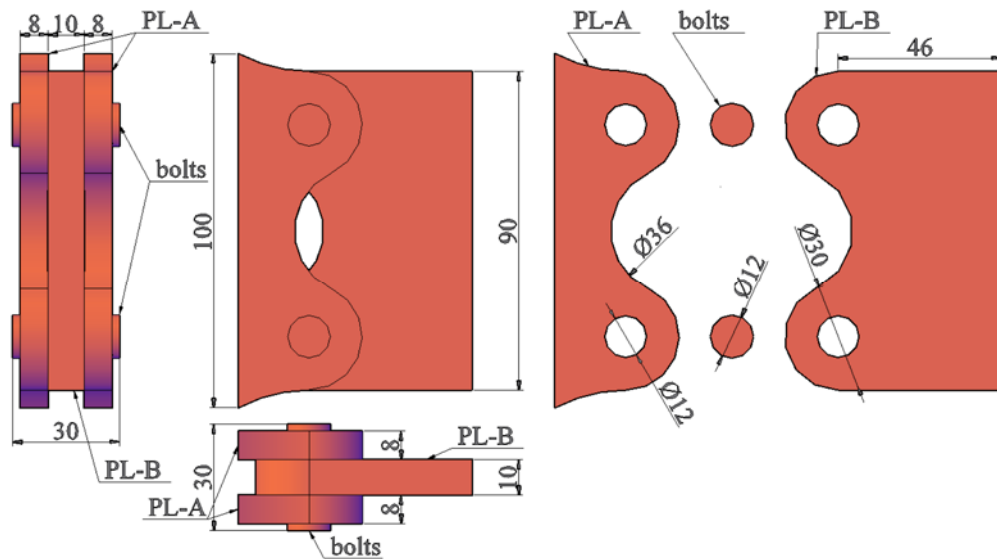


Figure 3-25: Details of beam to node connections in a full-scale gridshell structure (dimensions are in millimetre).

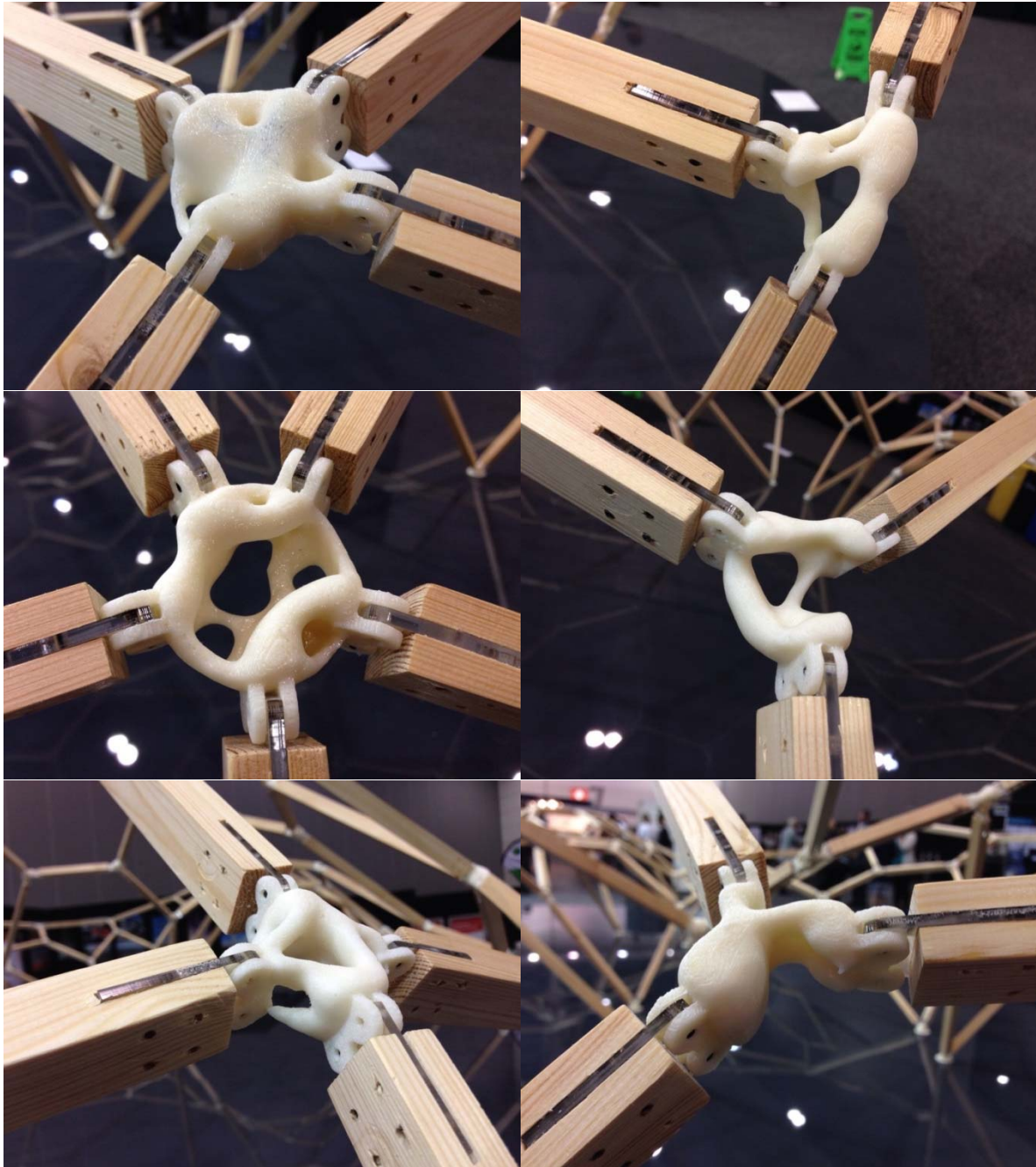


Figure 3-26: Nodes designed by BESO and 3D printed in plastic for the scaled prototype of a gridshell structure.

A number of designed nodes are shown in Figure 3-26. Although the nodes are designed using BESO and supposed to be the most efficient structural connections for the imposed loads, their topologies and geometries do not demonstrate the structural efficiency at the first glance. The reason is that, unlike the traditional design routines in which multiple load cases from different loading scenarios are considered in the design procedure, only one load case is

used in this project. Structural optimisation in this study results in a specific topology which is efficient on for the predefined loading conditions.

3.4.2. Design of nodes for arbitrary load conditions

To design nodes for arbitrary load conditions, the BESO design for out-of-plane bending is firstly compared with the design for out-of-plane shear. The dimensions of the initial model used for both designed nodes are shown in Figure 3-25 and the design loads are shown in Figure 3-27.

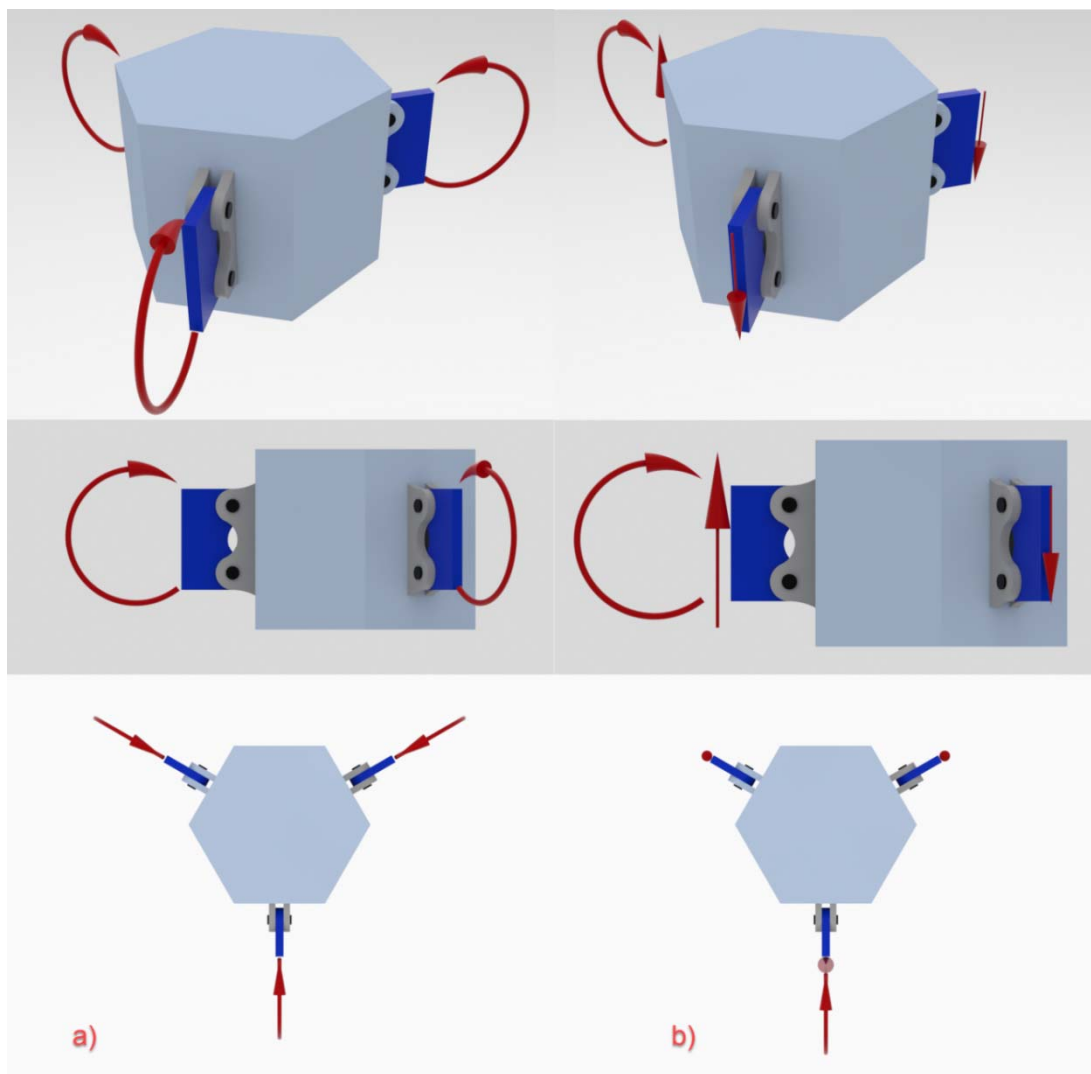


Figure 3-27: Boundary and loading conditions of a symmetrical three-way node subjected to a) symmetrical out-of-plane bending moments and b) combination of out-of-plane shear forces and bending moments.

The symmetrical bending moments in the first case are simulated by applying two equal push and pull forces at the end of the connected beam members. The second loading case is simulated by applying two vertical loads equally at the ends of two connected beam members and fixing the third connected member. The control parameter is the maximum volume removal ratio, also known as volume fraction. Technically speaking, the decision of a suitable volume fraction to be set at the start of BESO design process is a matter of trial-and-error as it depends on two factors. The first is that the stress level of the final solution should not exceed the allowable value. The second factor is that the slenderness of the elements should meet both buckling and 3D printing requirements. The suitable volume fraction is selected in a way that both stress level criterion and slenderness criterion are satisfied. In case 1, iteration 57 is selected as the final solution. In case 2, iteration 41 is selected as the final solution. Figure 3-28 shows the results of the BESO design for out-of-plane bending and combination of out-of-plane shear force and bending moment.

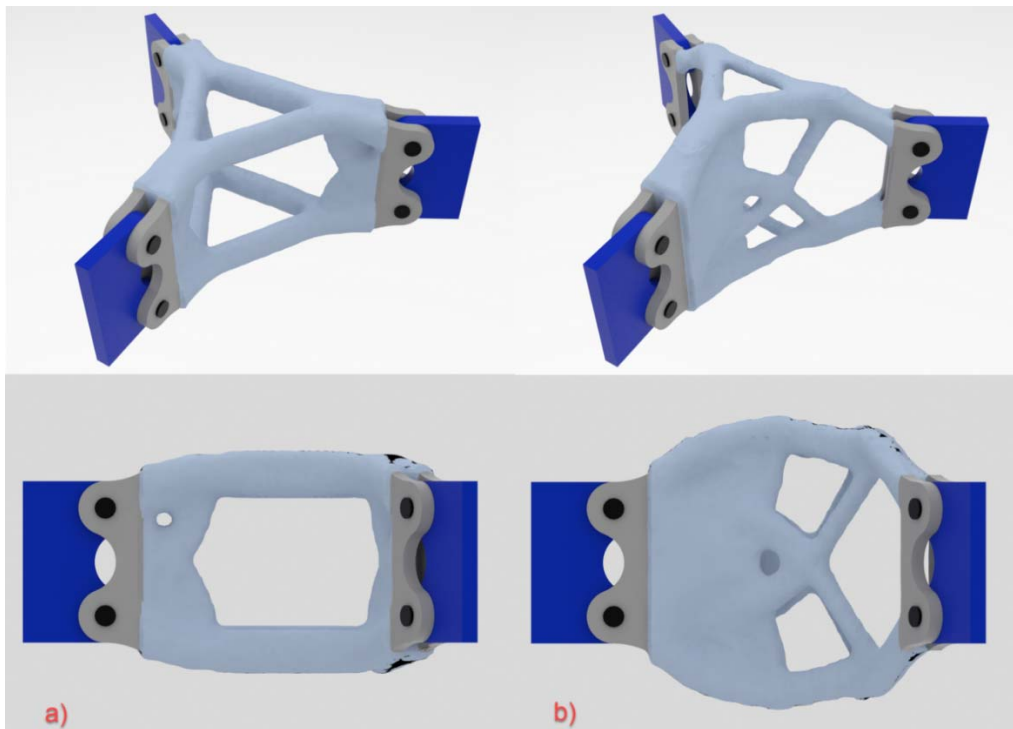


Figure 3-28: Results of BESO design of a symmetrical three-way node subjected to a) symmetrical out-of-plane bending moment and b) combination of out-of-plane shear force and bending moment.

In the final topology of the bending node, a truss-like structure is formed between the planar substructures as the non-design connection is weakened in the middle. In both designs, a triangular topology is formed at two levels as a result of the presence of out-of-plane bending. The triangle in the first node (bending node) is symmetrical due to the uniform bending moment. This is not the case in the second node (shear node) as the bending stress varies throughout the design domain. The same reason also applies to the different planarity of the substructures in the two nodes. Besides, compared to the bending node, the final structural members of the shear node are generated closer to the surface of the design domain, which is due to the eccentricity of the imposed shear load similar to the node designed for torsion in the previous section. In the shear node, two vertical planar parts are generated between top and bottom substructures which are responsible for transferring the shear force from the two sides subjected to shear forces to the side under the combination of shear force and bending moment.

Figure 3-29 shows the stress contours obtained from the structural analysis for both cases. It can be seen that, in both cases, the stress is distributed uniformly in the designed domain.

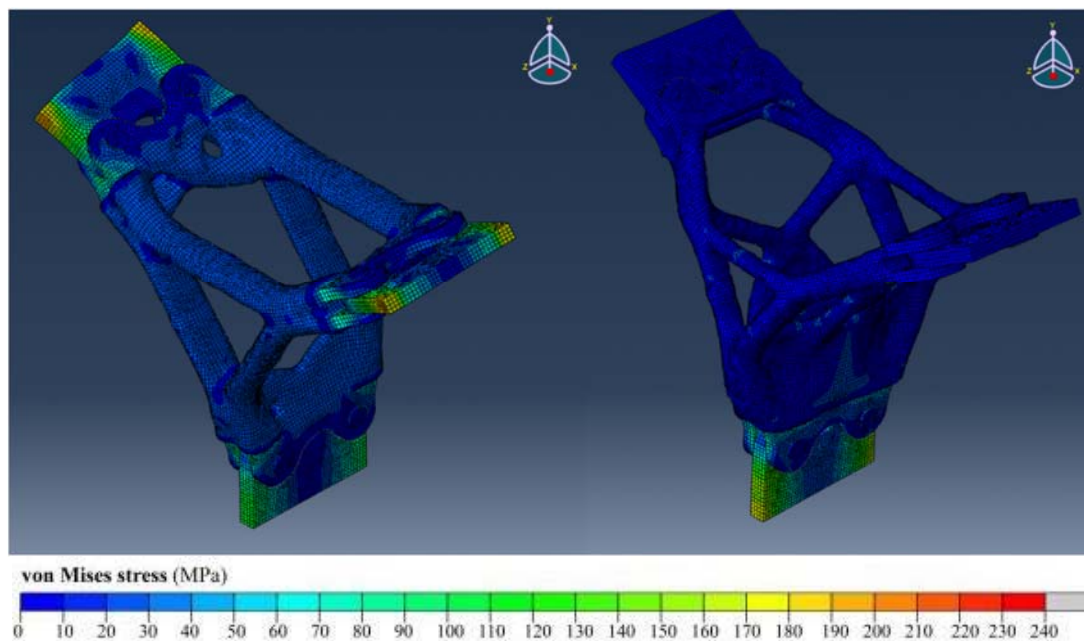


Figure 3-29- Stress contours of optimised nodes under bending and shear loads.

Figure 3-30 shows the BESO design for the 3-way node subjected to two out-of-plane shear loads. Compared to the node shown in Figure 3-22, a similar truss-like structure is also formed at the two sides with shear loads.

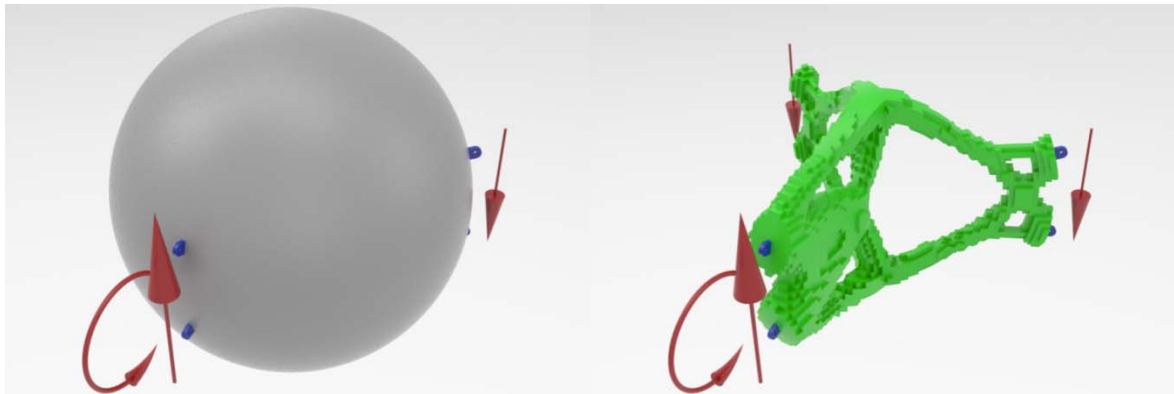


Figure 3-30: Symmetric 3-way node with 6 eye connections structurally optimised by BESO for out-of-plane shear force.

To explore more complicated loading situations, a number of nodes are designed for arbitrary geometrical and loading conditions. The results are shown in Figure 3-31.

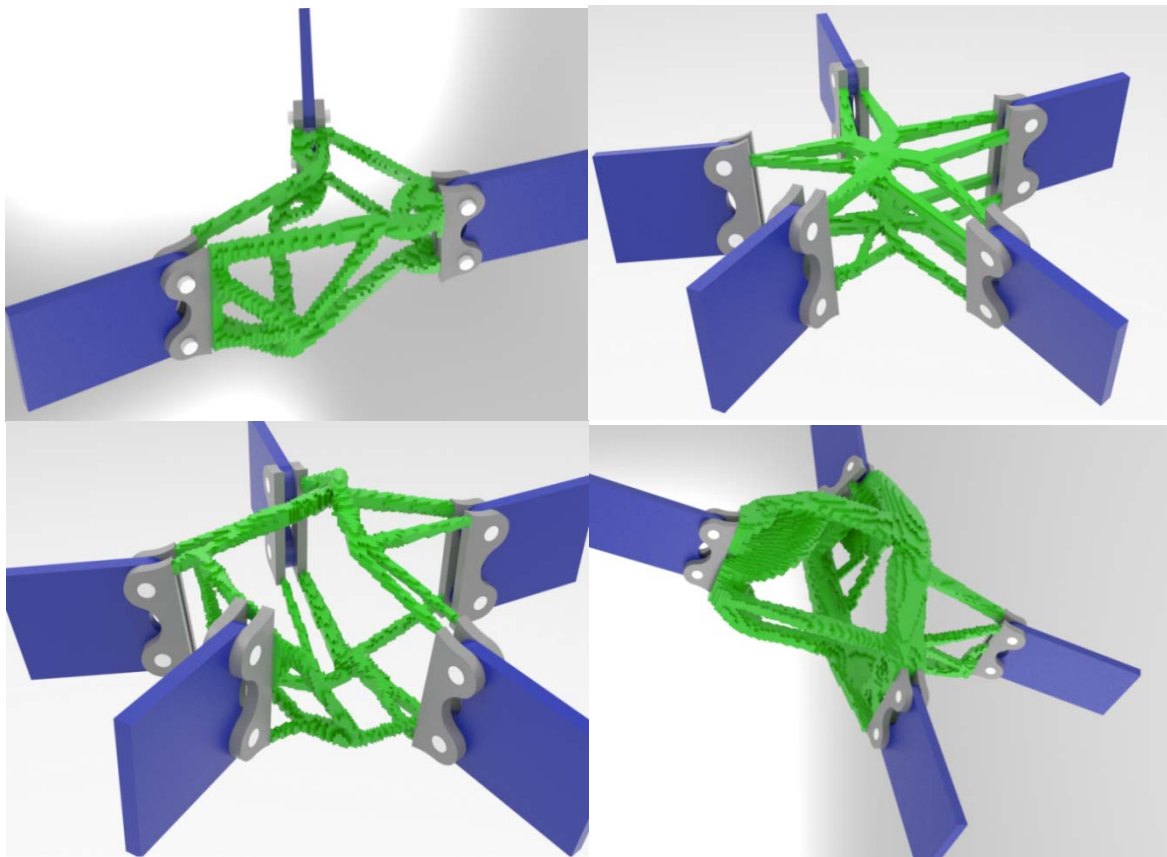


Figure 3-31: BESO design of nodes with three, four and five connecting members subjected to arbitrary loads.

The evolution of BESO design for a 3-way node is shown in Figure 3-32.

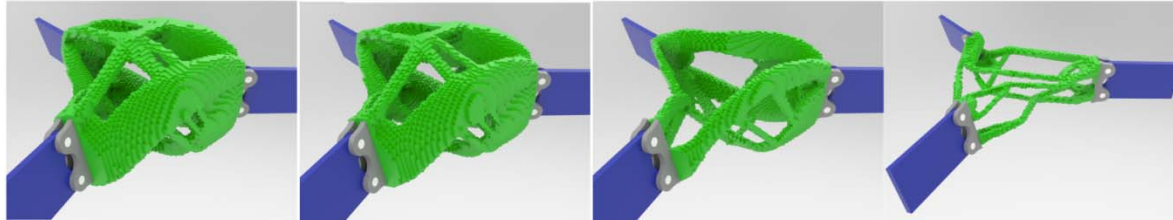


Figure 3-32: The evolution of BESO design for an arbitrary 3-way node subjected to an arbitrary load case.

As can be seen from the arbitrary designs, the optimum topology is topologically and geometrically complex and does not follow any obvious trend to be classified in a conventional design method. In other words, these topologies are not obtainable from conventional methods.

3.5. Effect of design domain size

The effect of design domain size on the BESO design is investigated in this section. Four nodes with three connected beams and different design domain sizes are optimised using BESO for similar out-of-plane shear forces. The dimensions of the nodes and the locations of shear loads are shown in Figure 3-33.

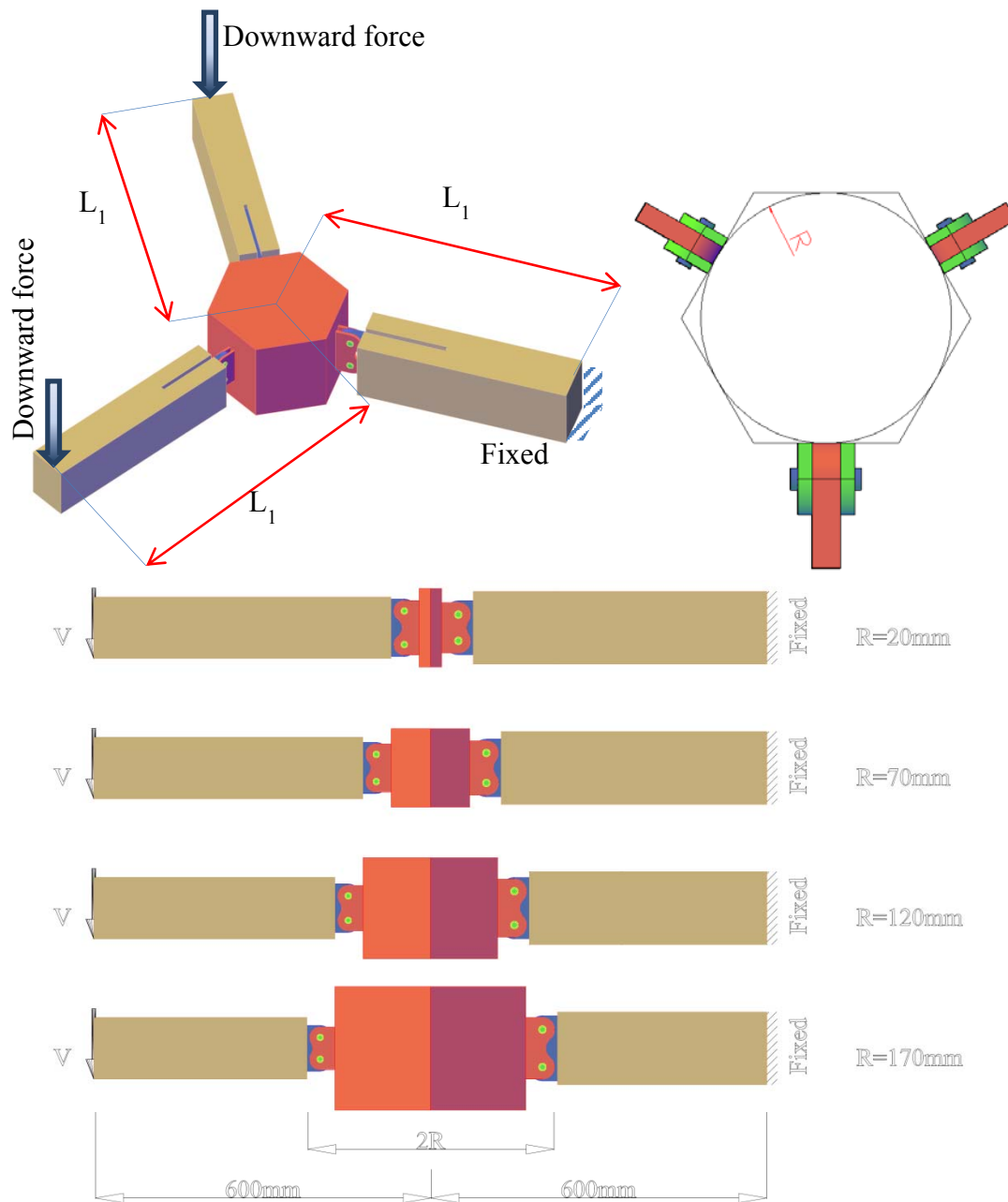


Figure 3-33: 3-way nodes with different design domain sizes subjected out-of-plane shear forces.

The results of the BESO design for different design domain sizes are shown in Figure 3-34.

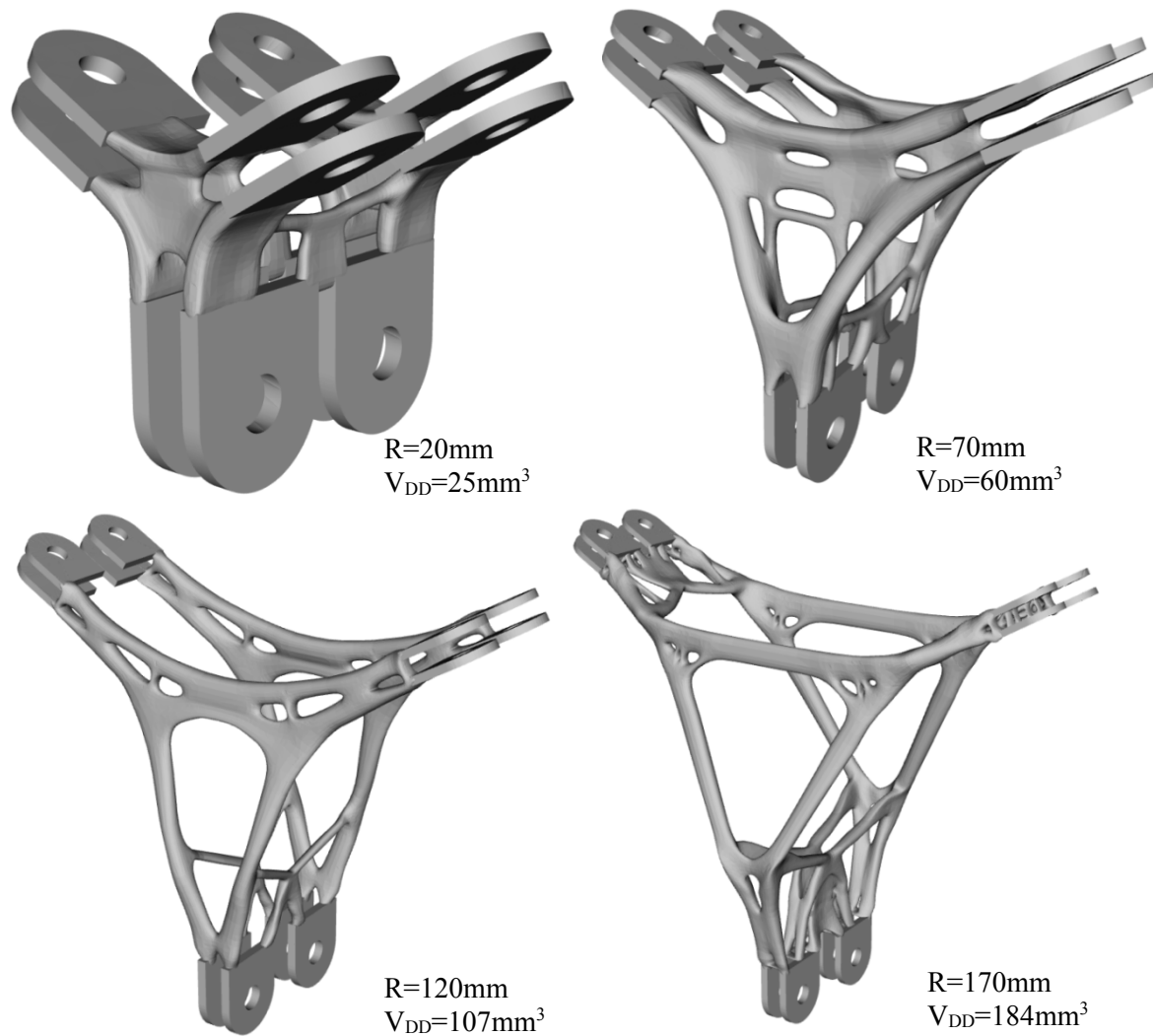


Figure 3-34: The results of BESO design for different design domain sizes.

The volume fraction for each of these structures is set in a way that the stress level of the final design is smaller than the allowable stress level (240MPa). With the increase in the design domain size, more details can be found in the topology obtained by the BESO design. The comparison of these nodes shows that decreasing the size of the design domain would decrease the volume of designed structure (V_{DD}), and consequently reduce the manufacturing cost of the node. The minimum size of the design domain is constrained by the space which is needed for connecting members not to intersect the neighbour connecting members. This space depends on the geometrical and topological properties of the node as well as the size of the member section.

3.6. Smoothing

The surface of the BESO model is always jagged as a result of removing elements from the initial mesh of the design domain (Figure 3-35). There are two disadvantages for the rough surface design. The first disadvantage is the stress concentration at the sharp edges of the BESO design, which would lead to inefficiency of the design. The second disadvantage of having a jagged surface is that it is difficult to be 3D printed as there are too many unprintable sharp corners. Therefore, the rough surface in the BESO model needs to be smoothed. For this purpose, two different methods are used in this study, namely the Laplacian smoothing algorithm and the Non-Uniform Rational Basis Spline (NURBS).

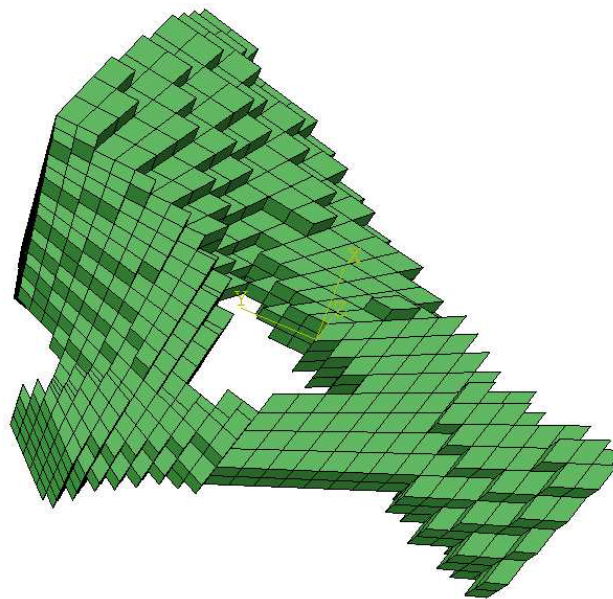


Figure 3-35: The jagged surface of BESO model.

Laplacian smoothing algorithm

The Laplacian smoothing algorithm is a mesh based smoothing method which iteratively modifies the locations of the surface nodes based on the weighted average of the neighbouring surface nodes in a finite element model [6]. In this method, a hollow surface model is firstly generated. Then for each node, a movement vector is calculated. The

movement vector is attained from averaging the vectors connecting the node with its neighbours.

The movement vector for one point of the mesh is illustrated in Figure 3-36.

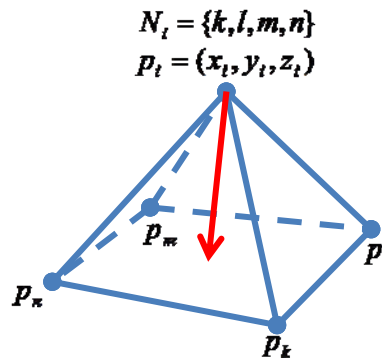


Figure 3-36: The movement of point p_k in an iteration of Laplacian smoothing algorithm.

The amount of the movement can be formulated as Equation (2).

$$\text{Movement vector} \quad \Delta p_i = \frac{1}{|N_i|} \left(\sum_{j \in N_i} p_j \right) - p_i \quad (2)$$

Then the nodes are moved along their movement vectors normalised by a suitable small factor. By iterating this process for a certain number, the final surface is smoothed. A comparison between the unsmoothed and smoothed structural nodes subjected to bending and shear forces (designed in 3.4.2) is shown in Figure 3-37.

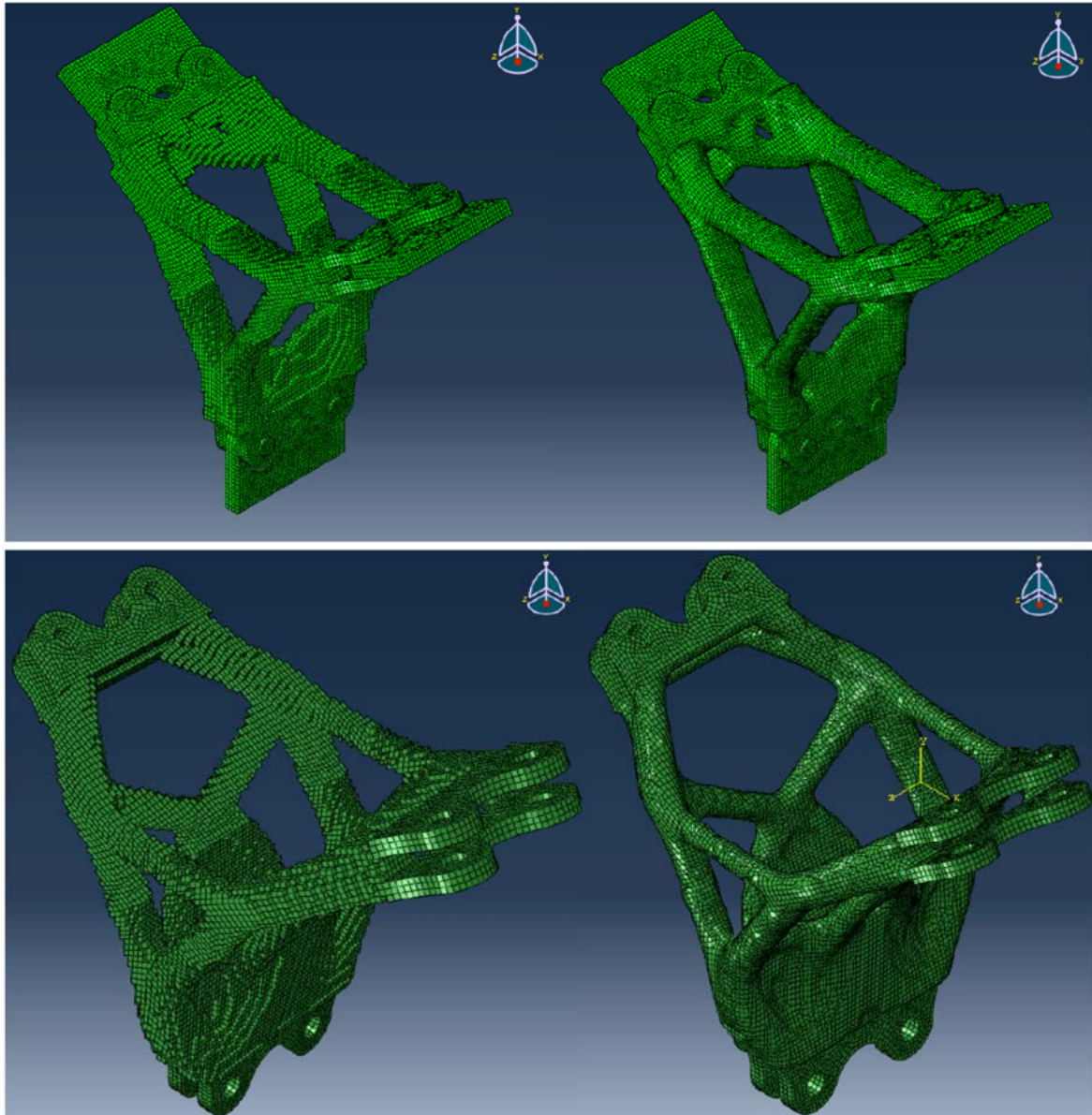


Figure 3-37: Smoothing by Laplacian algorithm.

Figure 3-38 and Figure 3-39 show two topologically and geometrically complex nodes which are designed by BESO and smoothed by Laplacian smoothing algorithm. In fact, the Laplacian smoothing algorithm is not related to the complexity of the topology and geometry of the designed node. Therefore, increasing the complexity of the model does not affect the smoothing performance.

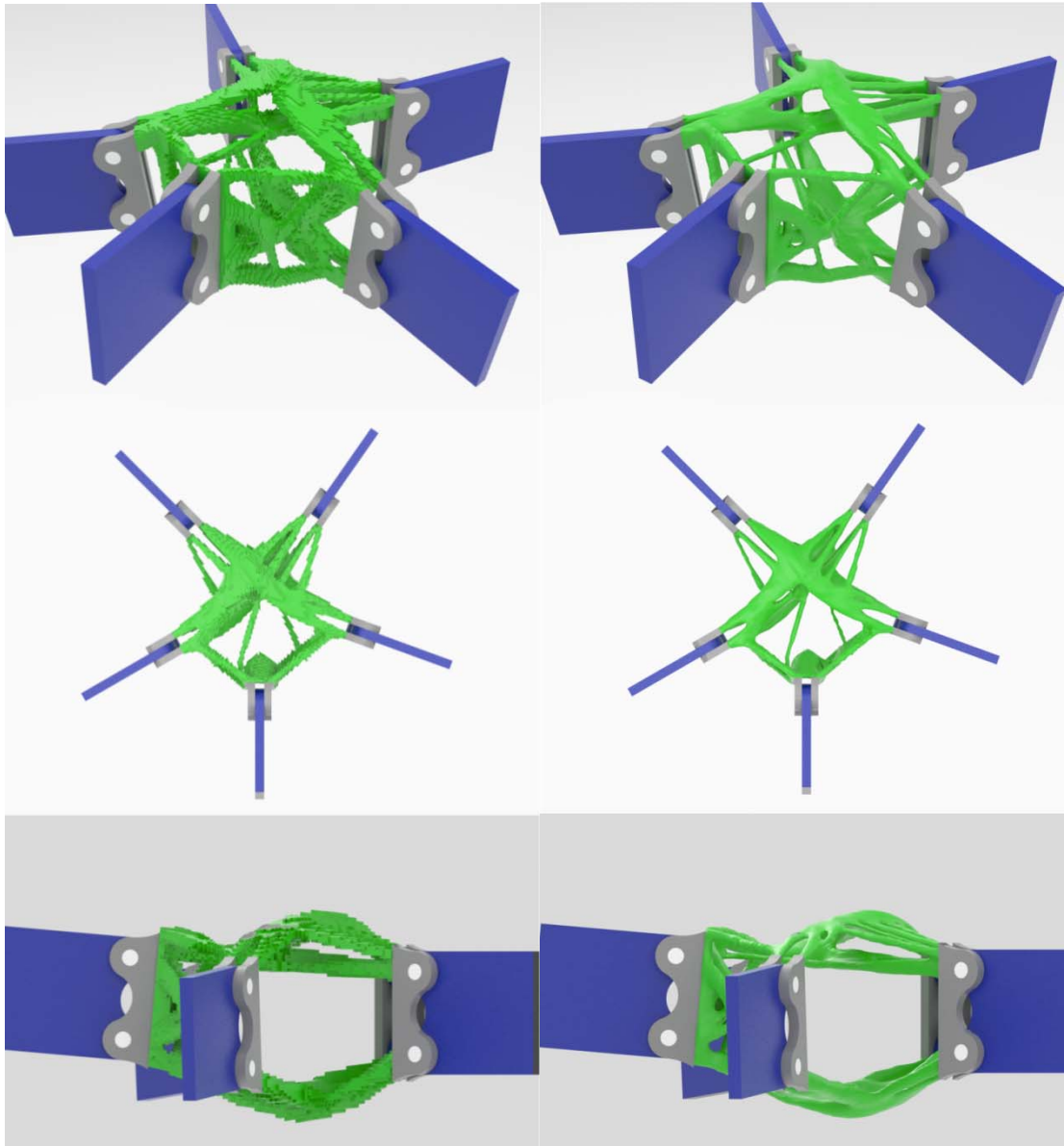


Figure 3-38: Smoothing by Laplacian algorithm.

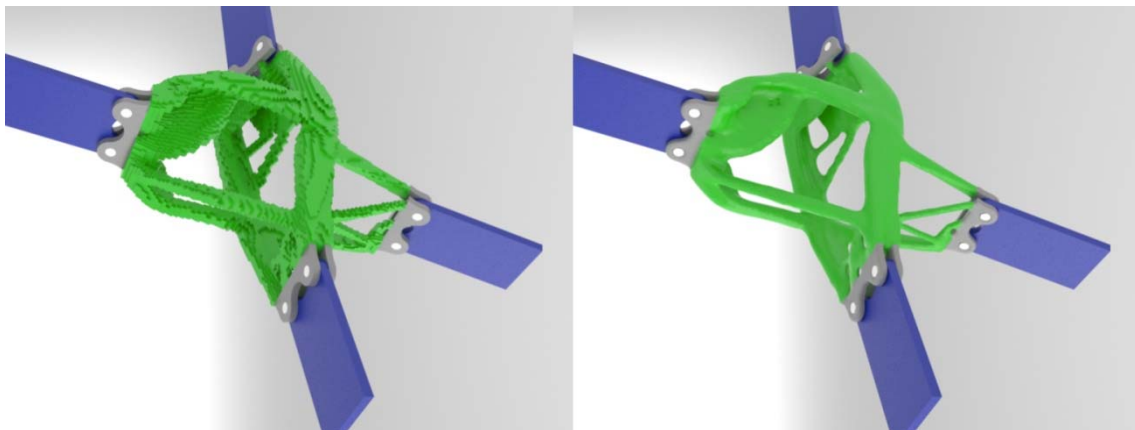


Figure 3-39: Smoothing by Laplacian algorithm.

Figure 3-40 shows unsmoothed and smoothed models of the evolution of the BESO design for a non-symmetrical three-way node designed by BESO under an arbitrary load condition.

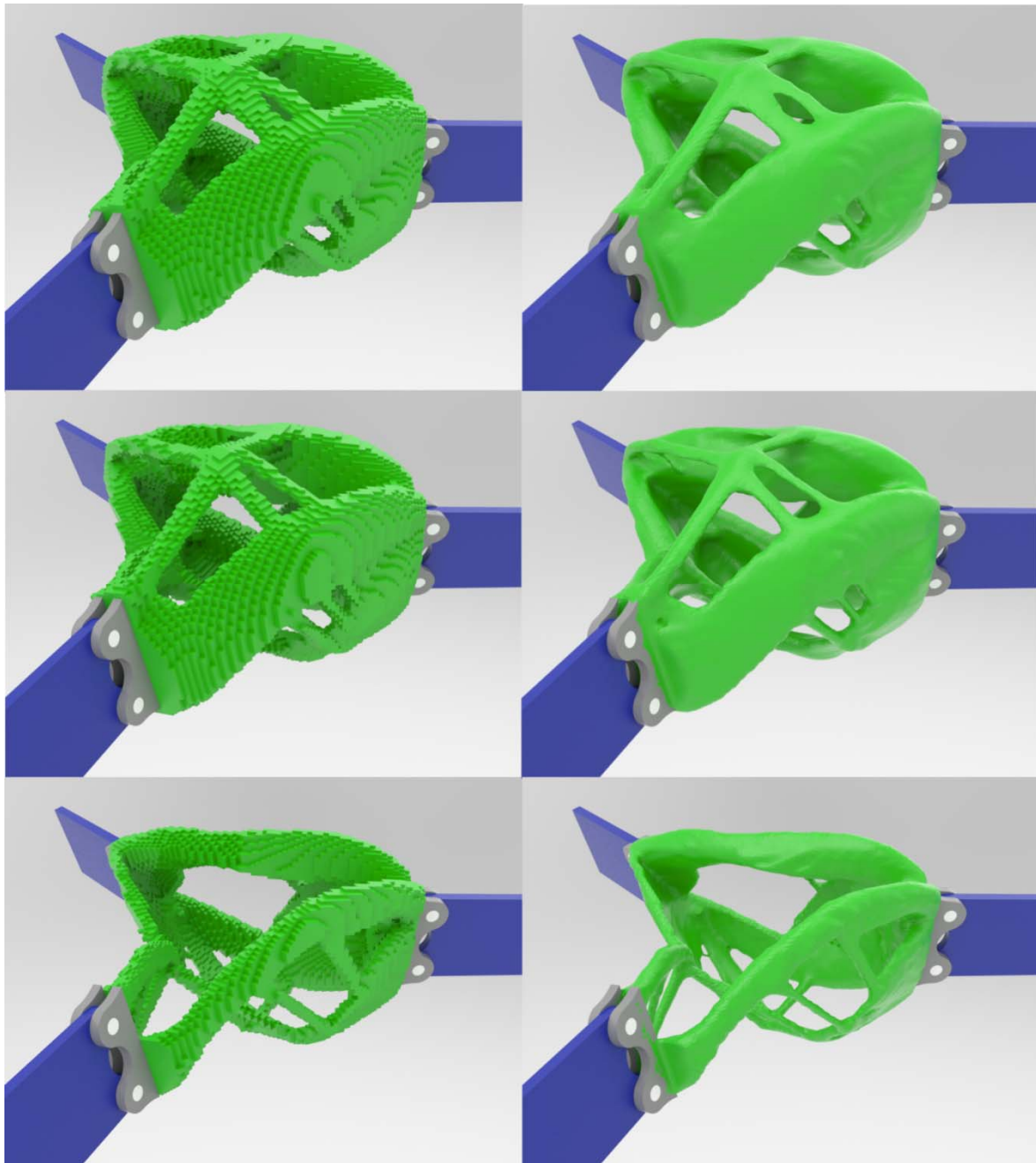


Figure 3-40: Smoothing different iterations of a node by Laplacian algorithm.

As can be seen in these samples, the size of some structural members is significantly decreased in the smoothed model compared to its original design. The reduction in size is dependent on the initial size of the member and the number of smoothing iterations. To have a better understanding of the changes in the cross-sectional area with the changing member

size, seven members with element number from 1 to 49 are modelled. Different iterations of Laplacian smoothing algorithm are applied to these models. Details of the seven models are shown in Figure 3-41.

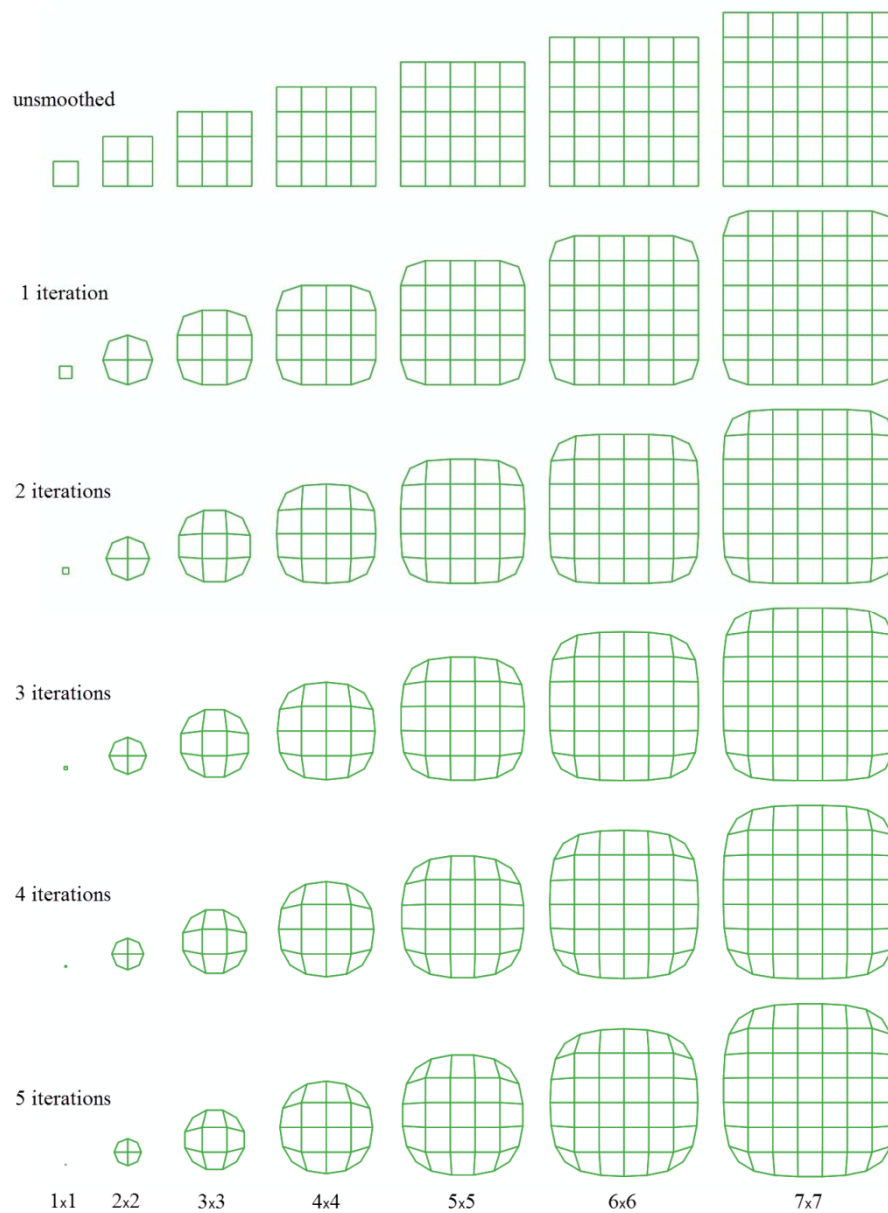


Figure 3-41: Smoothing members with different sizes and iterations of Laplacian smoothing algorithm.

The area reduction ratios for these members with different iterations of smoothing are shown in Figure 3-42. Based on this diagram, to limit the area reduction ratio to 10% in five loops of

smoothing, the number of elements in the cross-section of a structural member should be more than 50 approximately (when a mesh of uniform element size is used).

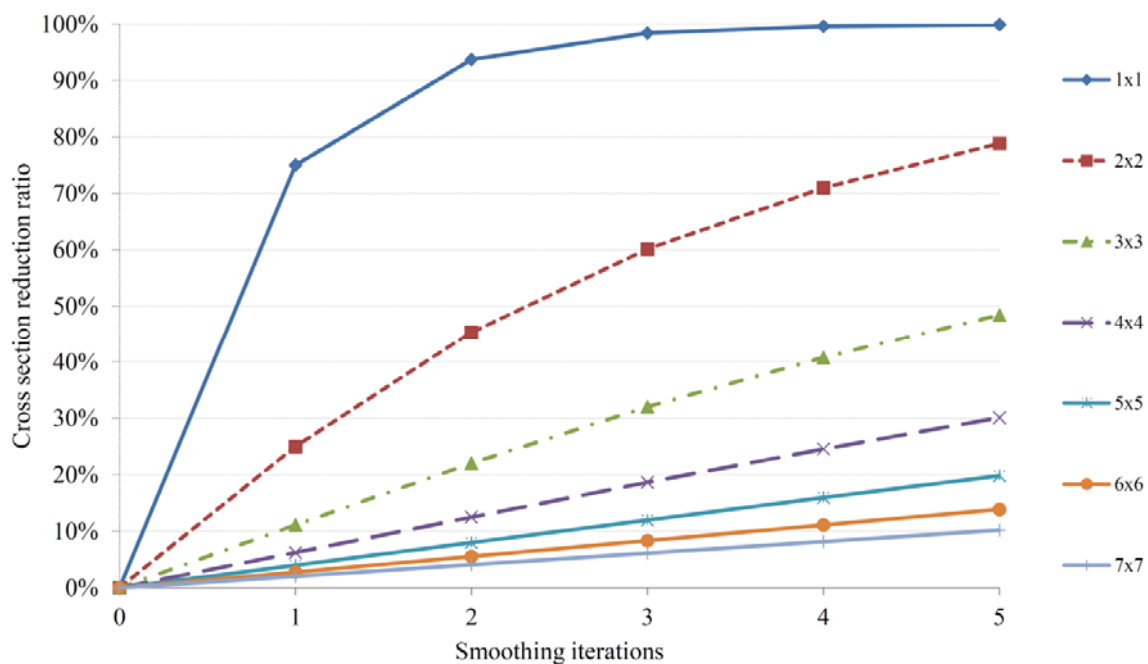


Figure 3-42: The area reduction ratio for members with different cross-section size smoothed by different iterations of Laplacian smoothing.

Non-uniform rational Basis spline (NURBS)

Non-uniform rational Basis spline (NURBS) is a mathematical model commonly used in computer graphics for generating and representing curves and surfaces. It offers great flexibility and precision for handling both analytic (surfaces defined by common mathematical formulae) and modelled shapes. The surface is controlled by a series of control points and a polysurface. A part of a polysurface, which is used to control the NURBS surface, is shown in Figure 3-43. Blue points and yellow lines are the control points and their connectivity respectively. In this study, EVOLVE 2016 [7] is used to smooth nodes using NURBS surfaces.

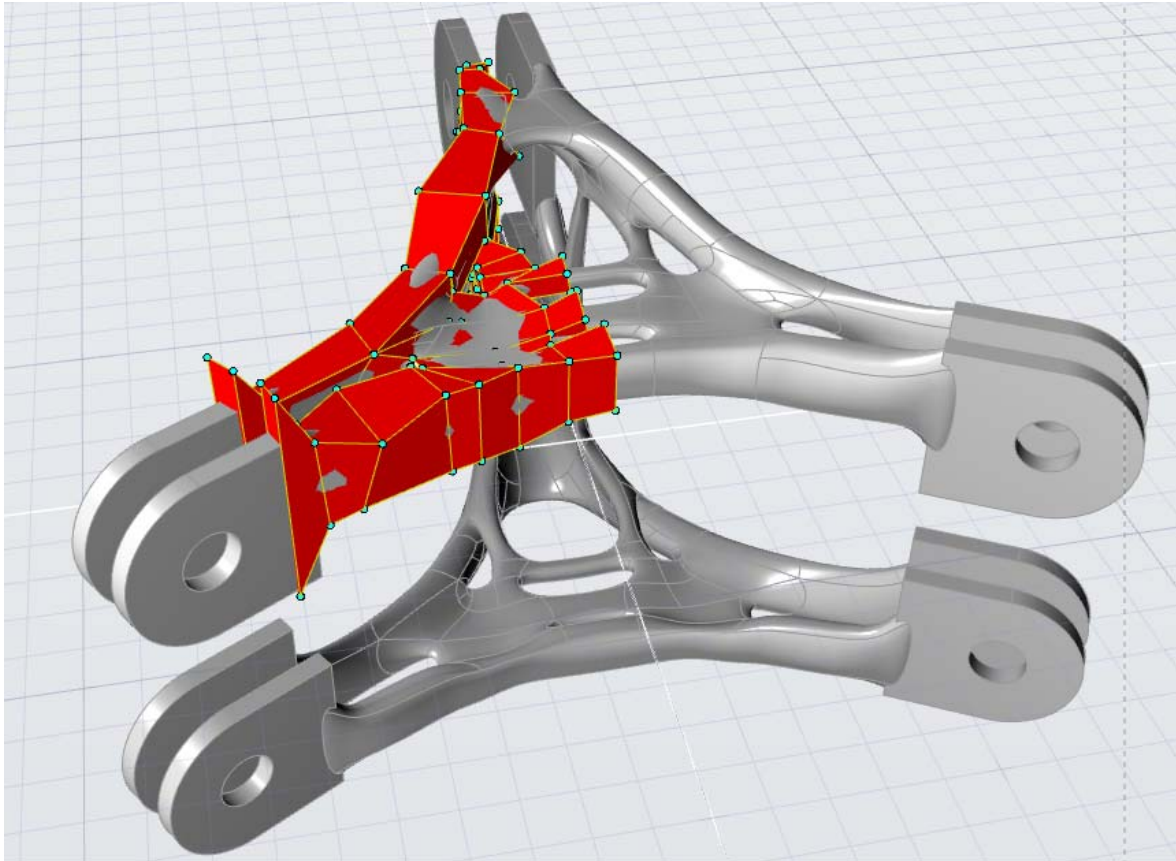


Figure 3-43: Red part: polysurface of control points for smoothing the node; gray part: Nurbified polysurface as the smoothed geometry for the node.

This NURBS smoothing procedure in Evolve 2016 is performed manually section-by-section. Non-design parts are modelled separately by normal solid objects and merged with the smoothed design part. The final surface of the smooth node is shown in Figure 3-44.

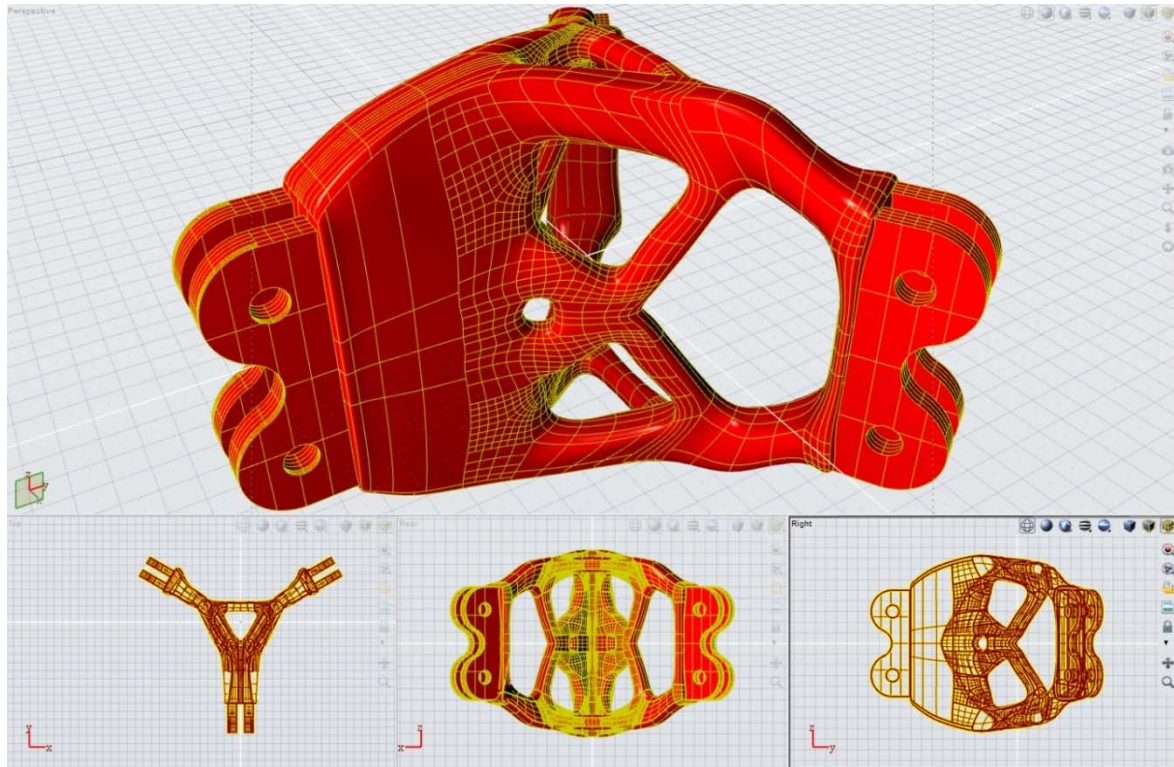


Figure 3-44: Different perspectives of the smoothed shear node using EVOLVE 2016.

The final result using NURBS surfaces leads to a perfectly smoothed surface which is suitable for 3D printing purposes. A rendered view of the smoothed shear node is shown in Figure 3-45.

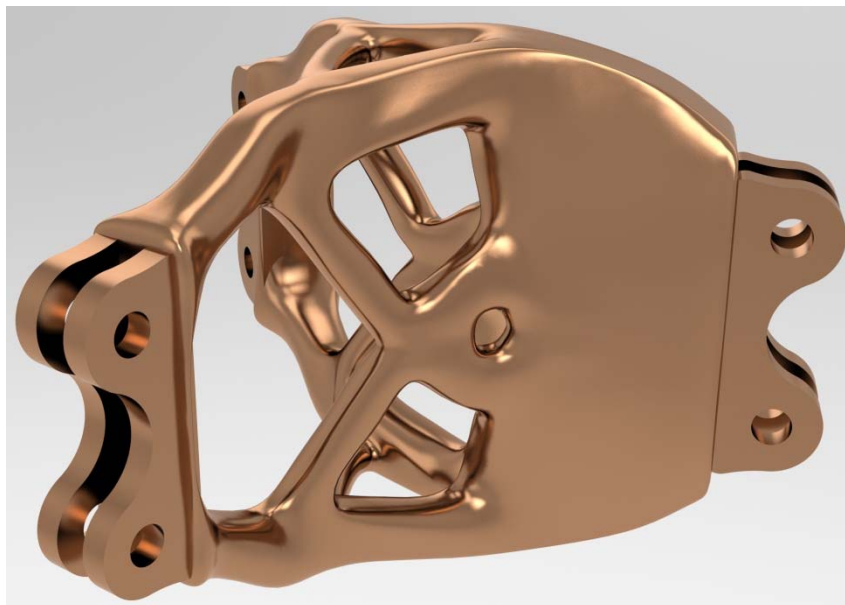


Figure 3-45: A rendered view of the shear node smoothed using EVOLVE 2016.

A comparison of the shear nodes smoothed by NURBS surfaces and Laplacian smoothing algorithm is given in Figure 3-46. It is seen clearly that the NURBS surface is smoother than that obtained from the Laplacian smoothing algorithm. Besides, no cross-sectional area reduction occurs in the members smoothed by the NURBS method.

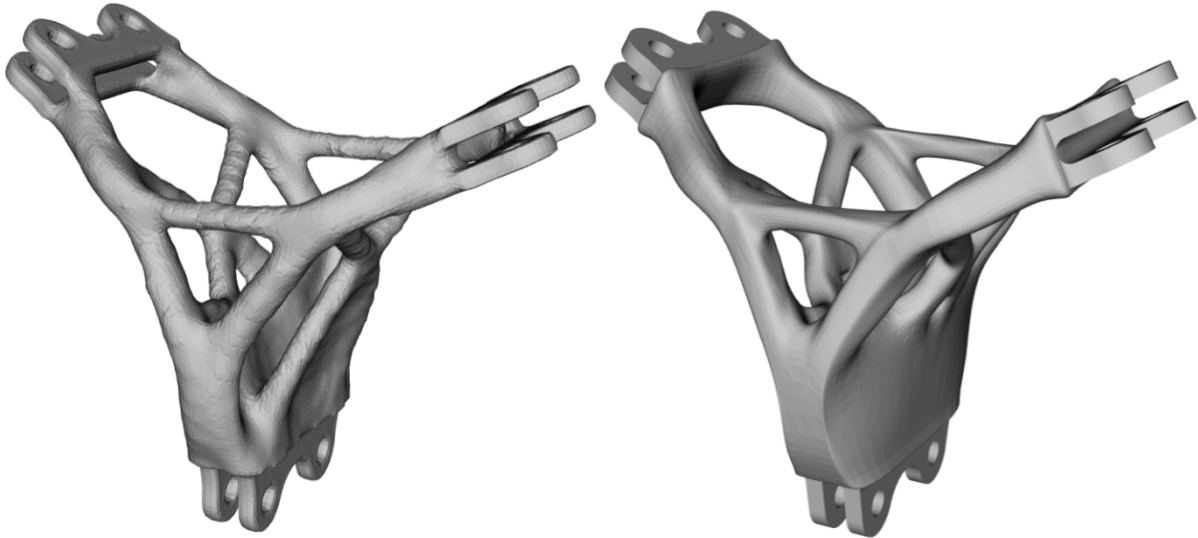


Figure 3-46: Comparison of shear nodes smoothed by Laplacian smoothing algorithm (left) and NURBS surfaces (right).

3.7. Manufacturing:

In this study, two additive manufacturing methods, namely Selective Laser Melting (SLM) and Binder Jet method, are used to manufacture the designed nodes and find out the challenges in 3D printing nodes.

In the Binder Jet method, a binder is selectively deposited onto the powder bed, bonding these areas together to form a fragile and porous part one layer at a time. Then a solid and strong part will be made by flowing bronze into the pores in an infiltration process [8]. The challenges of this method are related to removing the unused powder from the fragile and porous part. In the de-powdering process, slender structural members of the 3D printed object are susceptible to failure due to the mechanical vibrations. Some comments that received

from the manufacturer about the additive manufacturing problems of bending node are shown in Figure 3-47 to Figure 3-48.

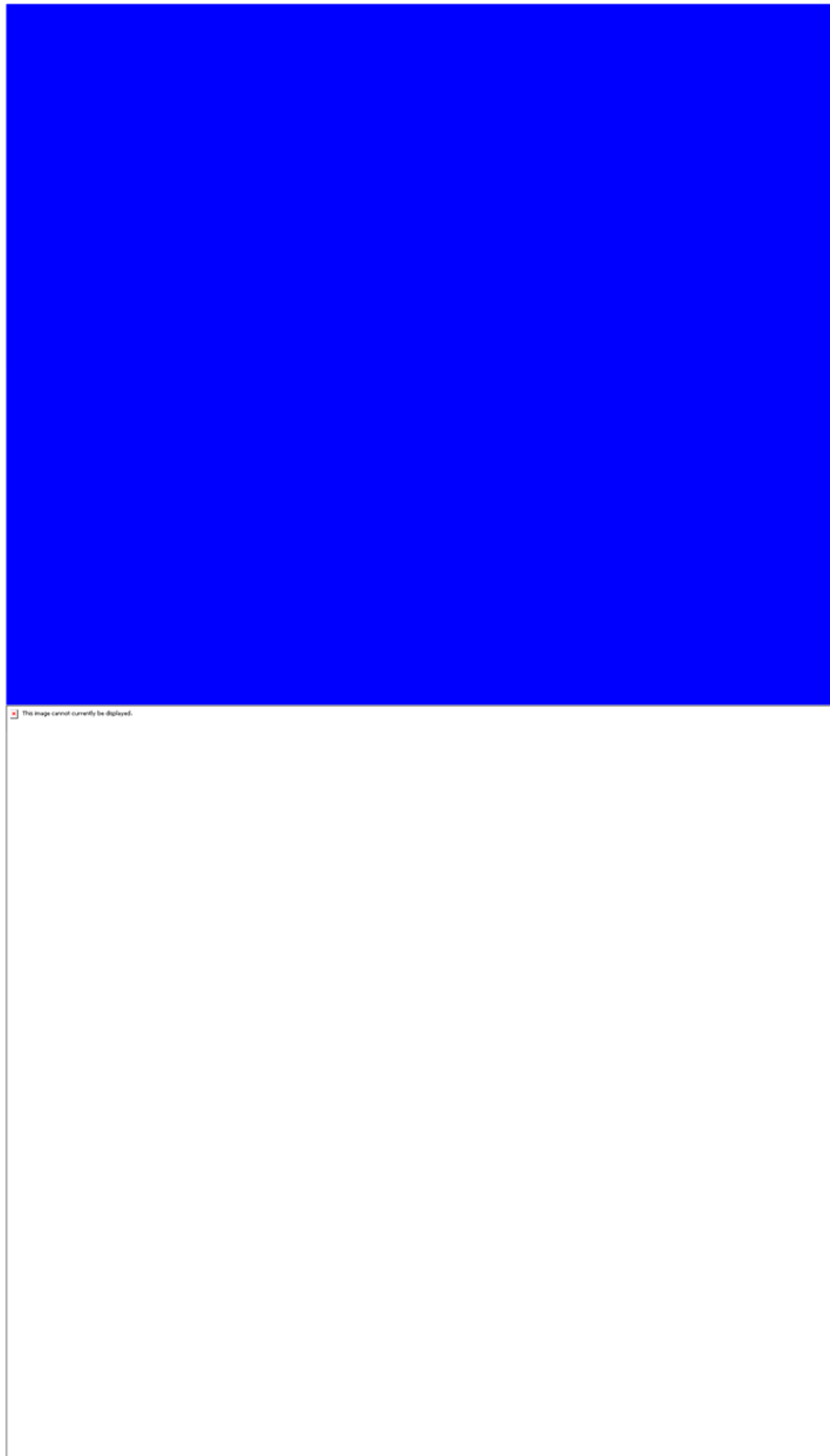


Figure 3-47: Slender members of the bending node need to be strengthened in order to avoid breaking during de-powdering in the Binder Jet method.

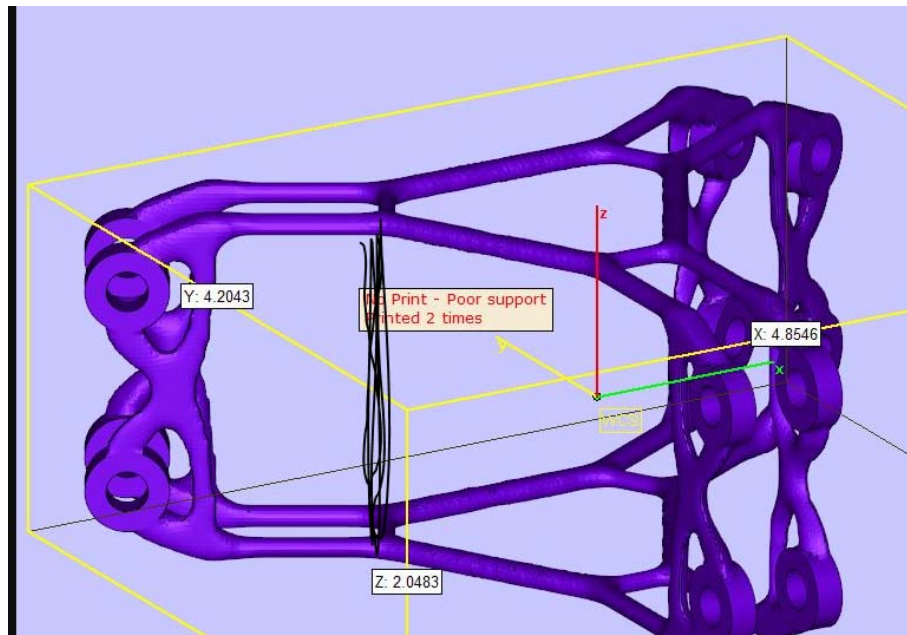


Figure 3-48: Additional members need to be added to the model in order to avoid breaking during de-powdering in the Binder Jet method. Similar comments are received for a five-way node as shown in Figure 3-49.

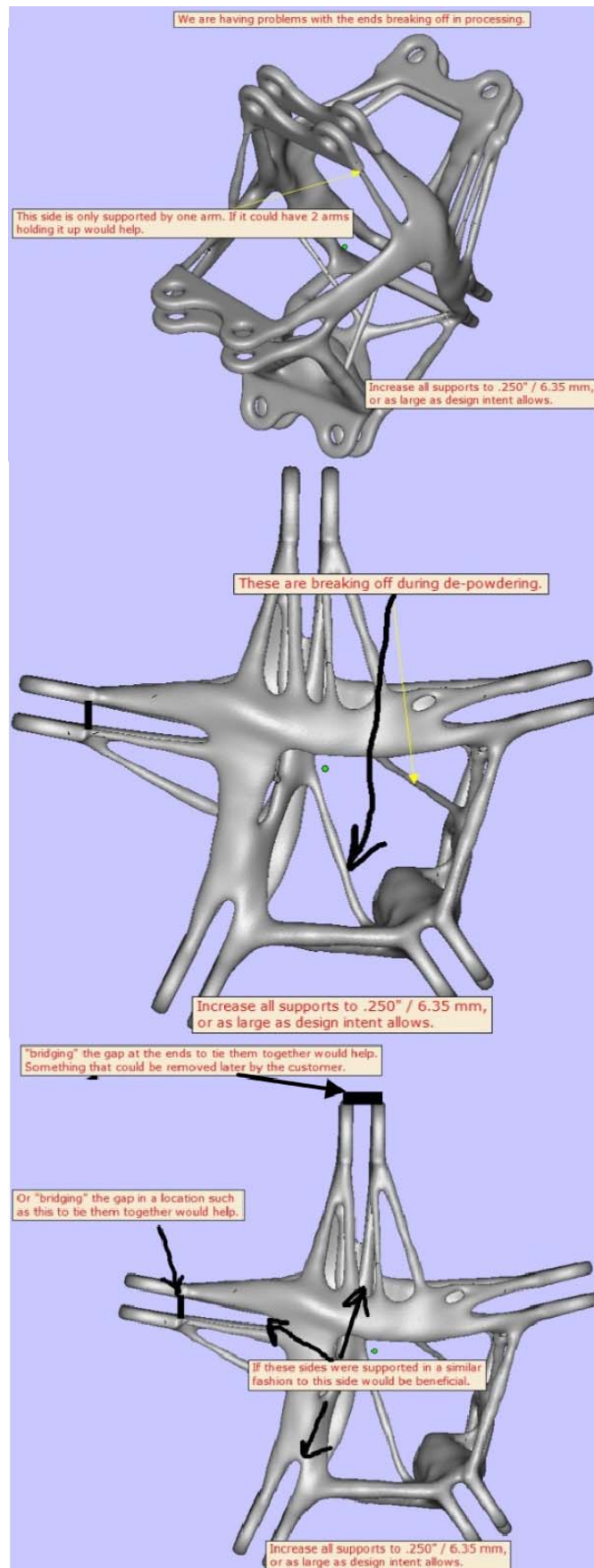


Figure 3-49: Weaknesses points of the models for 3D printing with the Binder Jet method



Figure 3-50: In-plane bending node successfully 3D printed by the Binder Jet method.

A successfully manufactured node using the Binder Jet method is shown in Figure 3-50. The contours of printing layers can be seen on the surface of the model.

In the SLM method a high power-density laser is used to melt and fuse metallic powders together. Additive manufacturing process in SLM can be summarised in Figure 3-51.

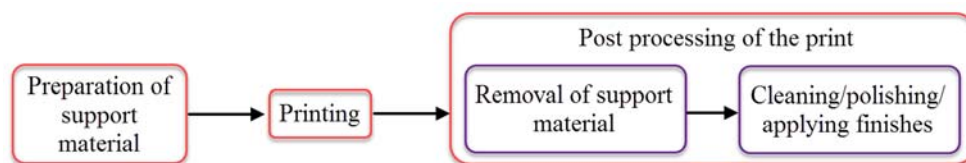


Figure 3-51: SLM additive manufacturing process.

Preparation

In this step, a lattice structure as supporting material is designed to be printed with the object. The supporting material provides temporary support for overhanging material during the printing process. In SLM printing method, the structure must be laid up on a layer below. As such, if the optimised form includes negative angles, large irregular openings or hanging

structure, additional support material will be required for a successful print as shown in Figure 3-53.

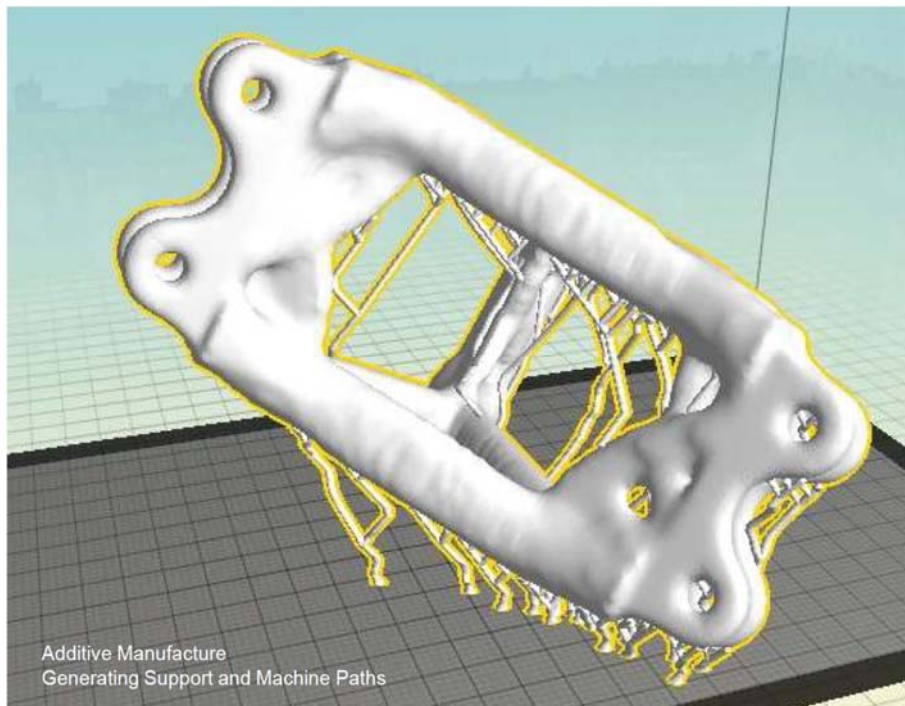


Figure 3-52: Additional support material for printing node using SLM method.

Although commercial software is available to generate the support material within the model, there is still a lot of manual work required from a competently trained AM printing technician. Minimising support structure could speed up the printing and save post-processing time, and hence significantly increase the economy of the product. Figure 3-53 shows the designs of support materials for 3D printing in two different directions.

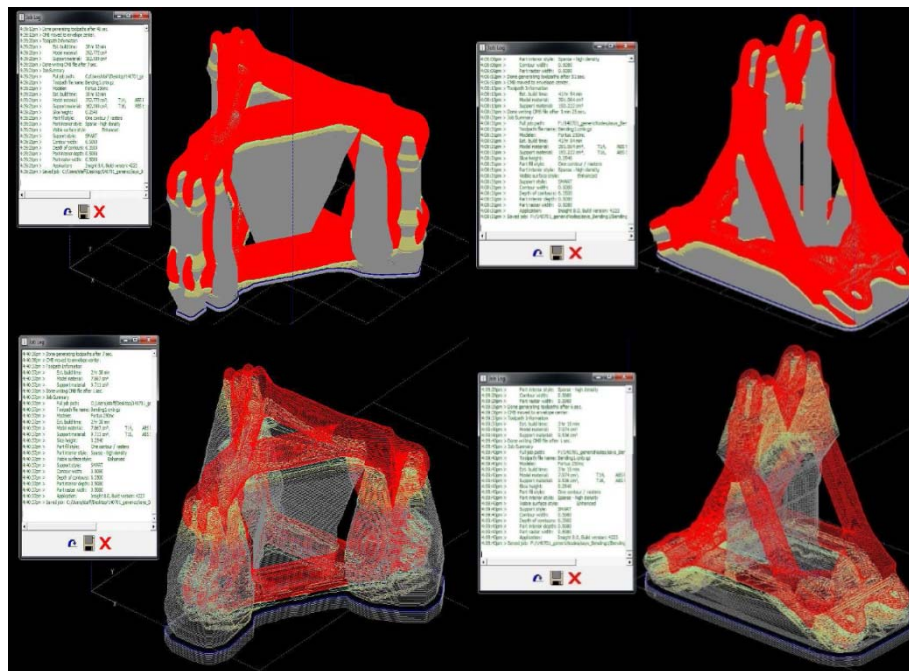


Figure 3-53: Designs of additional support material for printing node using the SLM method.

Printing

In this study, a selective laser melting machine in the Advanced Manufacturing Precinct (AMP) at RMIT University is utilised to print metal node using alloy powders. The metal powder is deposited in fine layers, and then a high intensity laser selectively melts the powder which forms the piece being printed. The process is repeating layer-by-layer until the final piece is “printed”.

Post processing

The final piece needs to be cut from the base plate. The support structure also needs to be removed and the surface smoothed, which adds time and cost to the process. Thus the optimisation of the support structure is an important step for achieving a cost effective solution.



Figure 3-54: Post-processing of a printed metal node.

3.8. Conclusions

In this chapter, a number of nodes are designed for various loading and boundary conditions to obtain a better understanding of the structural behaviour of nodes. The configuration of the node is different for basic load cases which are perpendicular to the node surface (axial, out-of-plane and in-plane bending) is different from the basic load cases which are tangent to the node's surface. Considering the double-layer connection system for the nodes (top and bottom bolts) which provides adequate out of plane resistance and stiffness for the nodes, the configuration of the BESO design consist of two separate top and bottom parts. In load cases where the direction of applied loads in top and bottom parts are the same (axial, in-plane

bending), the substructures are separated. But, in load cases where the top and bottom loads are reverse (out-of-plane bending), a connection forms between top and bottom substructures. In torsion load case the BESO design is a spherical lattice. A case study of a gridshell structures with topologically optimised and additively manufactured nodes is described. The challenges of smoothing and additive manufacturing of nodes are investigated. The Laplacian smoothing algorithm is very simple to apply regardless of the complexity level of the node. But the resolution of result depends on the mesh size of the node. Besides, the member sizes are node accurate after Laplacian smoothing. In contrast, using NURBS surfaces for smoothing, results in a very smoothed and accurate geometry, but the hardship of manual process of applying this method highly depends on the complexity of the topology and geometry of the node.

Manufacturing a number of the nodes using different additive manufacturing methods showed that unlike the conception which is induced by the definition of AM as an automatic manufacturing method, in most of the time, manual process is involved in both design and manufacturing steps. In design step, providing the reinforcement for specific loads involved in AM process should be considered. In manufacturing step, post processing of the nodes surface should be carried out.

References

1. Peters, B. and H. Whitehead (2008), Geometry, form and complexity, *Space Craft*. 20-33.
2. Querin, O.M., Steven, G.P. and Xie, Y.M. (1998). Evolutionary structural optimisation (ESO) using a bidirectional algorithm. *Engineering computations*. **15**(8): 1031-1048.
3. Huang, X. and Xie Y.M. (2010), *Evolutionary topology optimization of continuum structures: methods and applications*: John Wiley & Sons.
4. Yang, X. Y., Xei, Y. M., Steven, G. P., & Querin, O. M. (1999). Bidirectional evolutionary method for stiffness optimization. *AIAA journal*. **37**(11).
5. Arup company, Retrieved from arup.com/
6. Herrmann, Leonard R. (1976), "Laplacian-isoparametric grid generation scheme", *Journal of the Engineering Mechanics Division*, **102** (5): 749–756.

7. Altair, Solid thinking Evolve, Retrieved from <http://solidthinking.com/product/evolve/>
8. Varotsis, A.B. *Introduction to Binder Jetting 3D printing*. Available from: <https://www.3dhubs.com/knowledge-base/introduction-binder-jetting-3d-printing>

CHAPTER 4

COMPARISON BETWEEN NEW DESIGN AND CONVENTIONAL
DESIGN OF NODES FOR GRIDSHELL STRUCTURE

Chapter 4: Comparison between new and conventional designs of nodes for gridshell structure

An important question in optimising structural design is how efficient it is compared to the conventional designs. In this chapter, two new design approaches are presented to design structural nodes of complex shapes for gridshell structures, seeking improved structural performance and design efficiency. One of the new approaches is to use the transitional section method, in which the NURBS surfaces are utilised to connect beam members with each other, assuming that additive manufacturing (AM) method is employed for the fabrication. Two versions of nodes are generated using this method: one with sharp edges, and the other with rounded edges obtained from the Laplacian smoothing algorithm. The second approach adopted in this study for node design is the topology optimisation using the bi-directional evolutionary structural optimisation (BESO) method. By using the BESO algorithm, a node with complex geometry can be automatically generated and manufactured through AM. In this study, various loading conditions are considered in the analysis and optimisation design processes. Detailed design methodologies are firstly introduced, and then the structural performances of the new designs are compared with those of conventionally designed nodes. Finite element analyses are conducted to evaluate the stress distribution, maximum stress and mean compliance of different node designs. The results show that the maximum von Mises stresses of the newly designed nodes are significantly lower than those of the conventional nodes. The BESO designed node is shown to be the most efficient due to the highest stiffness, lowest structural volume and lowest maximum stress among all four nodes. The newly designed nodes also have more uniform stress distributions, as well as higher tolerance to a broad range of loading conditions. Moreover, the results show that the application of Laplacian smoothing in node design could effectively reduce the stress concentration. Prototypes of the newly designed nodes are successfully fabricated by additive

manufacturing, which enables the rapid and precise manufacturing of customized nodes designed to suit specific loading and boundary conditions.

4.1. Introduction

Gridshells, also called lattice shells or reticulated shells, are created by combining the geometry of shell and topology of a grid.

Figure 4-1 shows six different grid types which are used in gridshell structures. Depending on the grid system, the number of connecting beam members in nodes varies. For example, the majority of nodes in grid type (a) in Figure 4-1 are three-way nodes, while the numbers of the connecting beam members for most of the nodes are four in grid types (b) and (c) and six in grid type (d). Most of the nodes in grid type (e) (which is also known as Voronoi grid system) are three-way nodes. There are equal numbers of eight-way nodes and four-way nodes in grid type (f).

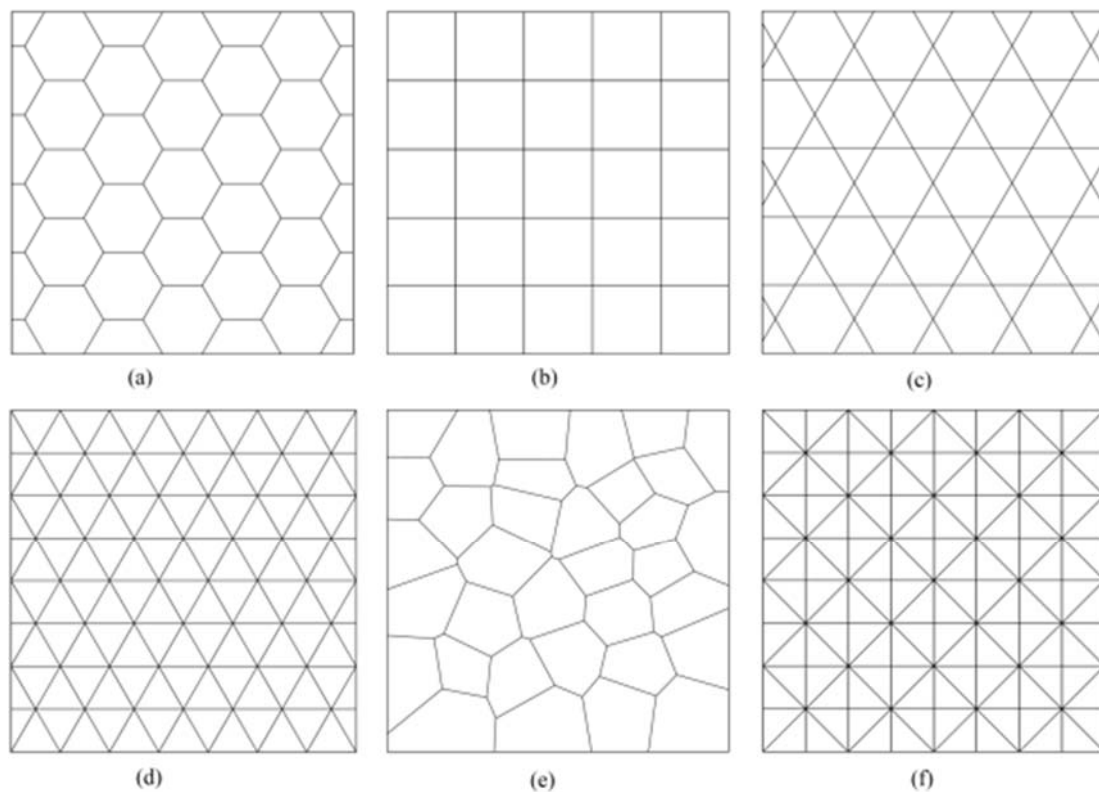


Figure 4-1: Different grid systems in gridshell structures

Geometric non-linearity in gridshell structures may lead to global instability, which is strongly influenced by both the geometric parameters and the joint rigidity [4-8]. It has been reported that, similar to continuous shells, gridshells could collapse in buckling mechanism which is sensitive to imperfections and the stiffness of structural members and nodes [9-13]. Many node configurations have been developed to connect members of gridshell structures [14-16]. However, most of them have limitations in moment capacity, stiffness and manufacturability which would affect the curvature of the gridshell surface [14]. In addition, the cost of manufacturing is a major issue [9-13].

Manufacturing of a large number of customised nodes with complex geometries is a big challenge in conventional manufacturing methods because these methods usually involve cutting and welding individual parts. It has been reported that structural node is one of the most costly parts in constructing 3D structures [14-17]. Also, in conventionally manufactured nodes, a large amount of welds and stress concentrations in sharp edges and connections increase the risk of fatigue failure under repeated loads. Therefore, in cases where complex nodes are exposed to repetitive loads, the transitional sections are used to generate a smoothed geometry and reduce the stress concentration. Besides, the complex form of node is manufactured by casting to avoid welding [18-20]. Laplacian smoothing, a mesh optimisation algorithm [21], is an effective design tool to transform the sharp edges to rounded connections. In Laplacian smoothing, nodes of the mesh are iteratively moved to the geometric centre by weighting the contribution of each neighbouring node in an averaging function [21-23]. Unfortunately, these smoothed nodes with transitional features cannot be precisely fabricated using the conventional manufacturing technologies. However, this can be achieved with high efficiency and accuracy by newly developed additive manufacturing (AM) technologies [24-27]. In this chapter, two different approaches are utilised to design structural nodes for gridshell structures, aimed at finding general ways for designing complex

structural nodes of better mechanical performance. These nodes are more likely to be fabricated through additive manufacturing as they are expected to be lighter than conventional nodes. The first approach is the transitional section design, which connects a simple node centre to the members by transitional volumes. The second approach is the bi-directional evolutionary structural optimisation (BESO) method, which seeks the best performance of the entire node whilst satisfy various constraints [28]. In this chapter, a typical six-way arbitrary node is extensively studied by using different design methods. The node is supposed to connect six rectangular hollow section steel beams. To make the study more general, all possible rotations of the connecting beams are defined, which brings the most general geometrical complexity for the node. To minimise the stress concentration in sharp edges, Laplacian smoothing algorithm is used to obtain the final topologies in both design approaches. Conventional concepts of structural node design which are used in Sun Valley project of the Expo 2010 Shanghai (Sun Valley node) [29] and Westfield Shopping Centre in London by Seele company (Seele node) [30] are utilised to design two nodes with similar geometrical, connectivity and topological conditions. The mechanical performances of the new and conventional nodes are assessed by finite element modelling and compared with each other. The volumes, stiffness and the maximum von Mises stresses of the newly designed nodes and the Sun Valley and Seele nodes are investigated. Prototypes of the newly designed transitional node and the BESO node are precisely fabricated by additive manufacturing.

4.2. Design of structural nodes for gridshell structures

4.2.1. Loading conditions

As discussed before, the internal forces in gridshell structures are mostly in-plane as a result of double curvature of the structure. In case of triangular grid, in which most of the nodes are

six-way nodes, the in-plane internal forces are mainly the axial loads acting in the beam members, and these axial loads usually govern the design process of the nodes. Therefore, the six-way transitional node is predominantly subjected to axial loads along the directions of the six connecting beams, i.e., p_1 to p_6 as shown in Figure 4-2. It should be noted that these loads are aligned with the centre line of the members. Therefore, they are not in the same plane. The direction of each of these loads in space is defined by three angles α , β and γ as shown in Figure 4-3. Considering the equilibrium equations of the node, the following equations should be satisfied by the applied loads

$$\sum F_x = \sum_{i=1}^6 p_i \times A_i \times \cos(\alpha_i) \times \cos(\beta_i) = 0 \quad (1a)$$

$$\sum F_y = \sum_{i=1}^6 p_i \times A_i \times \sin(\alpha_i) \times \cos(\beta_i) = 0 \quad (1b)$$

$$\sum F_z = \sum_{i=1}^6 p_i \times A_i \times \sin(\beta_i) = 0 \quad (1c)$$

where p_i is the pressure applied on the end surface of member i , A_i is the cross-sectional area of member i , and α_i and β_i are the directional angles of member i . The number of variables is six and the number of equations is three. This means there are infinite answers for the equations. But, for the design purpose, 25 answers are generated randomly and sorted based on the sum of the squared stresses, $S = \sum_{i=1}^6 (p_i)^2$. Top five load cases (LC_1 to LC_5) are selected to study the structural responses of the designed nodes.

Table 4-1 lists the five different load cases which are used for all the designs and numerical simulations in this study.

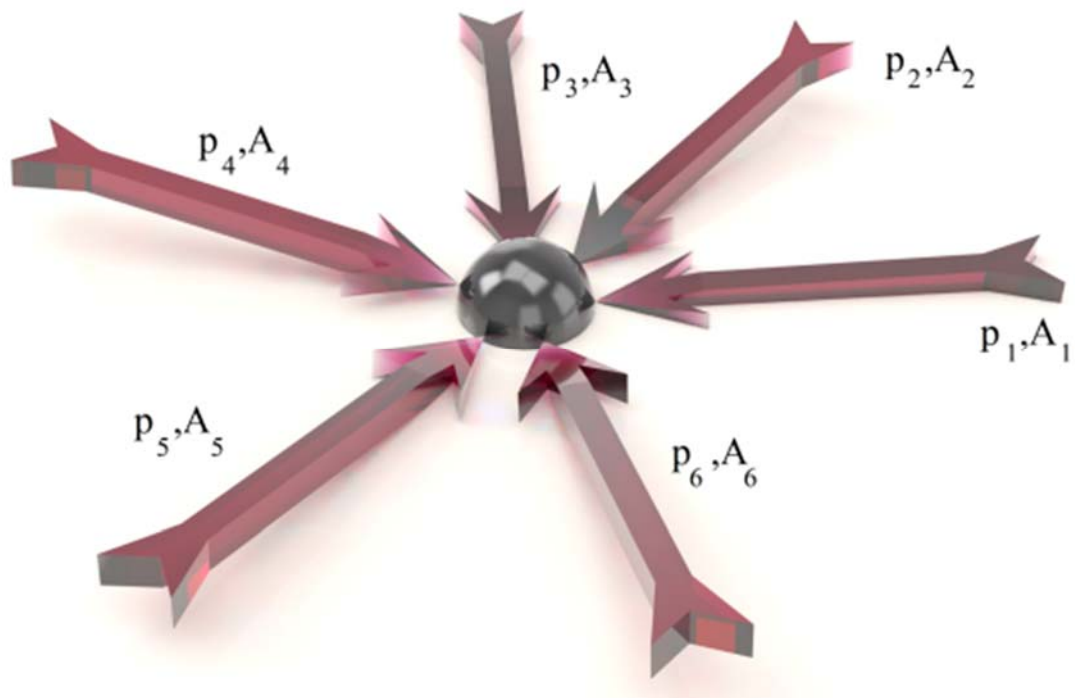


Figure 4-2: Loading and boundary conditions of a transitional node.

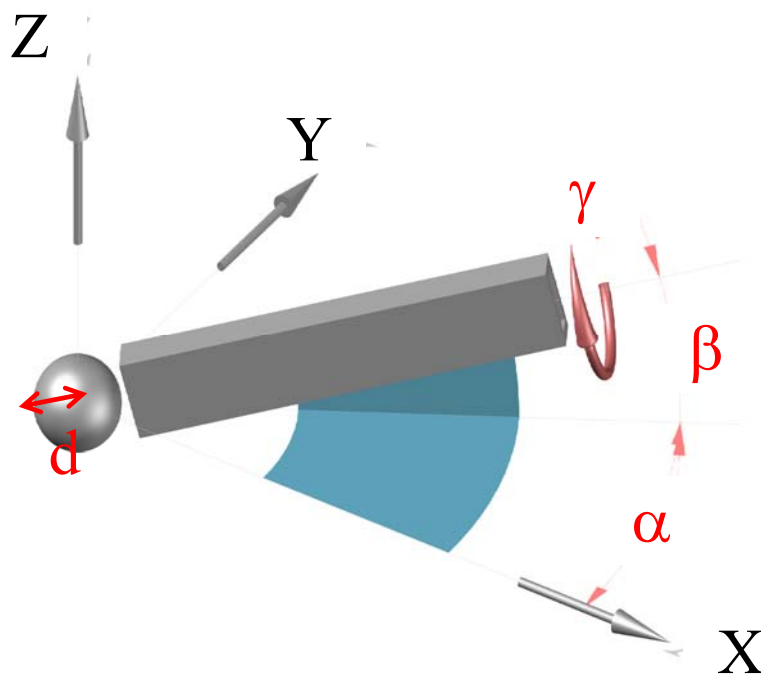


Figure 4-3: The spatial position of a member determined by three rotation angles in Cartesian coordinate.

Table 4-1: Summary of the five different load cases in this study.

Load cases	Directional axial pressure on members (MPa)*					
	P_1	P_2	P_3	P_4	P_5	P_6
LC_1	60	-60	-47	60	-34.375	-55.9
LC_2	20.7	20.7	-60	20.7	41.9	-58.9
LC_3	-27.1	68.6	-24.3	-26.1	68.6	-15.1
LC_4	60	-35.65	60	-18.45	60	-23.75
LC_5	-48	14.72	4.42	-7.6	-48	48

*Negative pressure values indicate tensile load.

4.2.2. Transitional section design

Structural nodes in gridshell structures are usually connecting beams coming from different directions with different sectional rotations. The technology used for manufacturing the nodes determines the level of simplicity needed for the node geometry and the node design concept. This is because a more advanced manufacturing technology enables the designer to utilise more complicated node geometries. In conventional manufacturing methods, the compatible design concept usually imposes high degree of constraints to the geometry of the node. These constraints make the geometrical properties of the node dependent on the geometrical and topological conditions of the structure rather than the structural requirements. Thus, the conventional nodes in gridshell structures are usually structurally overdesigned. In the transitional design approach applied to the node design in this section, the geometrical parameters of the node are more affected by the structural requirements compared to the conventional design approaches. This approach contains two successive stages. The first stage is the design of the centre part of the node, assuming a flat situation for the connecting beams, i.e. all beam members are laid in the plane of the node and have no rotation in section. In the second stage, the beam members and the centre part are connected using transitional volumes. As shown in Figure 4-4, the transitional volume contains curved transitional side surfaces and two flat ends. The flat ends are connected to the member at one end and the

centre part of the node at the other as shown in Figure 4-5. The side surfaces are generated using b-spline curves. This arrangement creates a smooth transition of the volume. The node designed by this method is named transitional node in this chapter.

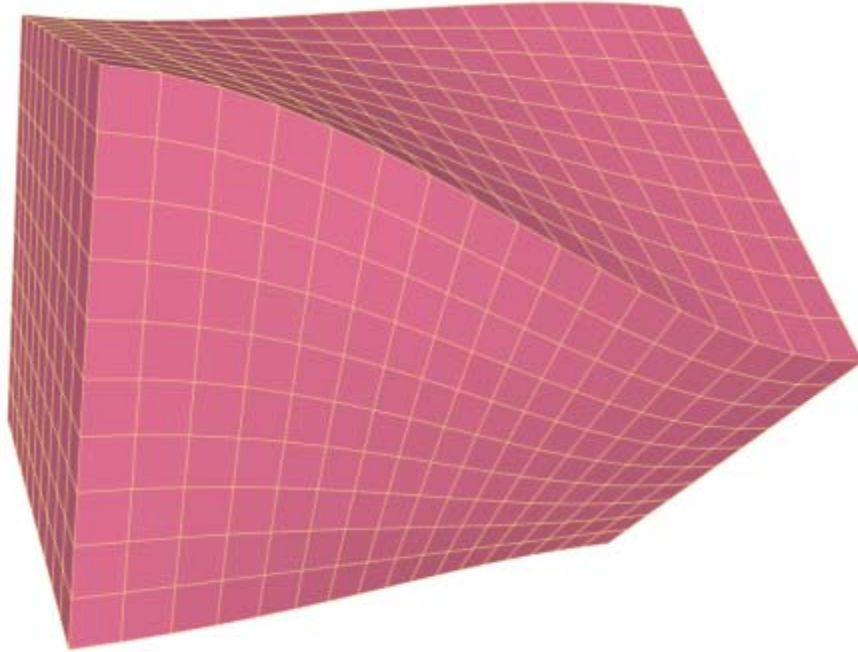


Figure 4-4: An illustration of a transitional volume with two rectangular end sections of different sizes in a twisted angle.

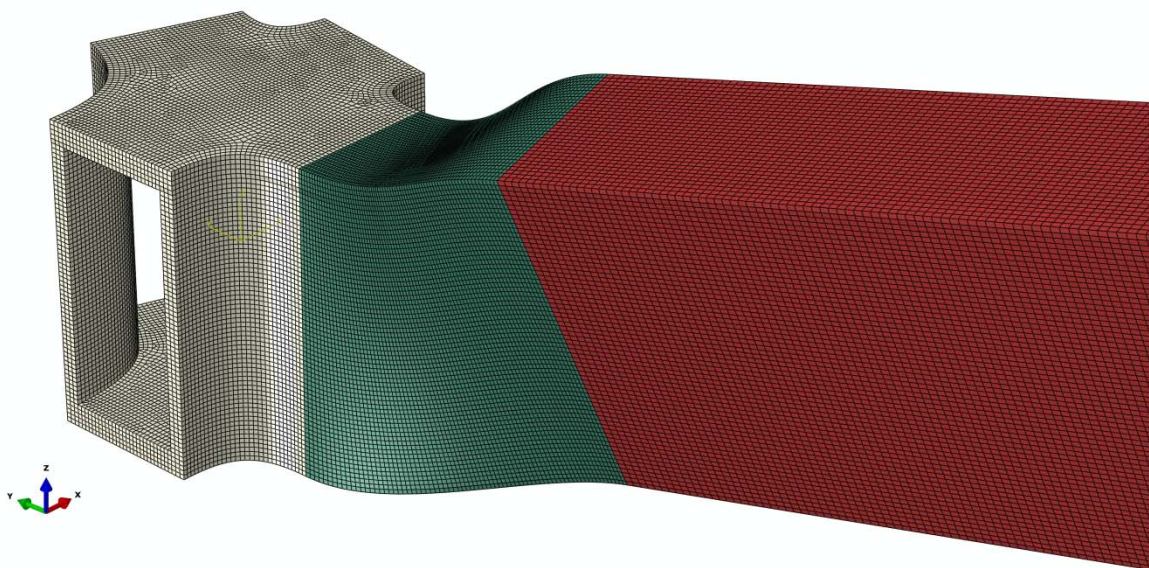


Figure 4-5: A transitional volume connecting a beam member to the centre part of a node.

The geometrical design parameters of the nodes in gridshell structures are categorised into two groups, including beam section parameters and beam orientation parameters. To define the geometrical design parameters related to the orientation of the beam, it is easier to use local axis of the node. The vector normal to the structure surface at the location of node is used as the third local axis (z). The tangent plane to the shell at the location of the node is called the node's plane. The projection of longitudinal axis of one of the connecting beams on the node's plane is considered as the first local axis (x). The second local axis (y) is the external product of the third local axis (z) and the first local axis (x).

Beam orientation parameters are defined based on the node's local axes and include three angles α , β , γ and a distance d , as shown in Figure 4-3, where α is the angle between the x axis and the projection of the member on the x - y plane, β is the angle between the member direction and the x - y plane, γ is the rotation angle of the beam member along its own centre line, and d is the distance from the centre point of the node to the end section of the beam member.

Beam section parameters for designing the six-way node are illustrated in Figure 4-6(a), including the width of the beam section (b), the height of the beam section (h), the web thickness of the beam section (t_w) and the flange thickness of the beam section (t_f). The geometric parameters for designing the centre part of the transitional node are illustrated in Figure 4-6(b)-(c), including the flange thicknesses of the centre part (t_{f1} and t_{f2}), heights of top and bottom flanges of the centre part (h_1 , h_1' , h_2 and h_2') and web thicknesses of the centre part (t_{w1} and t_{w2}). Figure 4-6(d) illustrates a node generated using the transitional section design method, which connects six rectangular steel tubes. The six-way nodes studied in this chapter are all generated according to the geometric parameters listed in Table 4-2, which also defines the directions of loads. The parameters for designing the central part of the transitional node are listed in Table 4-3. The volume of the designed transitional node is

6328cm^3 , i.e., 49.67 kg for steel node when the density is 7850 kg/m^3 . Figure 4-7(a) shows the original transitional node designed for further structural analyses with unsmoothed edges and connections.

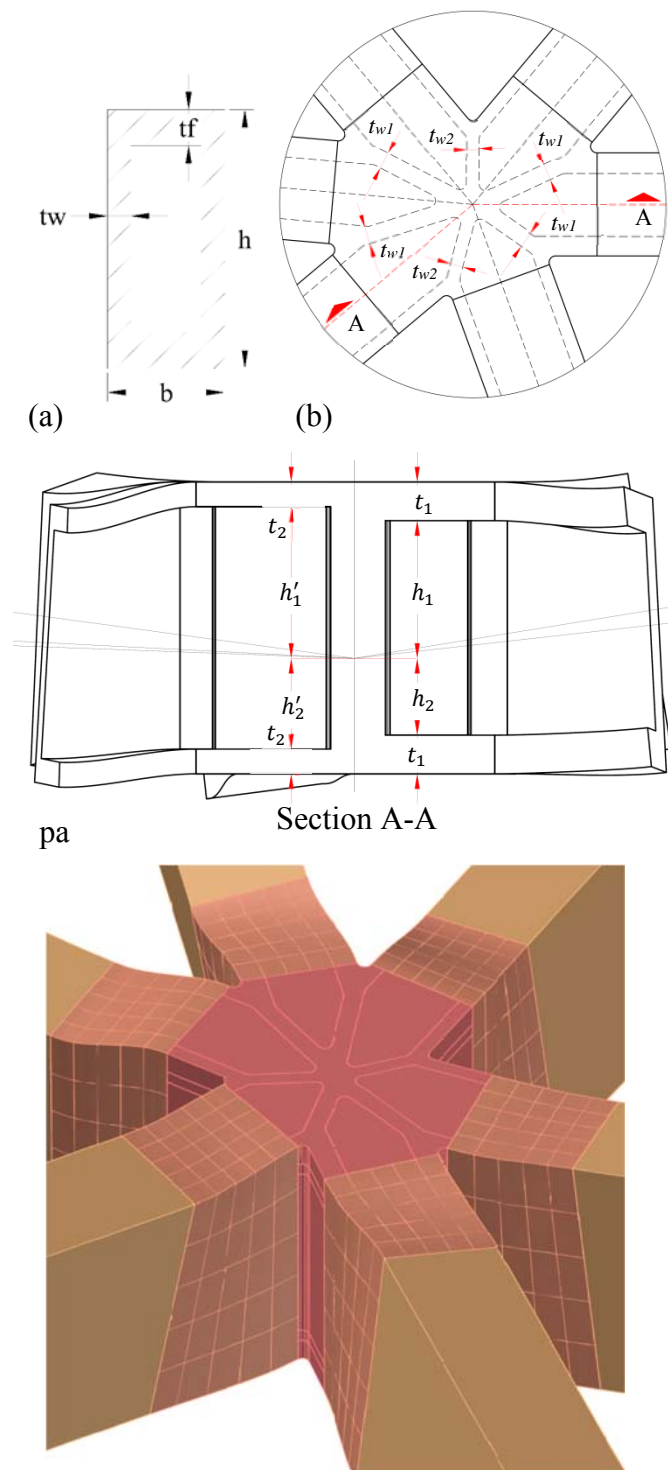


Figure 4-6: (a) The cross-section of the steel rectangular tube member; (b) top view of the node and its internal structure; (c) view on A-A section of the node showing the internal structure of the centre part and the transitional volume of the node; (d) a designed node connecting to six rectangular tube members by the transitional section design approach.

Table 4-2: Geometric design parameters of case study node.

Member	Rotation angles (degrees)			Distance of the member from the centre (mm)	Geometric parameters of the member (mm)			
	α	β	γ		d	b	h	t_f
L_1	0	6	8	195.712	80	180	25	16
L_2	50	8	4	199.272	80	180	16	10
L_3	130	1	7	198.155	80	180	16	10
L_4	175	7	9	208.345	80	180	25	16
L_5	220	2	4	199.771	80	180	16	10
L_6	290	10	3	173.877	80	180	16	10

Table 4-3: Geometric design parameters of the centre part of the transitional node.

Parameters	t_{w1}	t_{w2}	h_1	h_2	h'_1	h'_2	t_1	t_2
Values (mm)	13	10	89	49.6	98	58.6	25	16

To apply the transitional section method for the node design, AM is used for manufacturing the nodes. This allows us to use curves in design so that the stress concentration can be reduced. In the design using transitional section method, the sharp edges of the node may lead to stress concentration. In this study, to eliminate the stress concentration, Laplacian smoothing algorithm with five iterations is implemented to round the edges and connections. The volume of the smoothed transitional node is 6476 cm³, which is slightly higher than that of the unsmoothed one. The final shape of the smoothed transitional node is shown in Figure 4-7(b).

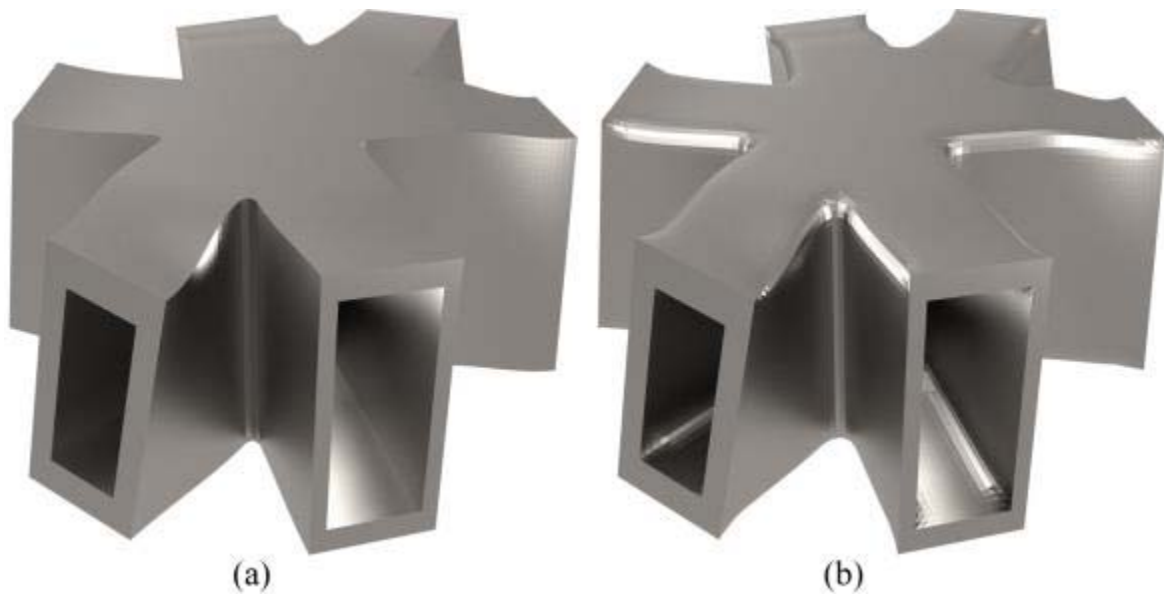


Figure 4-7: Shapes of the designed transitional nodes: (a) unsmoothed transitional node; (b) smoothed transitional node by Laplacian smoothing algorithm.

4.2.3. BESO design

In this chapter, topology optimisation is used to search for the stiffest structure with a given volume of material. In the BESO method, a structure is optimised by removing inefficient elements and adding elements where needed [28]. In this study, the BESO code is linked to ABAQUS which is used as a structural analysis engine for optimising the node stiffness.

The process of adding and removing elements in BESO is applied to a predefined domain, called the design domain. In the first step, the transitional node is considered as the design domain for BESO. The results of BESO design show that more material is removed from regions with lower strain energy density in the design domain, and the regions with higher strain energy density remain unchanged or strengthened. In the BESO design process, parameters maximum volume fraction, evolutionary rate and admission ratio, are set to 50%, 2%, and 2% respectively. The filter radius, which is the parameter to control the physical size of the members in BESO design, is set to 10 mm. The results of BESO design are strongly dependent on the loading conditions of the node (Figure 4-8).

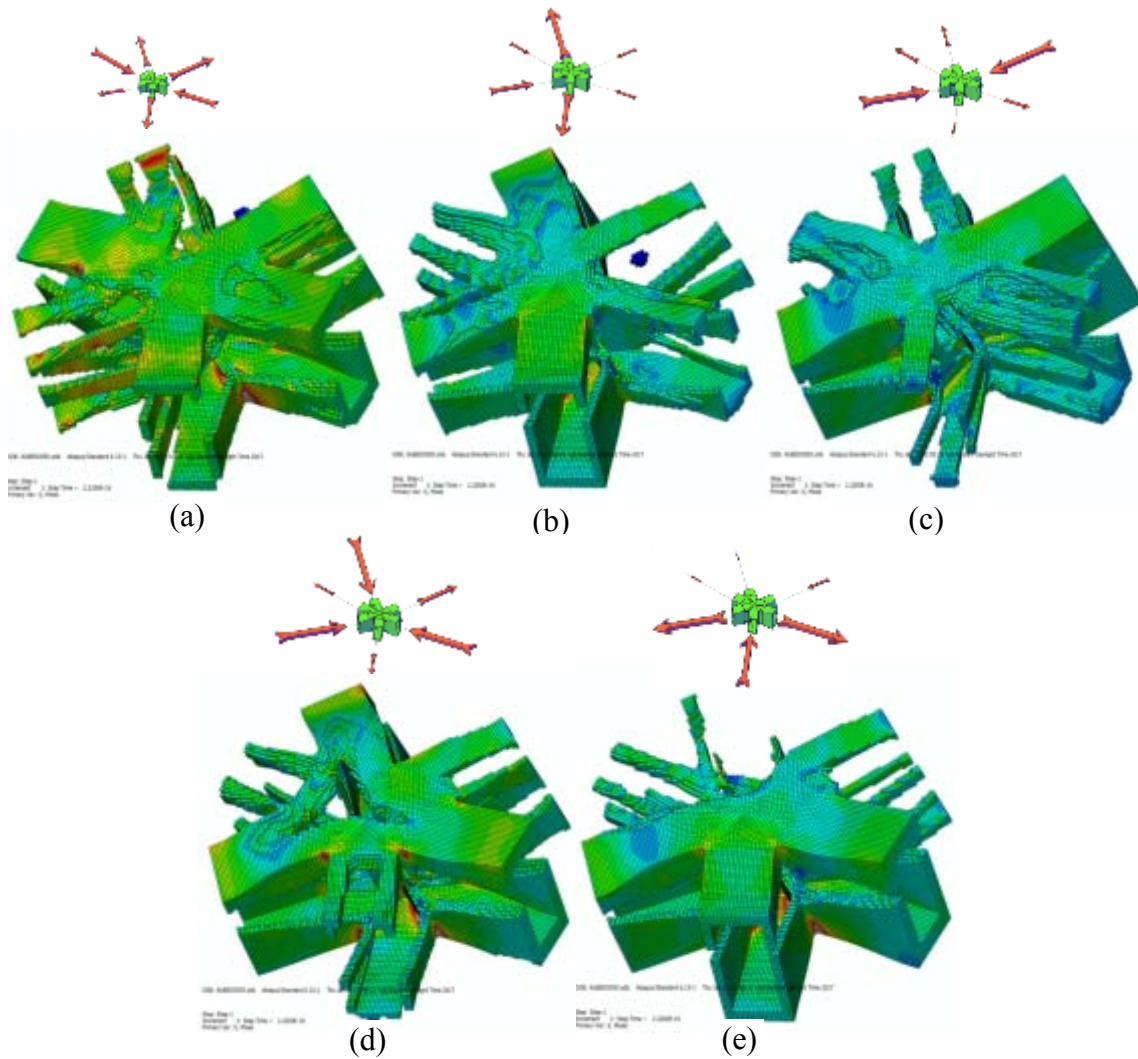


Figure 4-8: The results of BESO for transitional node under different loading conditions : (a) LC₁, (b) LC₂, (c) LC₃, (d) LC₄, and (e) LC₅.

To accommodate a combination of different loading conditions, BESO needs to solve the problem for multiple load cases. The objective function in the optimisation process for the multiple load cases is defined by a weighted average of the stiffness of the nodes with the same weight for all studied load cases.

The results of BESO for transitional node under a combination five load cases LC₁ to LC₅ are smoothed with three (L₃), four (L₄) and five (L₅) Laplacian iterations and shown in Figure 4-9. It can be seen that the Laplacian smoothing process increases the slenderness of the slender members more than the other members. To avoid this problem, sufficiently large filter radius should be selected in the BESO process to avoid excessively slender members.

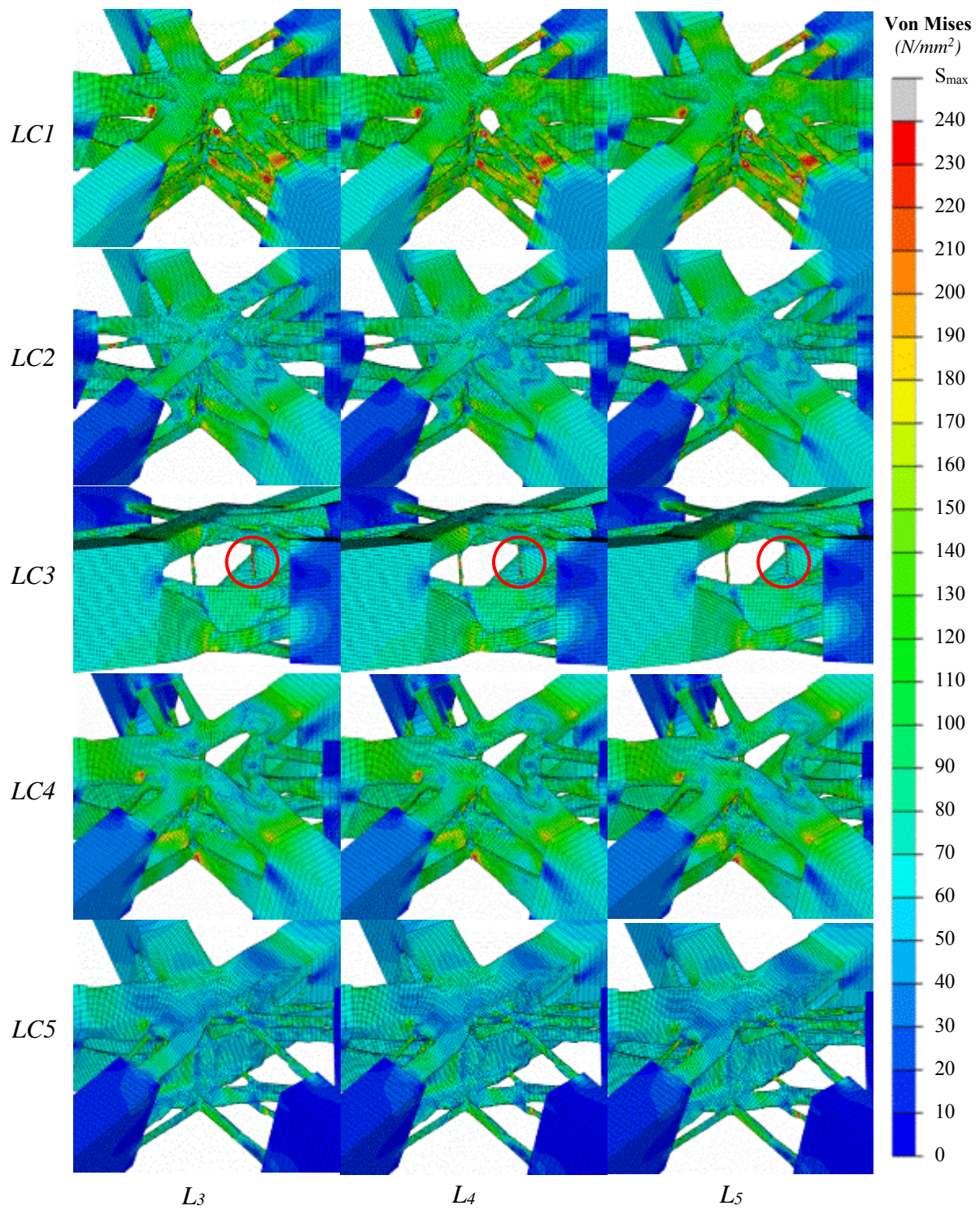


Figure 4-9: The smoothed geometry of the BESO results for transitional node under load combinations LC_1 to LC_5 with three (L_3), four (L_4) and five (L_5) iterations of Laplacian smoothing.

Generally speaking, it is preferable that the final design do not touch the boundaries of the design domain. Otherwise the efficiency of the design is affected by the limitations of the design domain. Therefore, when transitional node is used as initial model, the BESO design process is significantly limited because the transitional node is hollow and no element can be added to the inside region. Therefore, in the next step, the design domain is expanded from the hollow node to a solid volume between the connecting members. Figure 4-10 (a) shows the new initial model with solid design domain. The solid design domain is enclosed between the end faces of the members and top and bottom planes. The distances to the top and bottom planes from the centre of the node are 180mm. In this arrangement, a total of 193,257 hexahedral solid elements (C3D8) with an average size of 7 mm are used to mesh the initial model. In the optimisation process, the maximum volume constraint is the volume of the material to be removed. Once the maximum is reached, the BESO stops removing more material and keeps iterating to find the stiffest structure. To obtain a designed node with a similar volume as the transitional node, the maximum volume fraction is set to 95.5% in the BESO process. In the design process, two parameters, evolutionary rate and admission ratio, which are the ratios of material removed and added to the model in each iteration, are set to 2%. In addition, the filter radius, which is the parameter to control the physical size of the members in BESO design, is set to 15 mm. Figure 4-10 (b) shows the result of the BESO process at iteration 135 with the node volume of 8194cm³.

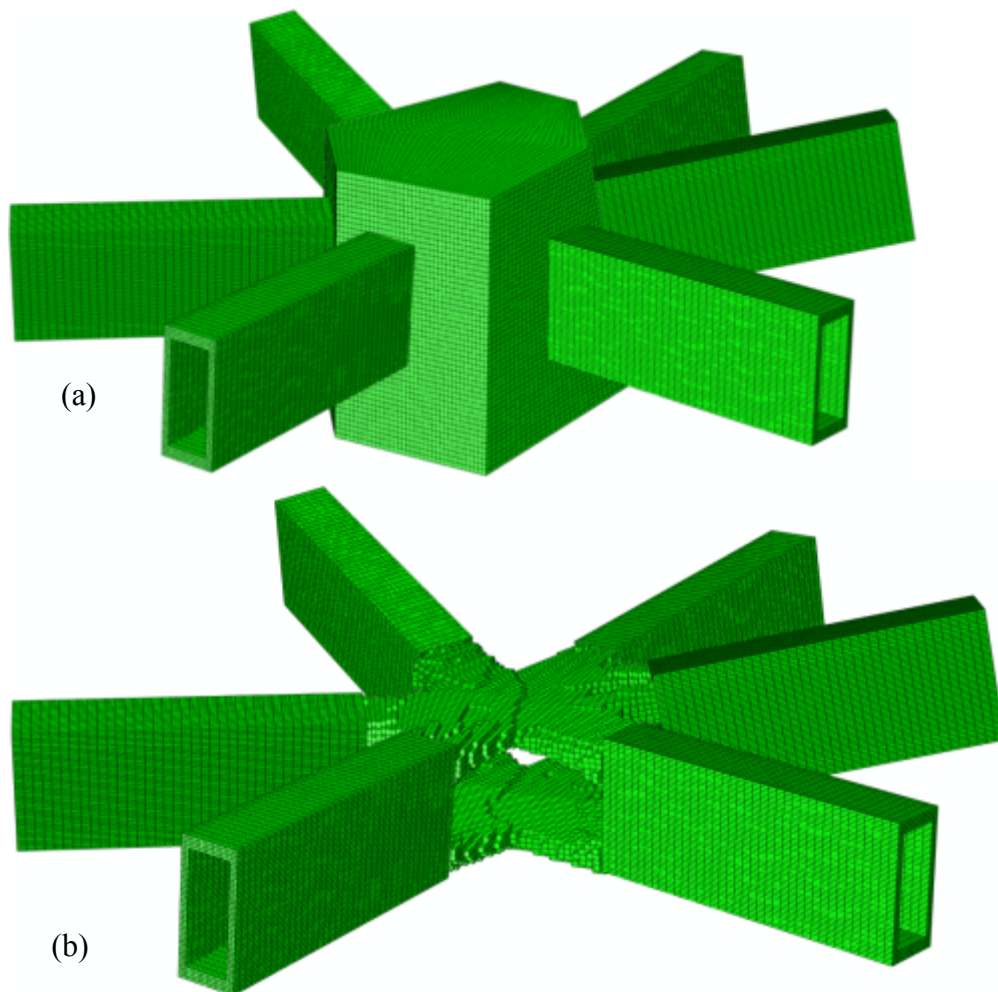


Figure 4-10: (a) The initial node model with a solid polyhedral design domain, (b) BESO result for multiple load cases at iteration 135.

Laplacian smoothing algorithm is used to smooth the final result obtained from the BESO design. As non-design domain remains unchanged, only design domain is smoothed. As shown in Figure 4-11, by applying the Laplacian smoothing algorithm to the design domain, the interfaces between the design domain and non-design domain are subjected to change. Therefore, the physical contact between the design domain and non-design domain is disconnected after smoothing. In the first attempt to deal with this deficiency, the nodes of the connected faces of the design domain are moved back to the original positions. As shown in Figure 4-12, the resulting model has sharp edges in the connecting region between the

design and non-design domains and shows a non-smooth transition of the geometry in this region.

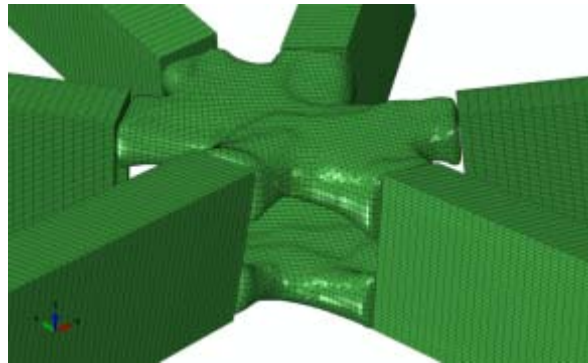


Figure 4-11- Smoothing of the BESO result when the nodes in the connecting faces of the design domain are allowed to moving during the smoothing process.

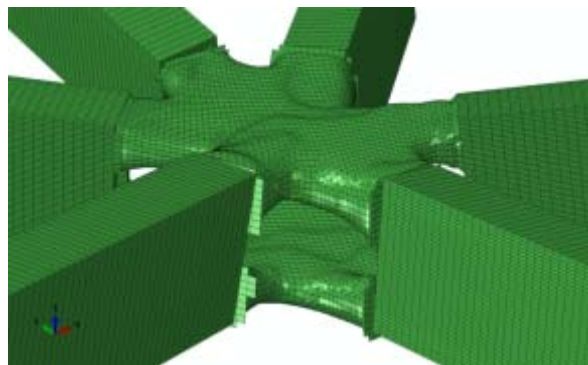


Figure 4-12- Smoothing of the BESO result when the connected faces of the design domain are moved back to the original positions.

To obtain geometry with better smoothness in the connecting region, instead of pushing the nodes back to their original locations, the nodes are constrained to the connecting face during the smoothing procedure. Figure 4-13 shows the result of the new smoothing procedure with nodes constrained to the connecting faces for the BESO design at iteration 173 ($V=6881\text{cm}^3$). It is clear in the figure that there is a sudden change and sharp edge in the connecting region when moving from the design domain to the non-design domain.

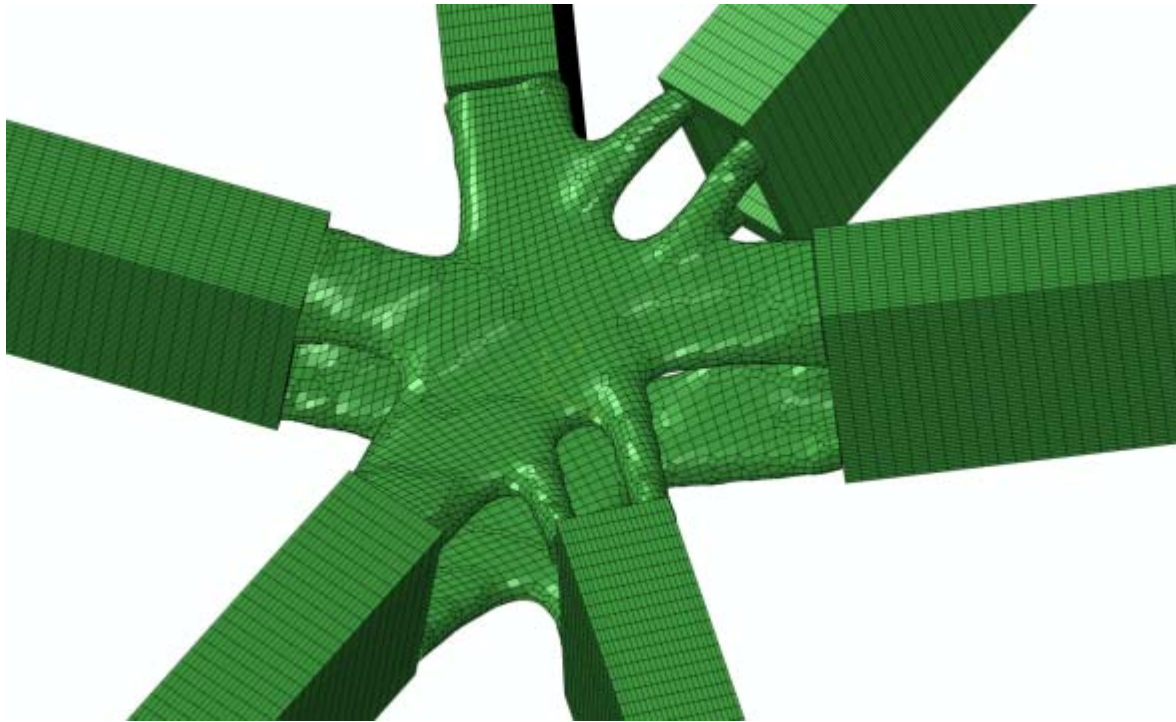


Figure 4-13: Smoothing of the BESO result when the nodes in the connecting faces of design domain are allowed to move in the plane of the connecting face only.

Another issue needs to be resolved in the current design is that the node is divided into two separate parts at the top and the bottom. In practice, it is difficult to control the exact positions of the two separate parts. Therefore, a small non-design part, which connects the two parts, is introduced in the current design to improve the feasibility in construction. The new design domain is generated by considering two parts, individually serving a specific duty. A solid part is defined in the middle of the design domain to give the BESO enough freedom for design. Also, transitional parts are defined at the connecting regions between the solid part and non-design domain with a transitional adaptive connection to non-design domain. The transitional parts avoid sharp edges that occur in previous designs. Figure 4-14(a) shows the new initial model for the BESO process, which has three different parts: non-design domain, transitional design domain and main design domain. The non-design domain contains six rectangular 10mm thick frames and keeps the connection between upper and lower parts of the designed node. The transitional design domain consists of six frames

with 30 mm depth, three times the thickness of the non-design domain. The main design domain is a solid space enclosed by six transitional volumes. In this arrangement, a total of 241,752 hexahedral solid elements (C3D8) with an average size of 5 mm are used to mesh the initial model. In the design process, the maximum volume fraction, evolutionary rate, and admission ratio are set to 72%, 2%, and 2% respectively. In addition, the filter radius, is set to 10 mm.

The optimised node is shown in Figure 4-14(b), which consists of two separated plate-like parts at the top and the bottom as expected. The plate-like parts are connecting the members through the non-designable rectangular frames. To obtain a suitable geometry for the construction purpose and remove the sharp edges, Laplacian smoothing algorithm is applied, and the final shape of the smoothed node is shown in Figure 4-14(c), which is considered as the final BESO design. The volume of the BESO designed node (BESO node) is 6298 cm³ (or 49.44 kg if it is made of steel), which is slightly smaller than the transitional node (6328cm³). In the BESO design, the mean compliance of the structure is optimised.

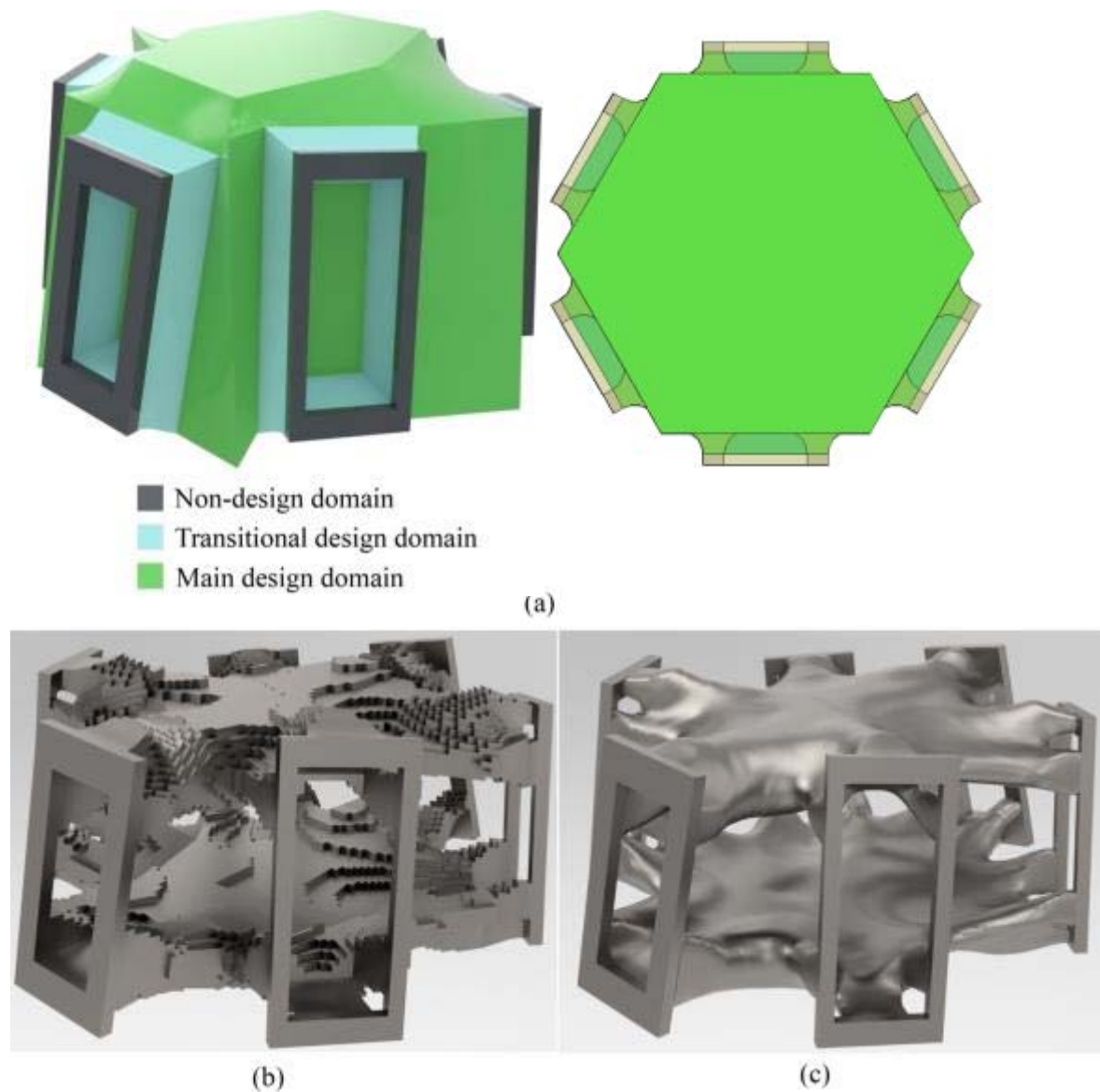


Figure 4-14: (a) The initial model for the BESO process; (b) the obtained unsmoothed topology of the BESO node; (c) the final smoothed topology of the BESO node.

4.2.4. Conventional designs

In timber gridshells, the structure is flexible as wood is a relatively soft material. Therefore, the initial deformations caused by manufacturing errors might not lead to much initial internal force in members. But in steel gridshells, the initial stresses caused by manufacturing errors are much higher. To avoid the high stresses, the manufacturing accuracy is of significant importance. Since the conventional manufacturing methods have limitations in

realising complicated shapes, it is challenging to fabricate a large number of three dimensional (3D) customised nodes with complex shapes. Besides, by using a design concept based on the conventional manufacturing methods, it is very difficult to create nodes with a large number of design parameters when the nodes are subjected to complicated spatial loads. Although beam section parameters, such as the width of the member (b), the height of the member (h), the web thickness of the member (t_w) and the flange thickness of the member (t_f), are independent on the method of manufacturing the section, different section manufacturing methods affect the conventional design concept of the node. Figure 4-15 shows two different methods of manufacturing a welded rectangular hollow section (WRHS).

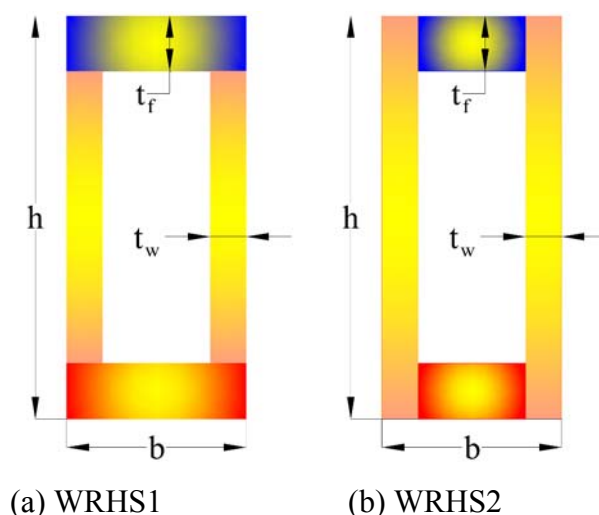


Figure 4-15- Beam section parameters of connecting beams

Two conventionally designed structural nodes selected from two well-known real projects are compared herein. One node is used in the Sun Valley pavilion of the Expo 2010 Shanghai (Sun Valley node), in which the beam member section is of type welded rectangular hollow section type 1 (WRHS1). The other is used in Westfield shopping centre roof in London by Seele company (Seele node), in which the beam member section is of type welded rectangular hollow section type 2 (WRHS2). The Sun Valley pavilion and Westfield shopping centre roof in London are shown in Figure 4-16. Although the design concept of the

two nodes are similar, both being rigid nodes under both axial loads and bending moments by forming an enclosed geometry, the structural details and design procedures are different. The Sun Valley node is a simpler node, because it only requires a three-axis cutting technology in the manufacturing stage, while the Seele node needs a five-axis cutting technology.



Figure 4-16: Sun Vally pavilion in Expo 2010 Shanghai [29] (left) and Westfield shopping centre roof in London [30] (right).

The overall design concept of the studied nodes is to connect six pieces of the connecting beams to a central part and provide end plates with suitable bolt holes at the end of each piece. The beam pieces are made of welded rectangular hollow section type 1 (WRHS1) in Sun Valley node and welded rectangular hollow section type 2 (WRHS2) in Seele node shown in Figure 4-15. As discussed before, the primary load cases in the gridshell structures are axial loads and out-of-plane bending. The major part of these loads is being transferred through the flanges of the beam section; therefore, the flanges are fully connected through top and bottom plates (called continuity plates herein) at the central part of the node. The geometry of the node is firstly designed, and then checked based on the applied loads.

The volume of the final design of Sun Valley node is 6877 cm³, or 53.98 kg if made of steel. The volume of the final design of the Seele node is 6441 cm³, or 50.56 kg if made of steel. For comparison, the internal structures of these two conventional nodes and the transitional node proposed in this chapter are illustrated in Figure 4-17.

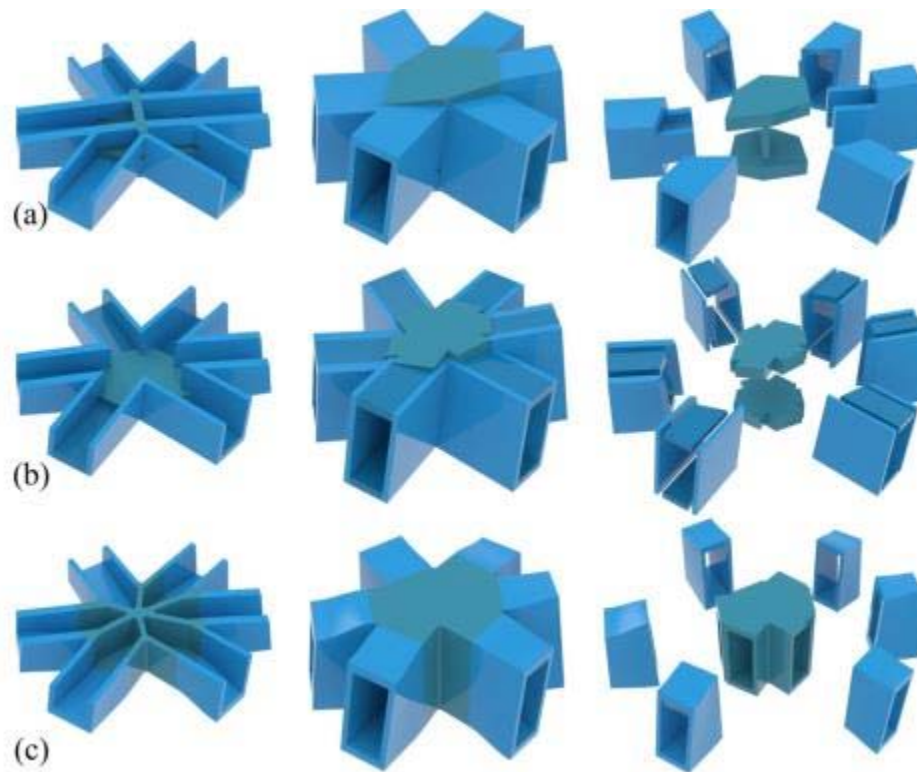


Figure 4-17: Internal structures and assembling of different types of nodes: (a) Sun Valley node; (b) Seele node; (c) transitional node.

Sun Valley node

In Sun Valley node, the core part of the node is composed of two parallel top and bottom continuity plates and a reinforcing plate in the centre. The dimensions and positions of the continuity plates are shown in Figure 4-18. To calculate the coordinates of the vertices of the hexagonal top and bottom plates, the dimensions of the flanges and the bounding sides of each connecting beam (Figure 4-18 (a)) are firstly calculated. Then the coordinates of vertices of the polygon for the top and bottom plates (Figure 4-18 (b)) are calculated from intersecting the bounding sides of the adjacent beams.

To calculate the thicknesses and positions of the top and bottom plates, the sides of the polygons are extruded vertically and the surfaces are intersected with the flanges (Figure 4-18 (c)). The maximum and minimum heights of intersection faces are used to determine the thicknesses and heights of the top and bottom plates (Figure 4-18 (d)).

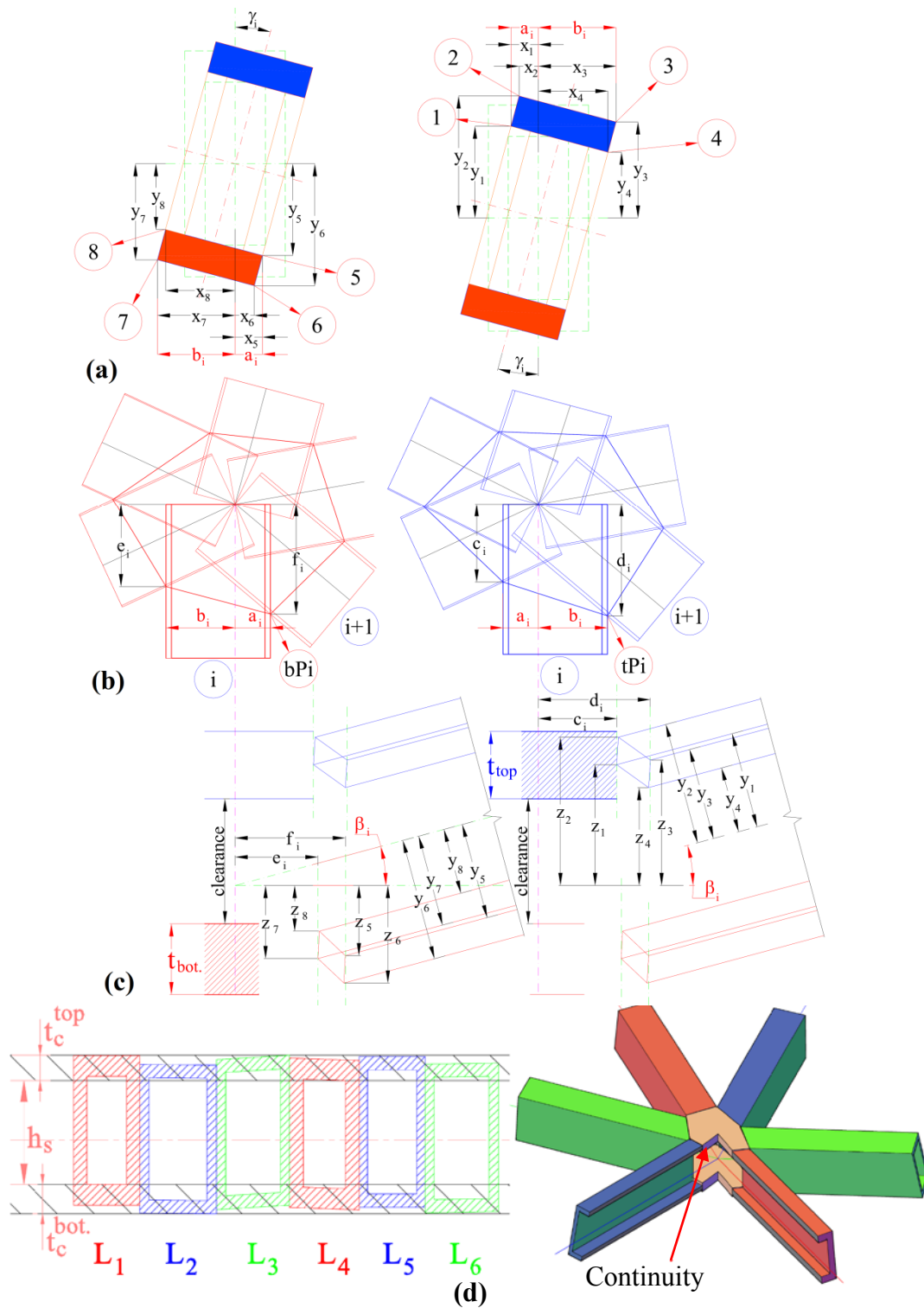


Figure 4-18- Geometries of the Sun Valley node.

The shape of the top and bottom continuity plates is prismatic. Therefore, the manufacturing can be easily carried out by using automatic 3-axis laser cutting technology or 3-axis water jet cutting technology. All flanges of the six beam pieces are welded to the faces of the

continuity plates. The distance between the top and bottom continuity plates determines the height of the reinforcing plate. The webs of the two members with the maximum internal forces are extended and welded to the reinforcing plate. The webs of the other four members are only welded to the neighbouring members to form an enclosed node [29]. Sufficient length for each connecting beam piece will be provided based on the end plate connection requirements. The 3D view of the Sun Valley node is given in Figure 4-17(a).

Seele node

In the Seele node, similar to the Sun Valley node, the flanges are connected through top and bottom plates, and the webs are welded together to form an enclosed node [30]. However, as a different section manufacturing method is used for the beam pieces in which the webs are continued over the flanges (Figure 4-15 (b)), the webs penetrate into the top and bottom continuity plates. Therefore, the continuity plates are not hexagonal shapes any more. The geometrical design of these nodes starts with intersecting the webs of the beam pieces as shown in Figure 4-19.

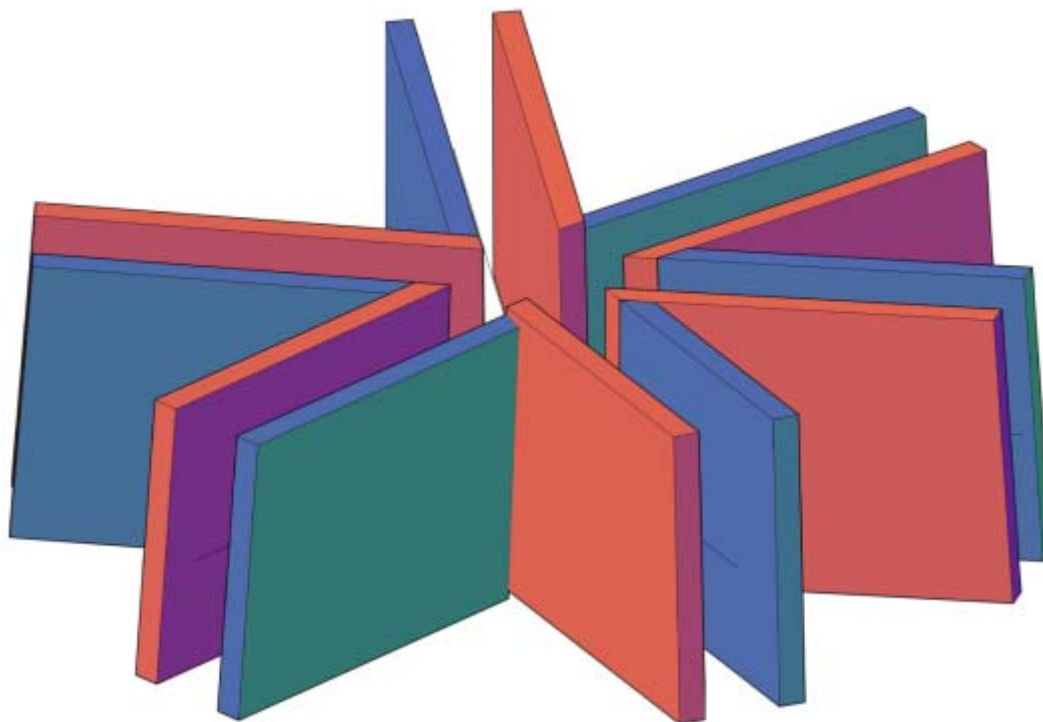


Figure 4-19: Intersecting the webs of the connecting beam pieces in Seele node.

The top and bottom flange faces of the connecting beam pieces are set back to provide a certain depth of groove in top and bottom continuity plates for beam webs (Figure 4-20). In this study, the minimum depth is considered to be 20mm.

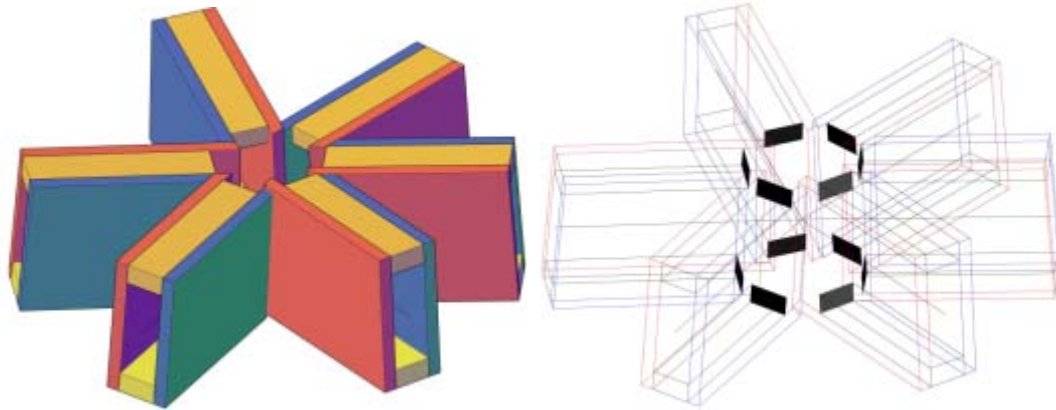


Figure 4-20: Set back of the flanges of the beam pieces.

Eventually, the thicknesses and positions of the top and bottom plates are determined from the maximum and the minimum heights of the intersected faces of the flanges of the beam pieces.

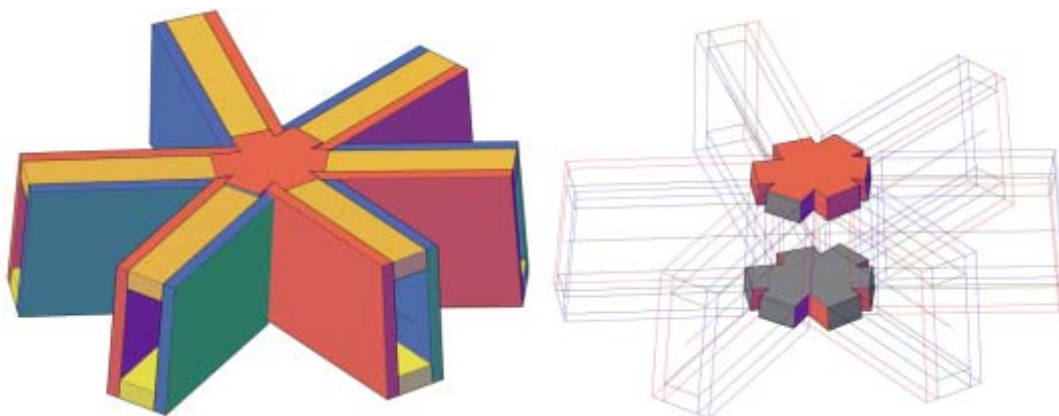


Figure 4-21: Top and bottom continuity plates of Seele node.

The faces of the grooves in top and bottom plates are not vertical in this design, and the shape of the plates is not prismatic anymore. Therefore, manufacturing of the plates is more

complicated and needs more advanced technologies, such as the 5-axis cutting facilities and precise quality control tools as shown in Figure 4-22.

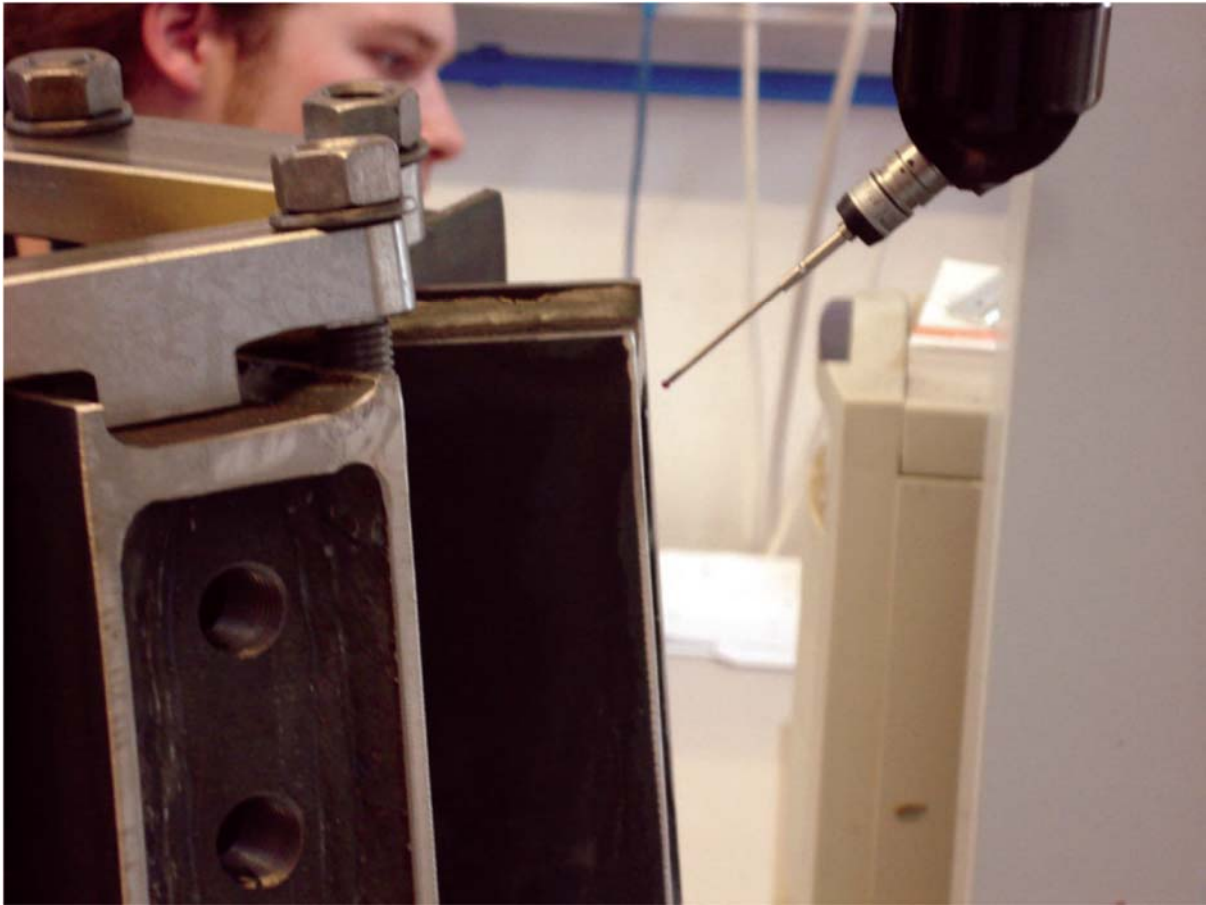


Figure 4-22: Final check of geometry for Seele nodes [30].

4.3. Finite element modelling

To validate the effectiveness of the new designs from using the transitional section method and the BESO approach, finite element modelling is performed to evaluate the mechanical properties of the new nodes, and they are compared to the conventionally designed nodes. Here a series of finite element models are created for modelling the five different types of nodes, including unsmoothed transitional node, smoothed transitional node, smoothed BESO node, Sun Valley node and Seele node. The commercial software package Abaqus Standard is employed for the quasi-static analysis. Linear elastic material model for steel is used with

Young's modulus of 210.83 GPa and Poisson's ratio of 0.3. Hypermesh v11.0 is used to generate the mesh for different nodes. Hexahedral elements (C3D8) are used for manually meshing the transitional and BESO nodes due to the complex geometries, while a combination of hexahedral elements (C3D8) and tetrahedral elements (C3D4) is used for automatic meshing Sun Valley and Seele nodes. The information of the finite element meshes for different nodes are summarised in Table 4-4. The average element size of all nodes is 5 mm. In the numerical simulations, one of the six members is fixed at its end and the loads are applied on other five members as a pressure at the end of each member. The mean compliance and the maximum von Mises stress in each model is used for assessing and comparing the mechanical performance.

Table 4-4: Meshing method of nodes.

Model name	Meshing method	Mesh size (mm)	Number of elements	
			C3D8	C3D4
Unsmoothed transitional node	Manually	5	51,190	0
Smoothed transitional node	Manually	5	51,190	0
BESO node	Manually	5	78,331	0
Sun Valley	Automatic	5	53,030	656,167
Seele	Automatic	5	51,219	698,001

4.4. Results and discussion

The von Mises contours obtained for the four different types of structural nodes (transitional nodes, BESO node, Sun Valley node and Seele node) under five loading cases from LC₁ to LC₅ are illustrated in Figure 4-23 to Figure 4-27. Smoothed and unsmoothed transitional nodes are also compared to demonstrate the effect of the smoothing algorithm. The results show that, for Sun Valley and Seele node, the centre parts of the node have evidently lower stress levels with a clear boundary between the members and the cores in all five loading cases. Also, stress concentration can be found around corners and connections of different

sections. While for the new designs, i.e. transitional and BESO nodes, the stress distributions are much more uniform without clear stress changes between the members and the centre parts. For transitional node, the application of smoothing algorithm reduces the stress level at the edges and connections between different sections.

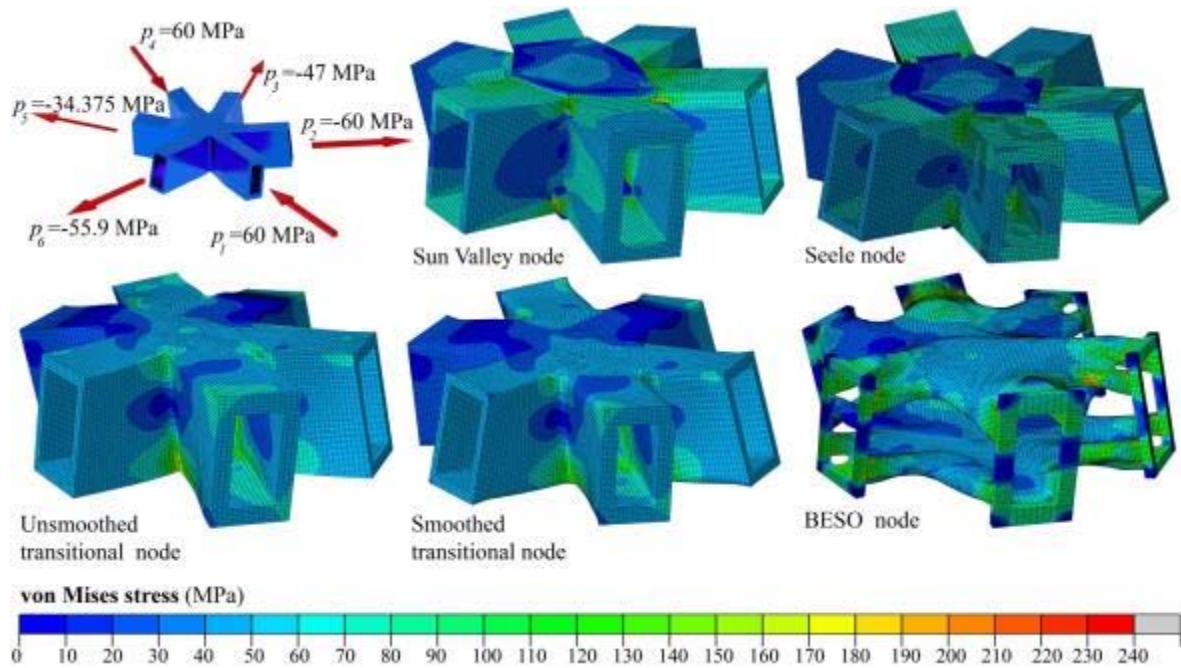


Figure 4-23: von Mises stress contours of new and conventional nodes under the same loading condition, LC₁.

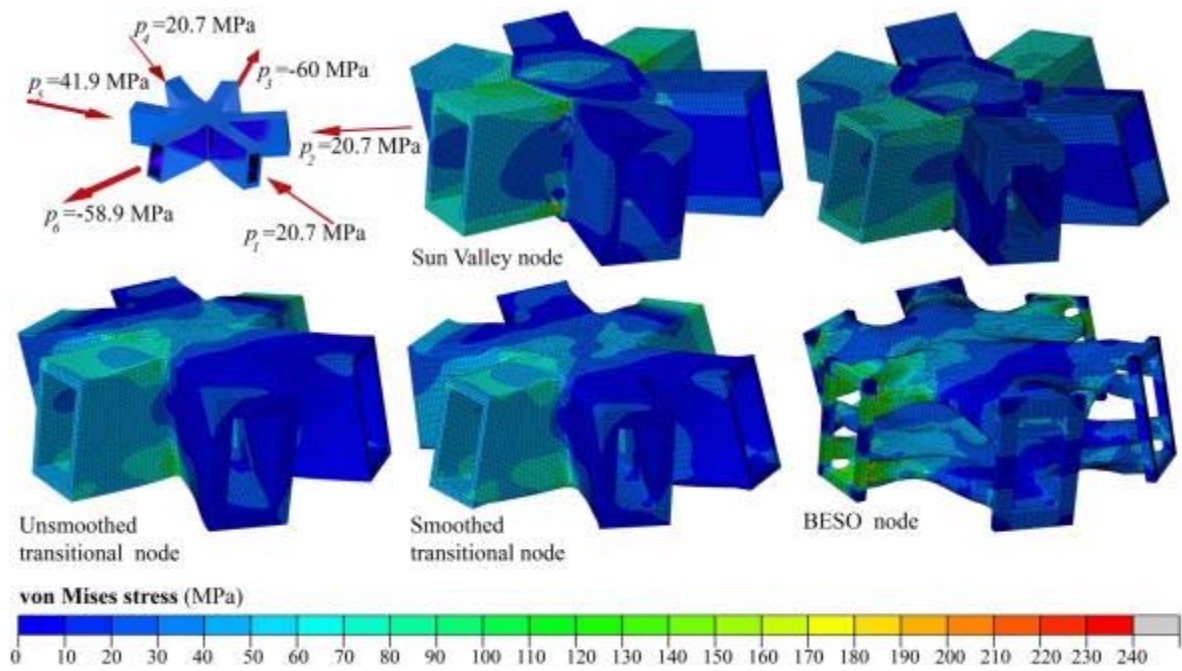


Figure 4-24: von Mises stress contours of newly designed and conventional nodes under the same loading condition, LC₂.

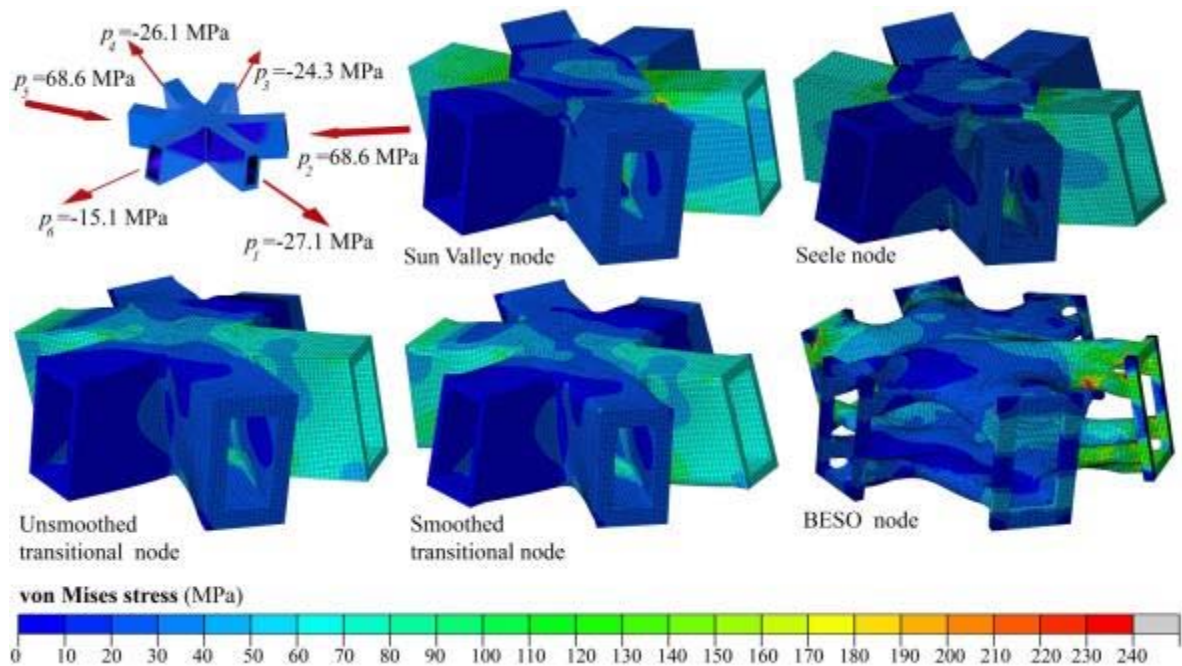


Figure 4-25: von Mises stress contours of newly designed and conventional nodes under the same loading condition, LC₃.

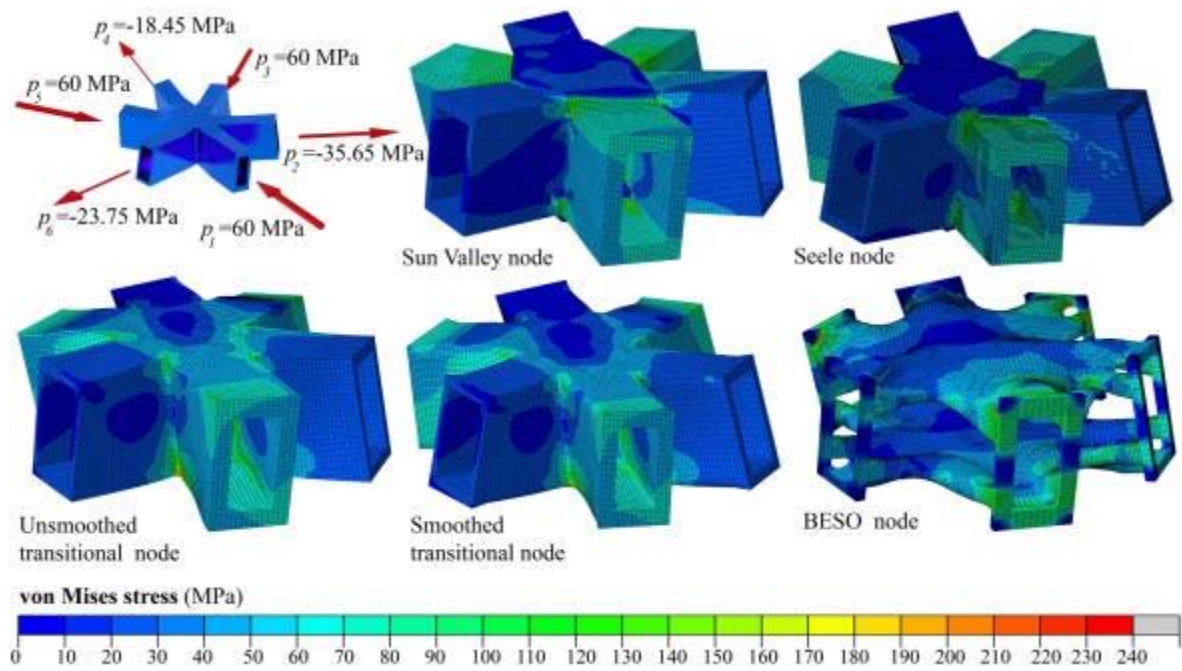


Figure 4-26: von Mises stress contours of newly designed and conventional nodes under the same loading condition, LC₄.

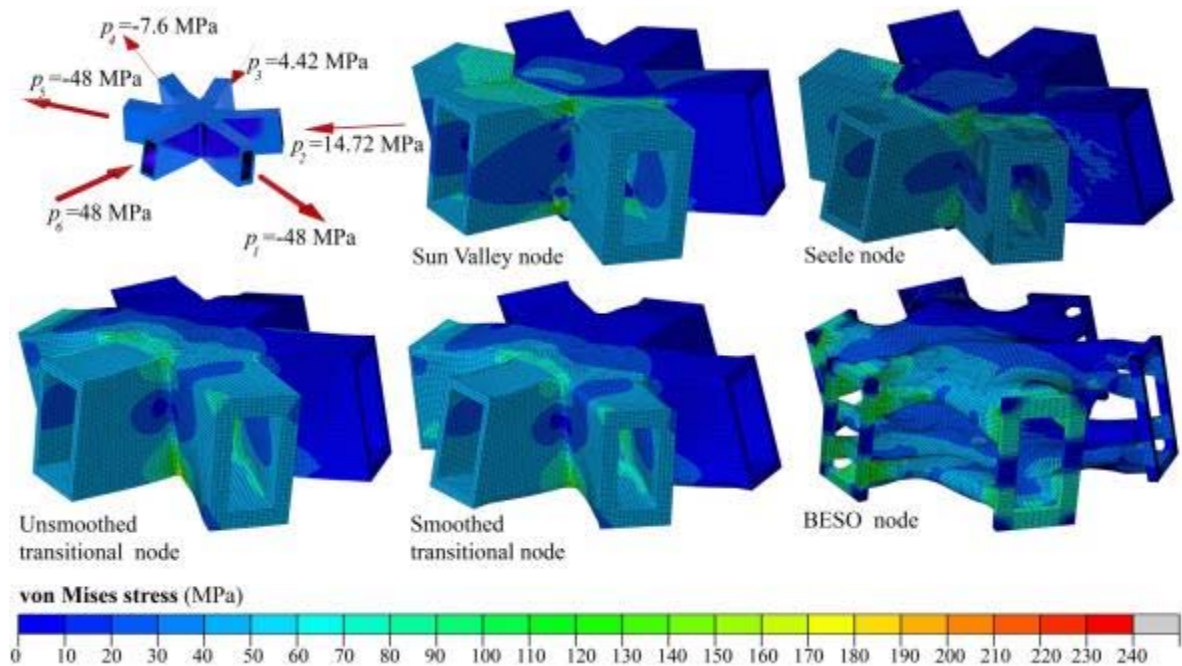


Figure 4-27: von Mises stress contours of newly designed and conventional nodes under the same loading condition, LC₅.

Table 4-5: The mean compliance, maximum von Mises stresses and volumes of different nodes.

Nodes	Mean compliance (N·m)					Maximum stress (MPa)					Volume (cm ³)
	LC_1	LC_2	LC_3	LC_4	LC_5	LC_1	LC_2	LC_3	LC_4	LC_5	
Unsmoothed transitional node	5.3	3.0	3.3	3.8	2.3	169	184	165	174	160	6328
Smoothed transitional node	3	3	8	9	6	146	146	147	154	133	
BESO node	4.9	2.5	2.8	3.1	1.8	177	159	160	153	117	6298
Sun Valley node	8	2	3	0	3	778	420	611	603	428	
Seele node	5.1	2.6	3.0	3.5	2.1	351	231	213	289	216	6441
	3	8	7	3	3						

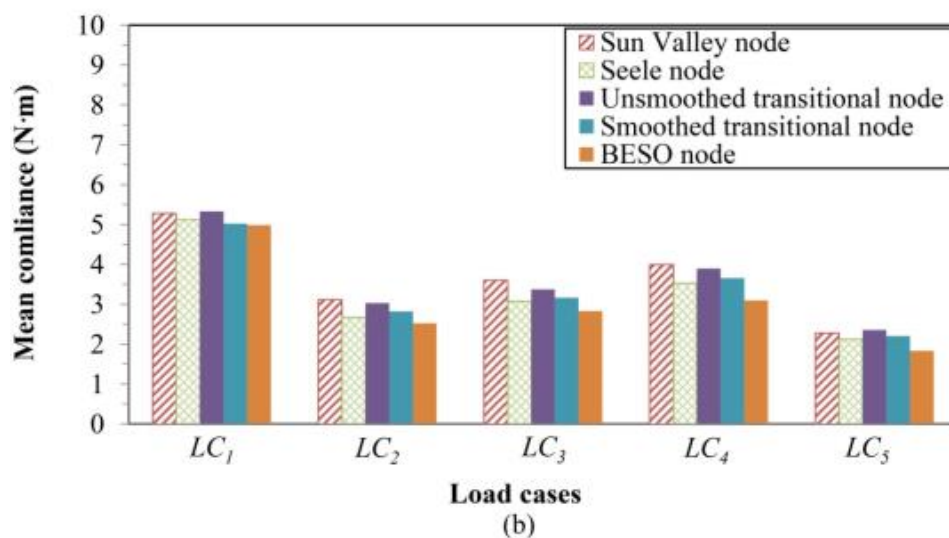
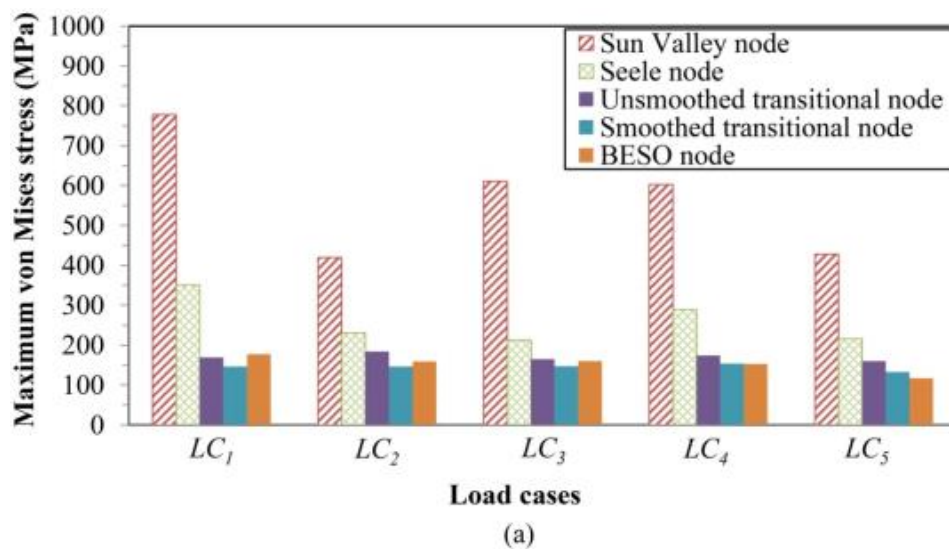


Figure 4-28: The maximum von Mises stresses and the mean compliances of different nodes under different loading cases LC_1 to LC_5 , (a) von Mises stress; (b) mean compliance.

In the following sections, the nodes are compared in three areas, including (a) volume and weight, (b) maximum von Mises stress and (c) mean compliance and stiffness.

Volume and weight

In order to have a meaningful comparison of the structural behaviour, the new nodes are designed to have similar weight as the conventional nodes. As listed in Table 4-5, Sun Valley node has the highest structural volume of 6876 cm^3 , which is approximately 7% higher than the Seele node (6441 cm^3), approximately 6% higher than the smoothed transitional node (6476 cm^3) and 9% higher than the BESO node (6298 cm^3). It is important to note that the volumes and weights of the conventionally designed nodes are dependent only on the geometrical parameters of these nodes. Therefore, it is not possible to design a lighter node for less critical loading conditions by using the conventional design methods.

Maximum von Mises stress

Figure 4-28(a) shows the maximum von Mises stresses for the four types of structural nodes. Detailed data are listed in Table 4-5. Overall, the maximum stresses of the newly designed transitional and BESO nodes are significantly lower than those of the Sun Valley node (56% to 81% lower) and the Seele node (20% to 58% lower) for all loading cases. For the first three loading cases LC_1 , LC_2 and LC_3 , the smoothed transitional node has the lowest stress level, while for the other two loading cases LC_4 and LC_5 , BESO node has slightly lower stress level. In spite of having the maximum amount of material among all five nodes, the Sun Valley node has the highest von Mises stress level in all loading cases.

In addition, compared to the unsmoothed transitional node, the maximum stresses of the smoothed transitional node in all loading cases are reduced by 10.9% to 20.7%. Therefore,

the Laplacian smoothing algorithm is able to effectively decrease the stress concentrations of the node.

Mean compliance and stiffness

Figure 4-28(b) illustrates the structural mean compliance of different nodes for various loading cases. It shows that the Sun Valley node has the highest mean compliance in loading cases LC_2 , LC_3 and LC_4 , followed by the unsmoothed transitional node, the smoothed transitional node and the Seele node. The BESO node has the lowest mean compliance in all loading cases. In the cases LC_1 and LC_5 , the unsmoothed transitional node has the highest mean compliance, slightly higher than the Sun Valley node.

Discussion

Conventional nodes: The results indicate that the Seele node is stiffer, lighter and has lower maximum stress compared to the Sun Valley node. It shows that, in conventional designs, the concept of penetrating webs into top and bottom continuity plates results in a more integrated structure, rather than the concept of connecting flanges to the continuity plates. Also, extending webs of the beams with the main loads is not effective in transferring loads.

The best mechanical performance: The new design approaches have reduced the maximum stress as compared to the Sun Valley and Seele nodes. Also, the BESO node has smaller maximum stress and smaller mean compliance compared to the transitional node, despite the smaller volume. Therefore, the BESO node has the best overall mechanical performance.

Uniform design: It should be mentioned that, in all loading cases, the maximum stress of the newly designed transitional and BESO nodes vary in a relatively smaller range compared to the maximum stresses of the conventionally designed nodes, indicating that they are more uniformly designed for different loading conditions.

The design guide: The stiffest BESO node consists of only two separated layers without any internal structures between them. This indicates that the material between the two layers is inefficient and can be removed during optimisation for pure axial loading conditions. Besides, comparing the Seele node with a hollow box structure to the transitional nodes with excessive internal walls, the Seele node is stiffer than the transitional nodes. This indicates that the internal walls have little contribution to the node performance when the nodes are axially loaded. Considering the fact that the out-of-plane bending consists of a couple of tension and compression loads, it is predictable that the internal walls are not efficient structural members for the out-of-plane bending either. Therefore, the hollow box configuration can be assumed as the best structural configuration for the nodes.

Aesthetical features: The gridshell structures are single layer structures with maximum exposure of their components compared to other structural types. To achieve beautiful landscape, it would be desirable to use members with organic shapes in structures. The newly designed nodes, especially the BESO node, are ranked much higher than the conventional nodes.

Fatigue: Gridshell structures are usually exposed to repeating loads, leading to fatigue stress in the structural members. The conventional design methods involve large amounts of cutting and welding of different parts as well as sharp edges, which increase the probability of defects and fatigue failure. The new design methods are generating the best geometry for fatigue resistance, as the sharp edges and the abrupt changes are avoided.

Manufacturing: The newly designed transitional node and the BESO node can be rapidly and precisely fabricated by using additive manufacturing. Figure 4-29(a) shows the prototype of the unsmoothed transitional node 3D printed in stainless steel, and Figure 4-29(b) shows the prototype of the BESO node printed in nylon material (to save the printing cost). The Sun Valley node can be manufactured in conventional manufacturing process by using 3-axis

laser cutting tool or 3-axis water jet tool. To manufacture the Seele node through the conventional methods, it is essential to use the 5-axis laser cutting tool or 5-axis water jet cutting tool due to the angled planes in design. In both conventionally designed nodes, large amount of welding, precise controlling and post-process machining of the surface are needed. On the other hand, the manufacturing process of the newly designed nodes is automatic; therefore, no significant post-processing, such as machining rough surfaces, is needed. However, the cost for 3D metal printing is still quite high nowadays.

Although a comprehensive comparison of the manufacturing intense and cost between the newly designed and the conventionally designed nodes is not possible as these factors are dominated by the market, a simplistic comparison of the unit price ratio in the two manufacturing methods, i.e. the additive manufacturing and the conventional manufacturing, is available. It has been advised by the industry references that this unit price ratio is about five. Based on this simplistic comparison, the newly designed nodes should weigh at most 20% of the conventional node to be practical and effective at this moment. This ratio is getting lower and lower with the rapid development of additive manufacturing technologies. Furthermore, other features also make the newly designed nodes promising, such as the aesthetical features, high stiffness, reduced structure size, reduced foundation requirement, high precision and less labour. It should be noted that, in this research, the five loading cases under consideration are representing the situation of a fully loaded node in a gridshell structure, which may be a rare case. If real loading conditions are taken into account in the design procedures, much lighter nodes will be generated using the new design methods, whereas the conventionally designed nodes may have little change in the weight, as they are designed based on the geometrical considerations only.

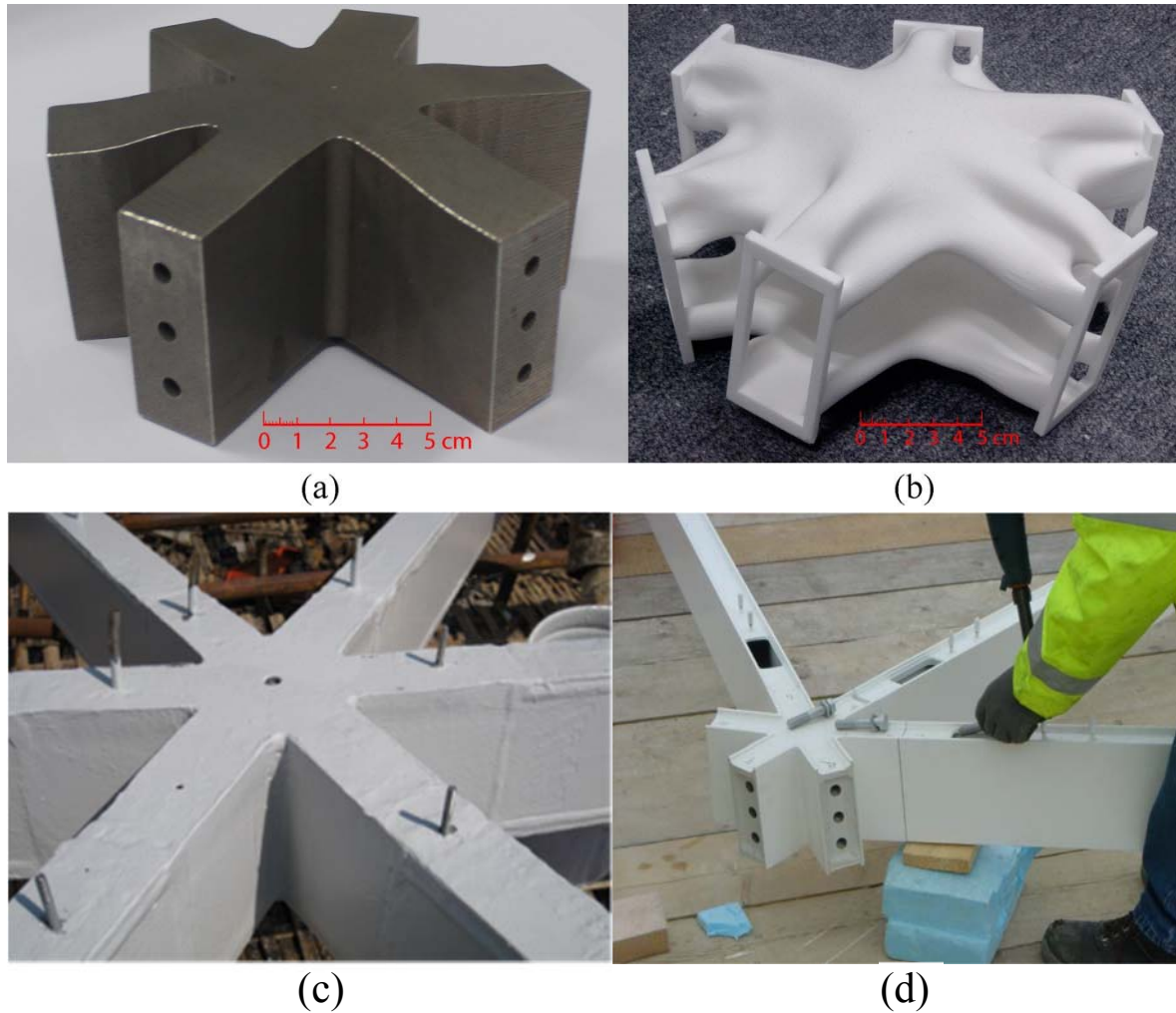


Figure 4-29- Manufactured samples of structural nodes: (a) unsmoothed transitional node with the end of each member prepared for bolt-connection additively manufactured in stainless steel; (b) BESO node additively manufactured in nylon material; (c) Sun Valley node conventionally manufactured for Expo 2010 Shanghai [29]; (d) Seele node conventionally manufactured for Westfield shopping centre roof in London [30].

4.5. Conclusions

In this chapter, two new designs of structural nodes for gridshell structures are introduced. The new designs are based on the transitional section method and the topology optimisation approach respectively. These new nodes are subjected to complicated axial tension and compression loads in six spatial directions defined by geometric parameters of the nodes.

Laplacian smoothing algorithm is applied to the new designs to generate a more practical geometry with less stress concentrations and better structural performance. A series of finite element modelling is conducted to evaluate the mechanical properties of these nodes in the elastic range. Prototypes of the newly designed nodes are additively manufactured using stainless steel and nylon materials. In addition, the conventionally designed nodes used in Sun Valley and Westfield shopping centre roof are studied under identical loading conditions for comparison.

The new design approaches have reduced the maximum stress compared to the Sun Valley and Seele nodes. The BESO node is demonstrated to be the most efficient, evidenced by the low von Mises stress, the highest stiffness and the smallest amount of material consumption. The newly designed nodes also have more uniform stress distributions. Furthermore, compared to the conventional nodes, the transitional and BESO nodes are more purposely designed based on specific loading and boundary conditions. The results also show that the Laplacian smoothing algorithm is effective in reducing the stress concentration in structural nodes.

References

1. Tonelli, D., Pietroni, N., Puppo, E., Froli, M., Cignoni, P., Amendola, G. and Scopigno, R. (2016). Stability of statics aware voronoi grid-shells. *Engineering Structures*. **116**: 70-82.
2. Liddell, I. (2015). Frei Otto and the development of gridshells. *Case Studies in Structural Engineering*.**4**: 39-49.
3. D'Amico, B. (2015). *Timber grid-shell structures: form-finding, analysis and optimisation*. PhD thesis, Edinburgh Napier University.
4. Lopez, A., Puente, I. and Serna, M.A. Numerical model and experimental tests on single-layer latticed domes with semi-rigid joints. *Computers & structures*. **85**(7): p. 360-374.
5. Fan, F., Ma, H., Cao, Z. and Shen, S. (2011). A new classification system for the joints used in lattice shells. *Thin-walled structures*. **49** (12): 1544-1553.
6. Lopez, A., Puente, I. and Serna, M.A. (2007). Direct evaluation of the buckling loads of semi-rigidly jointed single-layer latticed domes under symmetric loading. *Engineering Structures*. **29**(1): 101-109.
7. Kato, S., Mutoh, I. and Shomura, M. (1998). Collapse of semi-rigidly jointed reticulated domes with initial geometric imperfections. *Journal of Constructional Steel Research*. **48**(2-3): 145-168.
8. Lopez, A., Puente, I. and Aizpurua, H. (2011). Experimental and analytical studies on the rotational stiffness of joints for single-layer structures. *Engineering structures*. **33**(3):731-737.

9. Borri, C. and Spinelli, P. (1988). Buckling and post-buckling behaviour of single layer reticulated shells affected by random imperfections. *Computers & Structures*. **30**(4): 937-943.
10. Forman, S.E. and Hutchinson, J.W. (1970). Buckling of reticulated shell structures. *International Journal of Solids and Structures*. **6**(7): 909-932.
11. Bruno, L., Sassone, M. and Venuti, F. (2016). Effects of the Equivalent Geometric Nodal Imperfections on the stability of single layer grid shells. *Engineering Structures*. **112**: 184-199.
12. Fan, F., Cao, Z. and Shen, S. (2010). Elasto-plastic stability of single-layer reticulated shells. *Thin-Walled Structures*. **48**(10): 827-836.
13. Yan, J., Qin, F., Cao, Z., Fan, F. and Mo, Y.L. (2016). Mechanism of coupled instability of single-layer reticulated domes. *Engineering Structures*. **114**: 158-170.
14. Ahmed, M. and Stutzki, C. (2015). *Steel/Aluminum Grid Shells for Skylights*.
15. Oh, J., Ju, Y., Hwang, K., Kim, S. and Lho, S. (2016). Free node for a single layer free-form envelope subjected to bending moment. *Engineering Structures*. **106**: 25-35.
16. Stephan, S., Sánchez-Alvarez, J. and Knebel K. (2004). Reticulated structures on free-form surfaces. *Stahlbau* **73**(8): 562-572.
17. El-Sheikh, A. (1996), Development of a new space truss system. *Journal of Constructional Steel Research*. **37**(3): 205-227.
18. Wang, L., Jin, H., Dong, H., & Li, J. (2013). Balance fatigue design of cast steel nodes in tubular steel structures. *The Scientific World Journal*.
19. De Oliveira, J. C., Willibald, S., Packer, J. A., Christopoulos, C. and Verhey, T. (2006). Cast steel nodes in tubular construction-Canadian experience. In *Tubular structures-international symposium*, Vol. 11, 523.
20. Haldimann-Sturm, S.C. and Nussbaumer, A. (2008). Fatigue design of cast steel nodes in tubular bridge structures. *International Journal of fatigue*. **30**(3): 528-537.
21. Wei, P., Lu, D., Huang, T., & Wang, L. (2015). Hexahedral mesh smoothing via local element regularization and global mesh optimization. *Computer-Aided Design*. **59**: 85-97.
22. Field, D.A. (1988). Laplacian smoothing and delaunay triangulations. *International Journal for Numerical Methods in Biomedical Engineering*. **4**(6): 709-712.
23. Zhang, H. and Zhao, G. (2010). Quality improvement method for graded hexahedral element meshes. *Computer Aided Geometric Design*. **27**(7): p. 563-575.
24. O'donnell, J., Seifi, H., Sitler, B., Williams, N., Crolla, K. and Xie, Y. M. (2015, August). Smart Nodes Pavilion–Bi-Directional Evolutionary Structural Optimization and Additive Manufacturing. In *Proceedings of IASS Annual Symposia, International Association for Shell and Spatial Structures (IASS)*. **2015**(2): p. 1-12.
25. Seifi, H., Xie, Y.M., O'donnell, J. and Williams, N. (2016). Design and fabrication of structural connections using bi-directional evolutionary structural optimization and additive manufacturing. *Applied Mechanics and Materials, Trans Tech Publ*.
26. Williams, N., Prohasky, D., Burry, J., Crolla, K., Leary, M., Brandt, M., Xie, Y.M. and Seifi, H. (2015). Challenges of scale modelling material behaviour of additive-manufactured nodes, in *Modelling Behaviour*. Springer, 45-51.
27. Galjaard, S., Hofman, S. and Ren, S. (2015). New opportunities to optimize structural designs in metal by using additive manufacturing, in *Advances in Architectural Geometry 2014*. Springer, 79-93.
28. Huang, X. and Xie Y.M. (2010), *Evolutionary topology optimization of continuum structures: methods and applications*: John Wiley & Sons.
29. Min, C., Dong, X., Yang, Z., Liang, S., Shilin, D., Dasui, W., Wei, F. and Anan, Z. (2010). Experimental research and finite element analysis on joints of Sun Valley steel structure for the Expo Axis project [J]. *Journal of Building Structures*. **5**: 006.
30. Knippers, J. and Helbig T. (2009), Recent developments in the design of glazed grid shells. *International Journal of Space Structures*. **24**(2): 111-126.

CHAPTER 5

EXPERIMENTAL AND NUMERICAL STUDIES ON THE NODES FOR
GRIDSHELL STRUCTURES

Chapter 5: Experimental and Numerical Studies of Nodes for Gridshell Structures

As discussed in previous chapters, design and manufacturing of nodes for gridshell structures are not easy to achieve due to their complex geometry and loading conditions. Besides, the validation of node design is challenging because it is difficult to apply the design loads in a laboratory test. In this chapter, an innovative experimental setup for quasi-static test of nodes under dominant design loads is proposed. Two different symmetrical three-way nodes are designed using bi-directional evolutionary structural optimisation (BESO) for pure axial loads and pure out-of-plane bending moments respectively, and then manufactured using additive manufacturing (AM). A test rig is designed in this study and manufactured for the node testing under design loads. In addition, a 3D finite element analysis is conducted, and the numerical model is validated against the test results. It is found that the bolt tolerances should be considered in the design of the test setup.

5.1. Introduction

Structural node is one of the most critical components in a gridshell structure, which is responsible for transferring loads in the system. Also, the node stiffness could significantly affect the behaviour of the gridshell structure [1-7]. Therefore, it is very important to evaluate the effectiveness of the node design concept. However, it is usually difficult to simulate the complex geometrical, topological and loading conditions of a node in experiment. In most cases, the node conditions are highly simplified in the experimental tests.

Several approaches have been used in the design of test setup for structural nodes. The first approach is to simplify the geometry, topology and loading conditions of the test specimen. In the experimental study carried out by Lopez et al. [8] on nodes for single layer structures, the nodes were simplified as 2-way nodes, and only the out-of-plane bending moment was applied. The effect of combination of different parameters on the improvements of joint stiffness and rotational capacity was investigated [8]. Conventional four-point bending tests were conducted with mobile supports as shown in Figure 5-1a. The specimens for the four-point bending test are shown in Figure 5-1b. The experimental results presented only the bending behaviour and the rotational stiffness of the joints.

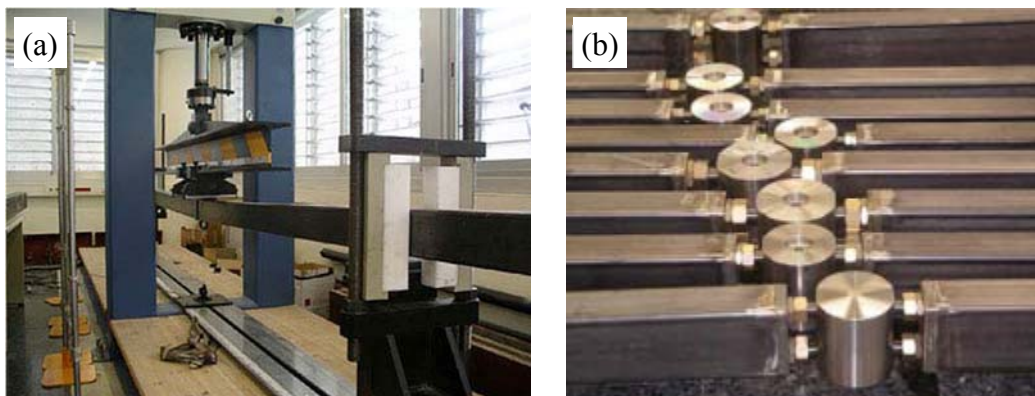


Figure 5-1: (a) Four-point bending test of the joint system, (b) specimens for the four-point bending test.

The second approach is to test the node when it is assembled in a structure by applying load on the structure. Although, in this method, the node is subjected to the internal loads from the connected members, which is similar to real life situation, the applied loads are usually different from the design loads. Besides, to test one node, other nodes and members in the structure might be damaged during the tests. This approach was used by Lopez et al. [1] in the numerical and experimental investigations of the influence of joint rigidity on the global behaviour of single-layer latticed dome structure. In their study, to validate the numerical analysis, two experimental tests were conducted. The first was on a simple structure with only one free node (Figure 5-2a) and the second was on a complete single-layer dome with seven meters span (Figure 5-2b). During the tests, the load was applied on the central node and the vertical displacement was measured.

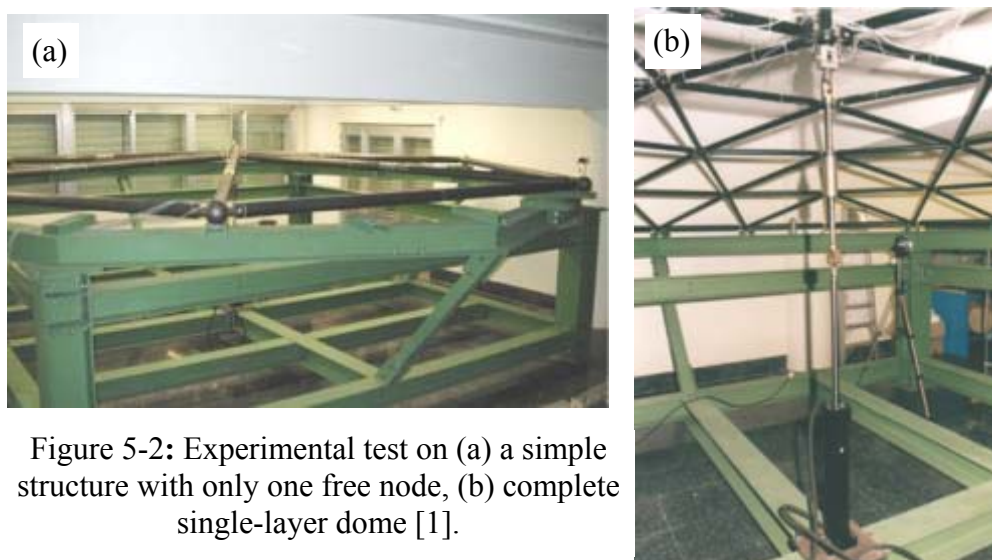


Figure 5-2: Experimental test on (a) a simple structure with only one free node, (b) complete single-layer dome [1].

Huihuan et al. [9] conducted experimental and numerical studies to investigate the influence of joint rigidity on the mechanical performances of squared plan-form single-layer structures. Limin et al. [10, 11] constructed a model of substructures to investigate the anti-progressive collapse mechanism of long-span single-layer spatial grid structures. Eight full-scale specimens were considered in their studies. Figure 5-3 shows the designed test setup in their

study consisted of a self-balanced spatial support system and a vertical reaction frame used to apply an upward load.

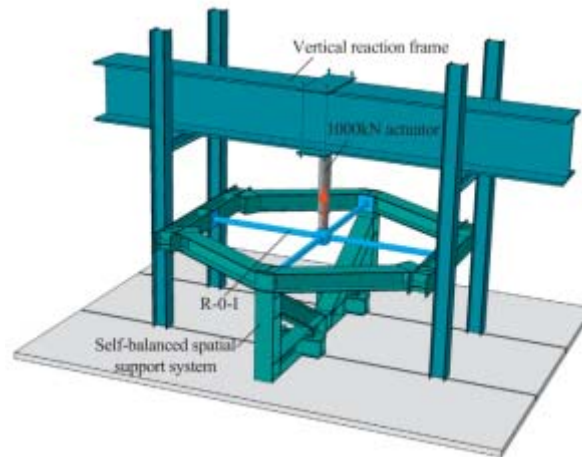


Figure 5-3: Test setup used in Limin et al. study [10].

The third approach is designed to be capable of covering all dominant loading and geometrical conditions of the node. In the full scale laboratory test conducted in Zhejiang University [12], loading devices were aligned with the directions of the design loads. In this test setup, a big spherical frame was needed to support the loading devices pointing to the node from different directions in space as shown in Figure 5-4. Although this test rig is versatile, it is very expensive and difficult to construct.



Figure 5-4: Overall view of experimental setup in Min et al. study [12].

In this study, an innovative test setup is designed, which is more flexible compared to the first two approaches, and is cheaper and easy to set up compared to the full scale loading device.

5.2. The design concept of test setup

The new test setup developed in this study is general, easily accessible and able to simulate the dominant loading conditions of the node of gridshell structure.

The idea of the test setup introduced in this section is to design a mechanism to distribute the applied vertical load to the connecting faces of the node. The distributed loads could properly simulate the design loads in the test. In the proposed test rig, pin connections are used, which would have minimum friction and reduce the influence on the rotational freedom. As discussed in previous chapters, due to membrane action of gridshell structures, the dominant load case in these structures is the axial load. Although out-of-plane bending and in-plane bending components are also affecting the design of the members, they are not as significant as the axial load. Shear forces and torsion moment are usually neglected as they are very small. Therefore, the axial load, out-of-plane bending moment and in-plane bending moment are considered in the designed test setup in this section.

To consider out-of-plane bending moments and in-plane bending moments, eccentricities of the axial loads are applied at each connecting face of the node (Figure 5-5).

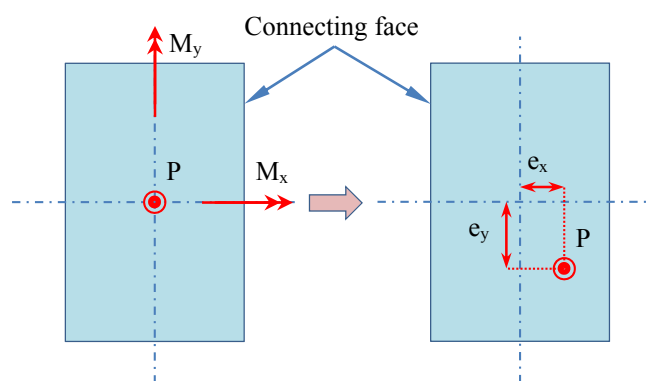


Figure 5-5: Application of out-of-plane bending moments and in-plane bending moments.

The concept of the test setup is based on the simple operation of changing the direction of the applied loads to the desired direction (vertical direction) by using a rotating part. This operation is schematically shown in Figure 5-6. As can be seen in Figure 5-6, two pairs of residual loads (dashed vectors) are generated in the reverse direction of the applied loads. These residual loads are combined and transferred to the ground through a pin support.

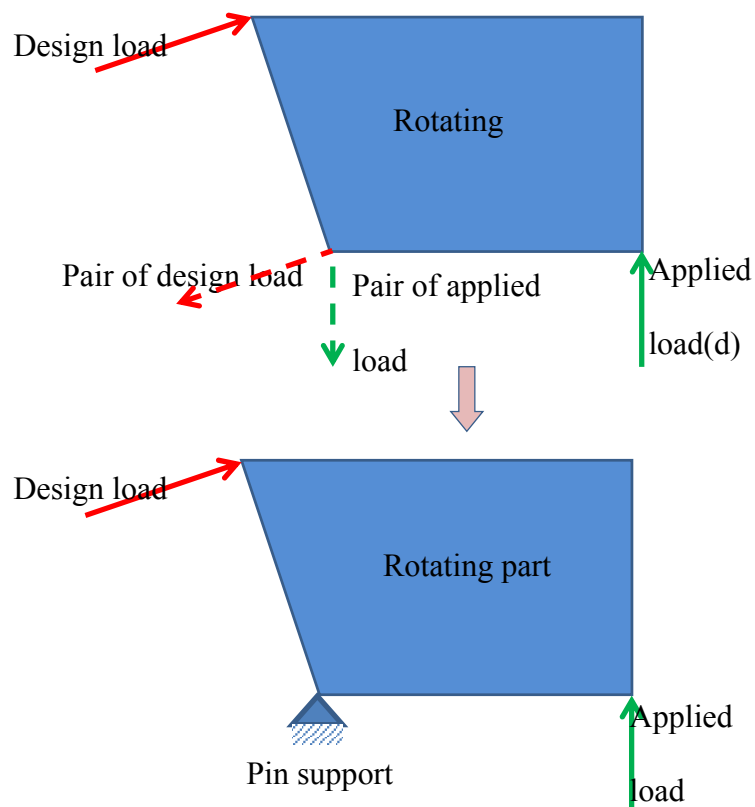


Figure 5-6: Schematic of changing the direction of the applied loads using a rotating part.

When all loads are in vertical direction, the resultant of the loads can be used as the only controlling load in the test setup (Figure 5-7).

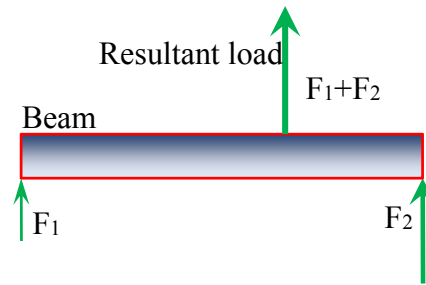


Figure 5-7: Using a beam to combine two vertical loads.

The design procedure of the new test setup is defined in a few steps. The arbitrary geometry conditions used for the nodes in Chapter 4: is selected to demonstrate the test rig design procedures. The perspective of a transitional node which is designed in Chapter 4: is shown in Figure 5-8.

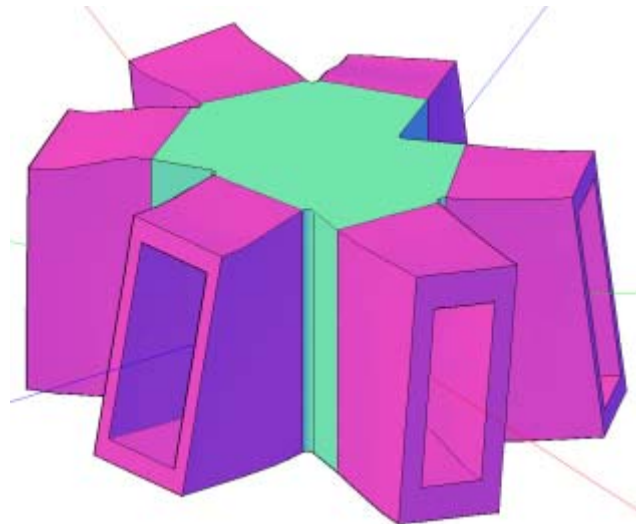


Figure 5-8: 3D node designed based on arbitrary geometrical parameters shown in Table 4-2. It should be noted that the procedures discussed here are for test rig design under individual load case. The first step is to apply the axial component of the load case to the centre of the connecting face. The direction of this axial component crosses the centre point of the node (Figure 5-9).

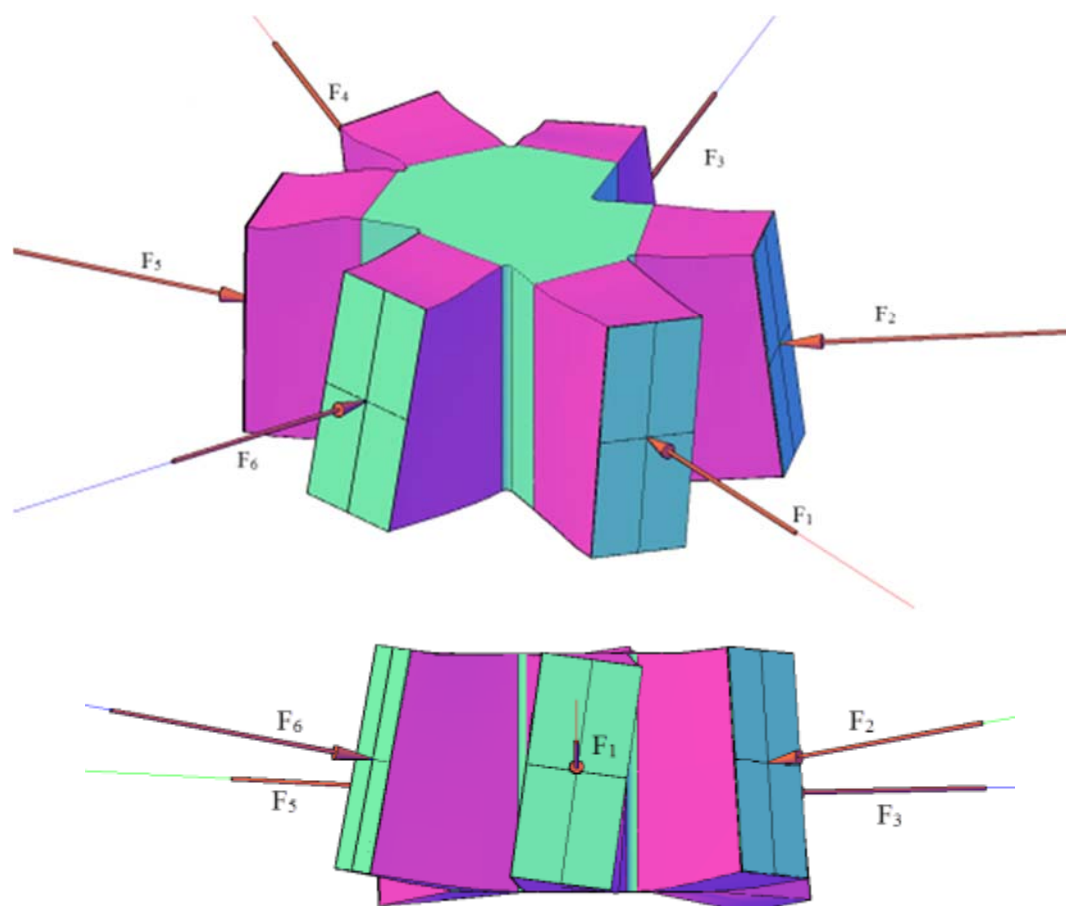


Figure 5-9: Axial loads applied concentrically on the node.

The next step is to apply the eccentricity calculated from the bending moments as shown in Figure 5-5. In this example, constant eccentricities of 30 millimetres are applied to the axial loads in both directions (Figure 5-10).

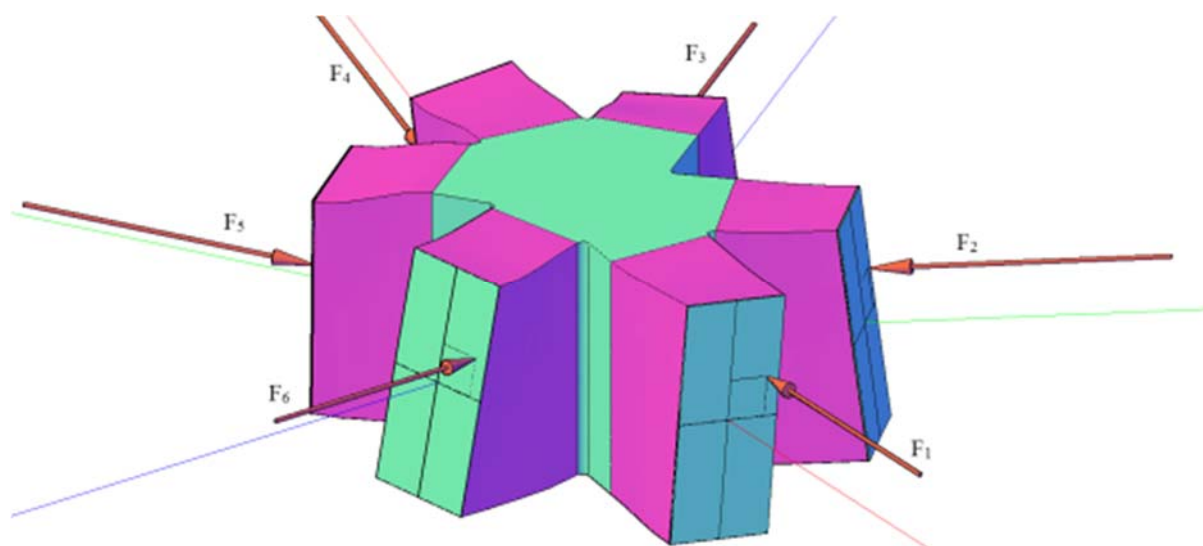


Figure 5-10: Eccentric axial loads applied on the node.

The vertical planes crossing through the point of the applied eccentric axial loads are needed to define the rotating plates in it. To define these planes on the connecting faces, z-vector and the vector of axial load are used. In this step, the position of the bolt hole for eye connection can be found by aligning the predesigned cleat plates to the lines obtained from intersecting vertical planes and connecting faces (Figure 5-11).

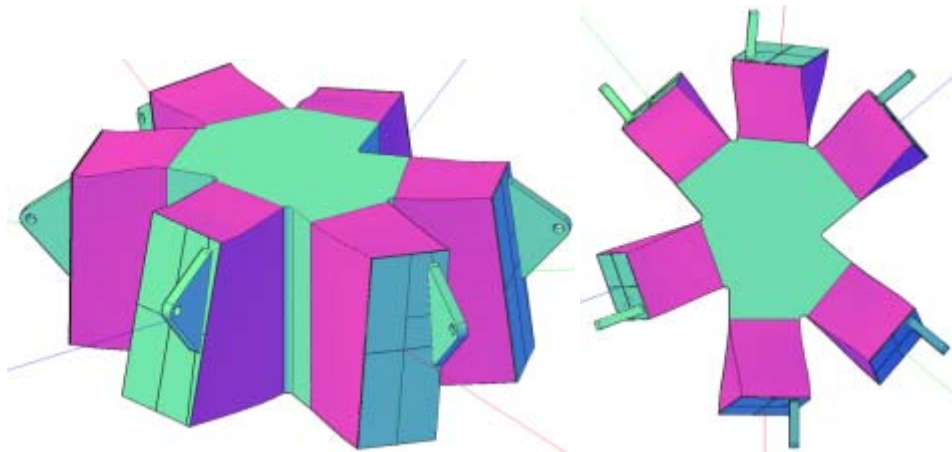


Figure 5-11: Definition of vertical planes.

The force applied vertically on each face can be calculated based on the dimensions of the plate used as the rotating part (Figure 5-12).

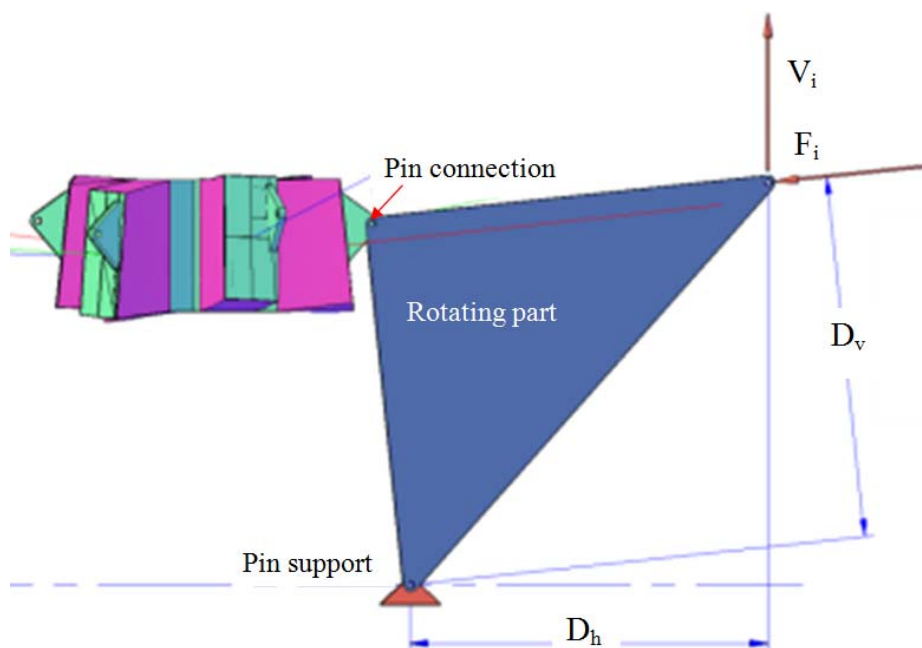


Figure 5-12: Solid plates used as rotating parts for changing the directions and magnitude of the applied vertical loads.

After determining the magnitude and location of all vertical forces, resultant force can be calculated. The process of calculating the location of the resultant force is shown in Figure 5-13. The vertical load F can be applied by using a support frame and a hydraulic jack.

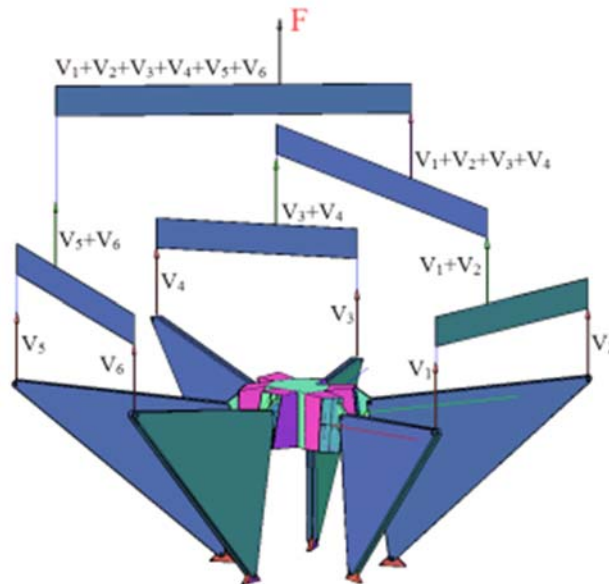


Figure 5-13: Generation of axial loads and bending moment loads.

5.3. Case study

In this study, a test rig is designed and manufactured to test nodes designed by BESO. The test rig evolved during a design process. The first test rig is proposed for testing symmetrical three-way node (Figure 5-14a) designed for two out-of-plane shear loads (Figure 5-14b). As shown in Figure 5-14c, the upper and lower parts of the test rig are clamped in the hydraulic jack and a tension is applied to the system.

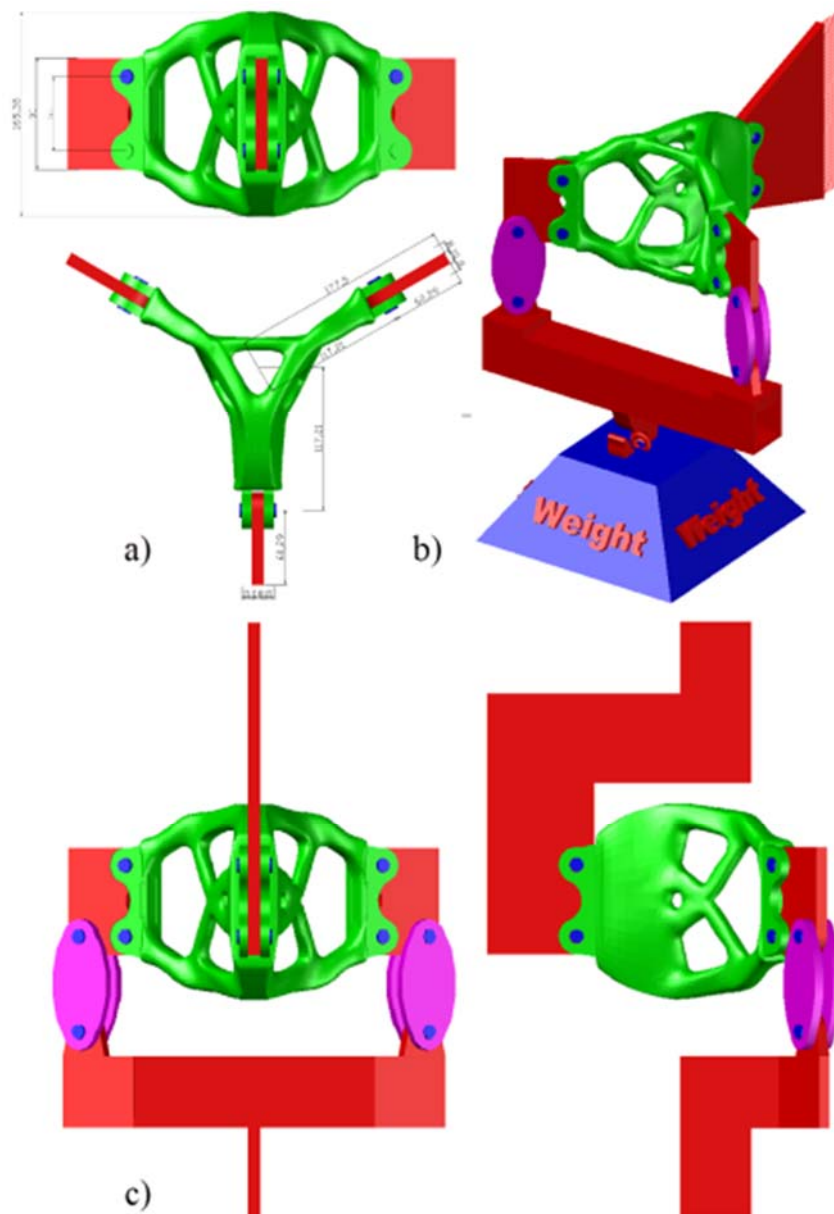


Figure 5-14: Test rig designed to test the shear node.

The advantage of this test rig is that it can be adapted to the conventional testing machines to test small size nodes. However, it cannot be applied to full scale node test. Besides, the test rig is customised for only one node and one loading case. Also, the lower part is made of plates intersecting with the angles of the node's connecting faces, which can be challenging in manufacturing.

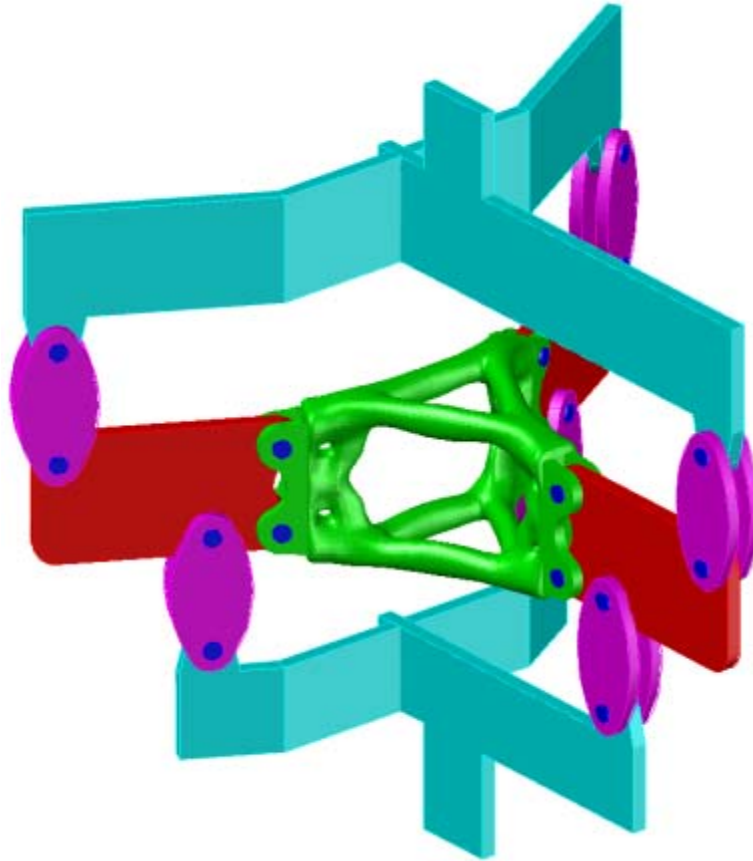


Figure 5-15: Test rig designed to test the bending node.

A similar test rig is designed for testing the node designed for out-of-plane bending (Figure 5-15). In this test rig, the out-of-plane bending on each connecting member is generated by applying two vertical forces in the opposite directions and with a certain eccentricity. This concept is later used in the design of a general test setup. In this design, the upper and lower parts of the test rig are still complicated to be manufactured. To design a simpler test rig for bending node, the concept of the coupled vertical loads is used with a simpler top and bottom parts as shown in Figure 5-16.

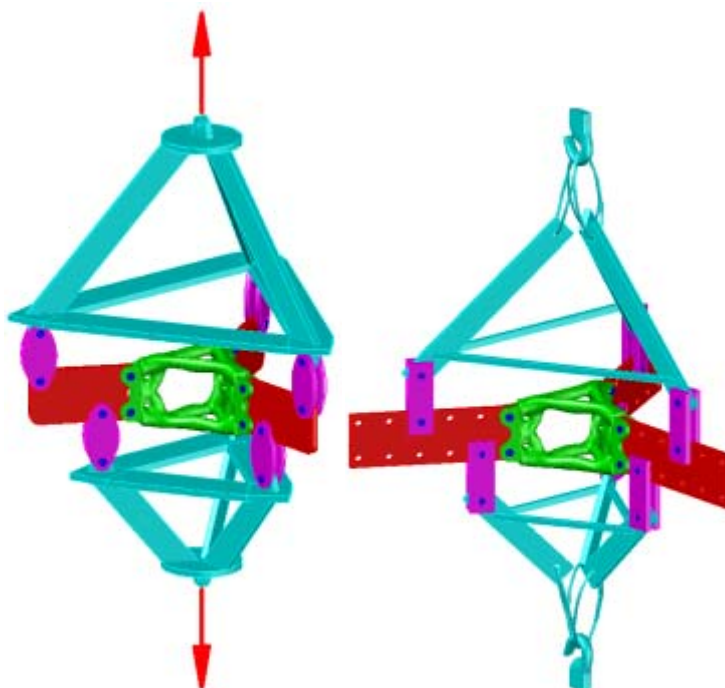


Figure 5-16: Test rigs designed for bending node.

In the third design version, designs for bending node test and shear node test are combined. In this test setup, different configurations of bolts and members are used to simulate different loading conditions for shear and bending nodes. Therefore, in this design, one end of the test rig is connected to the abutment, and the other two ends are connected to the loading device. The design is shown in Figure 5-17.

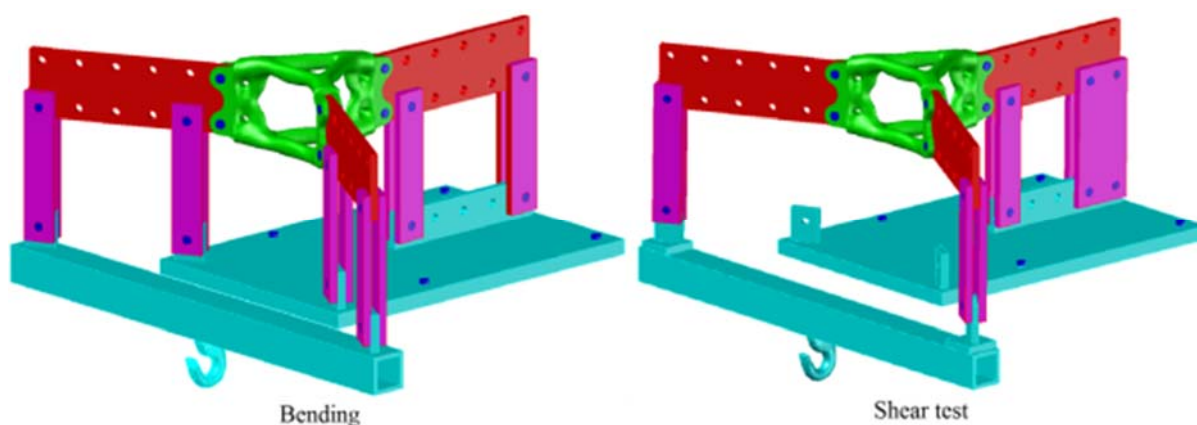


Figure 5-17: Test rig designed for both bending node and shear node.

With a small change in the direction of the applied load, it is re-designed to fit to the application of hydraulic jack (Figure 5-18).

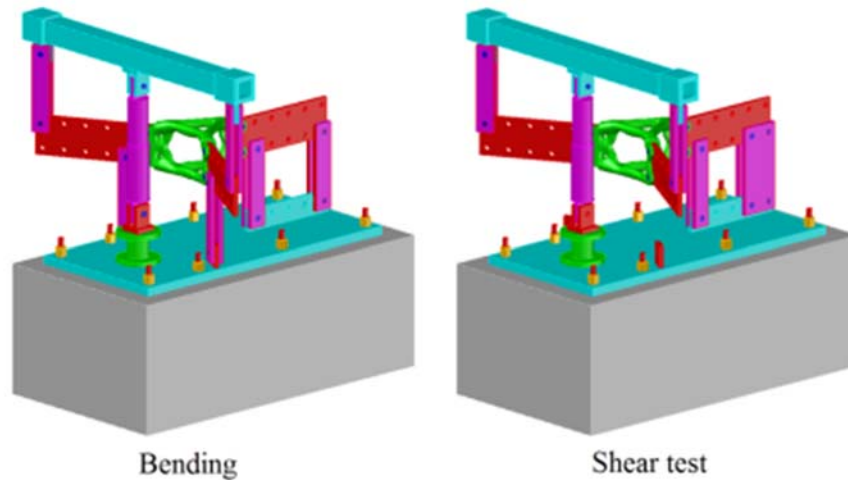


Figure 5-18: Test rig designed for both bending and shear experiment using one hydraulic jack.

The structural system and the internal force diagrams of different configurations of the test rig are shown in Figure 5-19. In shear test configuration, the node face connected to the foundation provides a fixed boundary condition, and the system behaves like a cantilever. In the case of bending configuration, the couples of vertical forces are provided at all three ends. However, as it is shown in Figure 5-19, the test rig is unstable to the horizontal movement.

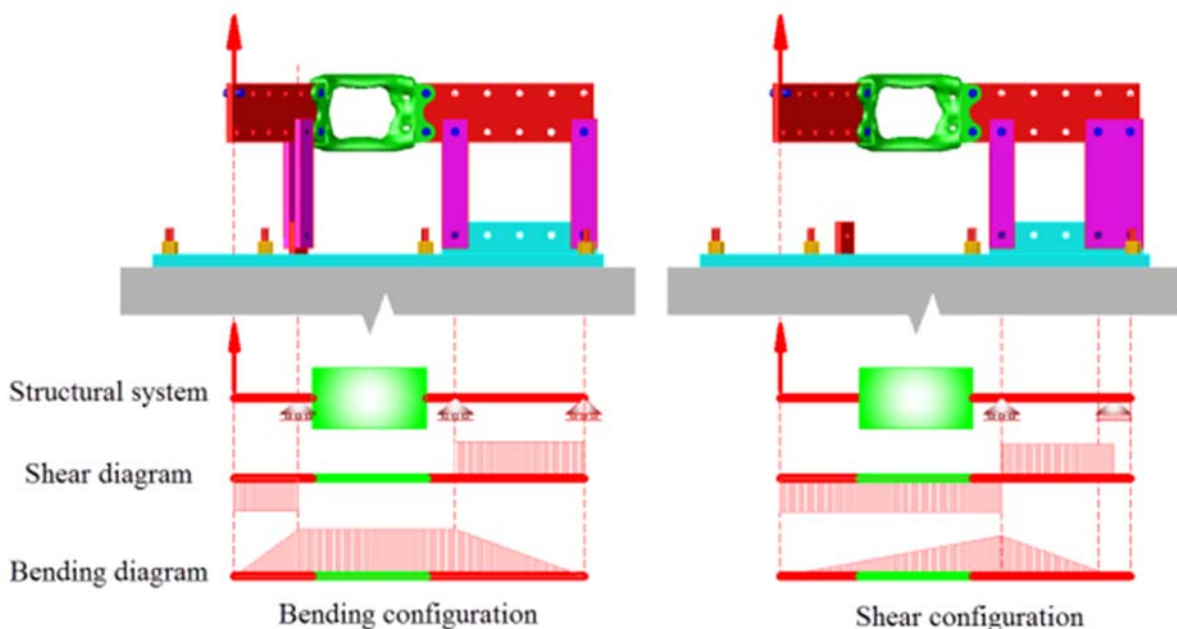


Figure 5-19: Structural system and internal force diagrams for bending node and shear node using one hydraulic jack.

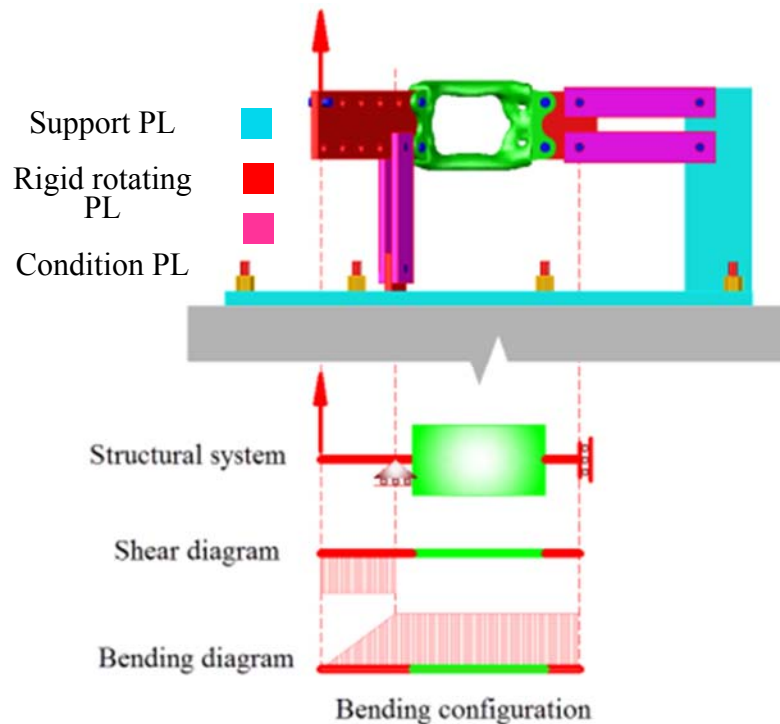


Figure 5-20: Bending configuration of the test rig.

To solve the instability problem of the test rig, the bending configuration of the test rig is modified, as shown in Figure 5-20. The modified test rig is consisted of three parts, including rigid rotating plates, support plates, and condition plates. The rigid rotating plates are used to change the direction of the applied loads. The support plates are connected to the ground to provide support for the node. The condition plates are employed to simulate the boundary conditions of the node.

In the next version, by determining the appropriate sizes for plates and the appropriate bolt holes in each plate, the test rig is designed for four different tests including bending, shear, compression and tension. The proposed test rig can be used to apply different loads to a three-way node by minimal changes in the configurations of bolts and plates. Different configurations of the final design for the test rig are shown in Figure 5-21 to Figure 5-24.

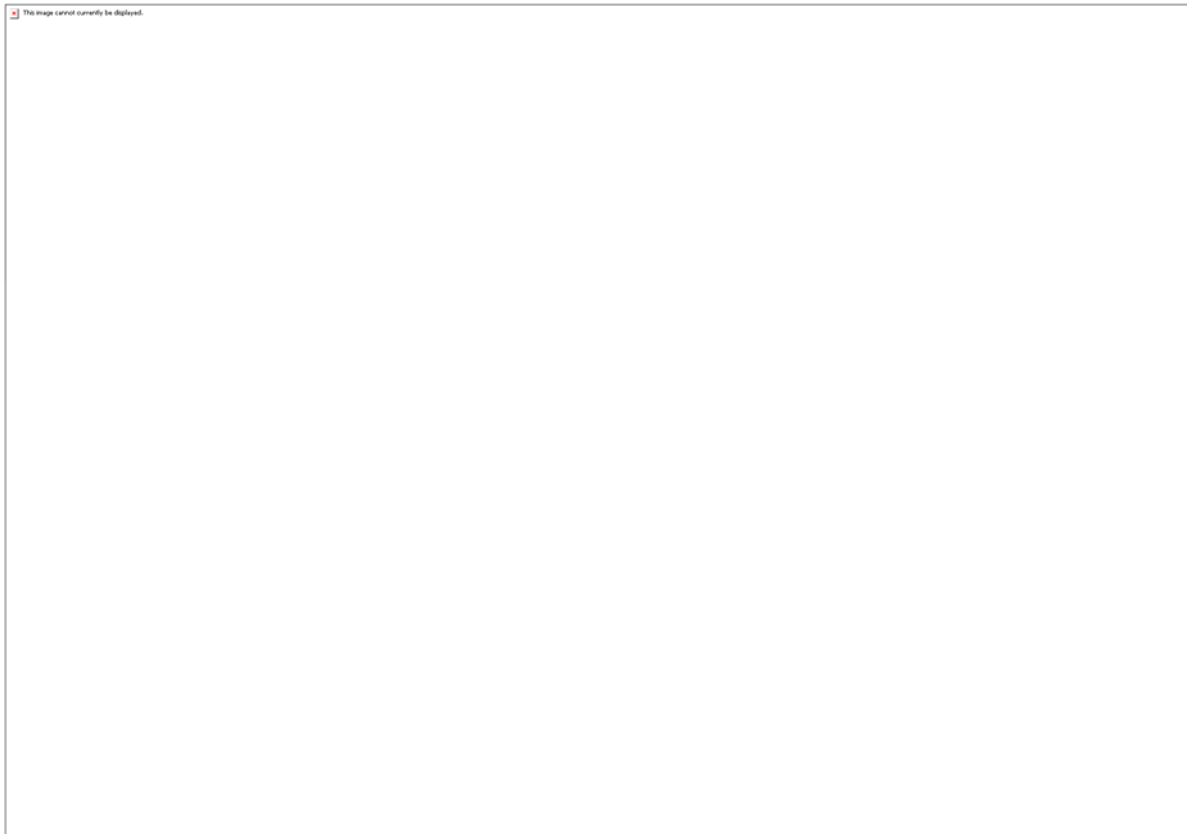


Figure 5-21: The configuration of test rig for shear test.

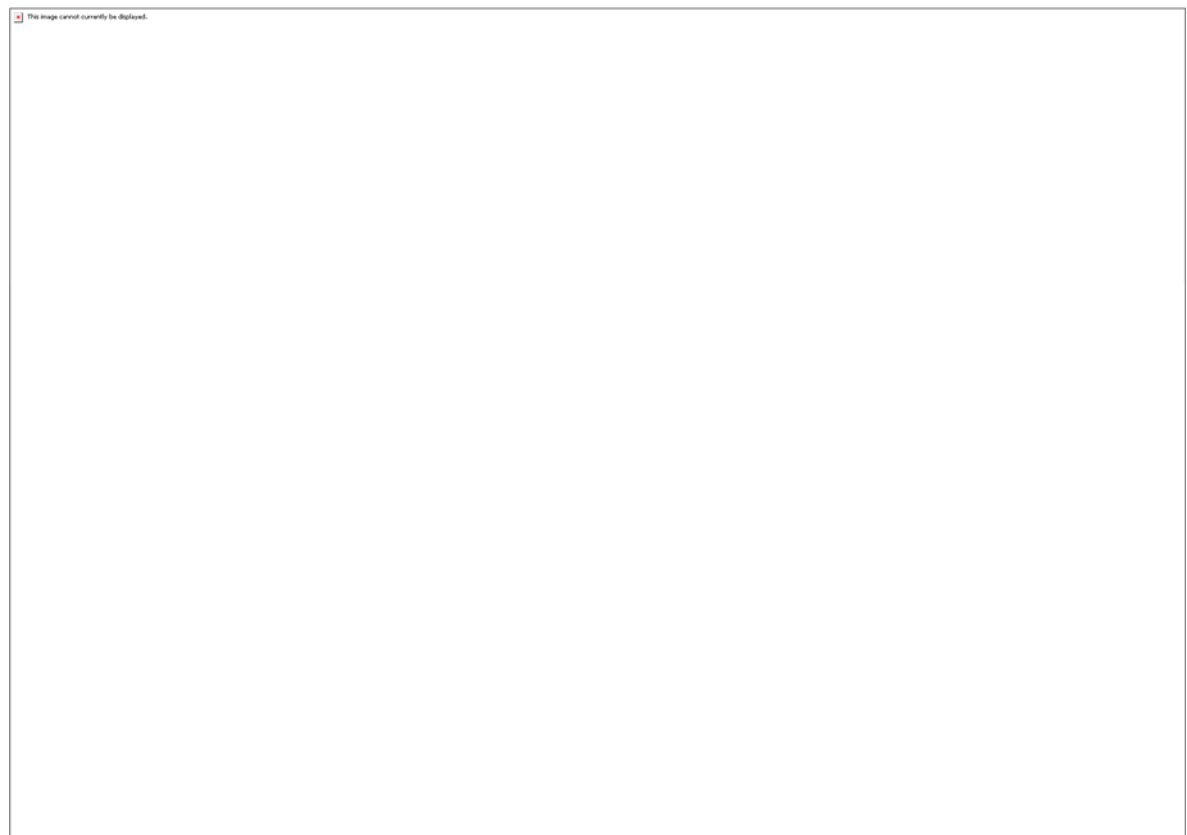
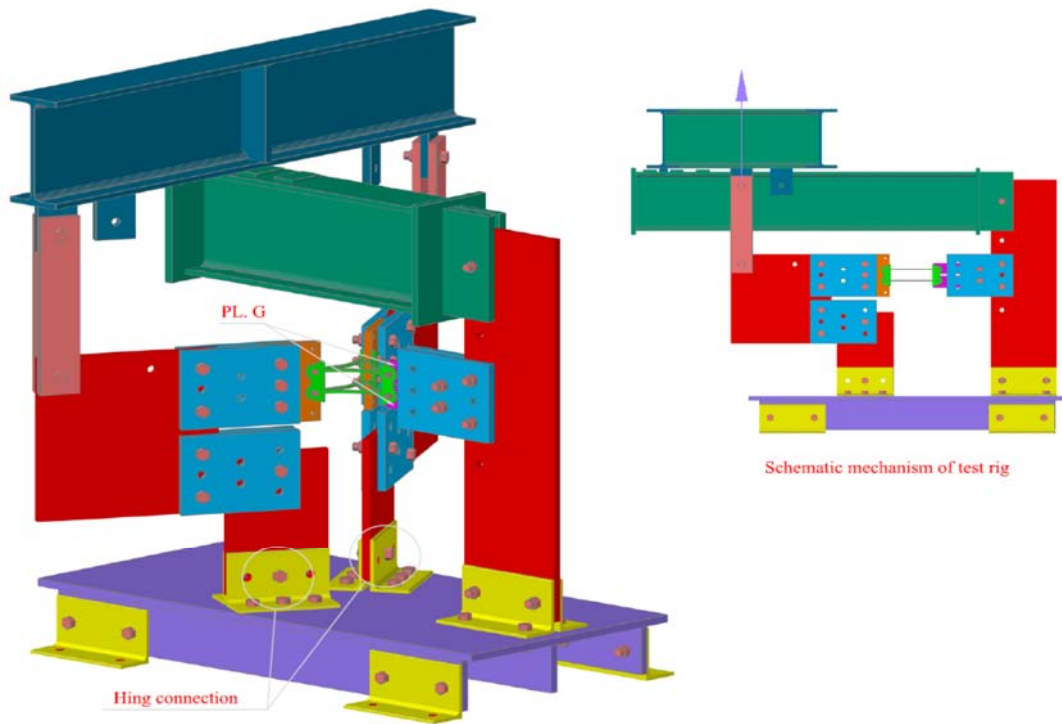
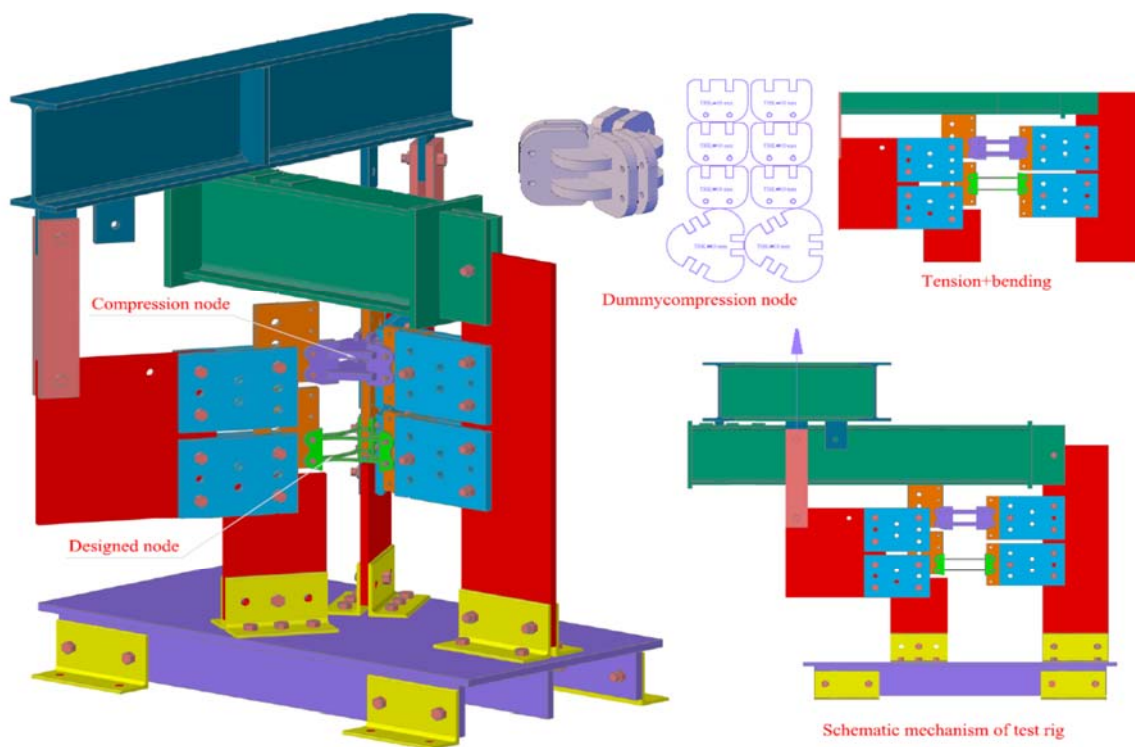


Figure 5-22: The configuration of test rig for compression test.



Configuration for bending test

Figure 5-23: The configuration of test rig for bending test.



Configuration for tension test

Figure 5-24: The configuration of test rig for tension test.

This test rig is manufactured and assembled for bending and axial node tests. Figure 5-25 shows the render and picture of the assembled test rig for axial test.



Figure 5-25: The render and picture of the assembled test rig for axial test.

5.3.1. BESO design

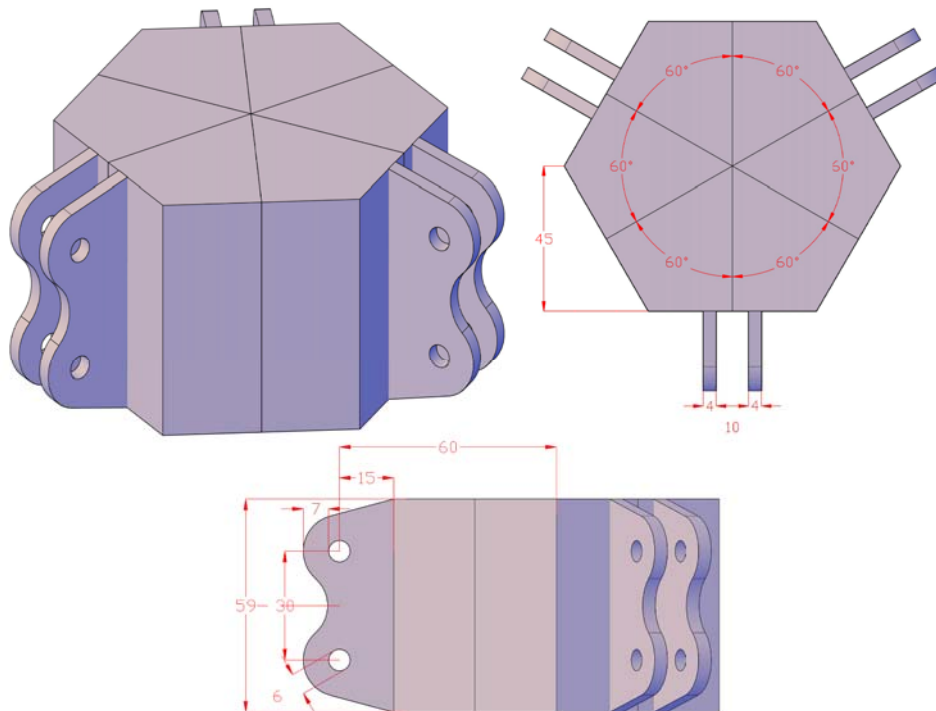


Figure 5-26: Dimensions of the initial geometry of the node for experimental study.

In this section, BESO design is carried out for axial loads. The dimensions of the node to be designed are shown in Figure 5-26. The result of BESO design is shown in Figure 5-27.

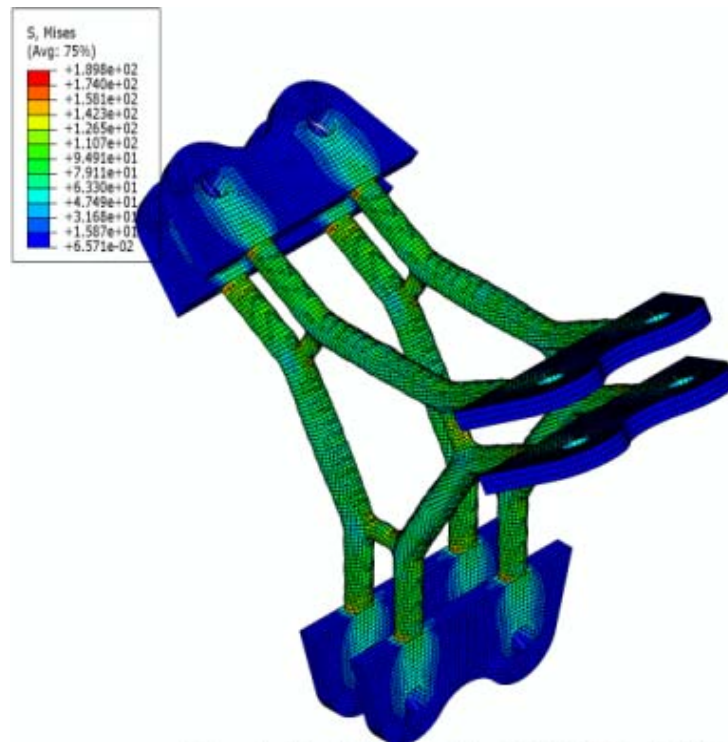


Figure 5-27: BESO design for axial load.

As it can be seen in Figure 5-27, the stress level in most parts of the non-design domain of the node is lower than that in the design domain. Therefore, the non-design domain is changed to a smaller part which is connecting top and bottom parts of the node. By reducing the volume of the non-design domain, the weight and cost of the node is reduced. The new non-design domain is shown in Figure 5-28.

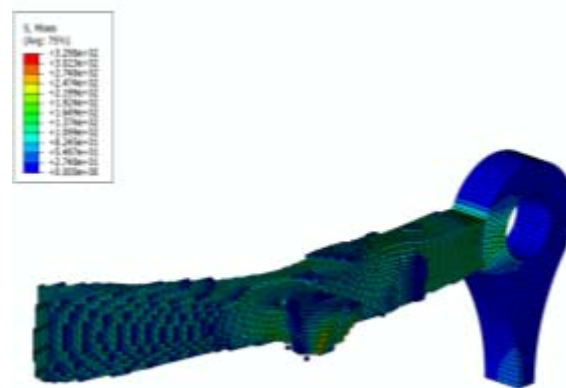


Figure 5-28: BESO design for axial load with a smaller non-design domain.

The BESO design for bending moment is also carried out and the result is shown in Figure 5-29. In this design, the non-design domain consists of small rings around the bolt hole.

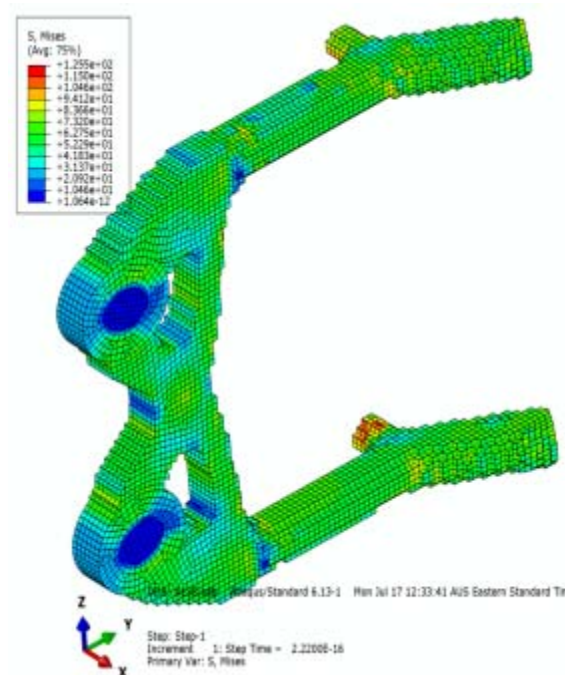


Figure 5-29: BESO design for bending moment.

Figure 5-30 shows the rendered perspective views of the nodes designed for symmetrical axial force and bending moment.

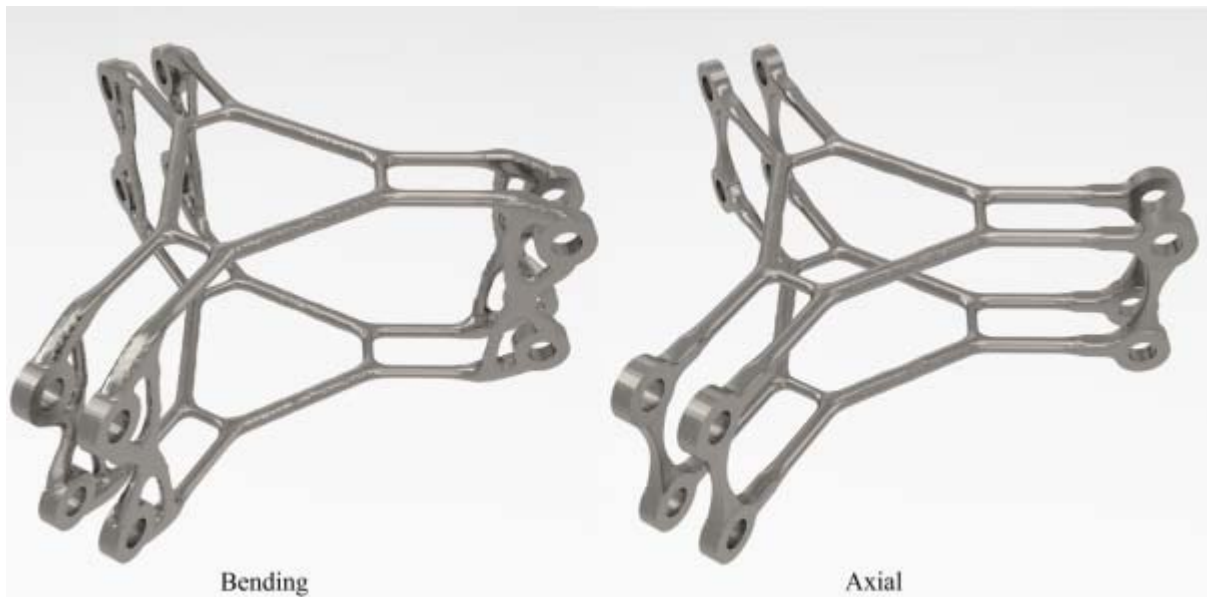


Figure 5-30: Perspective render of BESO design for bending node and axial node.

5.3.2. Material test

The nodes are 3D printed using stainless steel. A series of tensile tests are carried out on dog-bone samples to obtain the stress-strain curve of the stainless steel. The dog-bone samples are also 3D printed. The results of the tensile tests are shown in Figure 5-31.

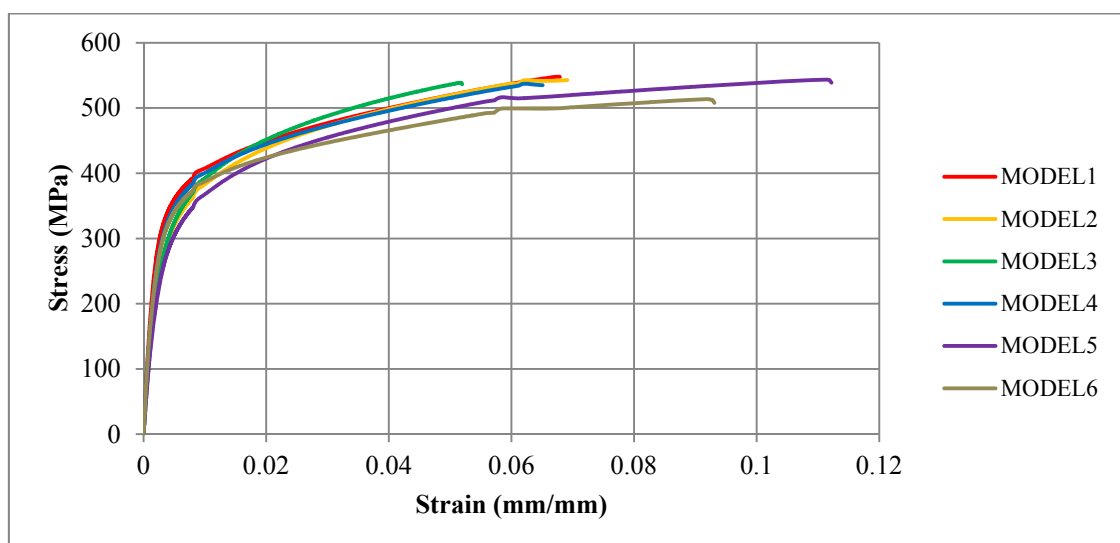


Figure 5-31: The results of tensile tests on 3D printed dog-bone samples. The stress-strain curve used for non-linear simulations is calculated based on the average of the test results. Figure 5-32 shows the strain-stress curve of the tensile test of the 3D printed stainless steel sample MODEL2 and the simplified curve for the simulations.

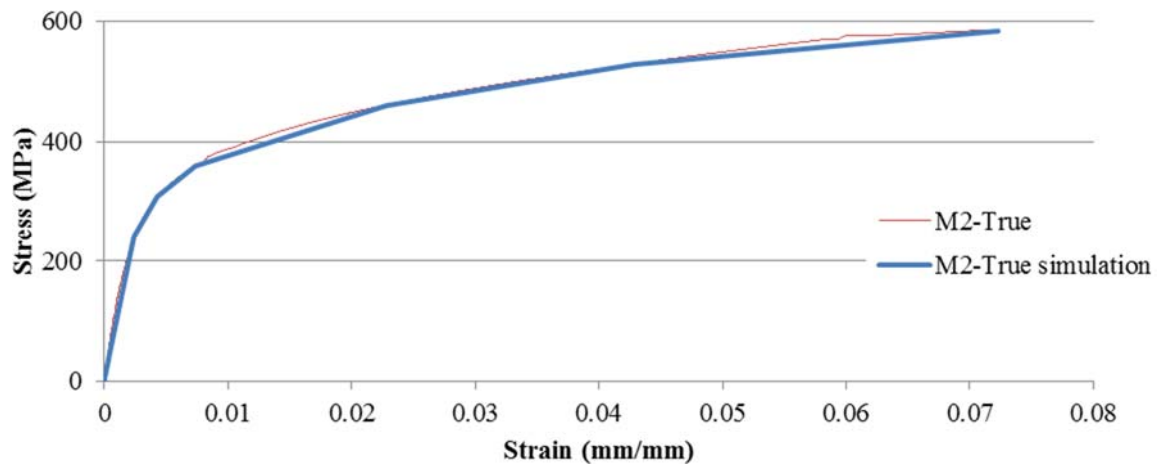


Figure 5-32: The simplified strain-stress curve for non-linear simulations.

5.3.3. Numerical simulation

Since BESO design is carried out based on linear analysis, the BESO results for both tension and compression lead to an identical geometry called axial node. However, the non-linear behaviours of the axial node under tension and compression are different due to the buckling of the slender members in compression. In this study, non-linear finite element analysis of structural nodes is carried out using Abaqus to study the behaviours of the symmetrical three-way nodes under symmetrical tension, compression and bending moments.

To apply loads, the joints which are on the internal surface of the bolt hole are constrained to a reference points. The loads are applied to these reference points. In axial node, the reference point is defined at the centre of the bolt hole. One set of the constrained joints and their attributed reference point is shown in Figure 5-33.

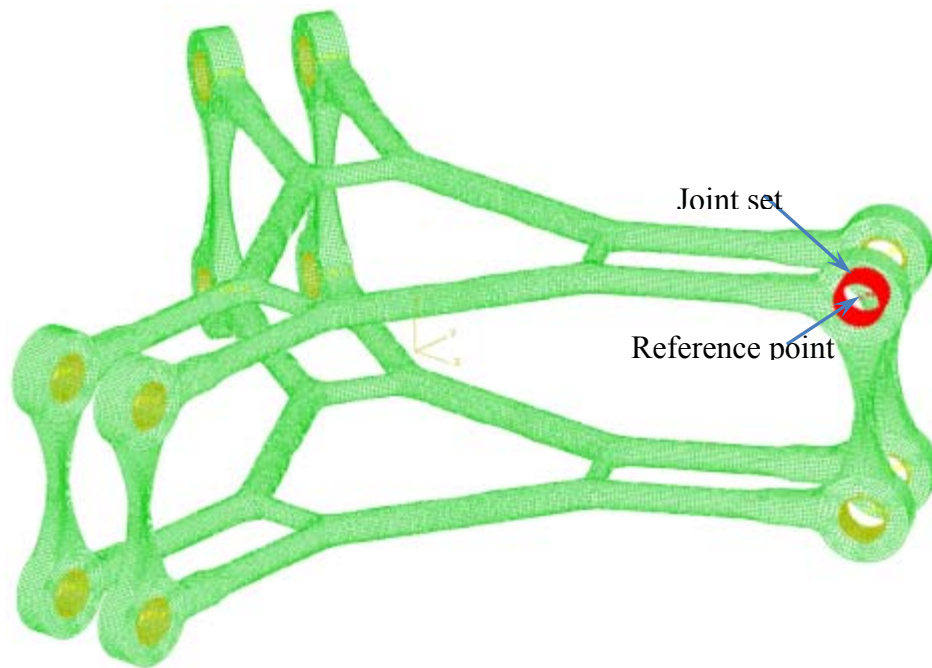


Figure 5-33: Constraint definition for a bolt hole in axial node.

In the numerical model of bending node, the reference point is defined at the centres of the four bolt holes of each face as shown in Figure 5-34.

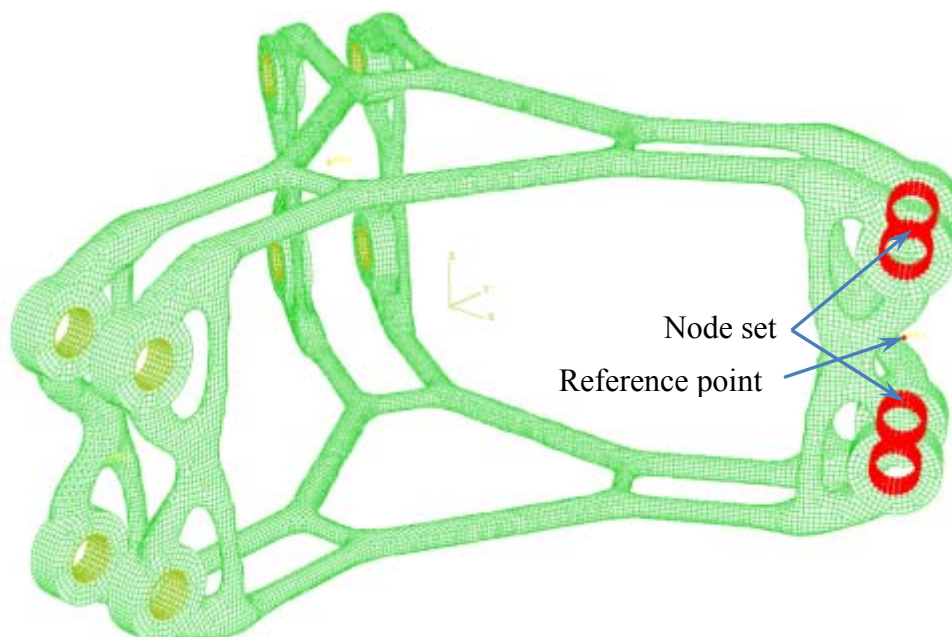


Figure 5-34: Constraint definition for bolt holes of one side of bending node.

The loading condition is simulated by applying displacements to the reference points. In axial nodes, translational displacements in the direction of the connected beam members are

applied to the reference points. In the bending node, out-of plane rotations are applied to the reference points. The applied displacements are shown in Figure 5-35.

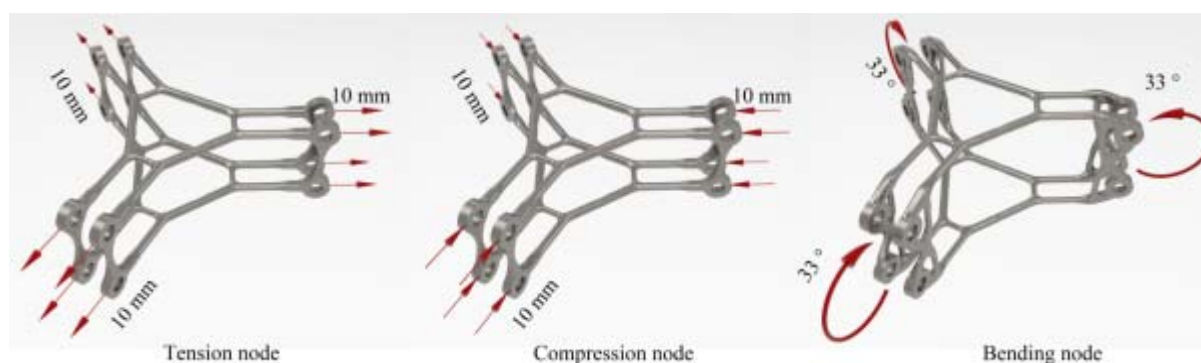


Figure 5-35: The loading conditions of axial and bending nodes.

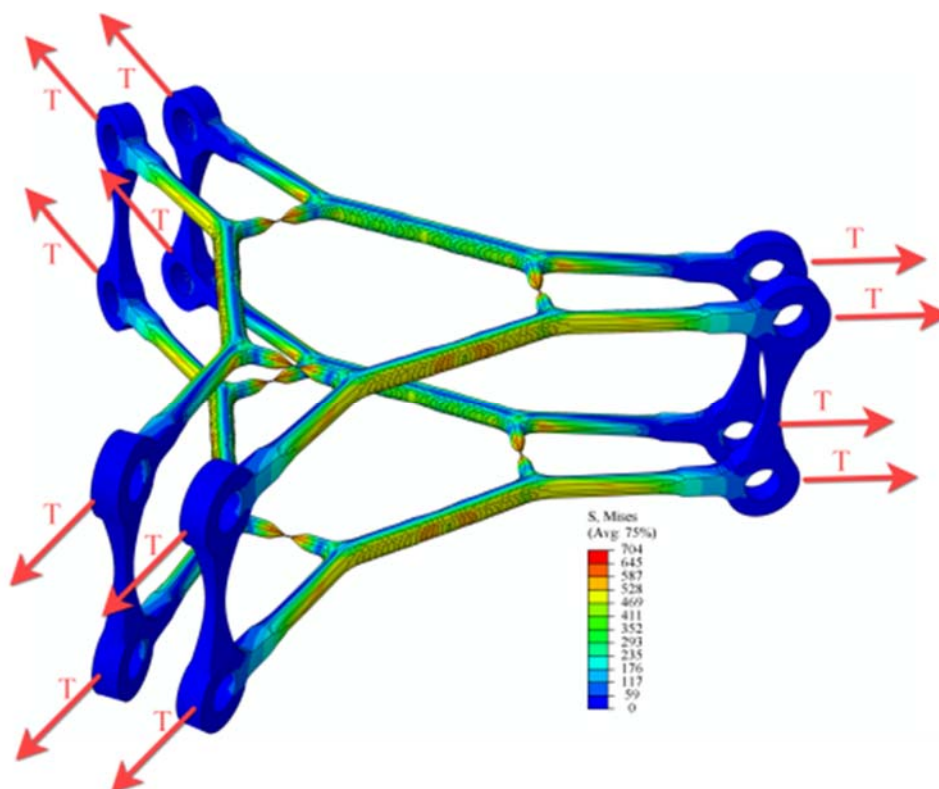


Figure 5-36: Failure of the node under outward axial loads (tension).

The failure mode of the axial node under the symmetrical tension load is shown in Figure 5-36. The force-displacement curve obtained from numerical model for a typical reference point of the tension node is shown in Figure 5-37. As can be seen in the figure, the maximum force applied to one bolt hole is 5kN. The failure of the node occurs in the member type three of the axial node as introduced in Chapter 3. To find the ratio of the internal force of the

failed member to the applied load, the equilibrium equation can be solved for the connection of the three types of members in the node. Figure 5-38 shows the internal forces of the members.

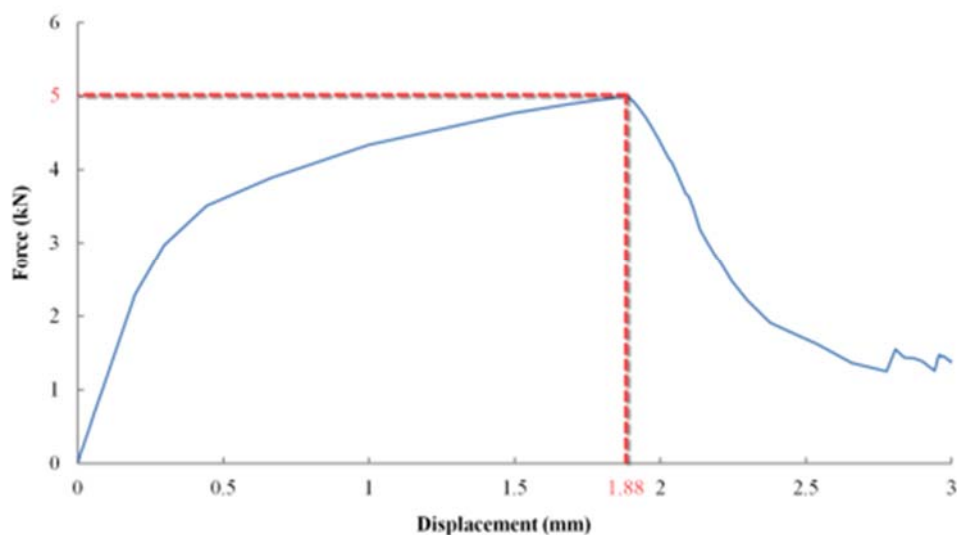


Figure 5-37: Force-displacement curve for tension node.

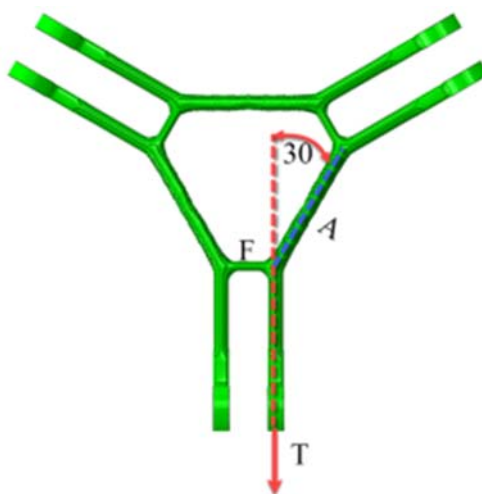


Figure 5-38: Applied load and internal forces of the members of tension node.

Considering the angle between member type one and the applied load, the internal force of member type one is equal to the applied force. Therefore, the equilibrium equations can be solved as follows:

$$\sum F_y = -T + A \cos(30) = 0 \quad \Rightarrow \quad A = \frac{T}{\cos(30)}$$

$$\sum F_x = -F + A \sin(30) = 0 \quad \Rightarrow \quad F = \frac{T \sin(30)}{\cos(30)} = T \times \tan(30) = 0.577 \times T$$

Therefore, the maximum internal force in the member type 3 which causes tensile failure of the member is equal to 2.89kN. The maximum tensile stress of the member is calculated by dividing the maximum tension of this member by the area of its cross section as:

$$\sigma_t = \frac{F}{Area} = \frac{2.89kN}{5.3mm^2} = 545MPa$$

which is matching to the maximum tensile stress of 586MPa as shown in Figure 5-32.

The failure mode of the axial node under the symmetrical compression load is shown in Figure 5-39.

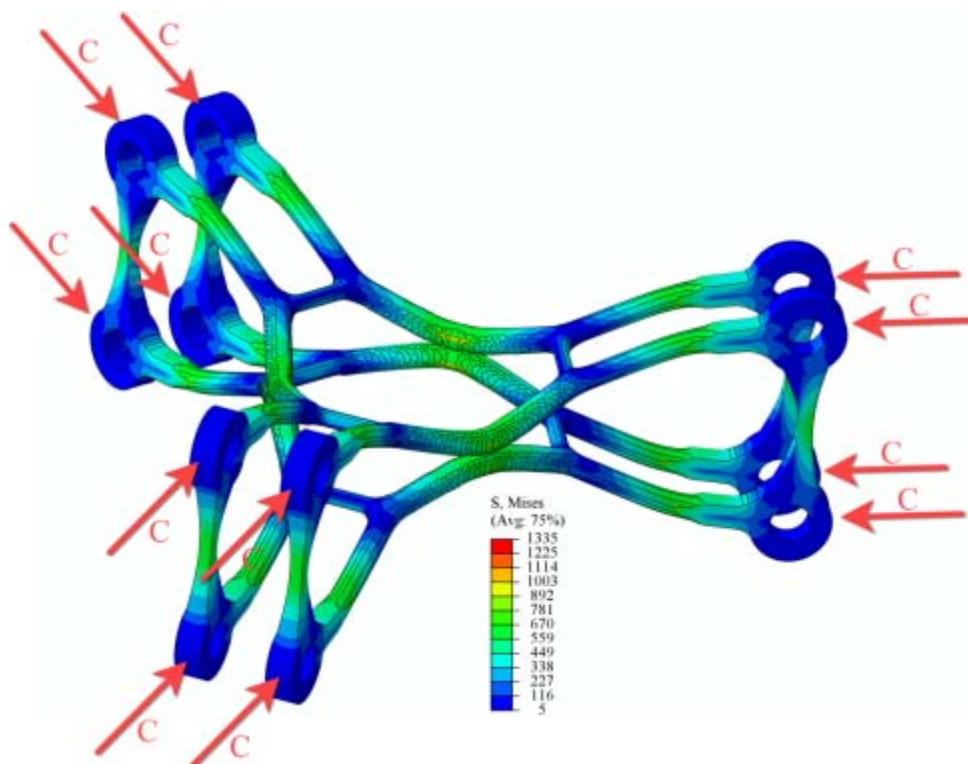


Figure 5-39: Failure of the node under inward axial loads (compression).

The axial node is failed under compression due to the global buckling of the planar substructures. The force-displacement curve of the axial node is shown in Figure 5-40

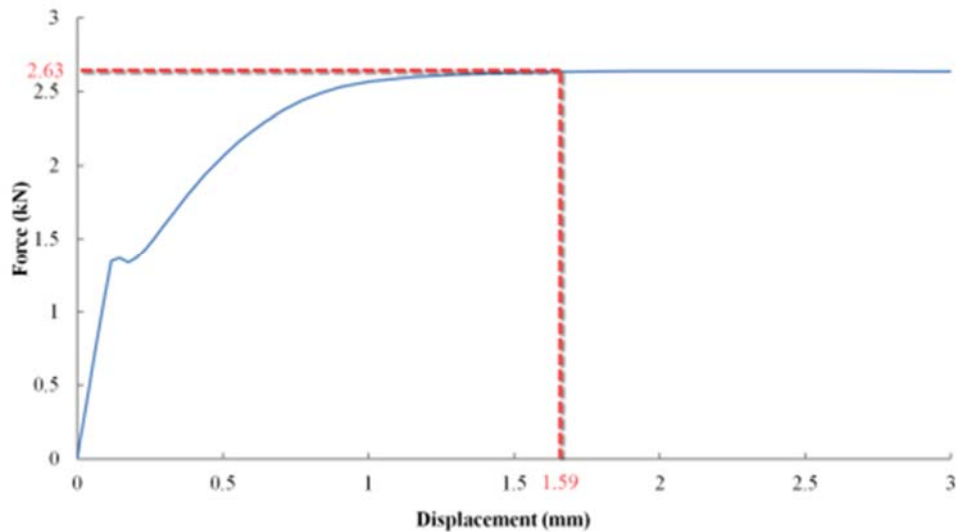


Figure 5-40: Force-displacement curve for compression node.

The applied maximum compression load is 2.63kN. The capacity of the axial node is decreased by 49% in compression compared to the tension capacity of the node.

The failure mode of the bending node under the symmetrical out-of-plane bending moment is shown in Figure 5-41.

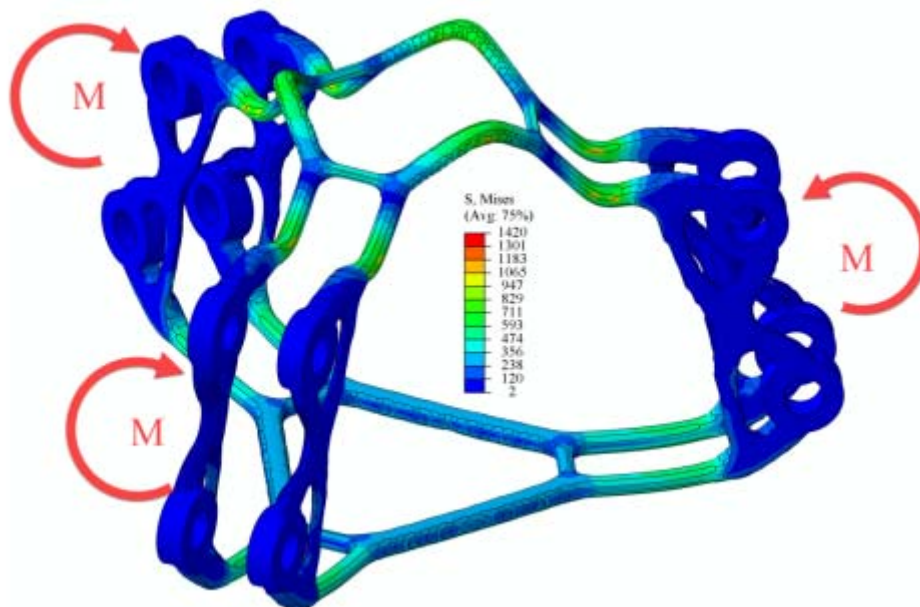


Figure 5-41: Failure of the node under out-of-plane bending moment.

The bending node is failed in buckling on the compression side. The moment-rotation curve of the node obtained from non-linear analysis is shown in Figure 5-42.

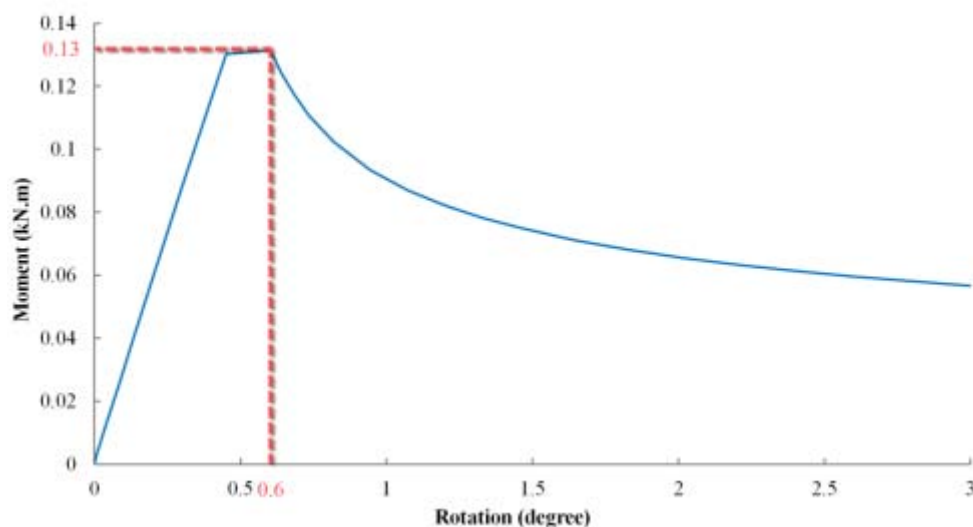


Figure 5-42: Moment-rotation curve for compression node.

As discussed in Chapter 3, the topology of planar substructures in both axial and bending nodes is similar, which is because in linear analysis the behaviour of bending moment is a precise combination of axial behaviour of tension substructure and compression substructure. But in non-linear analysis as shown in Figure 5-41, there are differences between the failure modes of substructures in bending node and their attributed node. The compression substructure of bending node is buckled in a different direction compared to the substructures in compression node which are buckled inside the node. Besides, both tension and compression substructures are subjected to the rotation of the bending node. Also, the tension substructure in bending node does not fail.

5.3.4. Estimation of load cell force

To measure the applied load by hydraulic jack, a load cell is used on top of the hydraulic jack. To select a proper load cell, the capacity of the load cell is estimated by calculating the maximum applied load of each node. The details of loads and dimensions of test rig of each node are shown in Figure 5-43 to Figure 5-45.

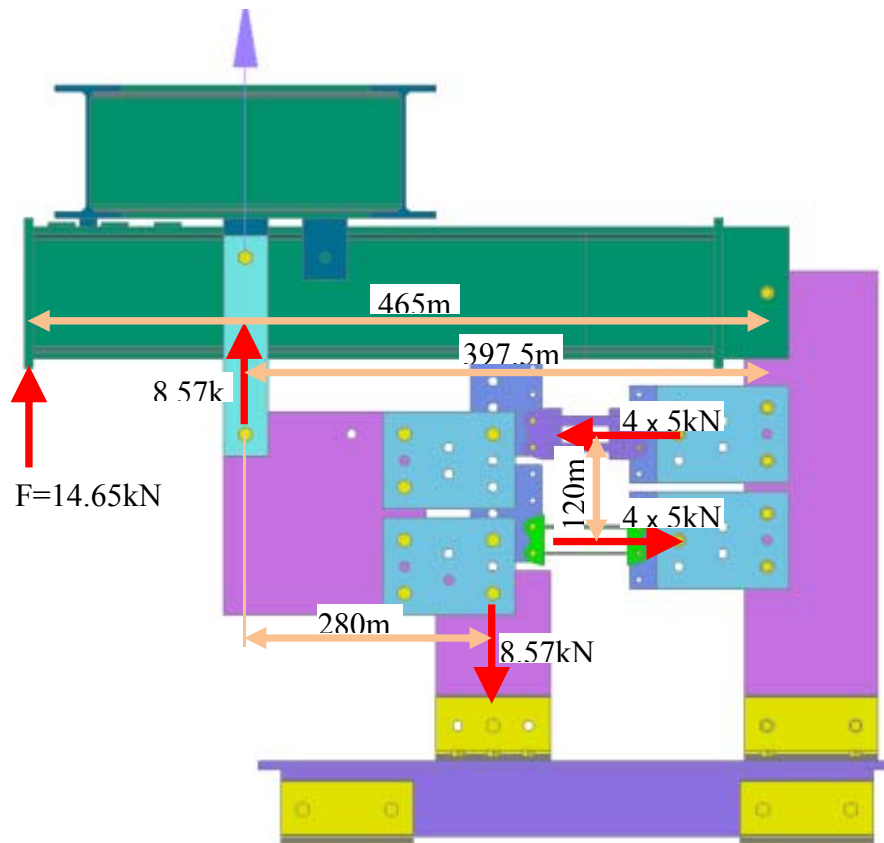


Figure 5-43: Dimensions and forces in test setup for tension node.

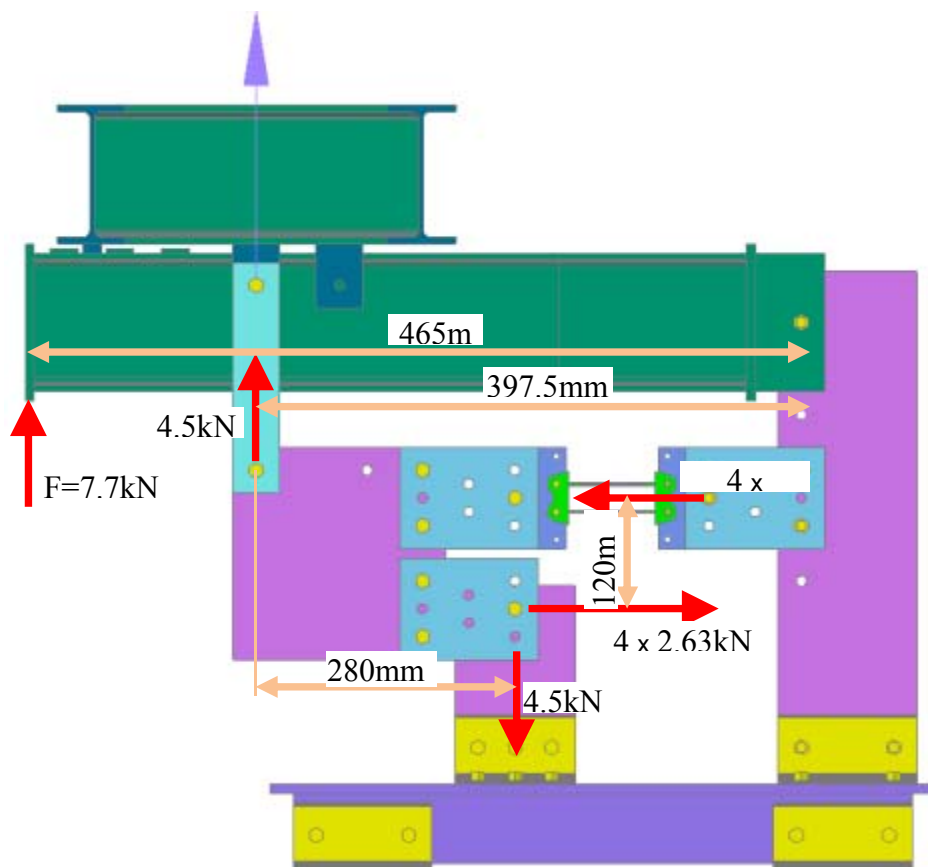


Figure 5-44: Dimensions and forces in test setup for compression node.

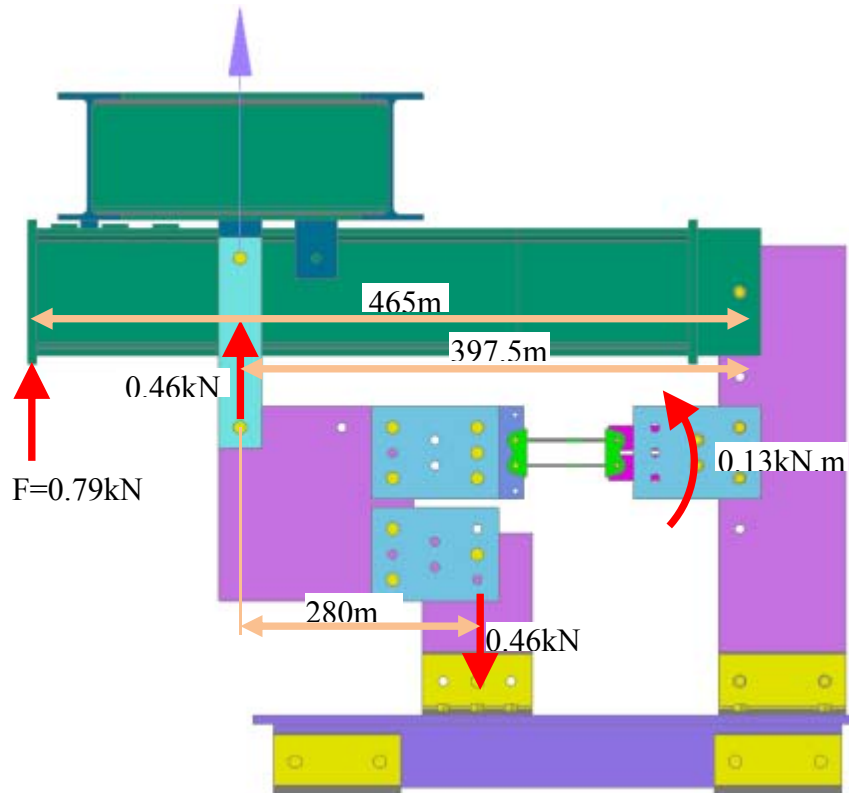


Figure 5-45: Dimensions and forces in test setup for bending node.

5.3.5. Manufacturing

The nodes are manufactured using binder jet method. In manufacturing process, as the slender members are broken in de-powdering step, temporary reinforcing members are added to the model. These members are removed from the nodes before testing. The 3D printed nodes are shown in Figure 5-46.

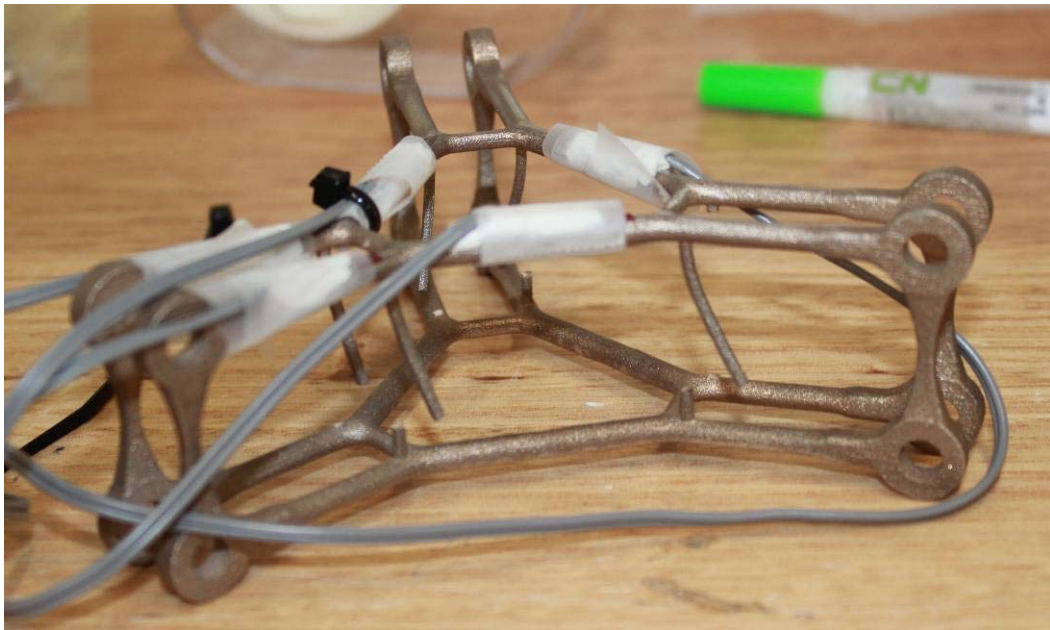


Figure 5-46: An axial 3D printed node used for experiment.

5.3.6. Experiments

Four axial nodes and one bending node are tested using the designed test rig which is demonstrated in section 5.2. After assembling the test rig and placing the node in it, an initial rotation in the rigid rotating plate is observed as shown in Figure 5-47.



Figure 5-47: The initial rigid rotation in the assembled test setup for axial node.

The reason of this initial rotation is that the difference between the diameter of the bolt and the diameter of the hole is not considered in the design process of the test setup, which may cause initial movement and rotation of the plates (Figure 5-48).

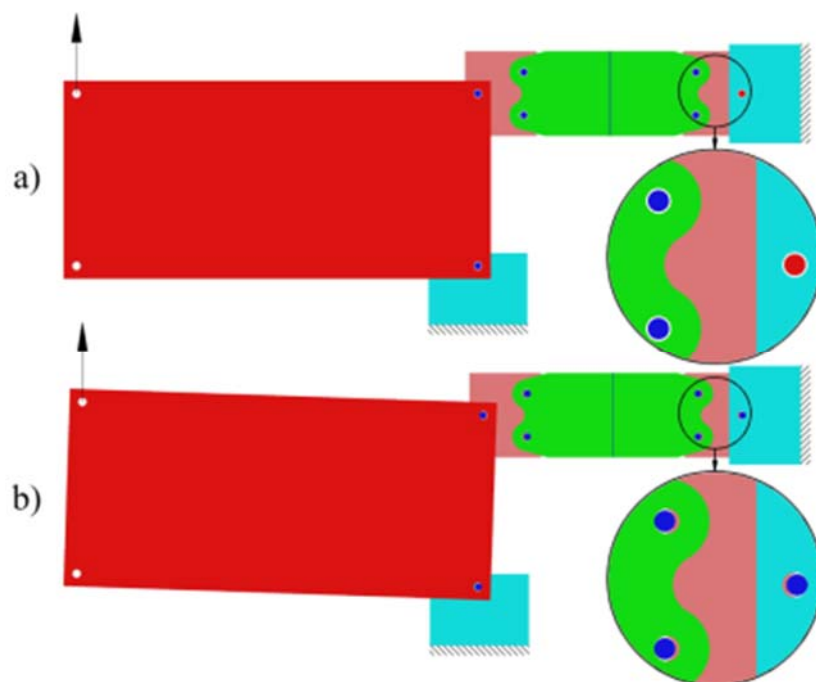


Figure 5-48: Test setup, a) before movement, b) after movement.

To include the initial movement in the simulation, two steps are considered. The first step is to simulate the movement of the node and plates before the surfaces of all bolts and holes are contacted tightly as shown in Figure 5-48b. The second step is to simulate the deformation of the node to failure. The predicted failure mode of the axial node is shown in Figure 5-49.

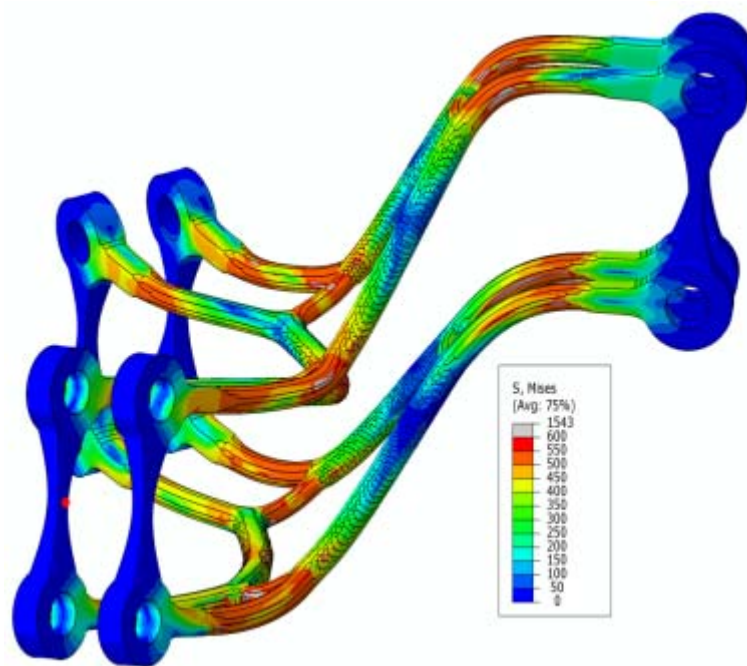


Figure 5-49: Failure mode of the axial node, a) non-linear simulation, b) experiment.

Figure 5-50 shows the force-displacement curve at the connection of the node to one of the rotating parts of the test rig. As can be seen clearly from the curve, the maximum applied load is equal to 8kN. The failure of the node under axial load occurs at the displacement of 3.2mm where node is deformed about 0.2mm at the location of the applied load.

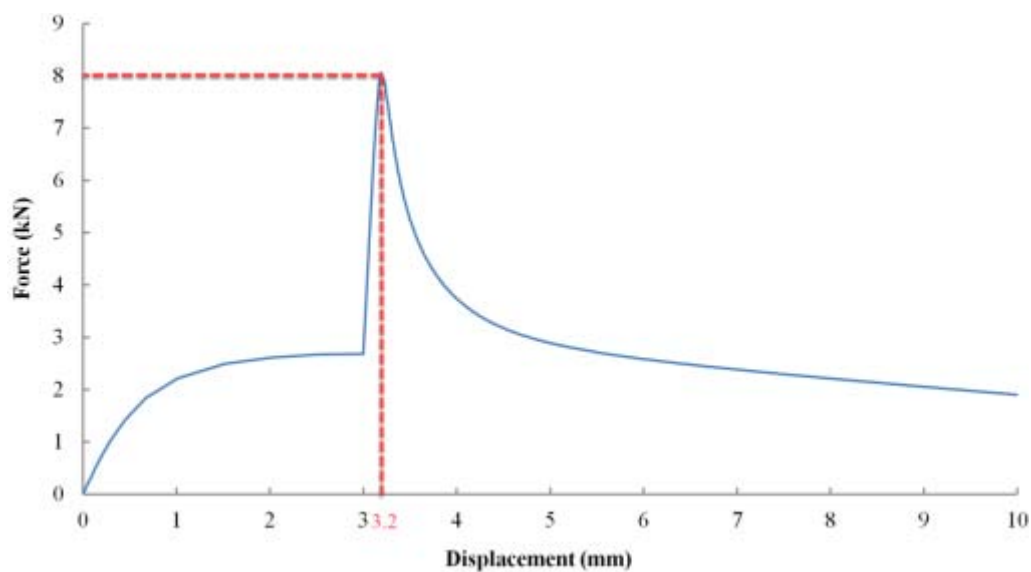


Figure 5-50: Force-displacement curve for compression node.

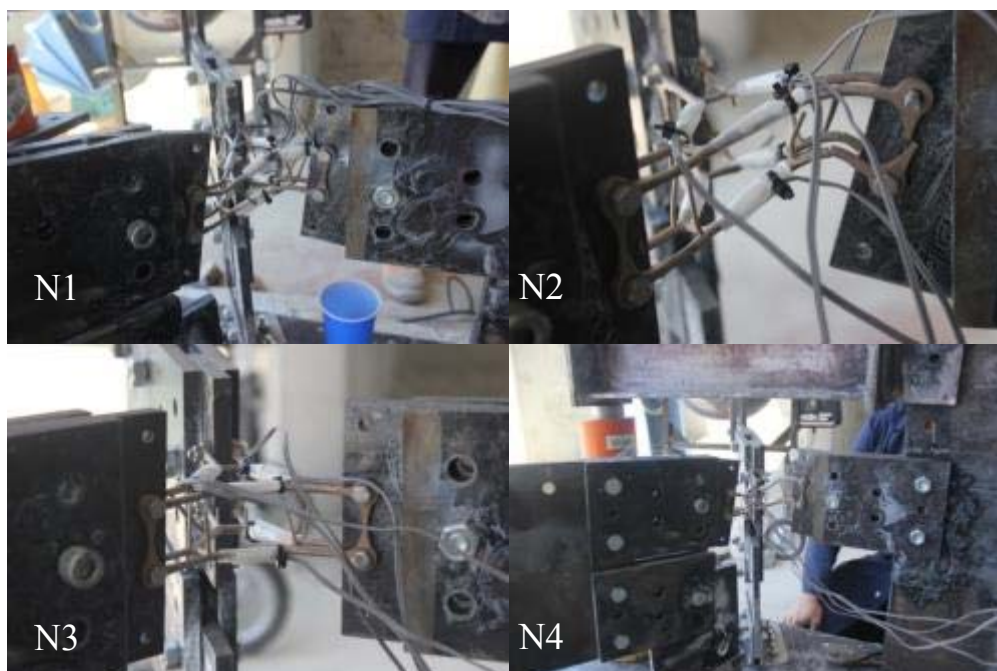


Figure 5-51: Four axial nodes are tested by using the proposed test rig.

Figure 5-51 shows the four axial nodes tested using the test rig. The maximum applied loads measured by the load cell for nodes N1, N2, N3, and N4 are 4.65kN, 5.72kN, 5.31kN, and 5.40kN respectively. By using the dimensions and the assembled configuration of the axial test rig shown in Figure 5-44, the maximum axial loads applied to the nodes by each of both rotating parts (**Figure 5-12**) of the test rig are equal to 6.35kN, 7.81kN, 7.25kN, and 7.38kN.

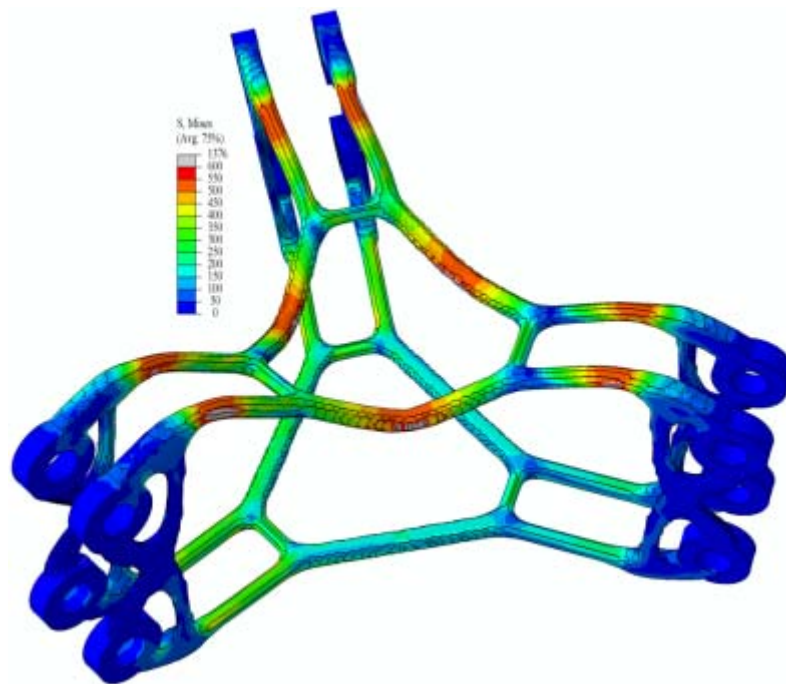


Figure 5-52: The deformation of the bending node simulated in Abaqus.

Figure 5-53 shows the moment-rotation diagram at the connection of the node to one of the rotating parts of the test rig. As can be seen, the maximum applied moment is equal to 0.13kN.m.

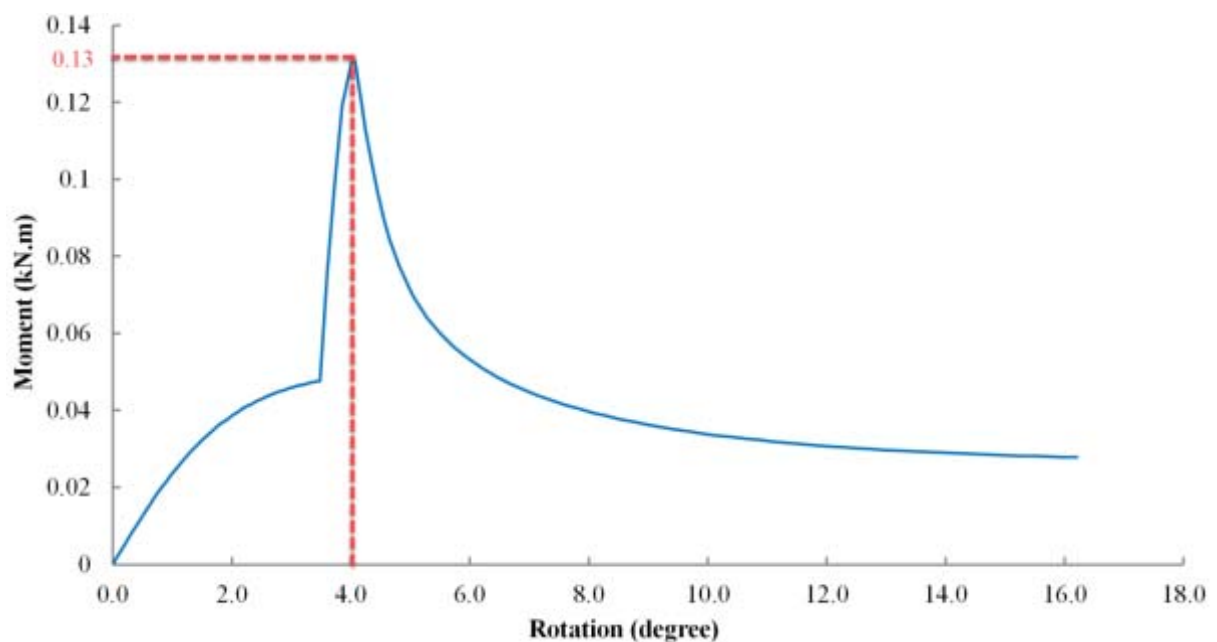


Figure 5-53: Force-displacement curve for compression node.

Figure 5-54 shows the failure of the bending node in experiment which is carried out using the proposed test rig. The deformed shape of the node in the non-linear simulation is shown in Figure 5-52.



Figure 5-54: One bending node is tested by using the proposed test rig.

The maximum applied load measured by the load cell for node M1 is equal to 1.18kN. By using the dimensions and assembled configuration of the bending test rig shown in Figure 5-45, the maximum bending moment applied to the node on each face is equal to 0.19kNm which is larger than 0.13kNm measured from non-linear analysis.

5.4. Discussion and conclusions

The proposed concept for test setup is based on changing direction of a vertical applied load to the desired direction by using the in-plane rotation of plate with specific dimensions and alignment. In the case study, a customised test rig is designed to test different types of nodes. The neglect of the differences in bolt diameter and hole diameter would cause a deviation of the real loading condition from the design condition. The node deformations obtained from

the numerical simulations agree very well with the experimental data. The maximum loads applied to the nodes are also close to the numerical predictions.

References

1. López, A., Puente, I. and Serna, M.A. (2007). Numerical model and experimental tests on single-layer latticed domes with semi-rigid joints. *Computers & structures*. **85**(7-8): 360-374.
2. Fathelbab, F.A. (1987). *The effect of joints on the stability of shallow single layer lattice domes*. PhD thesis, University of Cambridge.
3. See, T. and McConnel, R.E. (1986). Large displacement elastic buckling of space structures. *Journal of Structural Engineering*. **112**(5): 1052-1069.
4. Fan, F., Ma, H., Cao, Z. and Shen, S. (2011). A new classification system for the joints used in lattice shells. *Thin-Walled Structures*. **49**(12): 1544-1553.
5. Kato, S., Mutoh, I. and Shomura, M. (1998). Collapse of semi-rigidly jointed reticulated domes with initial geometric imperfections. *Journal of Constructional Steel Research*. **48**(2-3): 145-168.
6. López, A., Puente, I. and Serna, M.A. (2007). Direct evaluation of the buckling loads of semi-rigidly jointed single-layer latticed domes under symmetric loading. *Engineering Structures*. **29**(1): 101-109.
7. Ma, H.H., Fan, F. and Shen, S.Z. (2008). Numerical parametric investigation of single-layer latticed domes with semi-rigid joints. *Journal of the international association for shell and spatial structures*. **49**(2): 99-110.
8. Lopez, A., Puente, I. and Aizpurua, H. (2011). Experimental and analytical studies on the rotational stiffness of joints for single-layer structures. *Engineering structures*. **33**(3): 731-737.
9. Ma, H., Fan, F., Wen, P., Zhang, H., Shen, S. (2015). Experimental and numerical studies on a single-layer cylindrical reticulated shell with semi-rigid joints. *Thin-Walled Structures*. 86: 1-9.
10. Tian, L., Wei, J. and Hao, J. (2018). Anti-progressive collapse mechanism of long-span single-layer spatial grid structures. *Journal of Constructional Steel Research*. **144**: 270-282.
11. Wei, J.-p., Tian, L.-m. and Hao, J.-p. (2018). Improving the progressive collapse resistance of long-span single-layer spatial grid structures. *Construction and Building Materials*. **171**: 96-108.
12. Min, C., Dong, X., Yang, Z., Liang, S. U., Shilin, D., Dasui, W., Wei, F. and Anan, Z. (2010). Experimental research and finite element analysis on joints of Sun Valley steel structure for the Expo Axis project. *Journal of Building Structures*. **5**: 006.

CHAPTER 6

CONCLUSIONS AND FUTURE RESEARCH

Chapter 6: Conclusions and Future Research

6.1. Conclusions

In gridshell structures, structural nodes connect the members coming from different directions. The direction and position of the connecting faces of the nodes should be adjusted to fit the requirements of the connecting members. This is applied as constraints in the geometrical design of nodes, so that most geometrical and topological information of the structure (e.g. number, position and direction of the connecting members) are stored in the final geometry of the nodes stores. As nodes connect beam members in gridshell and transfer loads between them, the structural efficiency of nodes would affect the performances of the connected beams and the stability and load capacity of the whole structure. In the past, the application of gridshell structures was limited due to the lack of advanced manufacturing technologies, high cost and difficulties in structural node design. With the development of new design algorithm, such as the structural optimisation algorithm, it is possible to obtain efficient node design with lighter weight. However, the geometries of these designs are normally too complex to be fabricated using conventional manufacturing methods. In recently years, with the development of Computer Aided Manufacturing (CAM), many manufacturing restrictions, such as labour intensity involved in manufacturing with strict tolerance and restrictions in mass production of customised items, have been removed. Thus, more complex design configurations are conceivable to be constructed for gridshell structures. The newly developed additive manufacturing (AM) technique is able to realise the most complex node geometries with a high level of accuracy and quality control during the manufacturing process. In this research, the behaviour of gridshell structures designed using topology optimisation method and fabricated with the new manufacturing methods has been extensively investigated. The general configurations of the nodes for different load cases

have been developed. The challenges of smoothing node design and additive manufacturing of nodes are investigated. By comparing the new design with the conventional designs, the efficiency and effectiveness of the new design methods have been demonstrated. An innovative experimental setup has also been proposed and validated.

In the first stage, the effects of a number of parameters, such as the loading type and the initial node size, on the final node design have been investigated. The comparison of the designed nodes with different initial design domain sizes under the same loading condition shows that the decrease in the design domain size would lead to the decrease of the volume of the designed structure, and consequently reduce the manufacturing cost. Therefore, the best design domain size for structural node depends on its specific geometrical conditions as well as the initial design domain size. In this study, Bi-directional evolutionary structural optimisation (BESO) has been used to optimise design for more than 20 different nodes with various initial geometries and loading conditions. Based on the designed nodes, it can be concluded that, in an efficient node topology, a top layer and a bottom layer have always been generated for the node. In order to prevent stress concentration at the sharp edges in the BESO design, two different smoothing methods have been employed, including the Laplacian smoothing algorithm and the Non-Uniform Rational Basis Spline (NURBS). A case study of the smart project has also been presented and finally, the challenges in the design, smoothing and additive manufacturing of nodes have been investigated.

In the second stage, complex structural nodes have been designed by employing two different methods, i.e. the transitional section method and the topology optimisation method. In the first method, a simple node centre is connected to the members using parts with varying cross sections. The second approach is the bi-directional evolutionary structural optimisation (BESO) method. A comparative study between the new node designs and the conventional

node designs have also been carried out under identical loading conditions. In order to evaluate the structural performances of these nodes, a series of finite element analysis have been conducted on a typical six-way arbitrary node. Compared to the conventional nodes, the transitional and BESO nodes have shown reduction in the maximum stress and more uniform stress distributions. Moreover, the new nodes are more purposely designed based on different load cases. Besides, the comparative study has demonstrated that the BESO node has the least amount of von Mises stress, the highest stiffness and the smallest volume of material.

Finally, an experimental setup has been proposed for quasi-static test of nodes under different loading conditions. The proposed test setup is general, easy to establish and able to simulate the dominant loading conditions of the node. The test rig made in this study can apply different loads onto a three-way node with minimal changes in the configuration of bolts and plates, including compression force, tensile force, shear force and bending moment. Two types of symmetrical three-way nodes designed by BESO for pure axial loads and pure out-of-plane bending moments have been tested using the new test setup. A series of non-linear numerical analysis have also been carried out and validated using the test results. The finite element model has been demonstrated to be able to predict the structural behaviours of the nodes with high accuracy. Also, the tests results show that the effect of bolt tolerance on the testing results is significant and it should be considered in the design of test setup.

6.2. Future Research

As the most critical components of gridshell structures, structural nodes with higher efficiency can be designed using topology optimisation algorithms and manufactured with the help of additive manufacturing. In this study, the objective function of the structural optimisation is the stiffness of the node, and the stress is checked in each iteration. As the

stress level is usually used as the design criterion, it would also be interesting to investigate the effectiveness of using topology optimisation for stress in the design of nodes.

In the node design, both stress level introduced by the applied load and deflection caused by out-of-plane bending are important. To further optimise the design and improve the performance, it will be beneficial to compare the optimised results obtained from the objective function with only strength as variable and that with a combination of strength and stiffness.

The BESO design is time dependent. When the size of the design domain increases, the number of elements in the model increases, leading to the increase in the time of BESO design. It is usually hard to find the minimum size of the design domain that provides enough freedom for BESO design. A suggestion for solving this problem is to select a large design domain and fill it with big elements. The inefficient elements can be removed from the design domain by applying BESO. The remained design domain is then divided into smaller elements to be used as design domain for the next round of BESO design.

With regard to the failure mode of the nodes observed in the non-linear simulations and experimental tests, it is suggested to include the material non-linearity and buckling in the design process.

The result of BESO node design is highly influenced by the loading conditions, while the conventional design is more constrained to the geometrical conditions. Therefore, to obtain a better understanding of the efficiency of the BESO design, a comparison between BESO and conventional designs for different nodes from different locations of a gridshell structure with different curvatures can be beneficial.

In the test setup concept proposed in this study, the connection details need to be reconsidered so that it can transfer loads in both directions, enable tests to be conducted under displacement control, and allow cyclic loading tests.

Lastly, in this study, a manual hydraulic jack has been used to apply loads to the test rig. Therefore, the applied load function could not be controlled. The configuration of the test rig can be easily modified in the future to accommodate computer controlled hydraulic jack for a better control over the applied load function.